Vol. 152, September 1, 1983
Complete in one issue

ISSN 0003-2670

ANALYTICA CHIMICA ACTA

International journal devoted to all branches of analytical chemistry

ELSEVIER SCIENTIFIC PUBLISHING COMPANY

ANALYTICA CHIMICA ACTA

International journal devoted to all branches of analytical chemistry
Revue internationale consacrée à tous les domaines de la chimie analytique
Internationale Zeitschrift für alle Gebiete der analytischen Chemie

PUBLICATION SCHEDULE FOR 1983

	J	F	M	A	M	J	J	A	S	O	N	D
Analytica Chimica Acta	145	146	147	148	149	150/1 150/2	151/1	151/2	152	153/1	153/2	154 155

Scope. *Analytica Chimica Acta* publishes original papers, short communications, and reviews dealing with every aspect of modern chemical analysis, both fundamental and applied.

Submission of Papers. Manuscripts (three copies) should be submitted as designated below for rapid and efficient handling:

Papers from the Americas to: Professor Harry L. Pardue, Department of Chemistry, Purdue University, West Lafayette, IN 47907, U.S.A.

Papers from all other countries to: Dr. A. M. G. Macdonald, Department of Chemistry, The University, P.O. Box 363, Birmingham B15 2TT, England. Papers dealing particularly with computer techniques to: Professor J. T. Clerc, Universität Bern, Pharmazeutisches Institut, Baltzerstrasse 5, CH-3012 Bern, Switzerland.

Submission of an article is understood to imply that the article is original and unpublished and is not being considered for publication elsewhere. Upon acceptance of an article by the journal, authors resident in the U.S.A. will be asked to transfer the copyright of the article to the publisher. This transfer will ensure the widest dissemination of information under the U.S. Copyright Law.

Information for Authors. Papers in English, French and German are published. There are no page charges. Manuscripts should conform in layout and style to the papers published in this Volume. Authors should consult Vol. 132, p. 239 for detailed information. Reprints of this information are available from the Editors or from: Elsevier Editorial Services Ltd., Mayfield House, 256 Banbury Road, Oxford OX2 7DH (Great Britain).

Reprints. Fifty reprints will be supplied free of charge. Additional reprints (minimum 100) can be ordered. An order form containing price quotations will be sent to the authors together with the proofs of their article.

Advertisements. Advertisement rates are available from the publisher.

Subscriptions. Subscriptions should be sent to: Elsevier Science Publishers B.V., P.O. Box 211, 1000 AE Amsterdam, The Netherlands.

Publication. *Analytica Chimica Acta* appears in 11 volumes in 1983. The subscription for 1983 (Vols. 145–155) is Dfl. 1980.00 plus Dfl. 220.00 (postage) (total approx. U.S. $880.00). Journals are sent automatically by airmail to the U.S.A. and Canada at no extra cost and to Japan, Australia and New Zealand for a small additional postal charge. All earlier volumes (Vols. 1–144) except Vols. 23 and 28 are available at Dfl. 200.00 (U.S. $80.00), plus Dfl. 15.00 (U.S. $6.00) postage and handling, per volume.

Claims for issues not received should be made within three months of publication of the issue, otherwise they cannot be honoured free of charge.

Customers in the U.S.A. and Canada who wish to obtain additional bibliographic information on this and other Elsevier journals should contact Elsevier Science Publishing Company Inc., Journal Information Center, 52 Vanderbilt Avenue, New York, NY 10017. Tel: (212) 867-9040.

ANALYTICA CHIMICA ACTA
VOL. 152 (1983)

ANALYTICA CHIMICA ACTA

International journal devoted to all branches of analytical chemistry

ELSEVIER Amsterdam–Oxford–New York

0003-2670/83/$03.0C

Printed in The Netherlands.

Analytica Chimica Acta, 152 (1983) 1—11
Elsevier Science Publishers B.V., Amsterdam — Printed in The Netherlands

Review

DETECTION OF ENZYMATIC ACTIVITY BY POST-COLUMN REACTION AFTER SEPARATION BY HIGH-PERFORMANCE LIQUID CHROMATOGRAPHY

E. CLIFFORD TOREN, JR.* and DOROTHY N. VACIK
Department of Pathology, University of South Alabama, Mobile, AL 36617 (U.S.A.)
(Received 23rd March 1983)

SUMMARY

This review covers the origins, selected applications, designs, and theoretical aspects of post-column reactors for the continuous detection and quantitation of isoenzymes following separation by high-performance liquid chromatography. Compensation for interferences present in biological samples and the dispersion properties of packed bed and coiled capillary reactors are discussed.

Enzymes usually are present in trace quantities in biological samples with concentrations often being in the femtomolar range or less. Therefore, the key to their detection and quantitation is in the determination of catalytic activity rather than direct measurement of concentration or mass.

Isoenzymes are frequently separated by high-performance liquid chromatography (h.p.l.c.) with subsequent collection of fractions of the eluate. The fractions may be assayed manually or automatically. For example, Kudirka et al. [1] manually collected fractions containing creatine kinase (CK, EC 2.7.3.2) isoenzymes and subsequently quantified the activity of the fractions manually. Later, they used an automatic fraction collector with an AutoAnalyzer to quantify the activity of each fraction [2]. In either case, separation was achieved in ca. 30 min; however, activity determinations required several hours. Hence, the need for continuous detection of enzymatic activity has been clearly demonstrated.

Post-column reactors are ideally suited for continuous detection of activity. In their simplest form, such reactors (Fig. 1) consist of a mixer into which the column eluate and a reagent stream are added. The effluent from the mixer is passed through a delay volume (reactor) to allow the reaction to proceed for a fixed time and then through a detector to measure the product of the reaction. Enzyme-catalyzed reactions are generally substrate-specific or specific to a class of substrates, hence the detection of an enzyme by its activity adds to the selectivity because only "active" peaks will be detected. This aids in improving resolution of the desired components and thus provides for somewhat less sophisticated reactor design.

0003-2760/83/$03.00

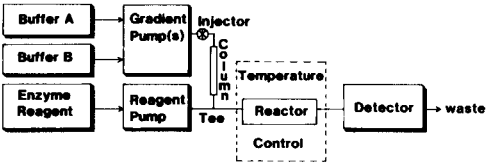

Fig. 1. An isoenzyme separation system based on h.p.l.c. and a single-detector, post-column reactor. A gradient system, useful for ion exchange, is illustrated. The mixer in this case is a simple T-joint (see text for other types). The reagent (substrates, buffers, activators, etc.) are mixed with the column effluent and the reaction proceeds in the thermostated reactor. The product or substrate concentration is continuously monitored by the detector. Reprinted from [7].

Spackman et al. [3] reported the first example of a post-column reactor in 1958. They mixed the column eluate with ninhydrin for the specific detection of the amino acids separated on the column. Later, Hicks and Nalevac [4] continuously quantified the activity of lactate dehydrogenase isoenzymes (LD, EC 1.1.1.27) as they emerged from a DEAE-Sephadex column by mixing the eluate with lactate and nicotinamide adenine dinucleotide (NAD). The reduced NAD (NADH) produced in the reactor was detected at 340 nm.

The introduction of additional post-column volumes must necessarily affect the resolution of the separation adversely by increased band-broadening (dispersion). Therefore, several reactors have been designed in an attempt to minimize dispersion yet provide sufficient time for the reaction to produce detectable concentrations of product. This paper reviews the progress of the post-column reaction detection of enzymes with regard to reactor types, theory, and selected applications. Other recent reviews have discussed enzymatic post-column reactors [5—7].

REACTOR DESIGN

Mixers

The first consideration in a post-column reactor system is the mixing device. The simplest design is a T-joint. Frei et al. [8, 9] have described several mixing-tee configurations and Huber et al. [10] have devised elegant experiments to measure the extent of mixing with T-joints for various angles between the arms. They recommend short columns packed with relatively large, non-porous beads as mixers. These provide mixing with only a minor increase in dispersion. Most enzymatic determinations, however, require long enough reaction times (usually 1—5 min) to develop sufficient measurable product, that a simple T-joint with a relatively large reactor suffices for adequate mixing with minimal effect on dispersion. Sophisticated mixers are generally necessary for fast reactions, e.g., tangential mixers for stopped-flow techniques.

Delay volume

Several designs for the delay volume device, the reactor itself, have been used. These include air-segmented flow reactors and unsegmented flow reactors. The latter have mainly been used with enzymatic separations because of their simplicity. The former have been used when high resolution is important. Because little has been published on segmented-flow reactors for post-column enzyme assay, this review will concentrate on non-segmented-flow reactors of which two types have been used: packed columns and open tubular capillaries.

Chang et al. [11, 12] first reported enzymatic post-column reactors designed with h.p.l.c. hardware for the determination of LD and CK isoenzyme activity. They used a 400 × 4.8 mm column packed with 40-μm nonporous Glycophase G for the delay volume. Schroeder et al. [13] used a tightly wound coil of stainless steel tubing (1.8 m × 0.5 mm i.d.) as the reactor for the detection of LD isoenzymes. Simultaneously, Schlabach et al. [14] compared the efficiency (plate number vs. flow rate) of a packed reactor (600 mm × 4.1 mm) filled with Whatman glass spheres with a capillary reactor (15.25 m × 0.5 mm); the results are shown in Fig. 2. Clearly, the dispersion characteristics of the packed-bed reactor are superior to those of the open tubular capillary. Decreasing the diameter of the capillary while proportionally increasing the length to provide similar delay volumes would improve the performance of the reactor at the expense of increased pressure drop and the risk of plugging; however, for isoenzyme determinations the selectivity of the reaction reduces the complexity of the chromatograms to an extent that the loss in resolution may become insignificant. Our experience indicates that with few exceptions, capillary reactors are adequate for

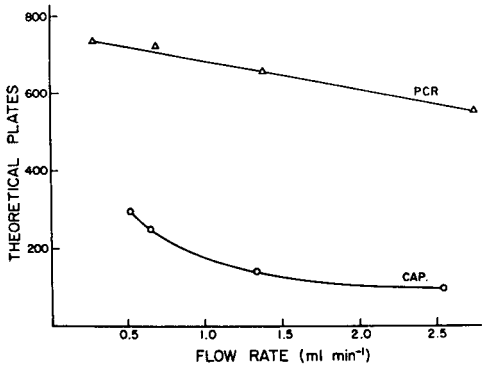

Fig. 2. Comparison of band spreading between a capillary tubing and a packed column reaction vessel (PCR). The capillary tubing was a 15.25-m coil of 0.5-mm i.d. stainless steel while the packed column was a 600 × 4.1 mm precision bore tube. The column was packed with Whatman glass spheres. The solute was 0.5 mM *p*-nitrophenol and the mobile phase was 0.01 M NaH_2PO_4 buffer driven at the same rate. Reprinted from [14], courtesy of the authors.

most enzymatic monitoring. They are easier to prepare and thermostat and are dimensionally stable to provide constant delay time for a constant flow. This is an important consideration in kinetic procedures.

As opposed to post-column reactions that proceed to equilibrium, enzymatic reactions can be adjusted to zero-order conditions with respect to substrate. Therefore, the peaks increase linearly with time while dispersion (band spreading) increases as the square root of time so that the "apparent resolution" is not as adversely affected by increased band spreading. This concept of apparent resolution has not been mathematically formulated, but qualitatively this phenomenon is used to advantage for enzymatic post-column reactors.

The recent interest in flow-injection systems has prompted several studies of band spreading in reactors. Although flow-injection techniques are similar to those for post-column reactions, the objectives are different. For example, the flow rate in post-column reactors is not completely selectable because it is determined primarily by optimal separation conditions; and the reagent flow rate is minimized, considering the flow-rate stability of the reagent pump and reagent solubility consistent with optimal substrate concentrations. Further, the sample frequency and volume are determined by the separation conditions. Therefore, not all of the optimizing conditions and techniques developed for flow injection systems are necessarily applicable to post-column work but do supply reasonable guidelines.

Levenspiel [15] has presented an excellent general treatment of reactor theory that is applicable to packed-bed reactors as well as open tubular capillaries. His discussion centers around the application of statistical moments to describe reactor performance, especially the first and second moments, i.e., the mean residence time and variance, respectively. (For pure Gaussian peaks, these correspond to the time at maximum peak height and the standard deviation squared). To summarize the general characteristics of band spreading in reactors:

$$\Delta\sigma^2/t_R^2 = 2D/uL \tag{1}$$

where $\Delta\sigma^2$ is the difference in the variance of a peak between two measuring points, t_R is the mean residence time between the measuring points, D is the axial dispersion coefficient, u is the linear flow rate, and L is the length of the reactor. The quantity D/uL is called the dispersion number and it characterizes a family of Gaussian distributions of equal areas. Small values indicate tall, narrow peaks that progressively flatten out as the dispersion number increases. It may be noted that $\Delta\sigma^2/t_R^2$ is $1/N$, where N is the number of theoretical plates in chromatographic theories. For flow in straight pipes (tubes), the axial dispersion coefficient is given by

$$D = D_M + u^2d^2/192\,D_M \tag{2}$$

where D_M is the molecular diffusion coefficient and d is the inside diameter of the pipe. Except for impractically low flow rates or extremely small i.d.

tubes, Eqn. (2) can generally be approximated by

$$D \simeq u^2 d^2 / 192\, D_M \tag{3}$$

From the above relationships for a given reactor, band spreading is increased by decreasing diffusion coefficients, an important consideration for macromolecules such as enzymes. Most theoretical and/or experimental studies have used solutes with $D_M \approx 10^{-5}$ cm^2 s^{-1} or have assumed that magnitude, whereas large enzymes may have values of $D_M \approx 10^{-7}$ cm^2 s^{-1}.

Another way of looking at the same problem is to consider the reactor as a series of N stirred tanks; this is identical to the chromatographic theoretical plate concept. For one tank, the distribution or peak shape is an exponential decay. As N increases, the peak shape becomes a Poisson distribution that becomes essentially Gaussian when N approaches 25, which is easily realized in most packed or open tubular reactors. Therefore, a column or reactor can be readily characterized by measurement of the standard deviation (peak width) and retention time. However, for small N, peaks are not Gaussian; also other mechanisms (e.g., adsorption) may account for non-Gaussian peaks and distortion of the peak shape; hence the moments should be calculated [16] or sophisticated graphical techniques should be used [17]. Also peak shapes in reactors depend on reaction order and absolute concentrations [15]. Fortunately, the zero-order kinetics generally used in enzyme assays should provide Gaussian peaks for reasonably large N, because zero-order reactions do not distort peaks.

Huber et al. [10] have stated optimal reactor conditions as $t_{Rc}^2/N_C \gg t_{Rr}^2/N_r$, where the c subscripts apply to the column and the r subscripts refer to the reactor. Simply stated, the reactor should be more efficient than the column. The residence time of the reactor, t_{Rr}, is established by the time required to produce sufficient quantifiable product; therefore, for a given t_{Rr}, the delay volume must be achieved with an increased N_r. Clearly, Huber et al. [10] and Schlabach et al. [14] have demonstrated the superiority of packed-bed reactors over open tubes. However, we have achieved good resolution ($N \approx 400$) for coiled tubes (see Fig. 2) primarily because, with enzyme-catalyzed reactions, the peak height and area increase linearly with the reaction time whereas the peak is broadened (width or σ) approximately as the square root of time; therefore, for enzyme reactors, conditions need not be as stringent as stated by Huber et al. [10].

Although reactors can readily be characterized experimentally by measurement of t_R or σ, it is useful to estimate reactor behavior for design purposes. Several equations are presented below that will approximate design characteristics for both packed-bed and helically-coiled reactors.

For inert, packed-bed reactors, the plate number, N, can be estimated [10] from

$$N = F t_R / 2\epsilon_f A \lambda d_p \tag{4}$$

where F is the volumetric flow rate, ϵ_f is the fraction of cross section flowed through (ca. 1), A is the cross-sectional area, λ is the packing constant, and d_p is the particle diameter.

For tubular reactors, Deelder et al. [18] have presented the most comprehensive correlation of parameters affecting band spreading and the design of such reactors. Coiled tubing introduces centrifugal forces that result in secondary flow profiles. Although this effect is beneficial, the mathematics tend to become intractable; but, numerical solutions have been developed. For coiled tubes (from Eqns. 1 and 3):

$$\Delta\sigma^2/t_R = \kappa d^2/96\, D_M \tag{5}$$

where κ depends on the flow profile [19] which is governed by the properties of the coiled tube, solvent, and solute. For straight tubes, $\kappa = 1$. More explicitly,

$$\kappa = 5.6\,(DnSc^{0.5})^{-0.67} \quad \text{for } 12.5 < DnSc^{0.5} < 200$$

$$\kappa = 1 \quad \text{for } DnSc^{0.5} \leqslant 12.5 \tag{6}$$

Here Dn is the Dean number given by $2ur\rho/\eta(r/r_c)^{0.5}$, r being the tubing radius, r_c the radius of the coil, and ρ and η the solvent density and viscosity, respectively. The Dean number describes the reactor itself and the solvent. The Schmidt number (Sc) describes the solute/solvent system and is given by $\eta/\rho D_M$. From these equations, the efficiency of coiled reactors can be estimated. Deelder et al. [18] and later Van den Berg et al. [20] correlated these relationships from literature reports and experimental data. Further comparisons of coiled tubes to packed columns have recently been reported [21—23].

Hofmann and Halasz [24], Huber et al. [10] and much, earlier, Horvath et al. [25] observed behavior that was not totally consistent with the above relationships. These deviations corresponded to local increases in N with u (Eqn. 3) and were ascribed to wall roughness [24, 25]. Such deviations have been observed in this laboratory, as has the fact that the dispersion of an LD-catalyzed NADH peak is intermediate between an authentic NADH injection and that of a protein aldolase of molecular weight 158,000 daltons (LD is a globular protein of m.w. = 140,000 daltons). We have also observed that Eqns. (5) and (6) hold qualitatively for macromolecule-tracers of $D_M \approx 10^{-7}$, but that the limits imposed in Eqn. (6) may be increased from 12.5 to ca. 100 and 200 to ca. 2000, respectively, for large molecules. Also complicating the picture, the tracer peaks with certain globular proteins in a stainless steel coiled reactor exhibit severe tailing, even with N values of 50—100. Therefore, it seems that adsorption of proteins on the reactor wall is likely, but the conditions for which this phenomenon occurs have not yet been completely defined.

INTERFERENCES

Interferences are a major problem in the analysis of biological samples. Hicks and Nalevac [4] recognized this problem in their early work. Also, drifting baselines (see, e.g. [13]) that result from chromatographic gradients and reagent decomposition (e.g., NAD → NADH) can seriously affect the measurement of activity. The approach to circumventing or compensating for these problems has been to use two detectors in several configurations: one to measure principally "noise" and the other to measure "signal + noise" and then to subtract the two to obtain the corrected "true" signal. The alternative is to eliminate interferences by prior sample processing, which can be very tedious.

The two detectors can be placed in parallel (Fig. 3) or in series (Fig. 4). Conceptually, the parallel mode is easier to understand. Hicks and Nalevac [4] maintained the sample channel at 37°C in which the LD-catalyzed conversion of NAD to NADH proceeded much more rapidly than in the identical reference channel maintained at 18°C. Because drifts and nonenzymatic interferences are not generally temperature-dependent, subtraction of the two signals yielded a response proportional to enzymatic activity.

Denton et al. [26] have described an unusual modification of this concept that incorporates an immobilized enzyme preparation in the sample channel. They immobilized hexokinase (HK, EC 2.7.1.1) and glucose-6-phosphate dehydrogenase (G-6-PDH, EC 1.1.1.49) so that the separated CK isoenzymes acted as catalysts in a reaction [27] that produced NADPH which was meas-

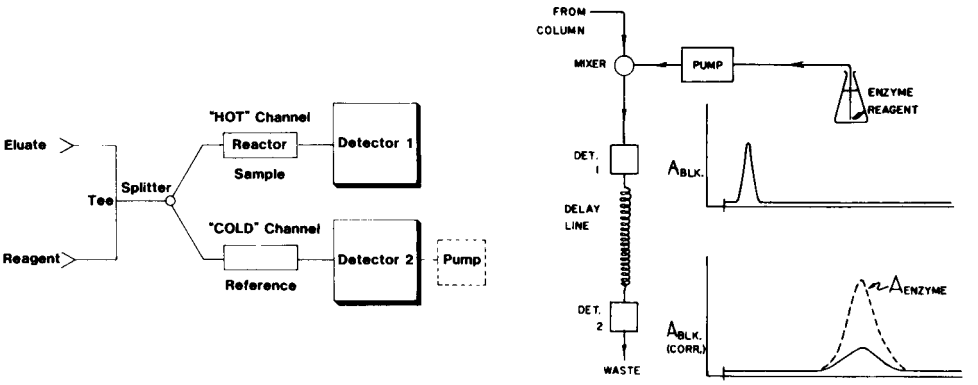

Fig. 3. Dual-detector post-column reactor, parallel mode. See text for description. Reprinted from [7].

Fig. 4. Enzyme reaction detector with a single-stream sequential arrangement. The blank (A_{BLK}) is obtained at detector 1 and must be mathematically shifted in time and broadened to reflect the band spreading in the coil. The resultant blank (A_{BLK} corr.) is subtracted from the response of detector 2 to obtain the response from the enzyme-catalyzed reaction. Reprinted from [13].

ured with a dual channel-absorbance detector; the reference channel contained no coupling enzymes and therefore served as a blank. The reagent and column eluates were pulled through the reactor with a peristaltic pump. Later, Denton et al. [28] extended the system to LD isoenzyme by immobilizing diaphorase to couple the NADH formed to produce the reduced form of 2,6-dichlorophenolindophenol that could be detected at 600 nm. Bostick et al. [29] further extended this approach by detecting LD and CK isoenzymes simultaneously. They determined LD specifically with amperometric oxidation of NADH on vitreous carbon and CK was specifically quantified by the bioluminescent detection of ATP coupled to the luciferin—luciferase reaction. A major advantage of the above approach is the reusability of the expensive coupling reagents.

Schlabach and Regnier [30] also immobilized HK and G-6-PDH, but on glass beads, for their single detector reactor. They obtained best results when only G-6-PDH was immobilized because of difficulty in reaching steady state when both coupling enzymes were immobilized.

The basic principles of dual serial detectors are illustrated in Fig. 4. Enzymatic peaks are distinguished from interferences, because their areas increase with time whereas areas of peaks caused by interferences, although broadened from detector 1 to detector 2, remain constant. To obtain a chromatogram, corrected point-by-point, the response of the first detector must be transformed with respect to time (the delay time of the reactor) and with respect to shape so that the response would appear as if it occurred at the second detector. Fulton et al. [31] developed a numerical solution to the mass-balance model based on a single adjustable parameter to provide this transformation. They evaluated this reactor system via the determination of LD isoenzyme profiles from human serum samples, using an open tubular capillary reactor [32]. Figure 5A illustrates the response of the two detectors, the upper trace being the output from the second detector. Figure 5B is the corrected chromatogram after transformation and point-by-point subtraction. There is some noticeable LD activity in the response from the first detector (Fig. 5A), which results from the inclusion of a pre-delay coil between the mixing T-joint and the first detector to allow for any lag time to pass (noticeable with CK and other coupled assay procedures) and to provide for temperature-equilibration before activity measurement. This system was subsequently evaluated for recovery, precision, linearity, and dynamic range for CK and LD determinations [31]. In this work, a simpler data reduction algorithm was used. Net areas rather than individual points were subtracted to obtain net activity to compensate for interferences. Later, this reactor system was used to identify the interferences in human serum in which CK isoenzymes were quantified by fluorescence detection [33].

Parallel-stream, dual-detector reactors do not require an on-line computer for data acquisition and reduction, but are mechanically more complex than serial stream reactors. Because the volume of a parallel reactor must be

nearly double that of an equivalent serial reactor, band spreading is increased and sensitivity is reduced.

DETECTORS

Ideally a detector for enzymatic reactions should be specific to product or substrate of the reaction, to eliminate the need for interference correction as discussed above. Therefore, detectors such as those based on refractive index that are unselective, insensitive, and subject to gradients have not been used for these applications. Conversely, fluorescence detectors, although widely used (see, e.g. [13, 33, 34]) require final products that fluoresce, a somewhat stringent condition that often requires coupling reactions. Because fluorescence detectors have lower detection limits and are more selective (in the sense described above), they are ideally suited for dehydrogenases, especially those that involve the NAD/NADH or NADP/NADPH couples, produced in either the main reaction (e.g., LD) or in subsequent steps (e.g., CK). Absorbance detectors are more generally applicable and are reasonably sensitive, especially the variable-wavelength types, but the wide variety of solutes in biological samples that absorb across the spectrum also makes them subject to very many interferences.

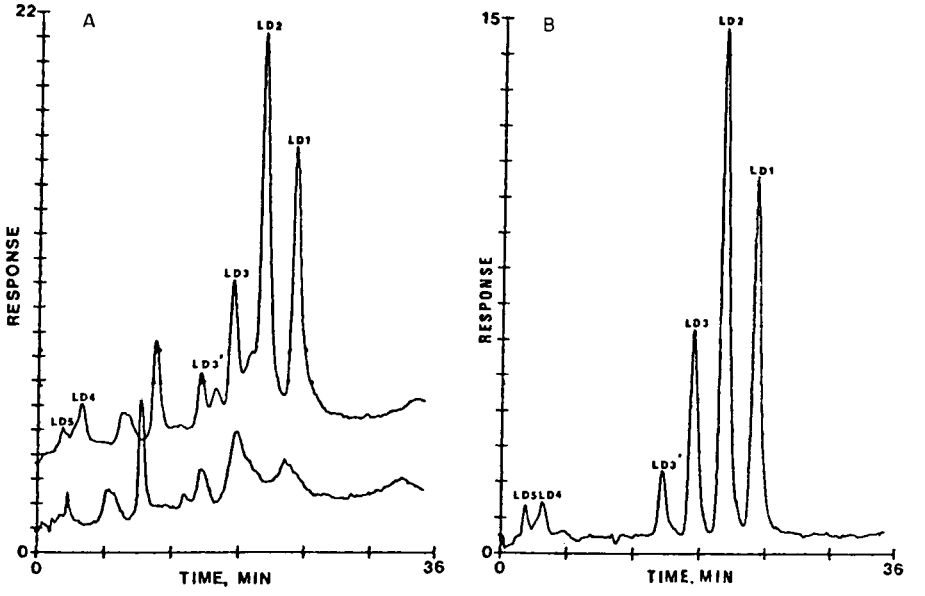

Fig. 5. Chromatograms of serum LD isoenzymes from a patient who had a myocardial infarction. (A) The upper trace was recorded at the downstream detector (detector 2); the lower trace shows the background absorbance, as it was observed at detector 1. (B) Profile resulting from the correction for background absorbance; the large artifacts (interferences) which appear in the 5—10 min region in the lower trace in (A) are eliminated by the subtraction process. (Column and chromatographic conditions similar to those described previously [32, 34].)

Further selectivity and reasonable sensitivity are available with electrochemical detectors because only a limited number of endogenous compounds are readily oxidized or reduced [29]. Bioluminescence detectors offer excellent selectivity, have acceptable detection limits and are easily constructed. Bostick et al. [29] detected the ATP produced by the CK-catalyzed reaction by coupling to luciferin/luciferase.

The post-column reactors with associated detectors of the types described above, however, do offer sufficient selectivity and sensitivity for the isoenzyme separations described herein. For future applications, novel detectors that provide increased selectivity and sensitivity would be desirable to eliminate the necessity for interference correction.

It can be concluded that post-column reactors are useful, and in many cases, essential tools for detecting and quantifying enzymes after separation by h.p.l.c. Although the addition of post-column volumes must necessarily increase band broadening, the additional selectivity, even occasionally specificity, gained by the post-column reactors tends to offset the loss in resolution. For these reasons, it is not possible to define under what circumstances a particular type of reactor should be used [35, 36]. Figure 5, for example, was obtained with reaction times of about 3 min using helically coiled reactors. Segmented-flow or packed-bed reactors may be required for enzymatic reactions that require longer times.

This work was supported by grant CHE 8101123 from the National Science Foundation. The authors appreciate the technical assistance of Joe Ann Thomas, Reede Cooley, and Dr. Peter Bloxham.

REFERENCES

1 P. J. Kudirka, M. G. Busby, R. N. Carey and E. C. Toren, Jr., Clin. Chem., 21 (1975) 450.
2 P. J. Kudirka, R. R. Schroeder, T. E. Hewitt and E. C. Toren, Jr., Clin. Chem., 22 (1976) 471.
3 D. H. Spackman, W. H. Stein and S. Moore, Anal. Chem., 30 (1958) 1190.
4 G. P. Hicks and G. Nalevac, Anal. Biochem., 13 (1965) 199.
5 F. E. Regnier and K. M. Gooding, Anal. Biochem., 103 (1980) 1.
6 L. D. Bowers and W. D. Bostick, in R. W. Frei and J. F. Lawrence (Eds.), Chemical Derivatization and Modification Techniques in Analytical Chemistry, Vol. 2, Plenum Press, New York, 1982.
7 D. N. Vacik and E. C. Toren, Jr., J. Chromatogr., 228 (1982) 1.
8 R. W. Frei, L. Michel and W. Santi, J. Chromatogr., 142 (1977) 261.
9 R. W. Frei and A. H. M. T. Scholten, J. Chromatogr. Sci., 17 (1979) 152.
10 J. F. K. Huber, K. M. Jonker and H. Poppe, Anal. Chem., 52 (1980) 2.
11 S. H. Chang, K. M. Gooding and F. E. Regnier, J. Chromatogr., 125 (1976) 103.
12 S. H. Chang, R. Noel and F. E. Regnier, Anal. Chem., 48 (1976) 1839.
13 R. R. Schroeder, P. J. Kudirka and E. C. Toren, Jr., J. Chromatogr., 134 (1977) 83.
14 T. D. Schlabach, S. H. Chang, K. M. Gooding and F. E. Regnier, J. Chromatogr., 134 (1977) 91.
15 O. Levenspiel, Chemical Reaction Engineering, 2nd edn., Wiley, New York, 1972.

16 E. Grushka, N. N. Myers, P. D. Schettler and J. C. Giddings, Anal. Chem., 41 (1969) 889.
17 W. E. Barber and P. W. Carr, Anal. Chem., 53 (1981) 1939.
18 R. S. Deelder, M. G. F. Kroll, A. B. Beeran and H. M. Van den Berg, J. Chromatogr., 149 (1978) 669.
19 K. B. Bischoff and O. Levenspiel, Chem. Eng. Sci., 17 (1962) 245.
20 J. H. M. Van den Berg, R. S. Deelder and H. G. M. Egberink, Anal. Chim. Acta, 114 (1980) 91.
21 R. Tjissen, Anal. Chim. Acta, 114 (1980) 71.
22 J. M. Reijn, W. E. van der Linden and H. Poppe, Anal. Chim. Acta, 114 (1980) 105.
23 J. M. Reijn, W. E. van der Linden and H. Poppe, Anal. Chim. Acta, 123 (1981) 229.
24 K. Hofmann and I. Halasz, J. Chromatogr., 173 (1979) 211.
25 C. G. Horvath, B. A. Preiss and S. R. Lipsky, Anal. Chem., 38 (1967) 1422.
26 M. S. Denton, W. D. Bostick, S. R. Dinsmore and J. E. Mrochek, Clin. Chem., 24 (1978) 1408.
27 S. B. Rosalki, J. Lab. Clin. Med., 69 (1967) 696.
28 M. S. Denton, W. D. Bostick, S. R. Dinsmore and J. E. Mrochek, in G. Hawk (Ed.), Biological/Biomedical Applications of Liquid Chromatography, II, Vol. 12, Dekker, New York, 1979.
29 W. D. Bostick, M. S. Denton and S. R. Dinsmore, 3rd Int. Liq. Chromatogr. Symp.: Biological/Biomedical Applications of Liquid Chromatography, Boston, MA, 1979.
30 T. D. Schlabach and F. E. Regnier, J. Chromatogr., 158 (1978) 349.
31 J. A. Fulton, T. D. Schlabach, J. E. Kerl and E. C. Toren, Jr., J. Chromatogr., 175 (1979) 269.
32 J. A. Fulton, T. D. Schlabach, J. E. Kerl and E. C. Toren, Jr., J. Chromatogr., 175 (1979) 283.
33 T. D. Schlabach, J. A. Fulton, P. D. Mockridge and E. C. Toren, Jr., Clin. Chem., 26 (1980) 707.
34 T. D. Schlabach, J. A. Fulton, P. D. Mockridge and E. C. Toren, Jr., Clin. Chem., 25 (1979) 1600.
35 R. W. Frei, Chromatographia, 15 (1982) 161.
36 R. W. Frei, in R. W. Frei and J. R. Lawrence (Eds.), Chemical Derivatization in Analytical Chemistry, Vol. 1: Chromatography, Plenum, New York, 1981.

Analytica Chimica Acta, 152 (1983) 13—24
Elsevier Science Publishers B.V., Amsterdam — Printed in The Netherlands

MICROPROCESSOR-BASED TENSAMMETRIC DETECTION FOR LIQUID CHROMATOGRAPHY

A. M. BOND* and R. D. JONES

Division of Chemical and Physical Sciences, Deakin University, Waurn Ponds 3217, Victoria (Australia)

(Received 18th January 1983)

SUMMARY

The electrochemical technique of tensammetry has not been widely used for routine analysis because of the likelihood of extensive interference problems. Separation procedures are required to make the technique analytically viable. The combination of high-performance liquid chromatography (h.p.l.c.) for separation with microprocessor-based tensammetric detection is examined. Computer control enables different waveforms to be applied to generate and optimize the tensammetric response. Tensammetric peak heights are used in quantifying the response. In order to use the tensammetric peak which has a position dependent on concentration, it is necessary continually to scan a range of potential and to apply a computer-based peak-search routine to locate the peak current. This approach is aided by the use of a static mercury drop electrode. When reverse-phase liquid chromatography is used, the minimum of organic modifier in the eluent must be taken, to achieve optimum tensammetric response. The combination of h.p.l.c. and microprocessor-based electrochemical detection provides new prospects for the determination of species which exhibit a tensammetric response. The examples studied are polyethylene glycol and phenol ethoxylates.

It has long been known that a wide range of organic compounds adsorbs on the mercury electrode [1]. The effects of adsorption have been studied extensively [2]. Under alternating current (a.c.) polarographic conditions, the base alternating current of the electrolyte is depressed at potentials where adsorption occurs and peaks are observed at positive and negative potentials where the compound is desorbed [3]. These adsorption/desorption a.c. peaks have been called tensammetric peaks [3]. They are non-faradaic in origin and generally are observed with most transient electrochemical techniques, e.g., pulse voltammetry [4, 5], a.c. voltammetry [3] and chronopotentiometry [6]. The height of the tensammetric peak is directly proportional to concentration at low concentrations but becomes independent of concentration at higher concentrations [3, 5].

Whilst tensammetric response has been advanced for analytical purposes, it has been noted that mutual interference effects exist when more than one adsorbing species is present in solution [3]. This is commonly the case, so that practical application of tensammetry has been very limited. The

0003-2670/83/$03.00

effect of the presence of more than one adsorbing species can be quite severe and in the worst case one component may mask the tensammetric response of all other species. The extent of the problem is influenced by the relative concentrations, and strengths and rates of adsorption of each species. At low concentrations, adsorption equilibrium frequently is reached very slowly [7], and at different rates which depend on the mobility of the species in solution. Interference effects can be minimized by exploiting these and other differences [8]. However, despite some advances of this kind, interference problems are still the main drawback hindering the development of tensammetry as a viable analytical technique.

The problems inherent with tensammetry are well illustrated in a recent publication on the determination of ethanol in spirit drinks [9]. The results obtained for vodka are excellent, the results for gin are approximately 25% low and the method failed for blended whisky. It is apparent that the results deteriorate as the matrix becomes more complex.

The obvious way to minimize the possibility of interference is to couple tensammetric detection with a separation procedure. Indeed, the studies outlined here suggest that this is the only way of using tensammetry reliably when solutions of unknown matrix are to be analysed. Liquid chromatography has been used widely for the separation of organic compounds [10] and the combination of liquid chromatography with electrochemical detection is very common [11]. Although faradaic processes are used almost exclusively for the detection step in liquid chromatography with electrochemical detection, some workers have used tensammetry [12, 13] with a.c. and alternating voltage (a.v.) techniques. Both approaches involve a detection method that relies on changes in the background rather than the actual tensammetric peak.

Lankelma and Poppe [12] stated that, because the tensammetric peak position is itself a function of concentration, the peak height cannot be used for liquid chromatography with electrochemical detection. However, this need be true only when the response for all concentrations has to be measured at a constant d.c. potential; in contrast to earlier work, it proved viable here to use data obtained from the tensammetric peak. As the peak position changes as a function of concentration, it is necessary to sweep a window of potential to ensure that the peak is observed and instrumentation was designed to achieve this. The electrochemical part of the experiment is under microprocessor control and a real-time program is used to scan the data collected during each sweep to find the peak position and the peak height. Only the peak data from each scan are retained and this allows a complete chromatogram to be constructed. Each sweep of potential is done at a fresh mercury drop. In this way there is no memory effect at the electrode. The use of microprocessor-based instrumentation is essential to the peak-finding and peak-measuring procedure and it also controls the potential waveform which is applied to the cell.

The aim of this new approach in tensammetry is to improve the sensitivity

and the selectivity of the tensammetric detector. The position of the peak can provide useful diagnostic information [6] whereas the techniques that rely on changes in the baseline are inselective. Furthermore, background faradaic processes that contribute to the baseline current may not be constant during the entire chromatogram.

The nature of liquid chromatography which can be used in tensammetric detection is restricted by the properties of the solvent system required. Solvents commonly used in reverse-phase liquid chromatography are organic/aqueous mixtures. However, organic solvents are commonly adsorbed themselves and even produce tensammetric responses in some instances. Clearly, the organic solvent should not interfere with the tensammetric response of the compound of interest. To satisfy this restriction, the optimum solvent should have the minimum possible organic component consistent with adequate separation of compounds. The use of normal-phase and non-aqueous molecular exclusion chromatography is essentially precluded because of the extensive use of organic solvents.

Because a separation procedure is considered to be essential if tensammetry is to provide a reliable and general analytical technique, the use of reverse-phase liquid chromatography was investigated with electrochemical detection and microprocessor-based instrumentation. The examples chosen for this investigation are predominantly the separation and detection of oligomers of phenol ethoxylate and the detection of polyethylene glycol. Both these compounds also can be detected by u.v. spectrophotometry. This detection method was used to validate data based on electrochemical detection.

EXPERIMENTAL

Instrumentation

The microprocessor-based waveform generator-data acquisition system has been described in part elsewhere [14]. A static mercury drop electrode (SMDE; EG & G Princeton Applied Research Corporation) was used as the working electrode. The reference electrode was Ag/AgCl (satd. KCl) and the counter electrode was a platinum wire. For measurement in a conventional electrochemical cell, solutions were degassed with high-purity nitrogen prior to obtaining voltammograms; the conventional electrochemical cell was thermostated at (25.0 ± 0.2)°C. The electrochemical detector cell for use with liquid chromatography was a Model 310 electrochemical detector cell (EG & G Princeton Applied Research Corporation).

The liquid chromatographic system consisted of a Waters Associates Model 6000A pump and Model U6K universal injector. A Waters Associates radial compression module RCM-100 equipped with a Rad-Pak-CN(10 μm) reverse-phase column was used for achieving separation of the phenol ethoxylate oligomers. Chromatograms were obtained at ambient temperature of (20 ± 1)°C.

Chemicals

Polyethylene glycol with molecular weight 1400 (PEG-1400; Polymer Laboratory, Church Stretton, Shrewsbury, U.K.) and phenol ethoxylate (ICI Laboratories, Ascot Vale, Victoria, Australia) were used. Acetonitrile (Waters Associates Liquid Chromatography grade) was used as the organic solvent and all other chemicals were of analytical-reagent purity.

RESULTS AND DISCUSSION

The need for separation of species prior to tensammetric detection is readily demonstrated. Figure 1 shows that the tensammetric response of sodium alkylbenzene sulphonate (SAS) under conditions of normal-pulse tensammetry (see later) is completely eliminated by the presence of relatively low concentrations of PEG-1400. Obviously, if the SAS and PEG-1400 could be separated by liquid chromatography, both species could be quantified easily with tensammetric detection provided that an appropriate detector system could be developed.

A substantial number of waveforms for detection of the tensammetric response was examined in this work. As the tensammetric peak position is a function of concentration, it is not possible simply to employ, for example, an a.c. waveform (alternating potential superimposed on d.c. potential)

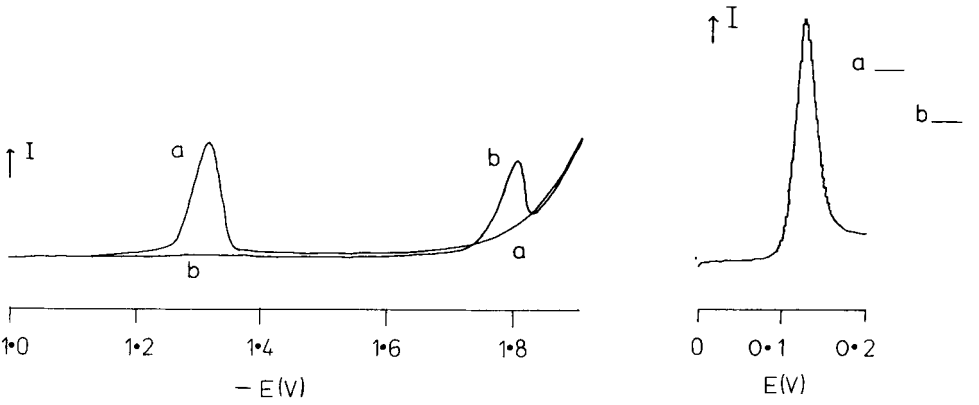

Fig. 1. Tensammetry of a mixture of sodium alkylbenzene sulphonate (SAS) and PEG-1400: (a) 100 μg ml^{-1} SAS in 0.05 M acetate buffer pH 5.9; (b) As for (a) plus 18 μg ml^{-1} PEG-1400. Normal-pulse tensammetry was used at a single mercury drop. Ramp step width 25.0 ms; pulse width 2.3 ms; T = (25 ± 0.2)°C.

Fig. 2. Normal-pulse a.c. tensammetry of 4 × 10^{-2} M cyclohexanol in 0.5 M Na_2SO_4 at a dropping mercury electrode. Drop time 1.0 s; pulse width 60 ms; a.c. frequency 530 Hz; a.c. amplitude 52 mV (p—p); alternating current measured at end of pulse; initial potential 0.0 V vs. Ag/AgCl; T = (25 ± 0.2)°C. (a) and (b) represent current levels recorded for a series of drops with continuously pulsed potential: (a) from 0.0 to 0.12 V; (b) from 0.0 to 0.14 V.

with a set d.c. potential and monitor the alternating current as the compound of interest elutes from the column if the optimum response is to be obtained. As an alternative, the possibility of pulsing the d.c. potential from a value where the compound of interest is adsorbed to a value past where it is desorbed whilst still maintaining the superimposed sinusoidal waveform was also examined. Figure 2 shows a complete current—voltage curve obtained by this approach (referred to as normal-pulse tensammetry) for cyclohexanol and indicates the current levels for particular pulse amplitudes. However, this approach was also not particularly successful under chromatographic conditions. The preferred detection method, and the one described in detail in this paper, requires that the complete current—voltage curve be recorded at many points in time as the compound elutes from the column and through the detector. With this approach the optimum response can be obtained even though the concentration of compound in the detection varies considerably because data obtained from peak currents (maximum values) are always available irrespective of the concentration.

In the past, tensammetry has been applied predominantly at a dropping mercury electrode with a slow scan of d.c. potential. This approach under most chromatographic conditions would be too slow to enable sufficient data to be obtained. However, a complete scan of potential at a hanging or stationary drop is possible in a very short period of time [14—17] and such systems can be utilized for tensammetric detection. The d.c. component of the potential may be scanned in a linear fashion (actually staircase with the digital equipment used in this work) versus time or in other formats and if required a sinusoidal potential, square-wave or other transient potential waveform may be superimposed on the (staircase) scan of potential. A microprocessor-based instrument is used to generate the required signals. All parameters may be varied under software control and the range of different square-wave and related formats available is correspondingly large. The choice of the most appropriate waveform and the subsequent optimization is very important; a computerized system provides the required flexibility in addition to enabling peak currents to be used.

Optimization of the waveform

Alternating current waveforms in tensammetry are well known [3]. Apart from sinusoidal and square waves, the two waveforms most extensively investigated in this work are similar to those used in differential pulse (d.p.) and normal pulse (n.p.) voltammetry (Fig. 3). All these techniques may be utilized at fast scan rates at the static mercury drop electrode and can be applied with the instrumentation used here. As the pulse techniques are generally useful, they are described in some detail with particular reference to their performance in tensammetric work. The d.p. technique involves taking the difference between the current measured before and after the pulse is applied and has been evaluated recently [5, 18]. The n.p. technique may be more useful because the potential between pulses is constant and, if

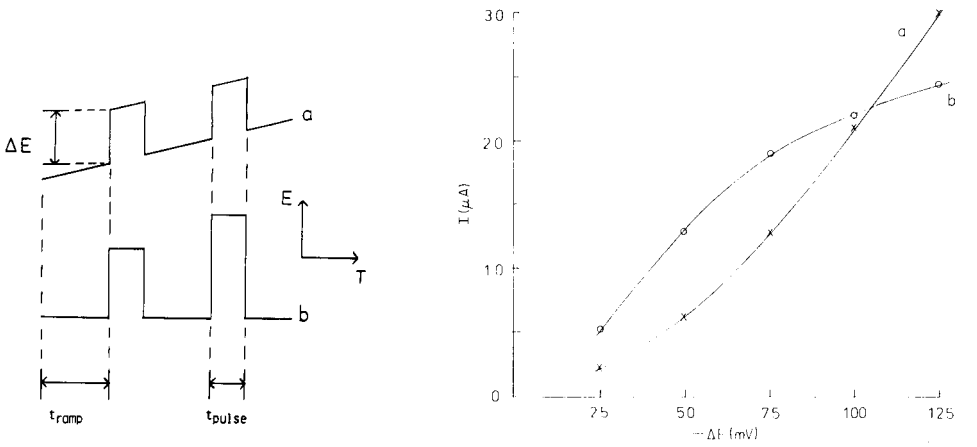

Fig. 3. The potential waveforms used in (a) differential pulse (d.p.) and (b) normal pulse (n.p.) tensammetry.

Fig. 4. Plots of d.p. current vs. ΔE: (a) phenol ethoxylate, 23.5 μg ml^{-1} in 0.1 M $NaNO_3$; (b) PEG-1400, 4.5 μg ml^{-1} in 0.1 M $NaNO_3$. Single mercury drop; ramp step width 20.0 ms, pulse width 0.7 ms, 25.0 ± 0.2°C.

the extent of adsorption is potential-dependent, the rest potential can be set for maximum adsorption. In our experience, this is the most generally useful waveform for tensammetry.

Table 1 shows a comparison of the tensammetric response with d.p. and n.p. techniques for low concentrations of two different surfactants. The n.p. technique is superior with respect to the current magnitude detected. The tensammetric peak for phenol ethoxylate is very broad. It has been noted [5] that the pulse height (ΔE) used in d.p. tensammetry is critical when a substance gives a broad response. A plot of peak height vs. ΔE for the d.p. tensammetry of the two surfactants is shown in Fig. 4. Changing ΔE has a significant effect on the response for phenol ethoxylate. By optimizing ΔE for both surfactants, the results for d.p. tensammetry approach those for n.p. tensammetry. However, with commercially available instrumentation, complete optimization may be restricted by the maximum value of ΔE. Use of n.p. tensammetry obviates the need to optimize ΔE and gives equal, if not superior, results.

After the mercury drop has been introduced into solution, there is a variable delay time which can be used prior to commencing the potential scan. Increasing this delay causes an increase in sensitivity for both the n.p. and d.p. techniques, because more time is allowed for accumulation of the surfactant on the surface of the electrode [5]. Increasing the delay time between pulses, t_{ramp}, has a similar effect. Results for PEG-1400 are presented in Table 2; the dependence of peak height on t_{ramp} is more pronounced for n.p. than d.p. tensammetry. For phenol ethoxylate, the d.p. tensammetric

TABLE 1

Comparison of tensammetric response[a] with normal-pulse and differential-pulse waveforms

Surfactant	Conc. (μg ml^{-1})	Peak current (μA)[b]	
		N.p.	D.p.[c]
PEG-1400	4.5	5.3	3.3
Phenol ethoxylate	18.8	18.7	2.0

[a]The hanging mercury drop electrode used had an area of 0.0098 cm^2. [b]Delay prior to pulse measurement 1 s; ramp step width 10.2 ms; pulse width 1.4 ms; initial potential —0.5 V vs. Ag/AgCl; resolution 4 mV; 0.1 M $NaNO_3$ supporting electrolyte; (25.0 ± 0.2)°C. [c]Pulse amplitude of —50 mV.

TABLE 2

Influence of ramp time on tensammetric peak height for PEG-1400 (4.5 μg ml^{-1} in 0.1 M $NaNO_3$) with n.p. and d.p. waveforms[a]

Total experiment time (s)	Ramp time (ms)	Peak current (μA)	
		N.p.	D.p.
5.04	10.2	5.3	3.3
8.47	20.0	8.9	4.8
18.83	49.6	19.7	9.3

[a]Other parameters as for Table 1.

peak height is independent of t_{ramp} for ΔE = —50 mV and only a small dependence is observed when ΔE is increased to —100 mV. The n.p. technique, however, shows a similar dependence of peak height on t_{ramp} for phenol ethoxylate as for PEG(1400).

The tensammetric current is capacitive in nature. Because it decays exponentially after pulse application, fast measurements are essential [5, 17]. This was confirmed for both d.p. and n.p. tensammetry. Pulse times of the order of 1 ms were used throughout this work. Unfortunately, most commercially available instruments do not offer such short pulse widths and so, without modification, could not be used with optimum results.

One of the major problems with both d.p. and n.p. tensammetry is their inability to discriminate effectively against background faradaic processes. This can be a severe problem because many tensammetric processes occur near the solvent limit. However, it is possible to improve n.p. tensammetry by making two current measurements during the pulse and using the difference response, because the faradaic current decays much more slowly than the capacitive current. Figure 5 shows schematically how this works. A similar approach has been used by Sokol and Evans [19] to minimize large background currents at solid electrodes. Excellent results are obtained by

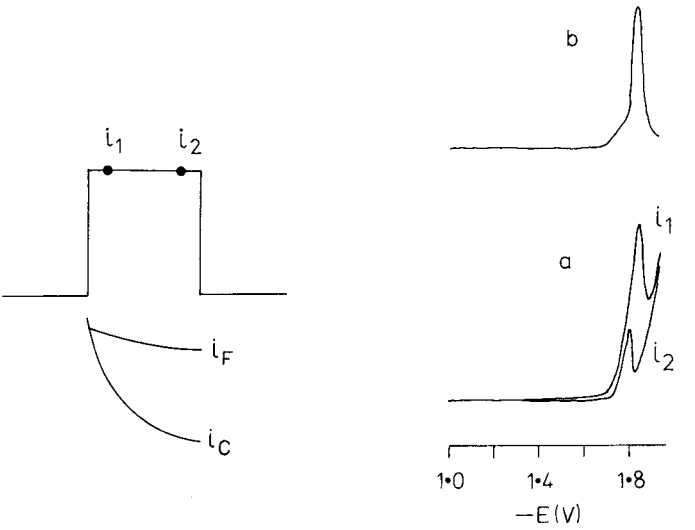

Fig. 5. Schematic diagram of n.p. technique with current difference approach; i_F and i_C are the faradaic and capacitive currents, respectively.

Fig. 6. Normal-pulse tensammetry with the current difference approach: (a) current components i_1 and i_2; (b) difference component $i_1 - i_2$ for 18 μg ml^{-1} PEG-1400 in 0.1 M $NaNO_3$. Ramp step width 40.0 ms; single mercury drop, 25.0 ± 0.2°C. Timing: 1.4 ms before i_1 and 1.4 ms between i_1 and i_2.

using this method (Fig. 6), though the difference current is slightly distorted because the peak positions of the two components are different. If required, symmetry can be improved by using software to make the individual peak positions coincide before the subtraction. Symmetry is also improved by increasing the time between current samples because the magnitude of the second component is further reduced; but this increased time will increase the overall pulse time and so decrease the sensitivity.

The relative simplicity and excellent performance of n.p. tensammetry relative to techniques with a superimposed pulse recommend the n.p. mode for evaluation of chromatography with electrochemical detection. Conclusions based on sinusoidal, square-wave or d.p. should be similar.

Combining tensammetry with liquid chromatography

The major problem encountered in combining liquid chromatography and tensammetry is that of finding solvent systems which are compatible with both chromatographic separation and electrochemical detection. Tensammetry is normally applied to aqueous solutions. Addition of typical organic modifiers such as methanol and acetonitrile have a deleterious effect on the tensammetry of various surfactants studied. Typically the tensammetric peak response becomes broadened and sensitivity is lost. In previous work with a.c. polarography, no organic modifier was used [12]. It is interesting

to note that in work in which lowering of the alternating voltage polarographic baseline was used, a relatively high component of organic modifier is tolerated [13]. Recently, the adsorption of tri(n)octylphosphine oxide (TOPO) on mercury electrodes was studied in methanol and methanol—water mixtures [20]. Results from this work indicate that the diminishment of the peak height after addition of methanol is much greater than the decrease in baseline depression. Thus in attempting to use the tensammetric peak height as an alternative to change in baseline, the restrictions on the nature of the solvent are more severe.

The separation of the oligomers of phenol ethoxylate was used as a model system. These compounds have u.v. chromophores and thus a u.v. detector can be used to provide a convenient comparison. The separation of oligomers having 2—12 ethylene oxide units can be readily achieved on a C_{18} reverse-phase column as shown by u.v. detection. However, separation can also be achieved with the C_8 and CN reverse-phase columns. Importantly, these columns require less organic modifier in the mobile phase to achieve adequate separation. In changing from the C_8 column to the CN column, the amount of methanol required can be reduced from 50% to 25%. Furthermore, it is possible to achieve an excellent separation on the CN column with only 10% acetonitrile. Thus the separation can be tailored to achieve the most favourable conditions for tensammetric detection. The tensammetry of phenol ethoxylate without separation of oligomers exhibits one broad peak at −1.66 V and would not be useful for analytical work.

Figure 7 indicates how the tensammetric detector functions in a practical situation. Initially, a range of potential is continually scanned on each mercury drop as the compound elutes from the column; the n.p. waveform is used and the potential is scanned from −1.0 to −1.9 V. Figure 7A shows the tensammetric response at four consecutive mercury drops for one of the oligomers as it passes through the detector. Figure 7B shows many scans of potential obtained from a large number of consecutive drops with the x-axis compressed; it is obvious that the changes in concentration can be followed as the oligomers elute. Figure 7B contains two major peaks and one minor peak. Between each scan of potential, a software-based peak search routine is employed to record the peak current during the previous scan. The result is shown in Fig. 7C; although the axes have been compressed, it is obvious enough that Fig. 7C is derived from the large set of data in Fig. 7B. In this example, each scan consists of 90 data points 10 mV apart. Because all scan data as well as peak data are stored in memory, it is only possible in this situation to obtain part of the total chromatogram. Obviously the resolution of the final chromatogram is restricted, because with the above conditions each scan required 5.5 s, i.e., a new stationary drop was grown every 5.5 s. The time required for one potential scan can be decreased by reducing (i) the range of the potential scan, (ii) the number of data points in each potential scan, at the expense of peak resolution, and (iii) the timing parameters such as t_{ramp}, at the expense of sensitivity. Thus the final choice

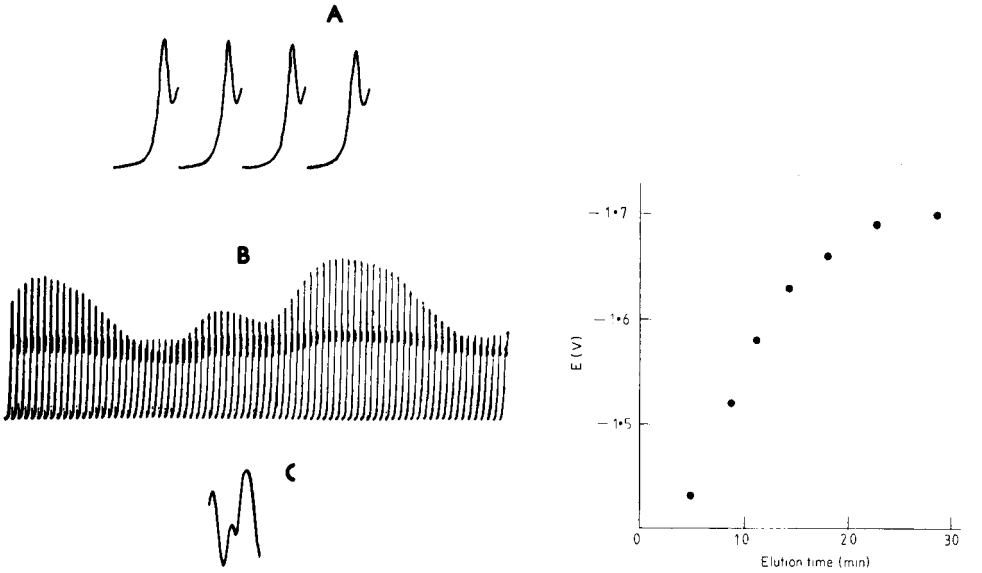

Fig. 7. Chromatogram of phenol ethoxylate (140 μg injected) with the tensammetric detector. Mobile phase is 10% acetonitrile in 0.05 M acetate buffer (pH 5.9) at 4.0 ml min^{-1} with a CN reverse-phase column; (20 ± 1)°C. (A) Normal pulse tensammetry scanning from −1.0 V to −1.9 V, ramp step width 49.6 ms, pulse width 1.4 ms, delay between scans 1.0 s; data collected during elution of seventh major peak of the chromatogram. (B) Many scans of potential under the same conditions as for A; data collected during elution of major peaks 7 and 8. (C) Plot of peak currents obtained using the peak-search approach during collection of data in B; note that the time axis was changed.

Fig. 8. Tensammetric peak potential vs. elution time. All conditions are as for Fig. 7 except that the initial potential was −0.6 V.

of parameters is important and depends on the particular characteristics of the problem being addressed.

The peak-search routine used in the present software relies on finding five points increasing followed by five points decreasing. The peak search is done after each scan (in real time) and no data smoothing is used. If a complete chromatogram is to be recorded, it is not possible to store all the data from each scan. After the peak has been found, the following scan is simply written-over the previous scan. Thus the bulk of the memory is free for the peak data.

Figure 8 shows a plot of the tensammetric peak potential versus the elution time for the oligomers of phenol ethoxylate. In general, the higher-molecular-weight species have the most negative peak potentials and give the most sensitive response because they adsorb more strongly on the electrode [13, 21]. In the present case, the first two oligomers are in fact not observed

with electrochemical detection at the concentration shown in Fig. 7. The ability to characterize the oligomer by peak position is a distinct advantage over using baseline depression and emphasises the enhanced ability to characterize the species giving zero tensammetric response. The strongest adsorbers on the reverse-phase column have the longest elution time. There is an interesting correlation between the strength of adsorption on the electrode and on the reverse-phase column, the compounds with the most sensitive response being most strongly retained on the column. Thus stronger eluting solvents would be required for a complete study of these compounds, but such mobile phases might be less compatible with the tensammetric detection.

Calibration curves of concentration versus peak current under chromatographic conditions are typical of those obtained in tensammetry, i.e., linear at lower concentrations and curved at higher concentrations. For the particular case of phenol ethoxylate the unresolved mixture of oligomers gave a detection limit of 1 mg l^{-1} with a linear response region of 1—10 mg l^{-1} when normal pulse voltammetry was used as the detection method.

Conclusions

Separation procedures are required to make tensammetry a viable analytical technique. A single drop (hanging drop) electrode is essential. Computer control is required for optimum performance and detection. The minimum possible organic component in the mobile phase is desirable. The peak detector is likely to be most reliable for detecting interferences and also for diagnostic purposes in correctly assigning the peak. Suppression of the baseline as previously used provides little information on which to characterize the electrode process.

The authors express their gratitude to the Australian Research Grants Committee for financial support of this project. Helpful discussions with Ian Russell, CSIRO, Belmont, Victoria, regarding the liquid chromatography substantially aided the development of the techniques described and are gratefully acknowledged.

REFERENCES

1 G. Gouy, Ann. Chim. Phys., 8 (1973) 793.
2 B. B. Damaskin, O. A. Petril and V. V. Batrakov, Adsorption of Organic Compounds on Electrodes, Plenum Press, New York, 1971.
3 B. B. Breyer and H. H. Bauer, Alternating Current Polarography and Tensammetry, Interscience, New York, 1963.
4 Z. Kozarac, B. Cosovic and M. Branica, J. Electroanal. Chem., 68 (1976) 75.
5 D. R. Canterford and R. J. Taylor, J. Electroanal. Chem., 98 (1979) 25.
6 P. Holmqvist, Anal. Chim. Acta, 90 (1977) 35.
7 P. Delahay and I. Trachtenberg, J. Am. Chem. Soc., 79 (1957) 2355.
8 B. Cosovic, N. Batina and Z. Kozarac, J. Electroanal. Chem., 113 (1980) 239.
9 M. C. Cheney, D. J. Curran and K. S. Fletcher, Anal. Chim. Acta, 126 (1981) 213.
10 N. A. Parris, in Journal of Chromatography Library, Vol. 5, Elsevier, Amsterdam, 1976.

11 K. Stulik and V. J. Pacakova, J. Electroanal. Chem., 129 (1981) 1.
12 J. Lankelma and H. Poppe, J. Chromatogr. Sci., 14 (1976) 310.
13 W. Kemula and W. Kutner, J. Chromatogr., 204 (1981) 131.
14 J. E. Anderson, A. M. Bond, I. D. Heritage, R. D. Jones and G. W. Wallace, Anal. Chem., 54 (1982) 1702.
15 D. Britz, Anal. Chim. Acta, 115 (1980) 327.
16 R. Samuelson, J. O'Dea and J. Osteryoung, Anal. Chem., 52 (1980) 2215.
17 R. A. Osteryoung and J. Osteryoung, Philos. Trans. R. Soc. London, Ser. A, 302 (1981) 315.
18 D. R. Canterford and R. W. Brown, J. Electroanal. Chem., 119 (1981) 355.
19 W. F. Sokol and D. H. Evans, Anal. Chem., 53 (1981) 578.
20 A. Anastopoulos, P. Karabinas and D. Jannakoudakis, J. Electroanal. Chem., 127 (1981) 219.
21 P. Holmqvist, Anal. Chim. Acta, 89 (1977) 315.

Analytica Chimica Acta, 152 (1983) 25—34
Elsevier Science Publishers B.V., Amsterdam — Printed in The Netherlands

A RETENTION PREDICTION SYSTEM IN REVERSED-PHASE HIGH-PERFORMANCE LIQUID CHROMATOGRAPHY BASED ON THE HYDROPHOBIC PARAMETER FOR ALKYLBENZENE DERIVATIVES

KIYOKATSU JINNO* and KAZUYA KAWASAKI
School of Materials Science, Toyohashi University of Technology, Toyohashi 440 (Japan)
(Received 25th February 1983)

SUMMARY

A retention prediction system for reversed-phase high-performance liquid chromatography (h.p.l.c.) is investigated. The system is based on the use of the hydrophobic parameter which is closely related to the retention mechanism in h.p.l.c. The system is evaluated by comparing the retention data between measured and predicted values. The predicted values were consistent with the measured values within a relative error of 15% for alkylbenzene derivatives.

In recent years, much effort has been directed to investigating the retention mechanism in reversed-phase high-performance liquid chromatography (h.p.l.c.) [1—6], and major advances in the understanding of the mechanism have been made. At present, it is generally considered that the retention of a solute in reversed-phase l.c. depends on the distribution equilibrium between the non-polar stationary phase and the polar mobile phase, i.e., the solvophobic theory. In liquid chromatography, the capacity factor, k', is used as a convenient description of retention index, because it shows a constant value under a particular set of conditions. The capacity factor of a solute is directly influenced by the distribution of the solute between stationary phase and mobile phase in reversed-phase l.c., i.e., there is some correlation between k' and the physicochemical parameters governing the equilibrium.

A somewhat similar approach has proved fruitful in investigating quantitative structure—activity relationships. The use of the partition coefficient (log P) of a compound in a 1-octanol/water system (Hansch's method), which is a good measure of its hydrophobicity, has become a standard method for such studies, which are concerned with establishing correlations between biological responses and physicochemical parameters describing molecular structure.

Various methods are in use for determinations of the partition coefficient in a 1-octanol/water system, such as the shake-flask method, counter-current distribution or continuous partitioning. However, the most promising method seems to be reversed-phase chromatography, either thin-layer chromato-

0003-2670/83/$03.00

graphy (t.l.c.) or high-performance liquid chromatography (h.p.l.c.). Several attempts have been made to use h.p.l.c. for such measurements [7—13]. Partitioning data from such h.p.l.c. studies are obtained from the observed linear relationship between log P and log k'.

It seems clear that the correlation between capacity factor and a hydrophobic parameter offers the possibility of predicting retention in reversed-phase l.c., if log P can be obtained from calculations. Much work has been published about this approach [14—16]. This paper is concerned with the construction of a preliminary retention prediction system for alkylbenzene derivatives based on the correlation between k' and log P.

EXPERIMENTAL

The liquid chromatographic system comprised a microfeeder MF-2 (Azuma Electric Co., Tokyo) as the pump and a Uvidec 100-III ultraviolet detector (Jasco, Tokyo) set at 208 nm.

The separations were done in two PTFE tubes (12.0 cm long, 0.5 mm i.d.) packed with Jasco FineSil C-8 (10 μm) and Jasco FineSil C-18 (5 μm), respectively, by the slurry technique. Mobile phases were mixtures of h.p.l.c.-grade acetonitrile (Tokyo Kasei, Tokyo) and purified water. All chemicals used were commercially available. Prior to measurements, the columns were washed with the relevant mobile phase until a constant value was obtained from the retention time of the eluate, t_R, according to $k' = (t_R - t_o)/t_o$. the columns as a solution in acetonitrile at room temperature, having a concentration of a few hundred mg l^{-1}.

The retention time of sodium nitrite in each mobile phase was taken as the unretained peak, t_o, [17] and the capacity factor, k', was evaluated from the retention time of the eluate, t_R, according to $k' = (t_R - t_o)/t_o$. All measurements were made in triplicate. The average reproducibility of each run was better than 1.0% relative.

DEVELOPMENT OF THE SYSTEM

In order to construct the retention prediction system, the following procedures were examined.

Measurement of capacity factors

Capacity factors of several standard compounds were measured for N mixtures of organic modifier and water, and the two kinds of packing. The results are shown in Table 1. The compounds selected as standard materials were representative alkylbenzenes. The capacity factors were measured with 40—70% (v/v) acetonitrile in the eluent for the C-8 packing and with 50—80% (v/v) acetonitrile for the C-18 packing; thus $N = 4$ in this instance. The difference in the solvent concentration ranges is due to the different efficiencies of the two columns.

TABLE 1

Hydrophobicity (log P) and logarithm of capacity factor (log k')[a]

Compound	log P[b]	log k'				
		% acetonitrile in mobile phase				
		80	70	60	50	40
For octylsilica (C-8) packing						
Benzene	2.13	—	—0.445	—0.286	—0.110	0.094
Toluene	2.69	—	—0.395	—0.222	—0.005	0.238
Ethylbenzene	3.22	—	—0.347	—0.157	0.091	0.378
n-Propylbenzene	3.75	—	—0.311	—0.084	0.198	0.378
n-Butylbenzene	4.28	—	—0.246	—0.003	0.310	0.705
n-Amylbenzene	4.81	—	—0.196	0.073	0.429	0.876
For octadecylsilica (C-18) packing						
Benzene		—[c]	—0.099	0.134	0.364	—
Toluene		—[c]	0.013	0.265	0.533	—
Ethylbenzene		—[c]	0.117	0.386	0.690	—
n-Propylbenzene		0.143	0.233	0.533	0.872	—
n-Butylbenzene		0.238	0.356	0.677	1.052	—
n-Amylbenzene		0.336	0.484	0.826	1.242	—

[a]Chromatographic conditions: 0.5 mm i.d., 12 cm column; acetonitrile—water mobile phase; flow rate 8 μl min^{-1}; column temperature 27°C; detection at 208 nm. [b]Hansch's method. [c]No resolved peaks were observed.

Calculation of log P values

The log P values were calculated by using Hansch's hydrophobic substituent coefficients, π. The calculation is expressed by the equation [14]:

$$\log P_{(S' x_1 x_2 \cdots x_n)} = \log P_{(S'H_n)} + \sum_{i=1}^{n} \pi(x_i) \quad (1)$$

where $S'H_n$ is a parent compound and $\pi(x_i)$ is the π constant of the x_i substituent. For example, log P of ethylbenzene can be determined from the equation

$$\log P(C_6H_5CH_2CH_3) = \log P(C_6H_6) + \pi(CH_2CH_3)$$
$$= \log P(C_6H_6) + \pi(CH_2) + \pi(CH_3) \quad (2)$$

The values used to calculate log P for the alkylbenzenes are shown in Table 2.

TABLE 2

Hydrophobic constants for alkylbenzene derivatives

log $P(C_6H_6)$	$\pi(CH_3)$	$\pi(CH_2)$	$\pi(CH)$	$\pi(C)$
2.13	0.56	0.53	0.40	0.30

Relation between log P and log k'

As there is a linear relationship between log k' and log P, as discussed above, the following N equations were obtained by the least-squares fitting for N experimental conditions.

$$\begin{aligned} x = x_1 \quad & \log k' = a_1 \log P + b_1 \\ x = x_2 \quad & \log k' = a_2 \log P + b_2 \\ \vdots \quad & \vdots \\ x = x_N \quad & \log k' = a_N \log P + b_N \end{aligned} \tag{3}$$

where x is the volume fraction of organic modifier in the mobile phase, and a and b are the slope and the intercept of each equation, respectively. The values for the slope and the intercept of each equation are listed in Table 3 with their correlation coefficients. Extremely good correlations were obtained for all solvent compositions.

If a and b can be expressed as functions of x (i.e., if x—a and x—b were correlated), the following two equations can be obtained by multiple regression analyses:

$$a = f_1(x) = \sum_{i=0}^{n} c_i x^i \tag{4}$$

$$b = f_2(x) = \sum_{i=0}^{n} d_i x^i \tag{5}$$

where n is a number less than N and c and d are constants. As can be seen in Table 3, a and b decrease as x increases. Therefore, the multiple regression analyses were done for the sets of x—a and x—b relations. A multi-order regression gave the most satisfactory correlation coefficient. The

TABLE 3

Results of linear regression analysis for the correlation between log P and log k'

Acetonitrile (%)	C-8 column			C-18 column		
	Slope (a)	Intercept (b)	r[a]	Slope (a)	Intercept (b)	r[a]
80				0.182	—0.540	1.000
70	0.092	—0.645	0.998	0.217	—0.571	0.999
60	0.135	—0.583	0.999	0.259	—0.431	0.999
50	0.200	—0.545	0.999	0.328	—0.348	0.999
40	0.293	—0.546	0.999			

[a]Correlation coefficient.

following equations were obtained:

$$a = f_1(x) = 1.246\,x^2 - 2.037\,x + 0.908 \quad (r = 1.000) \tag{6}$$

$$b = f_2(x) = -0.955\,x^3 + 0.553\,x - 0.705 \quad (r = 0.998) \tag{7}$$

for the C-8 packing

$$a = f_1(x) = 0.429\,x^3 - 1.031\,x + 0.788 \quad (r = 0.999) \tag{8}$$

$$b = f_2(x) = 1.502\,x^3 - 2.652\,x + 0.802 \quad (r = 0.961) \tag{9}$$

for the C-18 packing. From Eqns. (3—5),

$$\log k' = f_1(x) \log P + f_2(x) \tag{10}$$

This equation means that if x, the concentration of organic modifier in the mobile phase, and log P, a characteristic of a compound, are known, the logarithm of the capacity factor, log k', can be determined for given chromatographic conditions. This consideration is the basic concept of the retention prediction system (RPS) investigated here for reversed-phase liquid chromatography.

In this instance, the equations obtained for the C-8 and C-18 packings were, respectively,

$$\log k' = (1.246\,x^2 - 2.037\,x + 0.908) \log P + (-0.995\,x^3 + 0.533\,x - 0.705) \tag{11}$$

$$\log k' = (0.429\,x^3 - 1.031\,x + 0.788) \log P + (1.502\,x^3 - 2.652\,x + 0.802) \tag{12}$$

Given these equations, it is possible to construct the RPS for alkylbenzene derivatives with C-8 and C-18 packings and acetonitrile/water mixtures as the mobile phase.

The flow diagram of the scheme is shown in Fig. 1. The system was constructed on a MELCOM 800 computer. In this program for RPS, only simple numerical calculations are included. The essential part of the program is the calculation of log P by Hansch's method. The flow chart of this calculation is shown in Fig. 2. In this program, each character which is input as the compound name or chemical formula of a given solute is compared, one by one, with the characters in the data base and a decision is made whether or not

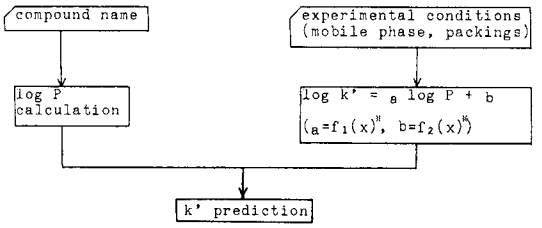

Fig. 1. The retention prediction system (RPS) in reversed-phase liquid chromatography based on log P as the parameter. x is the volume fraction of organic modifier.

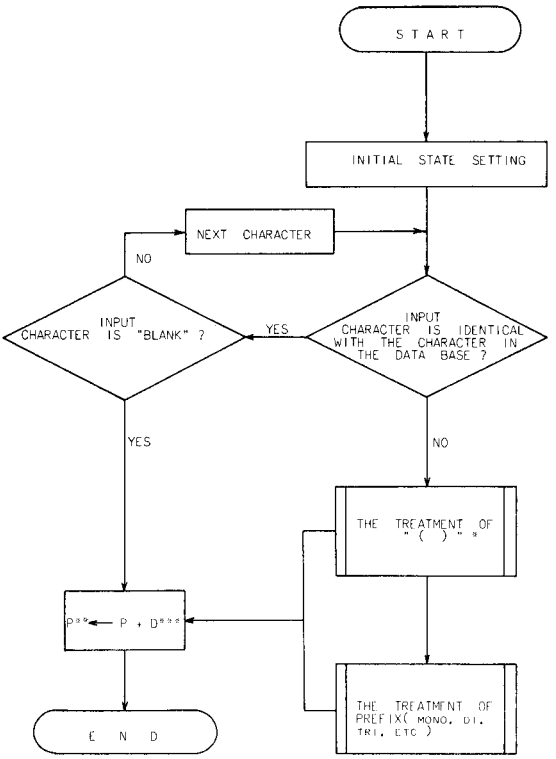

Fig. 2. The flow chart of "log P" calculation. *For example, $C_6H_5CH(CH_3)_2$, $C_6H_4(CH_2CH_3)_2$. **Calculated "log P". ***π-value corresponding to the character in the data base.

the input character is identical with the character in the data base. This procedure is repeated until a blank character, " ", appears.

With the interactive style, the following data should be input: (i) the compound name or the chemical formula of the given solute; (ii) the type of packings (stationary phase selection); (iii) the kind of eluent (mobile phase selection); (iv) the volume fraction of organic modifier in the eluent. The main feature of this RPS is that the possibility of retention of any solute can be assessed by the use of chemical formula and/or compound name of the solute. Table 4 shows examples of how the RPS works.

EVALUATION OF THE RETENTION PREDICTION SYSTEM

With the program for RPS, the following chromatographic systems were assessed. System I consisted of octylsilica packing as the stationary phase and acetonitrile—water mixture as the mobile phase. It was evaluated by comparing predicted and observed k' values as shown in Table 5. The conditions for the k' measurements by h.p.l.c. are shown in the footnotes in Table 5. Most of the capacity factors for the compounds predicted are in good agreement with the measured values.

TABLE 4

Examples of using the RPS with (i) compound name and (ii) chemical formula (sec-amylbenzene)[a]

(i)
SAMPLE?
?1,2-DIETHYLBENZENE

STATIONARY PHASE?
1. FINESIL C18
2. FINESIL C8
3. FINESIL C2
?1

MOBILE PHASE?
1. CH3CN/H2O
2. CH3OH/H2O
?1

CONCENTRATION OF ORGANIC MODIFIER? (F6.2)
?75.00

EXPERIMENTAL CONDITIONS;
STATIONARY PHASE/FINESIL C18
MOBILE PHASE/CH3CN: H2O = 75.00: 25.00
SAMPLE/1,2-DIETHYLBENZENE

LOG P: 4.31
PREDICTED CAPACITY FACTOR: 1.951

(ii)
SAMPLE?
?C6H5CH(C2H5)2
STATIONARY PHASE?
1. FINESIL C18
2. FINESIL C8
3. FINESIL C2
?2

MOBILE PHASE?
1. CH3CN/H2O
2. CH3OH/H2O
?1

CONCENTRATION OF ORGANIC MODIFIER? (F6.2)
?45.00

EXPERIMENTAL CONDITIONS;
STATIONARY PHASE/FINESIL C8
MOBILE PHASE/CH3CN: H2O = 45.00: 55.00
SAMPLE/C6H5CH(C2H5)2

LOG P: 4.71
PREDICTED CAPACITY FACTOR: 3.987

[a]Underlined items are the input data needed for accessing the RPS.

TABLE 5

Predicted and observed k' values of some alkylbenzenes[a]

Benzene derivative	log P	k' values		
		Observed	Predicted	$\Delta k'(\%)$[b]
Isopropyl	3.65	2.14	2.20	2.7
1-Ethyl-2-methyl	3.78	2.11	2.37	11.0
1-Ethyl-3-methyl	3.78	2.24	2.37	5.5
1-Ethyl-4-methyl	3.78	2.26	2.37	4.6
1,2,3-Trimethyl	3.81	2.10	2.41	12.9
1,2,4-Trimethyl	3.81	2.19	2.41	9.1
1,3,5-Trimethyl	3.81	2.22	2.41	7.9
Isobutyl	4.18	3.15	2.96	6.4
sec-Butyl	4.18	2.86	2.96	3.4
tert-Butyl	4.11	2.63	2.85	7.7
1-Isopropyl-4-methyl	4.21	3.03	3.01	0.7
1,2-Diethyl	4.31	2.92	3.19	8.5
1,3-Diethyl	4.31	2.89	3.19	9.4
1,4-Diethyl	4.31	2.91	3.19	8.8
1,2,3,4-Tetramethyl	4.37	2.63	3.30	20.3
1,2,3,5-Tetramethyl	4.37	2.64	3.30	20.0
1,2,4,5-Tetramethyl	4.37	2.77	3.30	16.1
sec-Amyl	4.71	3.87	3.99	3.0
tert-Amyl	4.64	3.45	3.83	9.9
n-Hexyl	5.34	5.92	5.67	4.4

[a]Chromatographic conditions: 0.5 mm i.d. × 12 cm octylsilica (10 μm) column; mobile phase acetonitrile/water 45: 55; flow rate 8 μl min^{-1}; column temperature 27°C; detection at 208 nm. [b]$\Delta k'(\%) = |k'_{\text{pred.}} - k'_{\text{obs.}}| \times 100/k'_{\text{pred.}}$

The capacity factors of structural isomers predicted by the RPS are the same, although the observed retentions are different. This can be attributed to the use of calculated hydrophobic parameters, log P, in the system; as the calculated log P values for structural isomers are the same, the predicted k' values will be the same. Accordingly, other parameters giving structural information must be introduced to improve the predicted values.

Table 6 shows a comparison of the observed and predicted k' values obtained for the octadecylsilica column packing and an acetonitrile/water mixture. In this table, $^1\chi^v$, V_w and A_w are the molecular connectivity index, van der Waals volume and surface area, respectively, and are used as parameters to construct the RPS. Log P, as can be seen in Table 6, is more promising than any other parameter in the system investigated. Therefore, the use of log P as the parameter for constructing the system for alkylbenzene derivatives with C-18 packing seems an appropriate compromise, though the system could be constructed with a combination of log P and any related parameter such as molecular connectivity index [18]. This will be discussed at a later date.

In conclusion, it is possible to predict retentions for alkylbenzene derivatives in reversed-phase h.p.l.c. within ±15% relative, by using the RPS

TABLE 6

Predicted and observed k' values of some alkylbenzenes[a]

Benzene derivative	Observed k'	Predicted k'			
		log P	$^{1}\chi^{v}$	V_w	A_w
Isopropyl	1.48	1.45(2.1)	1.43(3.5)	1.49(0.7)	1.52(2.6)
1-Ethyl-2-methyl	1.67	1.55(7.7)	1.46(14.4)	1.52(9.9)	1.55(7.7)
1-Ethyl-3-methyl	1.51	1.55(2.6)	1.45(4.1)	1.52(0.7)	1.55(2.6)
1-Ethyl-4-methyl	1.56	1.55(0.6)	1.45(7.6)	1.52(2.6)	1.55(0.6)
1,2,3-Trimethyl	1.63	1.56(0.6)	1.36(19.9)	1.55(5.2)	1.57(3.8)
1,2,4-Trimethyl	1.47	1.56(5.2)	1.36(8.1)	1.55(5.2)	1.57(6.4)
1,3,5-Trimethyl	1.64	1.56(5.1)	1.35(21.5)	1.55(5.8)	1.57(4.5)
Isobutyl	2.06	1.85(11.4)	1.80(14.4)	1.88(9.6)	1.93(6.7)
sec-Butyl	1.84	1.85(0.5)	1.86(1.1)	1.88(2.1)	1.93(4.7)
tert-Butyl	1.80	1.79(0.6)	1.66(8.4)	1.88(4.3)	2.00(10.0)
1-Isopropyl-4-methyl	2.11	1.87(12.8)	1.59(32.7)	1.92(9.9)	1.96(7.7)
1,2-Diethyl	1.97	1.95(1.0)	1.91(3.1)	1.92(2.6)	1.97(0.0)
1,3-Diethyl	1.78	1.95(8.7)	1.90(6.3)	1.92(7.3)	1.97(9.6)
1,4-Diethyl	1.90	1.95(2.6)	1.90(0.0)	1.92(1.0)	1.97(3.6)
1,2,3,4-Tetramethyl	1.97	2.03(3.0)	1.66(18.7)	2.00(1.5)	2.03(3.0)
1,2,3,5-Tetramethyl	1.94	2.03(4.4)	1.66(16.9)	2.00(3.0)	2.03(4.4)
1,2,4,5-Tetramethyl	1.82	2.03(10.3)	1.66(9.6)	2.00(9.0)	2.03(10.3)
sec-Amyl	2.34	2.34(0.0)	2.36(0.8)	2.38(1.7)	2.45(4.5)
tert-Amyl	2.25	2.27(0.9)	2.17(3.7)	2.38(5.5)	2.54(11.4)
n-Hexyl	3.41	3.12(9.3)	3.11(9.6)	3.01(13.3)	3.12(9.3)

[a]Chromatographic conditions as for Table 5, except for use of octadecylsilica (5 μm), and 75:25 acetonitrile/water. The values in parentheses indicate $\Delta k'$(%) as in Table 5.

constructed as outlined above. If such procedures are done with various packings and organic modifiers for the compounds as standard substances, retentions of any substances which are members of a homologous series of model compounds, can be predicted at any concentration of eluent. However, it must be emphasized that this system is only for alkylbenzene derivatives at present because the model compounds used to construct the system are representative of this class. To construct a system for other series, it is necessary to select suitable model compounds and to find the best parameters to express their retention behaviour. Retentions for solutes having more electron-withdrawing or -releasing groups or more bulky groups may not be predicted correctly by a system based on log P. Retention prediction systems are needed not only for isocratic elution but also for gradient elution, as the latter is more generally useful in practical h.p.l.c. separations. These approaches are being studied.

REFERENCES

1 E. J. Kikta, Jr. and E. Gruschka, Anal. Chem., 48 (1976) 1098.
2 C. Horvath, W. Melander and I. Molnar, J. Chromatogr., 125 (1976) 129.

3 C. Horvath and W. Melander, Am. Lab., 10 (1978) 17.
4 W. Melander and J. Stoveken, J. Chromatogr., 199 (1980) 35.
5 C. R. Yonker, T. A. Zwier and M. F. Burke, J. Chromatogr., 241 (1982) 257.
6 C. R. Yonker, T. A. Zwier and M. F. Burke, J. Chromatogr., 241 (1982) 269.
7 K. Miyake and H. Terada, J. Chromatogr., 157 (1978) 386.
8 K. Miyake and H. Terada, J. Chromatogr., 240 (1982) 9.
9 B. McDuffie, Chemosphere, 10 (1981) 73.
10 G. L. Biagi, O. Gandolfi, M. C. Guerra, A. M. Barbaro and G. Cantelli-Forti, J. Med. Chem., 18 (1975) 868.
11 G. L. Biagi, A. M. Barbaro, O. Gandolfi, M. C. Guerra and G. Cantelli-Forti, J. Med. Chem., 18 (1975) 873.
12 K. Jinno, Chromatographia, 15 (1982) 667.
13 K. Jinno, Anal. Lett., 15 (A19) (1982) 1533.
14 C. Hansch and A. Leo, Substituent Constants for Correlation Analysis in Chemistry and Biology, Wiley, New York, 1979.
15 R. F. Rekker, The Hydrophobic Fragmental Constant, Elsevier, Amsterdam, 1977.
16 M. d'Amboise and T. Hanai, J. Liq. Chromatogr., 5 (1982) 229.
17 K. Jinno, M. Ozaki and T. Sato, Chromatographia, in press.
18 K. Jinno and K. Kawasaki, Chromatographia, in press.

Analytica Chimica Acta, 152 (1983) 35—44
Elsevier Science Publishers B.V., Amsterdam — Printed in The Netherlands

RESONANT FREQUENCY MEASUREMENTS AS AN ALTERNATIVE TO PHASE-SELECTIVE A.C. POLAROGRAPHY IN TENSAMMETRY AND PSEUDOCAPACITANCE DETERMINATIONS

M. BOS* and W. H. M. BRUGGINK

Department of Chemical Technology, Twente University of Technology, Enschede (The Netherlands)

(Received 30th December 1982)

SUMMARY

A new method is proposed for the determination of the double-layer capacitance and pseudocapacitance of electrochemical cells. The method is based on the measurement of the resonant frequency of the circuit consisting of the electrochemical cell connected in series with a standard inductor. The performance of the method is demonstrated with double-layer capacitance measurements at the dropping mercury electrode in 1 M KCl and butanol-1/1 M KCl mixtures and with the determination of heterogeneous charge-transfer rate constants ranging from 10^{-2} to 10^{-5} m s^{-1}.

Several papers have appeared that describe the use of on-line digital computers in methods for the determination of the double-layer capacitance [1—5]. In this field, three lines of approach can be distinguished: (1) adaptation of phase-selective measurements with lock-in amplifiers or network analyzers to computer control as described by Bongenaar et al. [3]; (2) the use of the computer to generate a non-sinusoidal cell excitation with a repeating sequence and to produce either Fourier or Hadamard transforms to obtain the cell impedance as first suggested by Creason and Smith [6] and improved by Seelig and de Levie [1]; (3) the use of computer-generated potential steps as cell excitation and processing of the resulting cell current/time profile as proposed by Bos [4] and Britz [5].

A comparison of the three categories shows that the first requires expensive extra hardware such as programmable function generators and network analyzers or lock-in amplifiers. The second category relies on a stringent time relationship between the excitation signal and the sampling of the cell response and requires special computer hardware. Both the first and the second category require analog circuitry for the potentiostat, iR compensation and i-to-E conversion functions. The accuracy of the results will depend on the quality of this circuitry with regard to flat frequency response, linearity, stability and the magnitude of the phase shift introduced by the iR compensation circuitry. In the presence of electroactive compounds, the measurements in the first and second categories can provide information on the double-layer capacitance as well as on the kinetics of the electrode reactions.

0003-2670/83/$03.00

The experimental set-up for the third category is rather simple; it consists of the electrochemical cell and the computer. Accuracy in the current measurements is the only important requirement. A drawback of the method presented earlier [4] is that in the presence of electroactive compounds broad pseudocapacitance peaks occur that prohibit tensammetric determinations in a certain potential range around their respective standard potentials.

The method proposed now also utilizes a simple experimental set-up. The electrochemical cell is connected in series with an inductor to form a resonant circuit, the resonant frequency of which is determined by measuring the frequency of the dampened sine wave that results if a single short pulse is applied to the system. The amplitude information in the cell response signal is not utilized, so demands with regard to the instrumentation are minimal. The accuracy of the results will be determined by the absolute value and the stability of the fixed rate with which the cell response is sampled by the computer. A simple crystal-controlled timer, such as can be found on most microprocessor boards, amply provides the required accuracy in timing for this purpose. The information produced by the new method is equivalent to that obtained from phase-selective a.c. polarography in which the cell current is measured exactly 90° out of phase with the applied a.c. voltage and can be used in the same way, i.e., in the study of the electrical double layer at the dropping mercury electrode and solid electrodes, adsorption phenomena on electrodes and in the study of the kinetics of electrode reactions.

THEORY

The equivalent circuit for the combination of the electrochemical cell and an inductor is given in Fig. 1. Its resonant frequency is given by

$$f_{\text{reson.}} = 1/[2\pi(LC_{\text{eq}})^{1/2}] \quad (1)$$

With this equation the equivalent capacitance of the circuit, C_{eq}, can easily be determined from the resonant frequency if a known inductor L is used. In the absence of electroactive components, C_{eq} equals the capacitance of the electrical double layer, C_{edl}; thus for adsorption studies in nonelectroactive electrolytes the method directly produces the quantity of interest. In the presence of an electroactive component, the electrochemical cell can be represented by the circuit given in Fig. 2, the lower branch of which constitutes the faradaic impedance. The latter consists of a frequency-independent activation resistance, Θ, and a frequency-dependent Warburg impedance, W. According to Sluyters-Rehbach [7], the following equations can be derived for the terms in the faradaic impedance

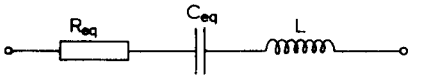

Fig. 1. Equivalent circuit of electrochemical cell/inductor combination.

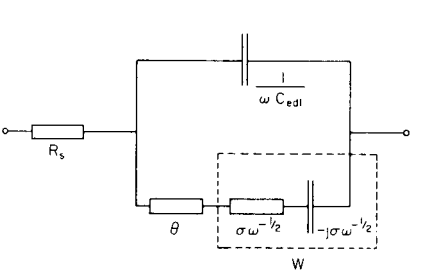

Fig. 2. Equivalent circuit of electrochemical cell with electroactive component.

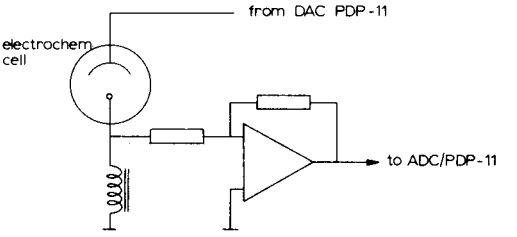

Fig. 3. Electrochemical cell circuitry.

$$\Theta = RT/[n^2F^2k_{sh}(C^0_{ox})^{\alpha}(C^0_{Red})^{1-\alpha}] \quad (2)$$

$$\sigma = (RT/n^2F^2 2^{1/2})\ \{[1/C^0_{ox}(D_{ox})^{1/2}] + [1/C^0_{Red}(D_{Red})^{1/2}]\} \quad (3)$$

$$C^0_{ox} = (C^*_{ox} + d^{1/2}C^*_{Red})/(1 + d^{1/2}e^{-\phi}) \quad C^0_{Red} = (C^*_{ox} + d^{1/2}C^*_{Red})/(e^{\phi} + d^{1/2}) \quad (4)$$

$$\phi = n\,F(E - E_0)/RT \quad d = D_{Red}/D_{ox} \quad (5)$$

(Symbols are defined in Table 1.)

For potentials far from the standard potential of the electroactive component, the faradaic impedance is infinite, so that in this case the system again measures directly the capacitance of the electrical double layer. In the region of the standard potential of electroactive components, the equivalent capacitance C_{eq} measured by the system comprises not only the double-layer capacitance C_{edl} but also depends on the value of the terms of the faradaic impedance. From a vector diagram of the circuit presented in Fig. 2, it can be found that

$$C_{eq} = \frac{\omega^2 C^2_{edl}\Theta^2 + 2\omega^{3/2}C^2_{edl}\sigma\Theta + 2\omega C^2_{edl}\sigma^2 + 2\omega^{1/2}C_{edl}\sigma + 1}{\omega^2 C_{edl}\Theta^2 + 2\omega^{3/2}C_{edl}\sigma\Theta + 2\omega C_{edl}\sigma^2 + \omega^{1/2}\sigma} \quad (6)$$

This equation can be used in several ways. The actual choice will depend on the goal of the measurements. Thus, the double-layer capacitance at a given potential in the presence of an electroactive compound can be determined from a single measurement, if Θ and σ are known. These latter values can be calculated from Eqns. (2) and (3) and the appropriate relationship for C^0_{ox} and C^0_{Red} as a function of electrode potential, as expressed by Eqns. (4) and (5). In this case the values of E_0, α, k_{sh}, D_{ox}, D_{Red}, C^*_{ox} and C^*_{Red} must be available. If these values cannot be readily obtained, Eqn. (6) can be used in a three-parameter (C_{edl}, σ and Θ) curve-fitting procedure using a number of C_{eq}, ω data pairs measured at different electrode areas, or at different concentrations using normalized parameters Θc and σc. This enables C_{edl} to be determined in the potential range of the a.c. wave of electroactive components [7, 8]. Should the method be used for the study of rate constants the Θ value found in the three-parameter curve-fitting procedure can be used together with Eqns. (2), (4) and (5) to give k_{sh}.

TABLE 1

List of symbols

a	interaction constant in Frumkin isotherm
B	adsorption coefficient in Frumkin isotherm
c	concentration of adsorbate
C^0_{ox}, C^0_{Red}	concentrations of oxidized and reduced form of electroactive component at electrode surface
C^*_{ox}, C^*_{Red}	concentrations of oxidized and reduced form of electroactive component in bulk of the solution
C_{eq}	capacitance of equivalent cell circuit
C_{edl}	double-layer capacitance
D_{ox}, D_{Red}	diffusion coefficients of oxidized and reduced form of electroactive component
E	d.c. potential of DME
E^0	standard potential of electroactive component
F	Faraday constant
f_{reson}	resonant frequency of electrochemical cell/inductor circuit
k_{sh}	standard heterogeneous reaction rate constant
L	inductance
n	number of electrons transferred in electrode reaction of electroactive component
R	gas constant
T	absolute temperature
α	transfer coefficient
σ	Warburg coefficient
Θ	activation polarization resistance [Eqns. (2) and (6)]
θ	degree of electrode coverage (Frumkin Equation)
ω	angular frequency

EXPERIMENTAL

Chemicals and equipment

The following compounds were used as received: potassium chloride, sodium sulphate, iron(III) ammoniumsulphate, oxalic acid, potassium oxalate, potassium sulphate, butanol-1 (all from Merck, quality "Zur Analyse"), cadmium chloride (AnalaR, analytical reagent), cadmium sulphate (Merck, Suprapur), nitrogen (Hoekloos, very pure) and mercury (Drijfhout, polarographic grade). All solutions were made with deionized water filtered through Millipore Q2 filters.

All measurements were done in solutions that had been stripped of oxygen by bubbling with nitrogen for 20 min.

The electrochemical cell consisted of a cylindrical vessel (57.1 mm tall, 34.3 mm diameter). A mercury pool at the bottom of this vessel was used as the counter electrode. The characteristics of the dropping mercury electrode (DME) were h = 40 cm, t = 3.6 s, m = 2.39 mg s^{-1} (1 M KCl, open circuit). A Radiometer drop-life timer, type DLT 1, was used for computer-controlled drop knock off. A schematic diagram of the connections of the electro-

chemical cell to the PDP-11/10 (Digital Equipment Corp.) on-line computer is presented in Fig. 3. The operational amplifier was from Keithley, model 301. The digital-to-analog converter (DAC) and analog-to-digital converter (ADC) were standard Digital Equipment Corp. interfaces contained in the laboratory peripheral system with 12-bit accuracy. The ADC was operated in the direct memory access (DMA) mode under control of the programmable real-time clock (LPSKW) of the computer. The inductor in series with the cell was a 88 mH toroid (Miller).

Computer program

A flow chart of the computer program that controls the experiments is given in Fig. 4. The program starts with an initial dialogue in which the operator can set the required experimental parameters for the d.c. scan, the drop time and the number of measurements at the same d.c. potential to be taken and averaged to improve the signal-to-noise ratio. Then the program applies the initial voltage of the wanted d.c. scan range to the cell and knocks off the first drop. If the mercury drop of the working electrode has reached its predetermined lifetime, the program continues with starting the ADC burst of 4096 data points. Directly after the start of this burst, a 5-μs 600-mV pulse is applied to the cell voltage. The corresponding amplitude of the a.c. voltage generated across the double layer depends on its impedance but is generally much less than 20 mV. The measurement cycle can be repeated a number of times at the same d.c. scan potential at successive mercury drops to improve the signal-to-noise ratio. If the wanted number of bursts has been acquired, the program calculates the Fourier transform of the 4096-point data buffer. This is followed by calculation of the power spectrum of the Fourier transform. The resonant frequency of the cell circuit is then calculated from the position of the maximum in this power spectrum. Finally, the equivalent capacitance of the circuit is calculated by using Eqn. (1), and printed on teletype together with the value of the resonant frequency. The capacitance value is also displayed on a stripchart recorder connected to a DAC. The whole process is repeated until the end of the scan range is reached.

RESULTS AND CONCLUSIONS

The accuracy of the system was checked against a standard capacitance decade bank. From the results given in Table 2, it can be seen that the mean error is ±2.3%, whereas the range that is covered with the fixed 88-mH inductor in the circuit extends from 0.05 μF to 2 μF. The performance of the system for samples not containing any electroactive compounds was tested by measurement of the differential capacity versus potential curve for 1 M potassium chloride (Table 3) and in the determination of the Frumkin adsorption isotherm constants for butanol-1 in this electrolyte (Fig. 5). As can be seen, the measured capacitance values for 1 M potassium chloride

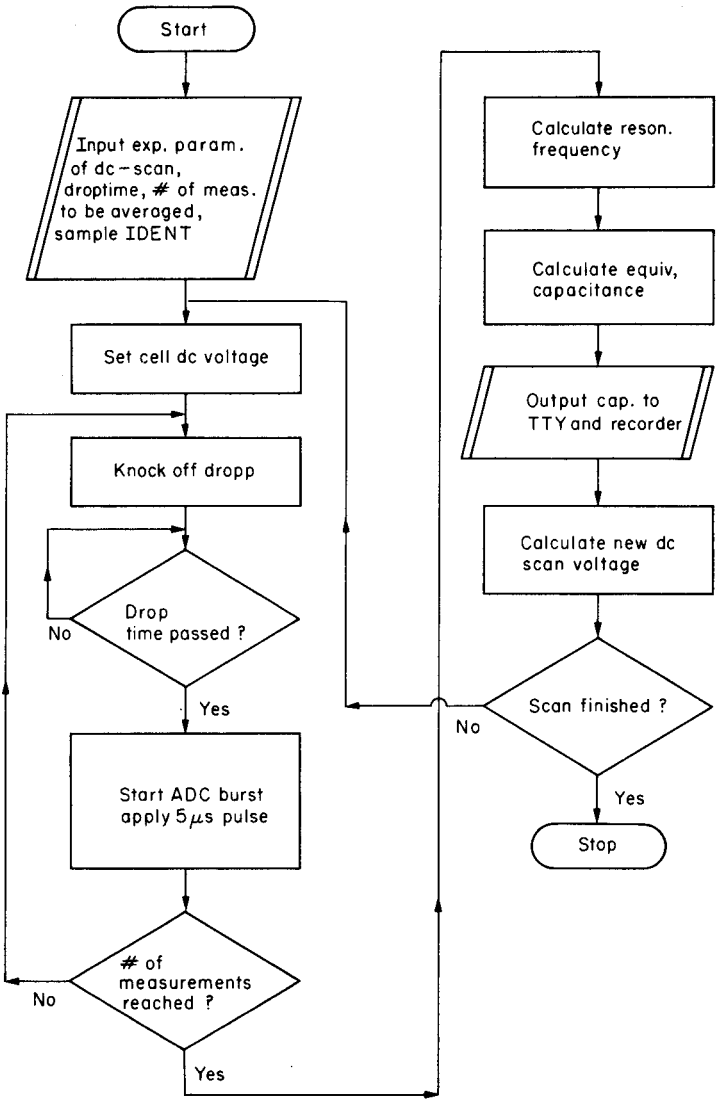

Fig. 4. Flow chart of computer program for resonant frequency measurements.

agree to within ±5% with the literature data [9]. From the adsorption isotherm in Fig. 5 the constants a and B for butanol-1 in 1 M KCl were calculated from the Frumkin equation $Bc = [\theta/(1-\theta)] \exp(-2a\theta)$, to be 1.29 and 10.7, respectively. Boravaya and Damaskin [10] reported values of 1.28 and 8.6.

The accuracy of the system at constant d.c. voltage across the cell was tested by using various drop times for a 0.5 M sodium sulphate solution. The results are given in Table 4.

TABLE 2

Performance of system with standard capacitances

Capacity used (μF)	Capacity found (μF)	Error (%)	Capacity used (μF)	Capacity found (μF)	Error (%)
0.050	0.048	−4.0	0.600	0.600	0.0
0.100	0.098	−2.0	0.700	0.678	−3.1
0.200	0.199	−0.5	0.800	0.771	−3.6
0.300	0.301	+0.3	0.900	0.885	−1.6
0.400	0.393	−1.8	1.000	0.952	−4.8
0.500	0.480	−4.0	2.000	1.923	−3.9

The use of the system to acquire data on electrode kinetics was tested for a number of electrochemical systems with heterogeneous charge-transfer rate constants ranging from 4×10^{-2} to 4×10^{-5} m s^{-1}. The experimental data are given in Table 5. The measurements were made at the d.c. potential of the pseudocapacitance peaks. For the fastest reaction (i.e., cadmium in 1 M KCl) the three-parameter curve-fitting procedure with the use of Eqn. (6) did not work because of the small magnitude of the Θ terms in comparison with the error in the capacitance measurements. If the Θ terms are neglected and the Warburg constant σ is calculated with the value 0.265 F m^{-2} for the double-layer capacitance for the different concentrations of cadmium, it shows a good inverse proportionality with the concentration ($\sigma \times$ conc. = $8.4 \times 10^{-3} \pm 0.5 \times 10^{-3}$ $\Omega m^{-1} s^{-1/2}$ mol).

The system iron(III) oxalate in 1.0 M potassium oxalate—0.05 M oxalic acid has a reported [11] k_{sh} value of 0.0148 m s^{-1}. Three-parameter curve-fitting of the data in Table 5 to Eqn. (6) gives the values $\Theta c = 3.8 \times 10^{-5}$ (Ω mol m^{-1}), $\sigma c = 3.5 \times 10^{-2}$ and $C_{edl} = 0.145$ F m^{-2}. Use of Eqns. (2), (4) and (5) with $D_{ox} = D_{Red} = 4.94 \times 10^{-10}$ m^2 s^{-1} produces a k_{sh} value of 0.014 m s^{-1}, which is in good agreement with the literature value mentioned above.

TABLE 3

Double-layer capacitance data at the DME for 1 M potassium chloride

DME potential (V vs. NCE)	Capacitance found (F m^{-2})	Lit. value [9] (F m^{-2})	DME potential (V vs. NCE)	Capacitance found (F m^{-2})	Lit. value [9] (F m^{-2})
−0.200	0.400	0.420	−0.800	0.178	0.192
−0.300	0.373	0.392	−0.900	0.170	0.172
−0.400	0.430	0.420	−1.000	0.155	0.164
−0.500	0.400	0.408	−1.100	0.155	0.160
−0.600	0.307	0.316	−1.200	0.162	0.164
−0.700	0.229	0.240			

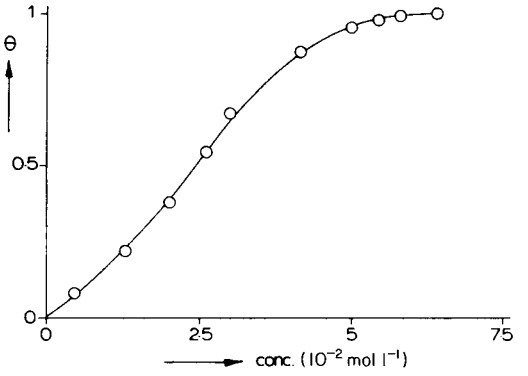

Fig. 5. Adsorption isotherm for butanol-1 in 1 M KCl at —0.6 V vs. SCE.

The k_{sh} value for cadmium-ion reduction in 0.5 M K_2SO_4 given by Tanaka and Tamamushi [12] is 8×10^{-4} m s^{-1}. The three-parameter curve-fitting procedure for this system gave $\Theta c = 3.2 \times 10^{-4}$, $\sigma c = 9.5 \times 10^{-3}$ and $C_{edl} = 0.22$ F m^{-2}. From the Θ value and $D_{ox} = 6.6 \times 10^{-10}$ m^2 s^{-1} and $D_{Red} = 1.53 \times 10^{-9}$ m^2 s^{-1}, the k_{sh} value is found to be 5.2×10^{-4} m s^{-1}. Although the agreement with the earlier value is somewhat disappointing, the result for the double-layer capacitance is in good agreement with the value measured in the absence of the electroactive component (0.22 vs 0.21 F m^{-2}). For the slowest reaction tested (i.e., zinc ions in 1 M KCl with $k_{sh} = 3 \times 10^{-5}$—$4 \times 10^{-5}$ m s^{-1}) the σ terms in Eqn. (6) are small compared to the Θ terms; thus in the three-parameter curve-fitting the results for σ will be unreliable. However, Θ and the double-layer capacitance can be found with satisfactory accuracy. The results found for the data given in Table 5 are: $C_{edl} = 0.166$ F m^{-2} and $\Theta c = 5.8 \times 10^{-3}$. This double-layer capacitance is in good agreement with the value measured in the absence of electroactive material (0.162 F m^{-2}). The product $\Theta c = 5.8 \times 10^{-3}$ together with $D_{ox} = 7.9 \times 10^{-10}$ and $D_{Red} = 1.6 \times 10^{-9}$ leads to $k_{sh} = 2.8 \times 10^{-5}$ m s^{-1} which is also in good agreement with its earlier value [9].

TABLE 4

Double-layer capacitance for the DME at —0.86 V vs. saturated mercury(I) sulphate at various drop times for 0.5 M Na_2SO_4

Drop time (s)	Capacitance (μF)	Drop area (mm^2)	Specific capacitance (F m^{-2})
0.96	0.314	1.48	0.213
1.44	0.393	1.94	0.203
1.92	0.507	2.34	0.216
2.40	0.566	2.72	0.208
			Mean 0.210 ± 0.006 F m^{-2}

TABLE 5

Pseudocapacitance measurements for systems with different k_{sh} values (peak values)

Active component	Conc. (mol m^{-3})	Drop time (s)	Specific capacitance (F m^{-2})	Frequency (Hz)
Cd^{2+}[a]	0.075	0.96	0.343	726
	0.075	1.44	0.350	625
	0.075	1.92	0.352	564
	0.075	2.40	0.378	504
	0.1875	0.96	0.645	524
	0.1875	1.44	0.530	504
	0.1875	1.92	0.612	423
	0.1875	2.88	0.626	363
	0.375	0.96	0.971	423
	0.375	1.44	0.994	363
Iron(III) oxalate[b]	0.98	0.48	0.423	826
	0.98	0.96	0.559	564
	0.98	1.44	0.574	484
	0.98	1.92	0.514	464
Cd^{2+}[c]	0.9	0.84	0.908	547
	0.8	0.84	0.952	516
	0.7	0.84	0.606	632
	0.6	0.84	0.683	581
	0.5	0.84	0.545	669
	0.4	0.84	0.291	847
	0.3	0.84	0.323	806
	0.2	0.84	0.254	907
Zn^{2+}[a]	7.39	0.96	0.464	826
	4.95	0.96	0.355	947
	4.95	1.44	0.354	826
	4.95	1.92	0.292	826
	4.95	2.40	0.494	586
	4.95	2.88	0.877	403

[a]In 1 M KCl. [b]In 1 M $K_2C_2O_4$/0.05 M $H_2C_2O_4$. [c]In 0.5 M K_2SO_4.

From these results, it can be concluded that the resonant frequency measurement technique for determining pseudocapacitances can be used to determine heterogeneous reaction rate constants up to 0.01 m s^{-1}. At the same time, it offers the possibility of establishing differential double-layer capacitance values in the presence of pseudocapacitance peaks.

The authors thank Prof. Dr. W. E. van der Linden for his helpful suggestions, Miss J. M. Boerrigter for preparing the manuscript, and Mr. R. H. Arends for making the drawings.

REFERENCES

1 P. F. Seelig and R. de Levie, Anal. Chem., 52 (1980) 1506.
2 M. Ichise, H. Yamagishi, H. Oishi and T. Kohima, J. Electroanal. Chem., 106 (1980) 35.
3 C. P. M. Bongenaar, M. Sluyters-Rehbach and J. H. Sluyters, J. Electroanal. Chem., 109 (1980) 23.
4 M. Bos, Anal. Chim. Acta, 122 (1980) 387.
5 D. Britz, Anal. Chim. Acta, 115 (1980) 327.
6 S. C. Creason and D. E. Smith, J. Electroanal. Chem., 40 (1972) 1.
7 M. Sluyters-Rehbach, Ph.D. Thesis, Utrecht, 1963.
8 D. Britz and H. H. Bauer, J. Electroanal. Chem., 16 (1968) 13.
9 M. Sluyters-Rehbach and J. H. Sluyters, Recl. Trav. Chim. Pays-Bas, 82 (1963) 535.
10 N. A. Boravaya and B. B. Damaskin, Elektrokhimiya, 8 (1972) 1529.
11 S. C. Creason and D. E. Smith, Anal. Chem., 45 (1973) 2401.
12 N. Tanaka and R. Tamamushi, Electrochim. Acta, 9 (1964) 963.

Analytica Chimica Acta, 152 (1983) 45—52
Elsevier Science Publishers B.V., Amsterdam — Printed in The Netherlands

MINICOMPUTER CONTROL OF MEASUREMENTS OF SPECTROELECTROCHEMICAL PROCESSES
Part 1. Instrumentation and Computer Programs

JANUSZ KRAWCZYK, MIĘCZYSŁAW ŁAPKOWSKI and JERZY W. STROJEK*

Institute of Inorganic Chemistry and Technology, Silesian Technical University, 44-100 Gliwice (Poland)

(Received 12th January 1983)

SUMMARY

The application of a NOVA-2 minicomputer is described for the control of a fast-scanning spectrophotometer and a potentiostat, with simultaneous recording of spectra and electrochemical curves. Previous difficulties with hysteresis effects in the spectrophotometer galvanometer are overcome.

The development of a rapid-scanning mirror spectrophotometer [1] made it possible to investigate the kinetics and mechanism of fast electrode processes and consecutive reactions [2—6]. The instrument can scan a wavelength range quickly because it has a special galvanometer; spectra are observed on the CRT display of a storage oscilloscope [7]. Minicomputers have been used to control the spectrophotometer and potentiostat, and to record the spectra [8, 9]. This method provides more precise recording of the observed phenomena and automatic on-line control of the measuring equipment.

The present paper deals with the application of a NOVA-2 minicomputer for the control of a potentiometer and a rapid scanning spectrophotometer and for simultaneous recording of the spectra and electrochemical curves. The system makes it possible to improve the performance of the galvanometer used in the spectrophotometer, with respect to hysteresis and oscillation when its position changes quickly. The subprograms which control the spectroelectrochemical process are also described.

EXPERIMENTAL

Instrumentation

Detailed descriptions of the fast-scanning mirror spectrophotometer and its static and dynamic characteristics are available [10, 11]. The spectrophotometer was controlled by a NOVA-2 minicomputer (DGC) equipped with two 8-bit digital/analog converters (DAC-14; ZDPUH, Kraków, Poland) and an 8-bit analog/digital converter (EH8B-1; DATEL, U.S.A.). Electro-

0003-2670/83/$03.00

chemical measurements were done in a spectroelectrochemical cell as described earlier [7]. The cell was controlled by a PRT-100-1X Tacussel potentiostat. The measured curves were recorded by means of a Yokogawa X-Y recorder or a 141B Hewlett-Packard storage oscilloscope. The data were also output by a line printer (DZM-180; MERA, Błonie, Poland) or on punched tape (DT-1058; MERA-ELZAB, Poland). The controlling program was introduced into the microcomputer memory by means of a fast paper-tape reader (CT-2100 MERA-KFAP, Poland). A block diagram of the system is shown in Fig. 1.

The minicomputer was connected to the spectroelectrochemical system by four lines; two D/A converters are used to control the electrochemical process and one two-input A/D converter serves to collect the results. The output OUT1 controls the potentiostat and the input IN1 is used for taking the electrochemical data. The analog output OUT2 controls the galvanometer mirror of the spectrophotometer, and the input IN2 is used to record the spectral data.

Procedures

The spectroelectrochemical process is controlled by a SPECTRUM program written in the computer language of the NOVA-2 minicomputer; it is added to the BASIC interpreter in the form of subprograms. A particular subprogram can be called by the instruction CALL *N*.

The complete control cycle (Fig. 2) consists of *W* steps in time *T*. At each step, the minicomputer sends a voltage controlling the potentiostat to the output OUT1, and receives the current intensity or the voltage of the working electrode through input IN1. The program can measure a 256-point spectrum within 8 ms. With a sweep width of 200 nm, the resolution obtained is better than 1 nm. If a 128-point spectrum is measured, the required time can be shortened to 4 ms. An essential limitation in decreasing the time

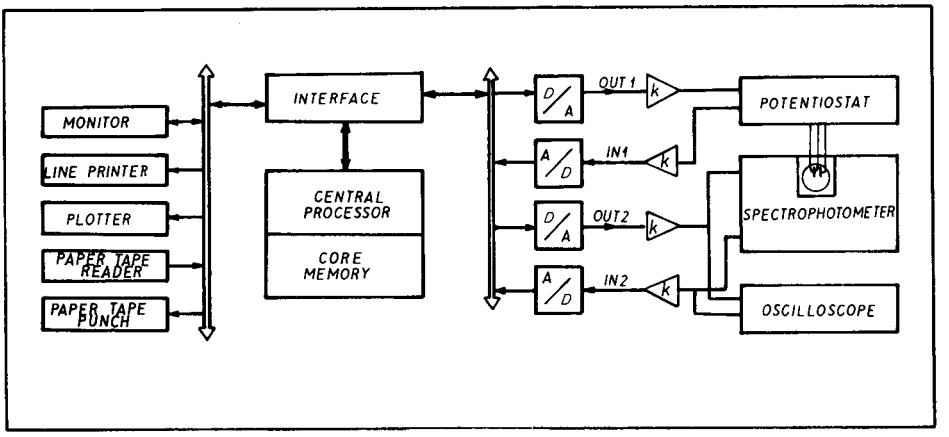

Fig. 1. Block diagram of the apparatus.

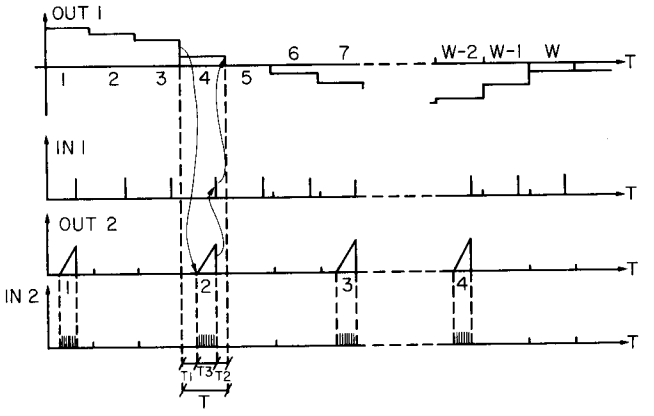

Fig. 2. Timing diagram of the controlled and measured signals.

of recording a spectrum is the inertia of the galvanometer and its mirror. Its limiting frequency is 500 Hz, so that for measuring times shorter than 2 ms, the galvanometer and its mirror cannot follow the changes of the controlling current. This damps the amplitude of the sweep, and the spectrum is shifted with respect to wavelength.

The SPECTRUM program provides six procedures, CALL 10 · · · CALL 15, which facilitate detailed determination of the spectroelectrochemical parameters and give easy access to the measured data.

(a) CALL 11, W, L, K. This procedure can be used to determine the parameters of measurements. The variable W determines the number of steps in the measuring cycle ($W < 4096$). The variable L controls the number of recorded spectra ($L < W$). The spectra can be recorded at constant or variable intervals or they may not be measured at all. For $L > 0$, the spectra are measured in the following steps $1, D + 1, 2 * D + 1, \ldots, (L - 1) * D + 1$, where $D = \mathrm{INT}[(W - 1)/(L - 1)]$. For $L < 0$, the spectra are measured in steps chosen by the user. For $L = 0$, the spectra are not recorded.

The variable K controls the number of steps of the D/A converter which controls the galvanometer ($K < 256$). If $K > 0$, the spectrum is recorded in N points: $N = \mathrm{INT}[256/K]$. If $K < 0$, the absorption is measured for one wavelength only, depending on the value of K. In this case, the mirror does not sweep the whole spectrum, but is fixed at the required wavelength and, for a particular chemical compound, the change in the height of its peak can be recorded in time. If $K = 0$, the absorption is not measured.

(b) CALL 12, I, F. This procedure makes it possible to store the value of the voltage function which controls the potentiostat and the intervals between the consecutive measurements of the spectrum. If $I > 0$, the value of the controlling voltage is established at the Ith step, depending on F ($F \leqslant 255$). If $I < 0$, the value of the time interval between the Ith and $(I - 1)$th measurement is stored (the variable F controls the number of

steps). It is worth noting that this procedure can control the potentiostat using any functional run.

(c) CALL 13, T1, T2, T3. This is the measuring procedure. It controls the potentiostat and the spectrophotometer, according to the data stored from procedures CALL 11 and CALL 12, and it conducts the measurements at predetermined intervals, using the time parameters $T1$, $T2$ and $T3$. $T1$ is the period of time measured from the voltage change at the potentiostat to the start of recording the spectrum. $T2$ is the period of time measured from the end of recording the spectrum to the next voltage change at the potentiostat. $T3$ is the time required for recording the spectrum. The measuring step is the sum of the three periods: $T = T1 + T2 + T3$. All the times are measured in milliseconds; for $T1$ and $T2$ the minimum is 100 μs with a maximum of 2 h, the maximum recording time being 30 s.

The potentiostat current is measured during 20 μs after the recording of the spectrum is complete, i.e., after a time equal to $(T1 + T3 + 0.02)$ ms calculated from the moment of the voltage change at the potentiostat. The time relationships are presented in the schematic block diagram of the measuring equipment shown in Fig. 3 (a, b).

(d) CALL 14, S, P, X. To obtain the maximum speed of measurement, the data obtained are recorded in the computer memory in binary form. Procedure CALL 14 provides access to these data using BASIC. To read the stored data, the value of the parameter S is needed; S represents the serial number of the measurement of the spectrum. If $S = 0$, the currents recorded from the potentiostat are read. The parameter P represents the number of consecutive measurements in the spectrum for $S > 0$, or the number of consecutive measurements of current for $S = 0$.

The data obtained by this procedure can be recorded by a line printer or a perforated tape or presented graphically on an X-Y recorder.

(e) CALL 15, I, X. This procedure is used to send the controlling voltage via the D/A converters directly to the OUT1 and OUT2 output or to conduct a measurement by using the inputs IN1 and IN2. Parameter I establishes the number of the converter ($I = 1, 2$ means reading the value X via the IN1 and IN2 inputs, but if $I = -1, -2$, the values X are sent to the OUT1 and OUT2 outputs). The variable X establishes whether the voltage value is to be read or sent ($X < 256$).

(f) CALL 10, R, H, T4. This procedure requires emphasis because of its essential role in the program. It is designed to improve the galvanometer dynamics. During the measurement, the galvanometer mirror moves periodically with a period T. To stabilize its movement, the mirror is forced to oscillate before the actual measurement. The parameter R determines the number of introductory periods. The galvanometer is controlled by a voltage of saw-tooth shape (Fig. 4). On the increasing slope of each pulse, the spectrum is swept and the decreasing slope makes the mirror return to its original position. However, the galvanometer mirror may be regarded as a second-order inertial element, and its behaviour can be compared with a

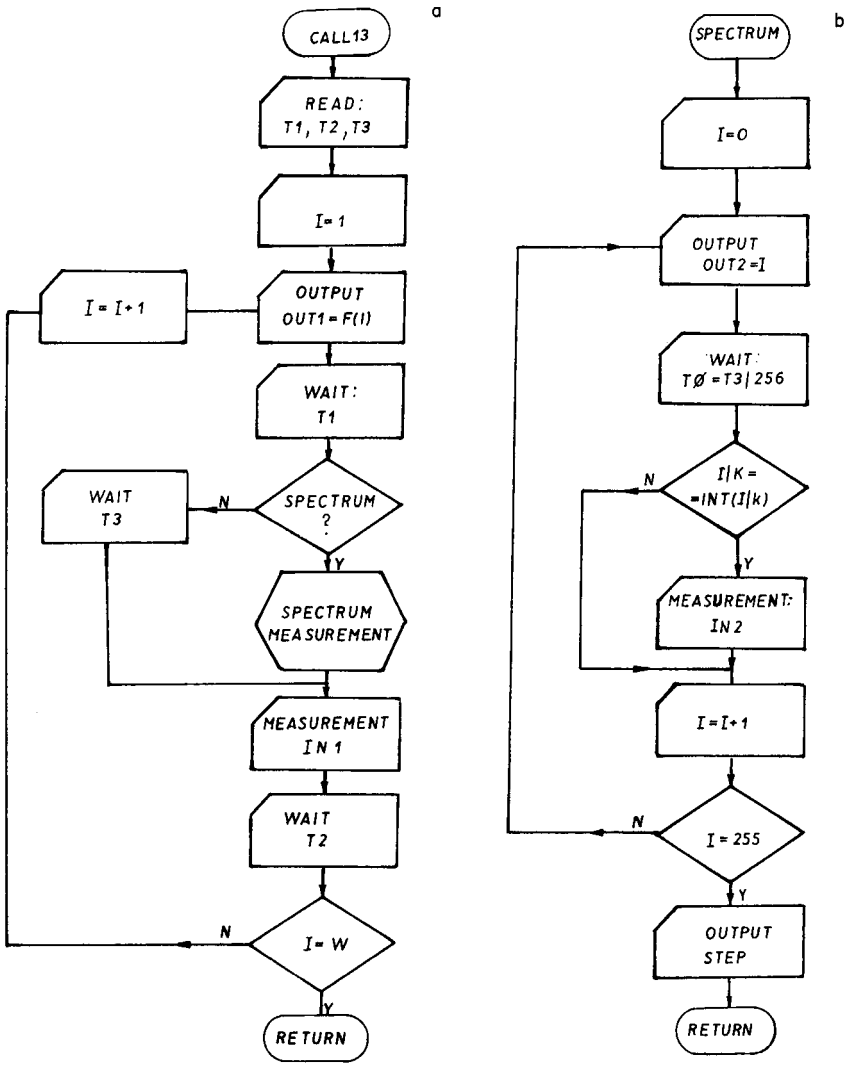

Fig. 3. Block diagrams of the measuring procedure CALL 13.

response to a unit pulse; thus during its fast return it starts to oscillate. Accordingly, in the case of high-speed spectrophotometric measurements, oscillations appear in the initial range of recording the spectrum (Fig. 5, b, c). Calculations showed that the voltage controlling the mirror at the time of its return to the original position should be changed in two steps, as shown in Figs. 4 and 5(d).

The height and width of the step are established by two parameters, H and $T4$. The height H is represented by a number within the range 0—255, time $T4$ being expressed in μs. The relation of these parameters was described by

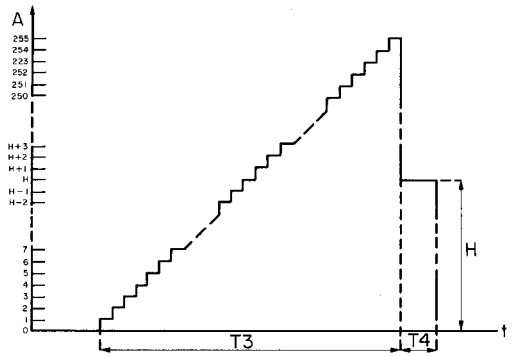

Fig. 4. Timing diagram for the voltage at the IN2 input controlling the galvanometer of the spectrophotometer. See text for details.

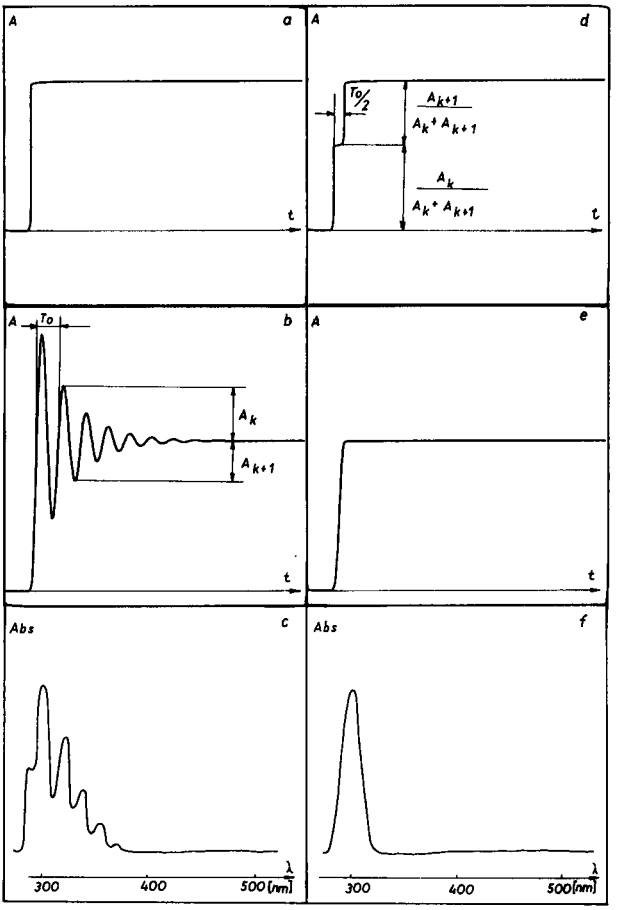

Fig. 5. (a, d) Voltage shapes controlling the galvanometer. (b, e) Plots of galvanometer movements as responses to runs (a) and (d). (c) Interference filter spectrum recorded with the saw-tooth shape voltage controlling the galvanometer. (f) Interference filter spectrum recorded with application of the voltage controlling the galvanometer as in Fig. 4 (step parameters as in Fig. 5d).

Brosens [12], and their effect on the response of the mirror to the unit pulse is shown in Fig. 5(b). Figure 5(e) shows the response of the mirror to the improved control pulse presented in Fig. 5(d). The parameters of the step were selected in such a way that the length of step $T4$ is equal to half the period of the free oscillation of the galvanometer. The amplitude H was calculated from

$$H = A_k/(A_k + A_{k+1})$$

where A_k is the amplitude of the mirror readjustment after a unit pulse has been applied to the galvanometer. These parameters are denoted in Fig. 5 as (b) and (d).

Based on these considerations, it can be concluded that the length of the next step should differ from a multiple of the periods of free oscillations of the galvanometer. T_0, and should conform to an odd multiple of half the oscillation period, T_0.

RESULTS

The oscilloscope traces of the spectrum of an interference filters, placed at the beginning of the recorded spectrum, are presented in Fig. 5(c) and (f). As shown in Fig. 5(f), application of the controlled run by means of a double step leads to a significant improvement in the recorded spectrum.

In order to check the correctness of the spectrophotometer performance and the control and recording subprograms, a series of neodymium filter spectra was recorded. Some examples of such recordings are presented in Fig. 6. Spectra (a, b) were recorded by utilizing a saw-tooth controlling voltage of the galvanometer mirror without additional runs to stabilize the galvanometer movement (parameter R in procedure CALL 10 is zero), whereas spectra 6(c, d) were recorded with prior application of twenty stabilizing runs. The parameters of the step were selected as in the case of the spectrum of the interference filter (Fig. 5, f). It can be seen from these figures that the recordings obtained according to subroutine CALL 10 (Fig. 6, c and d) are better than those in Fig. 6(a, b). The recorded spectra do not change their position while being recorded. Therefore, averaging of the results is better and leads to an increase in the signal-to-noise ratio.

The procedures described above facilitate efficient control of the fast-scanning mirror spectrophotometer and the potentiostat for electrochemical systems (e.g., chronoamperometry, chronopotentiometry) so that simultaneous recording of the spectra of the reaction substrates and products, and of electrochemical measurements become reasonably convenient and accurate. Experimental results obtained with the instrumentation and programs described will be presented in a subsequent paper.

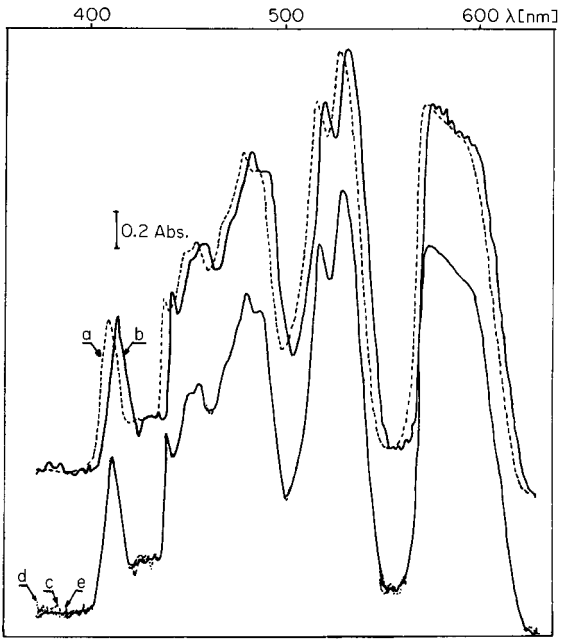

Fig. 6. Neodymium filter spectra: (a, b) without previous stabilizing pulses of the galvanometer mirror; (c, d) with previous application of 20 stabilizing pulses; (e) spectrum calculated by the program as the average of 30 spectra recorded in the same way as (c, d). (a, c) Spectrum 1; (b, d) spectrum 30.

REFERENCES

1 J. W. Strojek, G. A. Gruver and T. Kuwana, Anal. Chem., 41 (1969) 481.
2 L. N. Mackey and T. Kuwana, Bioelectrochem. Bioenerget., 3 (1976) 596.
3 H. N. Blount, N. Winograd and T. Kuwana, J. Phys. Chem., 74 (1970) 3231.
4 N. Winograd and T. Kuwana, J. Am. Chem. Soc., 92 (1970) 224; 93 (1971) 4343.
5 H. N. Blount, J. Electroanal. Chem., 42 (1973) 271.
6 W. R. Heineman, T. Kuwana and C. R. Hartzell, Biochem. Biophys. Res. Commun., 50 (1973) 892.
7 Z. Uziel and J. W. Strojek, Pol. J. Chem., 53 (1979) 1843.
8 E. E. Wells, Jr., Anal. Chem., 45 (1973) 2022.
9 R. M. Wightman, R. L. Scott., C. N. Reilley, R. W. Murray and J. N. Burnett, Anal. Chem., 46 (1974) 1492.
10 J. W. Strojek and Z. Uziel, Pol. J. Chem., 53 (1979) 1619.
11 J. W. Strojek, Z. Uziel and T. Kuwana, Pol. J. Chem., 54 (1980) 1215.
12 P. J. Brosens, Electro-Opt. Syst. Design, (1971) 21.

Analytica Chimica Acta, 152 (1983) 53—59
Elsevier Science Publishers B.V., Amsterdam — Printed in The Netherlands

A COMPARISON OF SCHEMES FOR THE ON-LINE ACQUISITION OF EXPERIMENTAL DATA

LOUIS MEITES*[a], MARIA PERLA COLOMBINI, LEONARDO LAMPUGNANI and TADDEO ROTUNNO

Istituto di Chimica Analitica Strumentale del C.N.R., Istituto di Chimica Analitica ed Elettrochimica dell'Università, Via del Risorgimento 35, 56100 Pisa (Italy)

(Received 14th April 1983)

SUMMARY

Two new schemes for the on-line acquisition of data in physicochemical experiments are proposed, and a comparison is made of their utilities in potentiometric titrations of weak acids. It is suggested that it will often be better to acquire data at equal increments of the dependent variable than, as is now the custom, at equal increments of the independent one.

There are many physicochemical experiments in which the independent variable is time, and many others in which it is some quantity that varies linearly with time. Constant-rate titrations and studies of the rates and mechanisms of reactions by following the dependence of absorbance, conductance, or some other property of a solution fall into the first group; the recording of absorption spectra and voltammograms falls into the second. In either case, some number of points is collected during an experiment, and their coordinates are used to evaluate some number of physicochemical parameters. Many such experiments are performed with the aid of microprocessors or computers that cause the points to be acquired in accordance with some previously established algorithm, and that invariably have access to a clock that makes it possible and easy to acquire them at uniform intervals of time. However, there appears to have been no inquiry into whether that is always, or ever, the best schedule for acquiring data. If it is not, the overall efficiency of experimentation might be increased by adopting a better one. This paper proposes two alternative schemes and shows that, in two different though related applications, one of them appears to be substantially superior to the one in general use.

One of us [1] recently investigated the conditions under which one weak acid can be detected in the presence of another, using data obtained in a potentiometric titration of their mixture with a base. Non-linear regression

---

[a]Permanent address: 22, Circle Drive, Potsdam, NY 13676, U.S.A.

0003-2670/83/$03.00

may be used to find the best values of the parameters in the equations that describe the titration of a single acid. If only one acid is actually present, the "deviation plot" [2] obtained by plotting the residuals against the independent variable (the volume of added base) will consist of points randomly scattered around the volume axis. The amplitude of the scatter will reflect the standard error of a single measurement of the dependent variable (pH). If, however, there are actually two acids present, a systematic error will arise from the falsity of the hypothesis implied by the choice of equations, and the deviation plot will be transformed into a random scatter around a smooth curve whose shape reflects the nature of that error. The smooth curve, called a "deviation pattern," has a maximum and a minimum whose heights increase as the relative concentration of the second acid increases, or as its dissociation constant becomes more widely different from that of the first acid. If c_2/c_1 is the ratio of the concentrations of the two acids, and if $\Delta(\mathrm{p}K)$ is the difference between their values of $\mathrm{p}K_a$, the amplitude A of the pattern, defined as the difference between the most positive residual and the most negative one, was found to be given by an equation of the form

$$A = g(c_2/c_1)[\Delta(\mathrm{p}K)]^2/[1 + h(c_2/c_1)] \qquad (1)$$

in which g and h represent constants whose values are influenced by the way in which the data are distributed. If the limit of detection is taken to correspond to a value of A that is just equal to three times the standard error of a single measurement of pH, and if that error is taken to be 0.002 pH unit, the values obtained for g and h indicated that it should just be possible, for example, to detect 1.0% of a second acid for which $\mathrm{p}K_a$ differs by only 0.57 unit from the corresponding value for the first one. This result was obtained on the basis of a data-acquisition schedule comprising 21 points equally spaced along the f axis from pH 3.0 to pH 7.0, or roughly $0.002 < f < 0.995$ if $c_1 = 0.1$ M, if c_2/c_1 is small, and if $\mathrm{p}K_{a,1} = 5$. The titration parameter f is defined [3] as the ratio of the number of moles of base added at any point to the total number of moles of acid being titrated, and in any one titration is proportional to the volume of reagent added.

The problem has a trivial case in which $\Delta(\mathrm{p}K)$ is large and c_2/c_1 is on the order of one. Confronted with a titration curve obtained in that case, the natural reaction of a chemist trying to decide how many acids were present would be to count the number of points of maximum slope. Though of course there is only one such point if both $\Delta(\mathrm{p}K)$ and c_2/c_1 are small, this suggests that the utility of an experimental point increases as the slope of the curve at that point increases.

Accordingly two different schemes for data acquisition were envisioned: (1) data are acquired at equal increments of pH; (2) data are acquired in such a way that the probability of acquiring a point is proportional to the slope of the curve at that point. After this work had been completed, Smit and Smit [4] described an autotitrator for which the algorithm governing the sizes of the successive aliquots of reagent was designed to yield points at roughly

equal increments of pH or potential of the indicator electrode. Shia and Meites [5] had previously effected controlled-potential coulometric analyses with a data-acquisition schedule in which a number of predetermined times were spaced in a way that led to roughly (but only roughly) equal increments of the quantity of electricity. Nothing else could be found in the literature to suggest that either of these procedures has been used, or contemplated, before.

METHOD

So that the results of these calculations would be easy to compare with those previously published [1], conditions and ranges were chosen to be essentially identical with those previously used. It was assumed that 25 cm^3 of the sample is titrated with 0.1 M strong base; that the major constituent of the sample is a monobasic weak acid having a conditional acidity constant equal to 1×10^{-4} M and present at a concentration of 0.1 M; and that the other constituent is a second monobasic weak acid which has a conditional acidity constant $K_{a,2}$ corresponding to $pK_{a,2} = 4.00 + \Delta(pK)$, where $\Delta(pK)$ is positive, and is present at a concentration c_2 equal to or less than 0.1 M.

To test the first of the algorithms suggested above, the pH of the original mixture was calculated and rounded upward to the nearest 0.1 unit, and the resulting value was assigned to the pH at the first experimental point. The value 6.50 was assigned to the pH at the last point, 23 additional values equally spaced between these extremes were generated, and the value of f at each of the 25 points was computed from the exact equation for the titration curve. If c_2/c_1 was small, this yielded a set of points that covered the range of values of f from approximately 0.025 to 0.997.

These "data" were fitted to the exact equation for the titration of a single monobasic weak acid. Terms involving the ion-product constant of water were always negligible, and three parameters were therefore involved: the concentration of the acid, its pK_a value, and a quantity that formally represents the single-ion activity coefficient of hydrogen ion [6]. The best values of these parameters were used to compute the values of the residuals, and the difference between the most positive residual and the most negative one was taken to be the amplitude A of the deviation pattern. Because the points are relatively sparse and arbitrarily spaced, this procedure yields values of the amplitude that tend to be slightly too small and that have relative standard errors on the order of 5—10% [1, 7].

"Data" for testing the second algorithm were generated in the following way. The pH of the original mixture was computed and subtracted from 8.0 (which was a crude estimate of the pH at the equivalence point) to obtain an estimate of the average slope, $\bar{S}$ (= dpcH/df), of the titration curve over the region expected to be of interest. Values of the pH at f = 2/260 and 3/260 were then computed, and the slope at the latter point was estimated from the equation

$S = (pH_{f=3/260} - pH_{f=2/260})/(1/260)$

A random number R lying between 0 and 1 was generated and compared with the quantity Q defined by the equation

$$Q = S/10\,\bar{S} \tag{2}$$

If R was smaller than or equal to Q, the point at $f = 3/260$ was retained; if R exceeded Q, that point was discarded, the pH value at the next point (where $f = 4/260$) was computed, a new random number was generated and compared with the value of $(pH_{f=4/260} - pH_{f=3/260})/[(1/260) \times 10\,\bar{S}]$, and so on. The procedure was stopped at $f = 258/260$, so that the widest range of values of f that could have been represented in any set of data extended from 0.0115 (= 3/260) to 0.992 (= 258/260), although there was no assurance that a point at either of these extremes would appear in any particular set. The factor of 10 in the denominator of Eqn. (2) reflected a desire to retain approximately one-tenth of the 256 points that would be generated and considered. In fact, the number of points that were retained varied between 13 and 25 in different sets, with an average of 18.5. An upper limit of 25 points was imposed arbitrarily, so that the results would not be biased in favor of this strategy, by repeating the entire procedure if it would have led to the inclusion of a 26th point in any set. Another reason why the average number of points retained was smaller than one-tenth of the number considered is that the procedure employed for evaluating $\bar{S}$ yields an overestimate of the average slope in the interval $3/260 < f < 258/260$. Nevertheless, repeating the procedure several times for each of several different pairs of values of c_2/c_1 and $\Delta(pK)$ to obtain sets containing different numbers of points revealed no substantial systematic dependence of the amplitude on the number of points retained. The amplitude A of the deviation pattern was again evaluated in the manner described above.

The computations were done in BASIC with a Tektronix Model 4051 microcomputer, using a general program for effecting non-linear regression [8] that is closely similar to, but somewhat more efficient than, predecessors that have been widely distributed and used.

RESULTS AND DISCUSSION

Table 1 shows the amplitudes that were obtained with points evenly spaced along the pH axis; Table 2 shows those that were obtained with points for which the probability of acquisition or retention is proportional to the slope of the curve. For the sake of compactness, each Table contains only about half of the values that were computed.

Table 3 summarizes the values of the parameters in Eqn. (1) for all three schemes of data acquisition. Those for data equally spaced along the f axis were taken from Meites [1]; the others were obtained by regression onto Eqn. (1) in such a way that the sums of the squares of the relative deviations in A were minimized.

TABLE 1

Amplitudes of deviation patterns for data equally spaced along the pH axis (The amplitudes are expressed in pH units)

$\Delta(pK)$	Amplitudes for c_2/c_1 values of						
	1	0.5	0.2	0.07	0.03	0.01	0.005
1	0.426	0.397	0.290	0.153	0.0777	0.0286	0.0147
0.4	0.0766	0.0690	0.0447	0.0203	0.00952	0.00333	0.00170
0.15	0.0110	0.00967	0.00606	0.00279	0.00126	—	—
0.06	0.00180	0.00158	0.00096	—	—	—	—

The following two conclusions are apparent. First, with points for which the probability of acquisition is proportional to the slope (scheme 2), the amplitudes are slightly smaller than with points evenly spaced with respect to the independent variable (scheme 1). Although the differences are too small to be statistically significant at any reasonably high level of confidence, these results provide no basis for thinking scheme 2 to be superior. Secondly, with points evenly spaced with respect to the dependent variable (scheme 3) the amplitudes are substantially larger than with those evenly spaced with respect to the independent variable. Moreover, scheme 3 becomes more advantageous as the amplitude decreases. For example, with $c_2/c_1 = 1$ and $\Delta(pK) = 1$, the amplitudes are 0.426 unit for points equally spaced along the pH axis, and 0.416 unit for points equally spaced along the f axis. Under these conditions, the two schemes are indistinguishable, but the presence of the second acid is so clearly revealed by cursory inspection of the titration curve that sensitive techniques for detecting it are hardly needed. However, with $c_2/c_1 = 0.005$ and $\Delta(pK) = 1$, the corresponding amplitudes are 0.0147 unit and 0.0094 unit. In this marginal case, where the detection of the second acid would be quite impossible by any classical technique, and would just be possible by the deviation-plot approach if the points were equally spaced with respect to the independent variable in the traditional and customary

TABLE 2

Amplitudes (in pH units) of deviation patterns for data having a probability of acquisition proportional to the slope

$\Delta(pK)$	Amplitude for c_2/c_1 values of						
	1	0.5	0.2	0.07	0.03	0.01	0.005
1	0.405	0.347	0.241	0.114	0.0444	0.0196	0.00902
0.4	0.0691	0.0605	0.0370	0.0153	0.00664	0.00308	0.00150
0.15	0.00946	0.00825	0.00518	0.00217	0.00106	0.00037	—
0.06	0.00153	0.00138	—	—	—	—	—

TABLE 3

Values of the parameters in Eqn. (1) for different plans of data acquisition

Scheme	g	h	Relative standard deviation from regression (%)
1. Equally spaced with respect to the independent variable (f)	1.882	3.307	6.6
2. Probability of acquisition proportional to the slope	1.776	3.010	7.7
3. Equally spaced with respect to the dependent variable (pH)	2.345	3.611	9.9

fashion, it would be much easier and more certain if the points were evenly spaced with respect to the dependent variable.

The detection, either by measurements of pH or by potentiometric titration, of one weak acid in the presence of a much larger concentration of another has always been assumed to be impossible unless the dissociation constants of the two acids were widely different, and the approach suggested in this paper and its predecessor [1] is the first that has been proposed for the situation in which they are not. Yet, titrations of solutions containing only one monobasic weak acid are very frequently done so that either the concentration of the acid or its dissociation constant, or both, can be evaluated, and a comparison of the two schemes for data acquisition for such purposes is therefore likely to be of more general interest than the comparison made above. Two sets of synthetic data were therefore generated for the titration, with 0.1 M base, of 25 cm^3 of a 0.1 M solution of a single monobasic weak acid for which the conditional acidity constant is 1×10^{-9} M. One set consisted of 25 points equally spaced along the f axis from $f = 0.025$ to $f = 0.975$, corresponding to the range of pH values from 7.41 to 10.49. The other consisted of 25 points equally spaced along the pH axis from pH 7.5 to pH 10.5, corresponding to the range of f values from 0.0306 to 0.9752. The standard errors of the values of c_a^0 and pK_a obtained from the two sets by non-linear regression onto the exact equation for the titration curve were computed by means of an updated version of a program previously described [8]. Assuming that the standard error of measurement of each pH-value is equal to 0.002 unit, the standard error of c_a^0 was found to be 0.0304% for data equally spaced along the f axis, but only 0.0178% for data equally spaced along the pH axis, while the standard error of pK_a was found to be 3.56×10^{-4} unit for data equally spaced along the f axis, but only 2.58×10^{-4} unit for data equally spaced along the pH axis. All these figures are small, but it is evident that the efficiency of experimentation and the certainty of its results are substantially improved by obtaining points for which the increments in the value of the dependent variable are equal.

CONCLUSIONS

Although no small number of examples could prove that one scheme for acquiring data is always superior to another, the advantages shown here to accure from spacing the points equally with respect to the measured or dependent variable, rather than with respect to the independent one, seem substantial enough to render the former scheme worthy of consideration in designing physicochemical experiments. In any particular circumstances, if the values of the parameters were known fairly closely in advance, a scheme superior to either could probably be deduced from pointwise variance analysis [9], but that schedule might prove to be an inferior one in slightly different circumstances. In particular, it can hardly be expected that the optimum schemes will be the same regardless of whether the qualitative behavior of the system is known or not. To acquire data at equally spaced values of the dependent variable may often be the best compromise between the ideal best plan and the restrictions imposed by uncertainty regarding the detailed behavior of the system under study.

This work was made possible by support from the Consiglie Nazionale della Richerche, and was aided in part by grant number CHE-8106103 from the National Science Foundation.

REFERENCES

1 L. Meites, Anal. Lett., 15 (1982) 507.
2 L. Meites, CRC Crit. Rev. Anal. Chem., 8 (1979) 1.
3 J. J. Lingane, Electroanalytical Chemistry, Interscience, New York, 1953, p. 74.
4 J. C. Smit and H. C. Smit, Anal. Chim. Acta, in press.
5 G. A. Shia and L. Meites, J. Electroanal. Chem., 87 (1978) 369.
6 D. M. Barry and L. Meites, Anal. Chim. Acta, 68 (1974) 435.
7 L. Meites, Anal. Lett., 15 (1982) 1149.
8 L. Meites, The General Multiparametric Curve-Fitting Program CFT4A, privately published, 1983.
9 L. Meites, Anal. Chim. Acta, 74 (1975) 177.

Analytica Chimica Acta, 152 (1983) 61—72
Elsevier Science Publishers B.V., Amsterdam — Printed in The Netherlands

WEIGHTING IN THE INTERPRETATION OF DATA FOR POTENTIOMETRIC ACID—BASE TITRATIONS BY NON-LINEAR REGRESSION

G. KATEMAN

Laboratorium voor Analytische Scheikunde, Universiteit van Nijmegen, Toernooiveld, 6525 ED Nijmegen (The Netherlands)

H. C. SMIT and LOUIS MEITES*[a]

Laboratorium voor Analytische Scheikunde, Universiteit van Amsterdam, Nieuwe Achtergracht 166, 1018WV Amsterdam (The Netherlands)

(Received 11th April 1983)

SUMMARY

In using non-linear regression to evaluate the concentration of the substance titrated and the other parameters that characterize the titration curve obtained when a weak monobasic acid is titrated potentiometrically with a strong base, it is customary to assume that the standard error of measurement of a single pH value is the same for all the points obtained. This is unrealistic because measurements of pH are known to be less precise in poorly buffered solutions than in well buffered ones, so that the data are least reliable in the regions where the curves are steepest. The consequences of these ideas are examined in detail, and it is shown how the standard error in measurements of the volume of reagent and the pH of the titration mixture affect the standard errors of the parameters that are calculated from the data by properly weighted regression analysis.

During the last decade there have been many studies [1—13] of the application of non-linear regression to the analysis and interpretation of data obtained in potentiometric acid—base titrations. There is no doubt that it provides better values, both of the concentration of the substance titrated and of the physicochemical parameters (such as dissociation constants, solubility products, and critical concentrations for micelle formation) that govern the curves, than can be obtained in any other way.

Questions have arisen, however, as to whether weighting factors should be applied, and how. Schwartz and Gelb [12] considered that the relative standard errors of their measurements of pH and the volume V_b of added base were roughly equal (and were approximately 0.1%), and concluded that neither of these variables could be considered to be error-free. The argument is open to the objection that the relationship between the errors is more important than their absolute or relative values. Consider, for example, the

*Permanent address: 22, Circle Drive, Potsdam, NY 13676, U.S.A.

0003-2670/83/$03.00

point at which a moderately concentrated solution of a monobasic weak acid HA, for which the conditional acidity constant K_a (= $[H^+][A^-]/[HA]$) is equal to 1×10^{-7} M, has been half neutralized. The pcH is equal to 7.000. If there is a relative error of 0.1% in the volume of reagent that has been added, so that the titration parameter f (= $V_b c_b / V_a^0 c_a^0$, where V_a^0 and c_a^0 denote the initial volume and concentration of the acid being titrated, while c_b denotes the concentration of the base) [14], is equal to 0.5005 rather than to 0.5000, the pcH should be 7.0009 instead of 7.0000. The resulting error is nearly an order of magnitude smaller than that corresponding to a relative error of 0.1% in the pcH. For data that are confined to the well-buffered portion of a titration curve, as were those obtained by Schwartz and Gelb, the error in f is nearly certain to be insignificant in comparison with the error in the pH, and is therefore hardly worth taking into account.

In the regions where the curve is steep, however — near $f = 0$ if the acid is very weak, and around $f = 1$ if it is sufficiently strong to yield a well-defined point of maximum slope — errors in measurements of V_b do become significant, and may greatly outweigh those in measurements of pH.

As Bishop [15] pointed out, every exact titration-curve equation is linear in f (and hence in V_b), although it may be a third-, fourth-, or higher-order polynomial in $[H^+]$. It is therefore much easier to solve for f or V_b than for $[H^+]$, and several authors [6, 12, 16] have consequently chosen to minimize quantities of the form $\Sigma_n W_n (V_{b,c,n} - V_{b,m,n})^2$, where $V_{b,c,n}$ is the calculated and $V_{b,m,n}$ the measured volume of base at the nth experimental point. The weighting factor W_n has sometimes been taken to be 1, but a different choice was made by Nowogrocki et al. [13] and will be discussed in the following paragraph. Those who are tempted to follow this lead should consider the "data" in Table 1, which also gives the values of the parameters obtained from them by linear regression onto the equations $y = a + bx$ and $x = a' + b'y$. Since these equations are algebraically equivalent, one might expect $b = 1/b'$ and $a = -a'/b'$, but the best values do not satisfy these equalities because the equations are not statistically equivalent. This is to say that it is the structure of an experiment, rather than the convenience or comfort of the programmer, that determines which is the independent variable and which is the dependent one. The discrepancy cannot be eliminated by weighting, for the proper weighting factors are $W_{n,y} = 1/[\sigma_y^2 +$

TABLE 1

"Data" for regression onto linear equations

$x = 0$	2.0	4.0	6.0	8.0
$y = 1.1$	2.7	5.0	7.3	8.9

Best linear equations:
$y = a + bx = 0.960\,000 + 1.010\,000\,x$
$x = a' + b'y = -0.926\,829 + 0.985\,366\,y$
$y = -a'/b' + (1/b')\,x = 0.940\,594 + 1.014\,851\,x$

$\sigma_x^2 (dy/dx)^2]$ for regression onto the equation $y = a + bx$ by minimizing the quantity $\Sigma_n W_{n,y} (y_{c,n} - y_{m,n})^2$, and $W_{n,x} = 1/[\sigma_x^2 + \sigma_y^2 (dx/dy)^2]$ for regression onto the equation $x = a' + b'y$ by minimizing the quantity $\Sigma_n W_{n,x} (x_{c,n} - x_{m,n})^2$. The denominators of the expressions for the two weighting factors are constant because $dy/dx = b$ while $dx/dy = b'$, so that all the points receive equal weight, and the values obtained for the parameters are the same, regardless of whether the weighting factors are included or not.

Nowogrocki et al. [13] employed the weighting factor $W_n = 1/[\sigma_{V_b}^2 + \sigma_{pH}^2 (dV_b/dpH)^2]$ in minimizing the sum of the squares of the differences of volume in regression onto the equation for a potentiometric acid—base titration curve. Although this factor is theoretically correct in form, its use actually compounds the error just discussed. If the titration curve has a well-marked point of maximum slope, the value dV_b/dpH is likely to be much smaller near that point than in any other region. For example, if an 0.01 M solution of a strong acid is titrated with 0.01 M strong base, the value of dV_b/dpH is 1.25×10^4 times as large, so that the term $\sigma_{pH}^2 (dV_b/dpcH)^2$ in the denominator of the expression for W_n is about 1.5×10^8 times as large at $f = 0$ as at $f = 1$. Points near the start of the titration will disappear in the calculations. The variation of dV_b/dpH is smaller in the titration of a weak acid, but again the only points that will receive any appreciable weight will be those in the immediate vicinity of the equivalence point unless the acid is very weak, in which event the inflection around the equivalence point disappears, and the greatest weight will be assigned to the points at the very start of the titration.

Unfortunately, these are precisely the regions in which measurements of pH are least reliable. Glass electrodes are ill-behaved in poorly buffered solutions, such as pure distilled water, where the standard error of a single measurement is more likely to be a few tenths than a few thousandths of a unit. Moreover, the pH values obtained in those regions may be drastically affected by traces of impurities, such as carbon dioxide and its conjugate bases, that would have no appreciable effect in the well-buffered regions of the curve. For both of these reasons, the weight that is assigned to a point should decrease as dpH/dV_b increases.

THEORY AND PROCEDURE

The foregoing discussion shows that one must minimize the quantity $\Sigma_n W_n (pH_{c,n} - pH_{m,n})^2$, where $pH_{c,n}$ is the calculated and $pH_{m,n}$ the measured value of the pH at the nth point, while the weighting factor W_n is given by

$$W_n = 1/[\sigma_{pH}^2 + \sigma_{V_b}^2 (dpH/dV_b)^2] \quad (1)$$

This takes the errors of measuring both V_b and the pH into account, and correctly assigns least weight to the data obtained in poorly buffered solutions.

The exact equation for the titration of a monobasic weak acid with a strong base can be written

$$[H^+] = \{c_a^0(1-f)/(1+rf) - [H^+] + [OH^-]\}K_a/\{c_a^0 f/(1+rf) + [H^+] - [OH^-]\} \quad (2)$$

where r is the dilution parameter defined by the equation $r = c_a^0/c_b$ [17]. Equation (2) is easily rearranged to give the cubic equation

$$[H^+]^3 + \alpha[H^+]^2 - \beta[H^+] - K_aK_w = 0 \quad (3)$$

where K_w denotes the conditional ion-concentration product $[H^+][OH^-]$ in the titration medium, and the subsidiary variables α and β are defined by

$$\alpha = c_a^0 f/(1+rf) + K_a; \quad \beta = c_a^0 K_a(1-f)/(1+rf) + K_w \quad (4)$$

Implicit differentiation and rearrangement yield

$$\mathrm{dpH}/\mathrm{d}V_b = (\mathrm{d}[H^+]/\mathrm{d}f)(\mathrm{dpcH}/\mathrm{d}[H^+])(\mathrm{dpH}/\mathrm{dpcH})[\mathrm{d}f/\mathrm{d}V_b]$$

$$= 0.4343\, c_b([H^+] + (1+r)K_a)/V_a^0(1+rf)^2\{3[H^+]^2 + 2\alpha[H^+] - \beta\} \quad (5)$$

In the course of regression analysis, Eqn. (3) must be combined with another equation that translates the concentration of hydrogen ion to a pH value:

$$\mathrm{pH} = -\log_{10}(y_{H^+}[H^+]) \; [= \mathrm{pcH} - \log_{10} y_{H^+}] \quad (6)$$

in which y_{H^+} represents the single-ion activity coefficient of hydrogen ion and also allows for the effect of a finite but constant liquid-junction potential. The equality within square brackets shows that the quantity dpH/dpcH, which appears in Eqn. (5), is equal to 1. In the absence of any prior information about the medium in which the titration is done or about the identity of the acid titrated, there are at least three parameters to be evaluated: c_a^0, pK_a, and y_{H^+}. Barry et al. [5], who avoided the problems of weighting by avoiding the regions near $f = 0$ and $f = 1$, showed that c_b could be evaluated as well, but it is assumed here that both c_b and V_a^0 are known *a priori*.

The present work was designed to evaluate the standard errors of these parameters, to elucidate their dependences on the value of K_a, and to study the effects of weighting on those dependences. The results should provide a reliable guide to the precision that can be expected in applying non-linear regression to data obtained in potentiometric titrations of monofunctional weak acids and bases.

The general structure of the computer program has been described previously [18] for the case in which the values of the independent variable are assumed to be free from random errors. The selected values of the parameters [$V_0(1)$, $V_0(2)$, etc.] are used to generate a set of n data points. The value y_1 of the dependent variable at the first point is changed by some arbitrary small amount Δy, and the corresponding values [$V(1)$, $V(2)$, etc.] of the parameters are computed. The values of $[V(1) - V_0(1)]/\Delta y$, $[V(2) -$

$V_0(2)]/\Delta y$, etc., are stored; then y_1 is returned to its original value, the value y_2 of the dependent variable at the second point is changed, a new set of values of the parameters is computed, and so on. Finally the variances of the parameters are obtained from equations of the form

$$\sigma^2_{V(1)} = \sigma^2_y \sum_{j=1}^{n} (\Delta V(1)/\Delta y_j)^2 \tag{7}$$

Repeated non-linear regression is required, and was effected with the aid of the most recent version of a program [19] that has been widely distributed and used.

Random errors in the independent variable x were taken into account in the same way. After the last of the quotients $\Delta V_i/\Delta y_n$ had been computed, y_n was returned to its original value, x_1 was changed by an arbitrary small amount, and a second series of fits was performed by perturbing the values of x one at a time. The variances of the parameters were obtained from equations of the form

$$\sigma^2_{V(1)} = \sigma^2_y \sum_{j=1}^{n} (\Delta V(1)/\Delta y_j)^2 + \sigma^2_x \sum_{j=1}^{n} (\Delta V(1)/\Delta x_j)^2 \tag{8}$$

All the computations were made in FORTRAN-IV with a Hewlett-Packard HP-1000 computer operated in a time-sharing configuration. Most of them entailed fifty non-linear regression analyses involving twenty-five data points, three parameters, and an equation [Eqn. (3)] that had to be solved by the Newton—Raphson method. Their results are afflicted both by round-off errors and by the arbitrary natures of the conditions that were set for terminating the individual fits. More precise values of the standard errors could have been obtained by double-precision computation, but their trends were considered to be more important than their exact values and seemed to be so clearly revealed by the results quoted here that further increases of the already substantial lengths of the calculations seemed unwarranted.

RESULTS AND DISCUSSION

It was always assumed that 25 cm^3 of an 0.1 M solution of an acid is titrated with 0.1 M base (so that $r = 1$), that $y_{H^+} = 1$, and that 25 data points are obtained. Table 2 shows the standard errors of c_a^0 and pK_a that resulted from unweighted calculations in which the values of V_b were considered to be free from random error. The values in the second and third columns were obtained for points equally spaced along the volume axis from $f = 0.025$ to $f = 0.975$; those in the fourth and fifth columns were obtained for points equally spaced along the pH axis over approximately the same range. It has been argued elsewhere [20] that the latter procedure is preferable, partly because it leads to more precise values of the parameters in calculations like these, and (except for the values of c_a^0 for the very weakest acids) these

results provide additional support for that argument. The exceptions, among which the one at $pK_a = 13$ is especially anomalous, result from rounding the pH value at the last point to the next lower tenth of a unit. This was done to ensure that the equivalence point would not be overstepped, for fear that the present comparison would be biased if it were. However, the slope is so small in the vicinity of the equivalence point of the titration of a very weak acid that f was only 0.80 at the last point on the curve for which pK_a was equal to 13.

Nevertheless the general trends are clear: the calculated relative standard error of c_a^0 is roughly independent of pK_a as long as pK_a is smaller than about 9, but increases rapidly as pK_a increases further, while the calculated standard error of pK_a is large if pK_a is either very small or very large, and passes through a minimum at values of pK_a between about 7 and 11.

Although these conclusions are not unreasonable, the behavior of the relative standard error of c_a^0 is sensitive to the range of values of f over which the data are acquired, as may be seen by comparing the values in the last two columns of Table 2 with those in Table 3, where that range is broadened by the inclusion of points out to $f = 1.125$. For a very weak acid ($pK_a > 10$) this has little effect, but for a stronger one it leads to a decrease of the calculated relative standard error of c_a^0, and that decrease exceeds an order of magnitude if $pK_a = 7$. Calculations were not done for still stronger acids because the variation of slope during a titration is already so large if $pK_a = 7$ that the size of an individual aliquot of reagent must vary from 3.7 cm^3 near $f = 0.5$ to only 0.045 cm^3 at the equivalence point to yield equal increments of pH over the range $0.025 < f < 1.125$. This is certainly feasible, but the required variation would be even larger with a stronger acid and would be so difficult to effect that the calculations could have no practical significance.

Because these calculations are unweighted, points near the equivalence point exert an overwhelming influence on the calculated relative standard error of c_a^0, as is shown in Fig. 1. In such a pointwise-variance-analysis plot, the ordinate represents the value of $\partial V_i/\partial y_j$ (or, more accurately, the finite-difference approximation to this) at the jth point to the largest value of that ratio at any point, and consequently it describes the relative influence of that point on the variance of the ith parameter. A point that has little influence on the variance of a parameter has little influence on its value as obtained from regression analysis. These plots therefore show that, for moderately strong acids, the values of c_a^0 obtained from unweighted regression analysis are almost entirely governed by the pH values at a very small number of points, which lie on the steepest portion of the titration curve and cannot be as reliable as they are assumed to be.

Table 4 shows the effects of proper weighting. Each value in this Table is the average of the results obtained in two calculations that were initialized and terminated in different ways to check their reproducibilities. The mean difference between the results in any pair was only about 2%. Several con-

TABLE 2

Standard errors of the parameters obtained by unweighted non-linear regression with data confined to the range $0.025 < f < 0.975$
(Each of these values was obtained with $\sigma_{pH} = 0.001$ and is proportional to that value. The assumed experimental conditions are described in the text)

pK_a	Standard errors for data equally spaced along the volume axis		Standard errors for data equally spaced along the pH axis	
	c_a^0, %	pK_a, unit	c_a^0, %	pK_a, unit
1	0.00559	0.0101	0.00530	0.0153
3	0.00578	0.00177	0.00432	0.00187
5	0.00588	0.000538	0.00461	0.000314
7	0.00586	0.000247	0.00517	0.000197
9	0.00827	0.000157	0.00651	0.000105
10	0.0170	0.000139	0.0151	0.000115
11	0.0454	0.000239	0.0521	0.000204
12	0.180	0.00107	0.214	0.000689
13	0.494	0.00232	0.165	0.00116

clusions can be drawn by inspecting these results and comparing them with the ones shown in Tables 2 and 3.

First, as expected, unweighted regression seriously overestimates the precision that can be attained. If the standard error of measurement of a single volume of reagent is equal to 0.04% of the volume required to reach the equivalence point, as it was in these calculations, the concentration of a moderately strong acid cannot be found with a precision better than about 0.015%, regardless of the value of pK_a or of how the points are distributed. This is clearly more reasonable than figures on the order of a few thousandths (Table 2) or ten-thousandths (Table 3) of a per cent.

TABLE 3

Standard errors of the parameters obtained by unweighted non-linear regression with data confined to the range $0.025 < f < 1.125$
(Each of these values was obtained with $\sigma_{pH} = 0.001$ and is proportional to that value. The assumed experimental conditions are described in the text. Each set of data consisted of 25 points equally spaced along the pH axis)

pK_a	Standard error of	
	c_a^0, %	pK_a, unit
7	0.000441	0.000420
9	0.00501	0.000586
10	0.0160	0.000836
11	0.0533	0.000860
12	0.237	0.000714

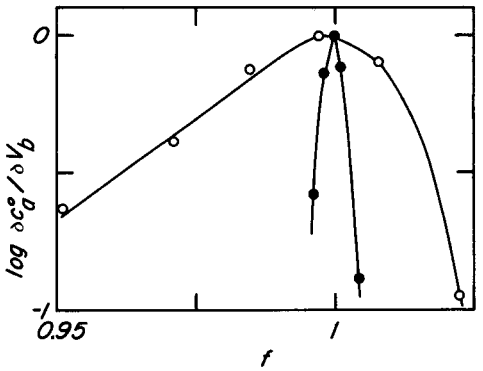

Fig. 1. Pointwise-variance-analysis plots for acids having pK_a values of 7 (solid circles) and 9 (open circles), according to unweighted regression with 25 points equally spaced along the pH axis over the range $0.025 < f < 1.125$. Every point having a relative influence (on the value of c_a^0) equal to, or greater than, 0.03 is shown.

Second, if the acid is very weak, the inclusion of points around and beyond the equivalence point worsens the precision with which c_a^0 can be evaluated. This is surprising, but the pointwise-variance-analysis plot in Fig. 2 shows why it is so. For points confined to the range $0.025 < f < 0.975$ there is a broad maximum in the relative influence at about $f = 0.35$: points at smaller values of f receive little weight in the calculations because they correspond to solutions so poorly buffered that the standard error of V_b corresponds to

TABLE 4

Standard errors of the parameters obtained by properly weighted non-linear regression (Each of these values was obtained with $\sigma_{pH} = 0.001$ and $V_b = 0.01$ cm^3; if both of these standard errors are multiplied by any factor F, the standard errors of the parameters will also be multiplied by F. The assumed experimental conditions are described in the text. Each set of data consisted of 25 points equally spaced along the pH axis over the specified range of values of f)

pK_a	Standard errors for data confined to the range $0.025 < f < 0.975$		Standard errors for data confined to the range $0.025 < f < 1.125$	
	c_a^0, %	pK_a, unit	c_a^0, %	pK_a, unit
1	0.0165	0.0189	—	—
3	0.0159	0.00277	—	—
5	0.0196	0.00122	—	—
7	0.0209	0.00132	0.0140	0.00168
9	0.0216	0.00104	0.0190	0.00158
10	0.0312	0.00093	0.0318	0.00138
11	0.0841	0.0089	0.0911	0.00140
12	0.230	0.0123	0.251	0.00151
13	0.479	0.0257	0.528	0.00178

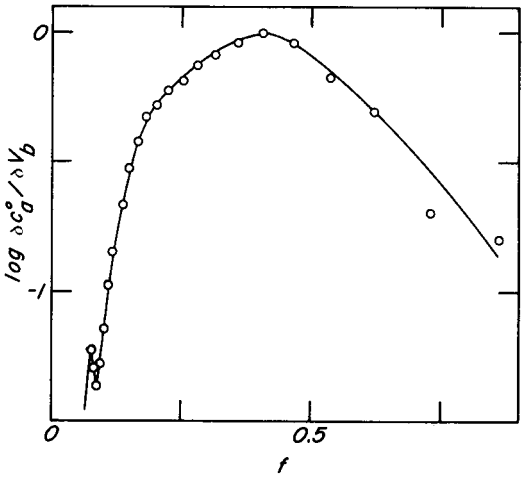

Fig. 2. Pointwise-variance-analysis plot for an acid having a pK_a value of 11, according to correctly weighted regression with 25 points equally spaced along the pH axis over the range $0.025 < f < 0.975$. No point falls outside the range of this plot.

a large uncertainty in the pH value, and points near the equivalence point also have little influence because the curve is nearly flat and featureless there in the titration of such a weak acid. Spreading the data over a wider range of values of f decreases the number of them that lie in the region of maximum influence, and therefore yields poorer results.

Third, if the acid is moderately strong, the inclusion of points around and beyond the equivalence point has little effect on the precision with which c_a^0 can be evaluated. This is because the additional information that these points would furnish about c_a^0 in an unweighted calculation is counterbalanced by the decrease in weight assigned to them by virtue of the fact that they correspond to relatively large values of $\sigma_{V_b}^2 (\mathrm{dpH/d}V_b)^2$.

Fourth, unweighted regression also overestimates the precision that can be obtained in evaluating pK_a, the standard error of which is, at best, very little better than that of the measurements of pH.

Although the general outlines of this picture are reasonable enough, some of its details are obscured by the tacit assumption that the value of K_w is known exactly. As this can scarcely be true unless the value of y_{H^+} is known as well, the calculations were repeated for data confined to the range $0.025 < f < 0.975$ (as for the second and third columns of Table 4), but with pK_w as a fourth adjustable parameter. The results given in Table 5 show three main features.

First, lack of knowledge regarding the value of K_w under the conditions of the titration has no appreciable effect on the precision with which c_a^0 can be evaluated for a moderately strong acid, but greatly worsens it for a very weak one. Of course, the first of these reflects the fact that the terms involving K_w in the equation that describes the titration curve are inappreciable for

TABLE 5

The effects of uncertainty regarding the value of pK_w on the standard errors of the parameters obtained by properly weighted non-linear regression
(Except for the inclusion here of pK_w as a fourth adjustable parameter, the calculations leading to these results were identical with the ones that led to the values given in the second and third columns of Table 4)

pK_a	Standard error of	
	c_a^0, %	pK_a, unit
5	0.0188	0.000484
7	0.0206	0.000513
9	0.0448	0.000586
10	0.156	0.00203
11	0.378	0.00542
12	1.03	0.0392
13	3.99	0.224

values of f below 0.975. As regards very weak acids, it may be emphasized that a titration curve obtained under these conditions has no point of maximum slope if pK_a exceeds about 11.5 [17], and that to achieve a relative standard error as small as a few per cent would be impossible by any technique that does not involve the use of non-linear regression.

Second, lack of knowledge regarding the value of K_w under the conditions of the titration improves the precision with which pK_a can be evaluated for a moderately strong acid, but worsens it for a very weak one. For a moderately strong acid the value of pK_w is not very precisely defined by data in this range, and part of the uncertainty that would otherwise be assigned to pK_a is assigned to pK_w instead. For a very weak acid, however, the value of pK_w is more reliably established by the data than that of pK_a, and both pK_a and y_{H^+} become very uncertain.

Third, the standard errors given in Table 5 correspond to particular values of σ_{pH} (= 0.001 unit) and σ_{V_b} (= 0.01 cm^3, or 0.04% of the volume required to reach the equivalence point). They would be inapplicable in other circumstances: if, for example, the pH meter could be read to only 0.01 unit, or if the reagent were added from a weight buret. The dependences of $\sigma_{c_a^0}$ and σ_{pK_a} on σ_{pH} and σ_{V_b} can be most compactly described by means of two new parameters defined by the equations

$$F = \sigma_{pH}/0.001; \quad G = \sigma_{V_b}/0.001 \; [= F\,\sigma_{V_b}/\sigma_{pH}] \tag{9}$$

The fundamental equation

$$\sigma_{V_i}^2 = \sigma_{pH}^2 (\partial V_i/\partial pH)^2 + \sigma_{V_b}^2 (\partial V_i/\partial V_b)^2 \tag{10}$$

can then be rewritten as

$$\sigma_{V_i} = F \{0.001 [(\partial V_i/\partial pH)^2 + (G/F)^2 (\partial V_i/\partial V_b)^2]^{1/2}\} = F\,\sigma_{V_i}^* \tag{11}$$

where $\sigma_{V_i}^*$ denotes the quantity within braces. It depends on the ratio G/F,

TABLE 6

Values of $\sigma^*_{V_i}$ for various values of G/F
(The significance of these values is described in the text. Values of $\sigma^*_{c_a^0}$ are relative standard errors and are expressed as percentages; values of $\sigma^*_{pK_a}$ are absolute standard errors and are expressed in pK units)

pK_a	G/F = 100		31.6		10		3.16	
	$\sigma^*_{c_a^0}$	$\sigma^*_{pK_a}$	$\sigma^*_{c_a^0}$	$\sigma^*_{pK_a}$	$\sigma^*_{c_a^0}$	$\sigma^*_{pK_a}$	$\sigma^*_{c_a^0}$	$\sigma^*_{pK_a}$
5	0.167	0.00743	0.0642	0.00511	0.0188	0.00484	0.00870	0.00282
7	0.222	0.00392	0.0716	0.00182	0.0206	0.000513	0.0129	0.000382
9	0.393	0.00631	0.177	0.00222	0.0448	0.000586	0.0250	0.000310
10	1.50	0.00654	1.41	0.00567	0.156	0.00203	0.146	0.00109
11	13.7	0.0537	2.30	0.00778	0.378	0.00542	0.360	0.00351
12	—	—	—	—	1.03	0.0392	1.01	0.0307
13	—	—	—	—	3.99	0.224	3.10	0.197

pK_a	G/F = 1		0.1		0.01	
	$\sigma^*_{c_a^0}$	$\sigma^*_{pK_a}$	$\sigma^*_{c_a^0}$	$\sigma^*_{pK_a}$	$\sigma^*_{c_a^0}$	$\sigma^*_{pK_a}$
5	0.00621	0.000960	0.00582	0.000487	0.00375	0.000152
7	0.00628	0.000308	0.00572	0.000250	0.00572	0.000201
9	0.0230	0.000292	0.0198	0.000269	0.0208	0.000255
10	0.144	0.000895	0.139	0.000780	0.140	0.000721
11	0.351	0.00273	0.328	0.00255	0.334	0.00202
12	1.02	0.0319	1.01	0.0316	1.01	0.0339
13	2.64	0.192	1.82	0.184	1.70	0.184

and does so in a complex way because a change of that ratio affects the relative weights assigned to the experimental points.

Table 6 summarizes the dependence of $\sigma^*_{V_i}$ on G/F. It provides the values of $\sigma^*_{c_a^0}$ and $\sigma^*_{pK_a}$ that correspond to the strength of the acid being titrated and the value of G/F that characterizes the precisions of the measurements. These values of $\sigma^*_{V_i}$ need only be multiplied by F to find the values of $\sigma_{c_a^0}$ and σ_{pK_a}. A wide range of conditions is covered: the value $G/F = 0.001$ corresponds, for example, to $\sigma_{V_b} = 0.0001$ cm^3 and $\sigma_{pH} = 0.01$, and thus to titrations employing weight burets together with pH meters that can be read to only two decimal places, whereas the value $G/F = 100$ corresponds, for example, to $\sigma_{V_b} = 0.1$ cm^3 and $\sigma_{pH} = 0.001$, and thus to a combination of inordinately crude measurements of volume with extremely precise ones of the pH.

Wider variations of σ_{V_b}/σ_{pH} are certainly possible. For example, σ_{V_b} might be as small as 5×10^{-6} cm^3 if the reagent were added from a microburet. However, all these calculations have been based on the assumption that 25 cm^3 of reagent is consumed at the equivalence point, and therefore the actual value of σ_{V_b} should be corrected to accord with that assumption before employing Table 6. Some error will arise because r is unlikely to be close to 1 when such a correction is necessary, but the magnitude of that error is unlikely to be large enough to distort the qualitative picture.

This work was made possible by support from the Nederlandse Organisatie voor Zuiver Wetenschappelijk Onderzoek, and was aided in part by grant number CHE-8106103 from the National Science Foundation.

REFERENCES

1 T. Anfalt and D. Jagner, Anal. Chim. Acta, 57 (1971) 165.
2 F. Ingman, A. Johansson, S. Johansson and R. Karlsson, Anal. Chim. Acta, 64 (1973) 113.
3 A. F. Isbell, Jr., R. L. Pecsok, R. H. Davies and J. H. Purnell, Anal. Chem., 45 (1973) 2326.
4 D. M. Barry and L. Meites, Anal. Chim. Acta, 68 (1974) 435.
5 D. M. Barry, L. Meites and B. H. Campbell, Anal. Chim. Acta, 69 (1974) 143.
6 T. N. Briggs and J. E. Stuehr, Anal. Chem., 46 (1974) 1517.
7 S. L. Young, E. Matijević and L. Meites, J. Phys. Chem., 78 (1974) 2626.
8 J. W. Frazer, W. Selig and L. P. Rigdon, Anal. Chem., 47 (1975) 1081.
9 L. Meites, J. E. Stuehr and T. N. Briggs, Anal. Chem., 47 (1975) 1486.
10 D. Murtlow and L. Meites, Anal. Chim. Acta, 92 (1977) 285.
11 S. R. Goode, Anal. Chem., 49 (1977) 1408.
12 L. M. Schwartz and R. I. Gelb, Anal. Chem., 50 (1978) 1571.
13 G. Nowogrocki, J. Canonne and M. Wozniak, Anal. Chim. Acta, 112 (1979) 185.
14 J. J. Lingane, Electroanalytical Chemistry, Interscience, New York, 1953, p. 74.
15 E. Bishop, Anal. Chim. Acta, 22 (1960) 101.
16 F. H. Clarke, Calculator Programming for Chemistry and the Life Sciences, Academic Press, New York, 1981, p. 87.
17 L. Meites and J. A. Goldman, Anal. Chim. Acta, 29 (1963) 472.
18 L. Meites, Anal. Chim. Acta, 74 (1975) 177.
19 L. Meites, The General Multiparametric Curve-Fitting Program CFT4A, privately published, 1983.
20 L. Meites, M. P. Colombini, L. Lampugnani and T. Rotunno, Anal. Chim. Acta, 152 (1983) 53.

Analytica Chimica Acta, 152 (1983) 73—82
Elsevier Science Publishers B.V., Amsterdam — Printed in The Netherlands

SYNCHRONOUS FLUORESCENCE SPECTROSCOPY WITH A SILICON-INTENSIFIED TARGET VIDICON

JAMES E. THOMPSON and HARRY L. PARDUE*
Department of Chemistry, Purdue University, West Lafayette, IN 47907 (U.S.A.)
(Received 11th January 1983)

SUMMARY

A silicon-intensified target vidicon is evaluated as a detector for synchronous fluorescence spectroscopy. Data acquired in the form of 180 emission spectra at each of 100 excitation wavelengths are stored in computer memory. Synchronous spectra are obtained as diagonals through the data matrix that correspond to fixed wavelength differences ($\Delta\lambda$) between excitation and emission wavelengths. Single- and two-component mixtures of anthracene, 9,10-diphenylanthracene, perylene, and tetracene were studied. Of the possible mixtures, synchronous spectra for three exhibited no detectable interactions; spectra for two exhibited one-way interactions; and spectra for one exhibited two-way interactions. Relative pooled standard deviations were in the range of 1% for single-component samples and 4—8% for two-component samples. Detection limits at the 95% confidence level were estimated between 0.005 mg l^{-1} (perylene) and 0.17 mg l^{-1} (anthracene).

Several earlier papers from this laboratory have described evaluations of imaging detectors for quantitative spectroscopy. Studies have included molecular absorption [1], molecular luminescence [2], atomic absorption [3], and atomic emission [4] spectroscopy. These and other studies have been summarized in recent reviews [5, 6]. This paper describes an extension of these studies to an evaluation of a silicon-intensified target vidicon (SITV) for synchronous fluorescence spectroscopy.

As implemented to date, synchronous fluorescence spectroscopy has involved the simultaneous scanning of excitation and emission monochromators with a small fixed wavelength [7] or frequency [8] difference ($\Delta\lambda$ or $\Delta\nu$) between them. This procedure provides a selection process in which only one of the several possible emission bands in a compound is monitored. The result is a relatively narrow emission band that reduces overlap among different components in mixtures. The resulting synchronous spectrum can offer improved selectivity and detection limits relative to the more conventional procedures in which several emission bands for all components in mixtures are superimposed [7].

Although mechanically-scanned spectrometers have been used effectively for synchronous fluorescence, they have some inherent limitations. Because different components in mixtures may require different operating parameters

0003-2670/83/$03.00

(e.g., $\Delta\lambda$ or $\Delta\nu$) for optimum performance, it may be difficult or time-consuming to achieve optimum performance with a mechanically-scanned system. It was judged that electronically-scanned imaging detectors could offer substantial improvements in versatility and speed relative to the more conventional systems. This paper describes initial results obtained with a silicon-intensified target vidicon applied to polynuclear aromatic hydrocarbons (PAH's).

Samples containing one or two PAH's were studied. Results confirm the feasibility of the concept and demonstrate advantages of versatility and speed inherent in the imaging detector. However, to date, detection limits are well above those reported with more conventional instrumentation [9].

EXPERIMENTAL

Instrumentation

The instrumental system is similar to that described earlier [2] except that the pulsed source is replaced with a continuous source and an excitation polychromator is arranged so that excitation energy is dispersed along the vertical axis of the sample cell [10]. In this way, emission spectra at different points along the vertical axis of the sample cell correspond to different excitation wavelengths. The resulting two-dimensional pattern of excitation/emission spectra is then monitored by the two-dimensional imaging detector (SITV) with the horizontal axis corresponding to emission spectra at different excitation wavelengths along the vertical axis. The output from the SITV is monitored by an on-line computer.

There are several options for using such a data set available on the active surface of the detector. These options include recording conventional emission or excitation spectra along the horizontal or vertical axes, recording the full excitation/emission spectra, or recording spectra along selected diagonal axes. It is easily shown that properly-selected diagonal axes can yield responses at emission wavelengths (λ_{em}) that are at fixed wavelength spacings ($\Delta\lambda$) from excitation wavelengths (λ_{ex}). This is analogous to the procedure used to generate synchronous fluorescence spectra with mechanically-scanned systems [7]. A potential advantage of the present system is that many scans with different values of $\Delta\lambda$ can be obtained in a fraction of a second. Thus, it is convenient to select the most suitable $\Delta\lambda$ value for each component in a sample.

The option used in this study was to record the entire excitation/emission spectra, and then to select the desired data as needed from computer memory. This permitted a variety of data-processing options to be evaluated.

More complete details of the instrument are described below.

Optical system. The excitation source is a 500-W, prefocused, xenon arc lamp (Optical Radiation Co., Azuza CA 91702), with an XIG-65 igniter, and a 533-02 power supply. The lamp module is enclosed in a water-cooled housing and is vented to a hood. Radiofrequency shielding and a power line

filter were used to protect other equipment from the effects of the high voltage pulse used to ignite the lamp.

Radiation from the lamp is passed through an attenuating pinhole and focused by a quartz lens (No. 2, 33-86-29, Bausch and Lomb, Rochester, NY 14602) onto the entrance slit of the excitation polychromator consisting of a visible grating (33-86-02, Bausch and Lomb) in an appropriate housing (33-86-26, Bausch and Lomb). The polychromatic light leaving the excitation polychromator is focused by a 75-mm focal length $f/3$ quartz lens (Oriel Corp., Stamford, CT 06902) into the center of a standard 1-cm pathlength quartz cuvette (Markson Science, Del Mar, CA 92014) held in a water-cooled holder. The 1350 groove mm^{-1} ruling density of the grating in the excitation polychromator yields an excitation range of 280 nm at the sample cuvette.

The fluorescence emission is gathered by a 150-mm focal length, $f/3$ glass lens and a 75-mm focal length lens (both Oriel Corp.) onto the entrance slit of an emission polychromator (prototype UFS-200, J-Y Optical Systems, Metuchen, NJ 08840). The custom mounting assembly used with this polychromator allows adjustment of the focus to obtain the best resolution over the wavelength range of 300—600 nm. The 50-μm slit width used throughout this work gave a theoretical bandpass of 5 nm and an observed bandpass of 7 nm. An electronically-controlled shutter is placed in front of the entrance slit of this polychromator to permit dark-current correction.

Silicon-intensified target vidicon. Schematics for the SITV interface circuitry are available on request; this discussion addresses only the most critical features.

The intensifier stage of the SITV (4804/P5, Radio Corporation of America, Lancaster, PA 17604) was operated at a potential of —9 kV. The potential at the focus/gating electrode is fixed at 98% of the intensifier voltage by a passive voltage divider network. The horizontal (emission) and vertical (excitation) axes are scanned in 180 and 100 steps, respectively, under computer (PDP-8/M, Digital Equipment Corp., Maynard, MA) control. Each of the 18 000 points in a complete scan corresponds to an excitation/emission wavelength pair. Wavelength calibration for both axes was accomplished with lines from a mercury pen lamp and confirmed by comparison of peaks for single-component samples with published spectra. A brief description of a typical sequence for data acquisition is presented below.

Prior to a run, the shutter is closed and the active surface of the SITV is erased using a conventional line scan format. At the end of this process, an end-of-scan pulse initiates loading of X and Y digital-to-analog converters with digital words corresponding to the first X and Y coordinates to be interrogated. After an integration period (50—75 ms in this work unless noted otherwise), the electron beam is unblanked, a sample-and-hold amplifier is gated to hold, and the analog-to-digital converter is signalled to being a conversion. This acquisition cycle is repeated for different XY coordinates until a complete horizontal scan has been acquired.

When the last X coordinate has been addressed, the SITV is placed in an erase mode and the data set just acquired is either negated (dark current run) or stored in computer memory (intensity run). After completion of this process, a new vertical and horizontal coordinate is output to the SITV interface and the cycle is repeated until all data have been acquired.

When all vertical levels have been interrogated, the data are written to several disk files for later processing. The data acquisition routines were written in the SABR assembly language (DEC).

Reagents

Stock solutions of anthracene (98+%), 9,10-diphenylanthracene (99+%) and perylene (99+%) (all from Aldrich Chemical Co., Milwaukee, WI 53233) were prepared at concentrations of 100 mg l^{-1} in cyclohexane (99.5%, Philips Chemical Co., Spec Chemical Division, Bartlesville, OK 74004). Tetracene (2,3-benzanthracene; Aldrich Chemical Co.) was prepared at a stock concentration of 10 mg l^{-1} in the same solvent. These stock solutions were diluted with cyclohexane to obtain the desired concentrations.

RESULTS

After the wavelength axes had been calibrated and it had been verified that the system responded linearly to changes in intensity, fluorescent spectra were recorded for one- and two-component samples of the four polynuclear aromatic hydrocarbons. Representative results are presented here.

Single-component samples

To establish reference data with which to compare mixture results, different concentrations of each of the four hydrocarbons were examined.

Figure 1 shows the spectrum of anthracene obtained with an excitation wavelength of 375 nm. This spectrum exhibits a width at half-height of 13 nm which is characteristic of the system. The spectrum also exhibits significant attenuation of the peak at 378 nm as a result of the glass window on the SITV. The peak at 400 nm was chosen for quantitative applications.

For each concentration of each hydrocarbon, three spectra were recorded on each of three aliquots of each sample to obtain estimates of within-run and between-run imprecision. For anthracene (0.25—1.0 mg l^{-1}), the pooled within-run relative standard deviation was 0.84% and the between-run RSD was not significantly different. The between-run scatter is observable in curve (e) of Fig. 2 which includes peak intensities for each of three aliquots at each concentration. The data also demonstrate good linearity.

Quantitative results for anthracene and the single-component samples are summarized in Table 1. Using the standard errors and the sensitivities, the 95% confidence level detection limits are estimated to be 0.17, 0.04, 0.005, and 0.08 mg l^{-1} for anthracene, 9,10-diphenylanthracene, perylene, and tetracene, respectively. These detection limits are well above values reported

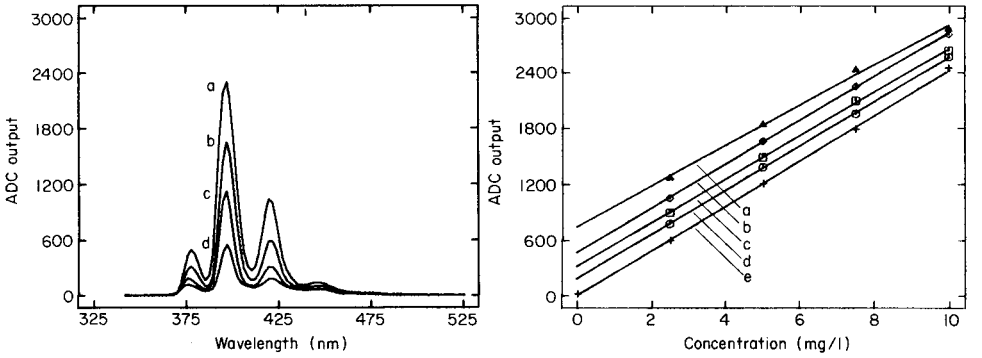

Fig. 1. Fluorescence emission spectra for different concentrations of anthracene (λ_{ex} = 375 nm). Curves (a—d) 10, 7.5, 5.0, and 2.5 mg l^{-1}, respectively.

Fig. 2. Calibration data for anthracene with and without 9,10-diphenylanthracene present: (a—d) anthracene with 1.0, 0.75, 0.5, and 0.25 mg l^{-1} 9,10-diphenylanthracene, respectively ($\Delta\lambda$ = 22 nm, λ_{em} = 400 nm); (e) pure anthracene (λ_{ex} = 375 nm, λ_{em} = 400 nm).

earlier [9]; however, it should be noted that much longer (×100) integration times were used in the earlier work [9], that detection limits are influenced by excitation source intensity, and that no attempts were made to optimize detection limits in this work.

Two-component samples

All possible two-component combinations of the four compounds were examined. Synchronous spectra for three mixtures (anthracene/perylene, tetracene/9,10-diphenylanthracene, and perylene/tetracene) exhibited no

TABLE 1

Least-squares statistics[a] for pure component samples of anthracene, 9,10-diphenylanthracene, perylene, and tetracene

Solute	Slope ± s.d. (10^2 ADC units/mg l^{-1})		Intercept ± s.d. (10^2 ADC units)		Corr. coeff.	Std. error (10^2 ADC units)	Pooled r.s.d. (%)
Anthracene (2.5—1.00 mg l^{-1})	2.28	0.01	0.014	0.08	0.999	0.20	0.84
9,10-diphenylanthracene (0.25—1.00 mg l^{-1})	23.2	0.3	0.44	0.2	0.997	0.49	0.95
Perylene (0.025—0.100 mg l^{-1})	260	3.5	0.82	0.24	0.997	0.60	1.4
Tetracene (0.25—1.00 mg l^{-1})	22.0	0.5	2.5	0.36	0.991	0.87	1.4

[a]Three measurements on each of four samples (n = 12) for each compound.

interaction; spectra for two mixtures (anthracene/tetracene and 9,10-diphenylanthracene/perylene) exhibited one-way interactions, and spectra for one mixture (anthracene/9,10-diphenylanthracene) exhibited two-way interactions. Representative results are discussed here.

No interaction. Emission spectra at the excitation maxima for perylene and tetracene shown in Fig. 3 exhibit significant overlap throughout the emission range for each compound. Accordingly, careful control of the excitation wavelength is needed to be able to quantify either component in the presence of the other. However, although there is overlap between the spectra, it is observed that the principal bands at 445 and 480 nm are well separated from each other, suggesting that the synchronous spectra may be independent of one another.

Figure 4 shows synchronous spectra that exhibit the expected separation. The most significant feature of the spectra is the fact that the peak height for the species that is kept constant does not vary in a systematic way as the concentration of the other species is varied. The same general behavior was exhibited for other concentrations of each of the two hydrocarbons. Figure 5 shows data for tetracene in the presence of four different concentrations of perylene. The scatter about the line is not significantly different from the scatter about the line for pure tetracene.

Mixtures of anthracene with perylene and of tetracene with 9,10-diphenylanthracene behaved in similar manner with no systematic interactions.

One-way interactions. Mixtures of anthracene with tetracene and of 9,10-diphenylanthracene with perylene exhibited one-way interactions with the apparent intensities for tetracene and perylene being enhanced by the presence of the anthracenes. The influence 9,10-diphenylanthracene on perylene is less surprising than the effect of anthracene on tetracene because of the relative proximity of the bands for 9,10-diphenylanthracene and perylene. Figure 6 shows the synchronous spectra for different concentra-

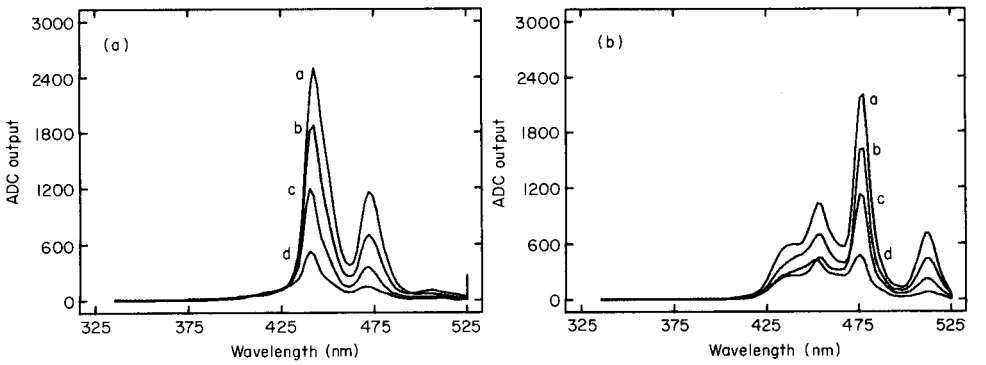

Fig. 3. Fluorescence emission spectra for different concentrations of perylene and tetracene. A. Perylene: curves (a—d) 0.1, 0.075, 0.05, and 0.025 mg l^{-1}; λ_{ex} = 438 nm. B. Tetracene: curves (a—d) 1.0, 0.75, 0.5, and 0.25 mg l^{-1}; λ_{ex} = 475 nm.

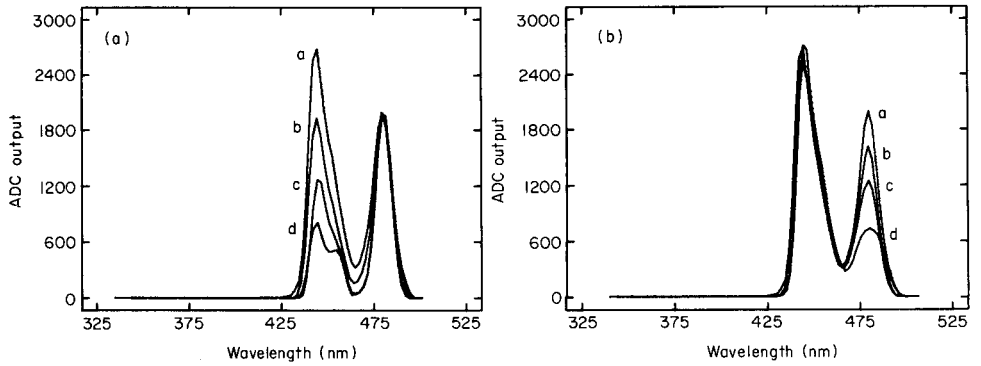

Fig. 4. Synchronous fluorescence spectra for perylene and tetracene ($\Delta\lambda$ = 5 nm). A. Perylene: conditions as in Fig. 3A. B. Tetracene: conditions as in Fig. 3B.

tions of tetracene in the presence of a fixed concentration of anthracene. Given the large separation and complete resolution of the bands, the effect of anthracene on the tetracene signal is surprising. The reason for this effect is not understood but probably relates to the fact that a rather large $\Delta\lambda$ value (10 nm) was used to excite the 400 nm band for anthracene. A detector that would be responsive to the anthracene band at 378 nm would likely reduce or eliminate this problem. This and other aspects of the problem are being studied.

The principal effect of the interaction in each case is to shift the calibration graph along the vertical (intensity) axis (see Fig. 2 for anthracene with 9,10-diphenylanthracene). The effect of anthracene on tetracene is quantified

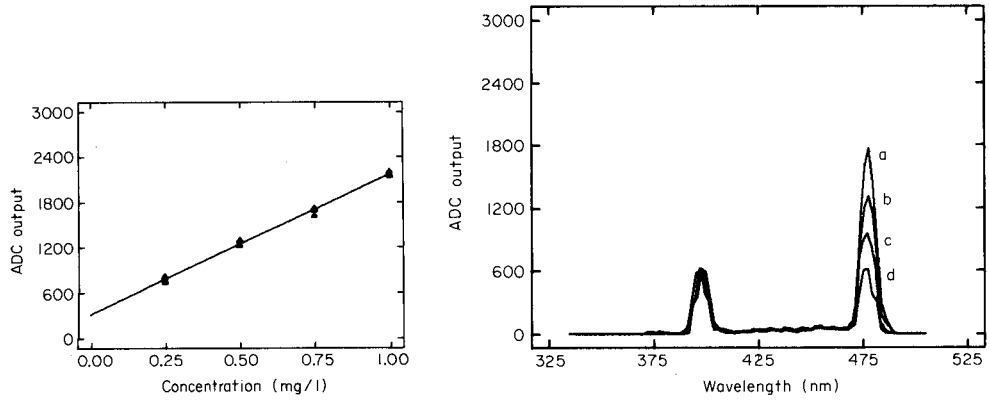

Fig. 5. Calibration plot for tetracene in presence of different concentrations (0.025—1.0 mg l^{-1}) of perylene.

Fig. 6. Synchronous fluorescence spectra for different concentrations of tetracene with anthracene ($\Delta\lambda$ = 10 nm). Curves (a—d): 1.0, 0.75, 0.5, and 0.25 mg l^{-1} tetracene, respectively, with 2.5 mg l^{-1} anthracene.

by the least-squares equation

$$I_{454} = 17 \times 100\, C_{tet} + 36\, C_{ant} + 3$$

in which I_{454} is the apparent peak height for tetracene and C_{tet} and C_{ant} are the concentrations (mg l^{-1}) of tetracene and anthracene. Standard deviations for the constants in sequence are 95, 9.5, and 88, respectively. The contribution of anthracene to the apparent tetracene signal for equal concentrations is about 2.1%; the intercept is not significantly different from zero.

The effect of 9,10-diphenylanthracene on perylene is quantified with the equation

$$I_{445} = 23 \times 10^3\, C_{per} + 1.4 \times 10^2\, C_{dip} + 8 \times 10^2$$

in which the standard deviations of the constants in sequence are 1.7×10^3, 1.6×10^2, and 1.5×10^2. The contribution of 9,10-diphenylanthracene to the perylene signal for equal concentrations is about 0.6%.

In each case, the interactions are significant only for substantial excesses of each interferent relative to the species with which it interferes.

Two-way interaction. The only combination for which two-way interactions were observed was anthracene with 9,10-diphenylanthracene. This interaction was imposed primarily by characteristics of the detector (SITV) and the optical system rather than a limitation of the general approach. Because the detector was insensitive to the 378-nm band for anthracene, it was necessary to use a relatively large value of $\Delta\lambda$ (22 nm) so that the 400-nm band could be used for anthracene. This large value of $\Delta\lambda$ also caused significant interference between the band at 400 nm for anthracene and that at 408 nm for 9,10-diphenylanthracene. It was possible to reduce the effect of anthracene on 9,10-diphenylanthracene by monitoring the band at 428 nm for the latter; however, it was not possible to eliminate the interactions.

Plots (a–d) in Fig. 2 show the effects of 9,10-diphenylanthracene on the peak intensity at 400 nm which results primarily from anthracene. The principal effect is to shift the calibration plots along the vertical axis with little significant change in the slope. Although the effect may appear small in the figure, the ten-fold difference in concentrations should be noted. The effect is quantified with the least-squares equation

$$I_{400} = 23.1 \times 10\, C_{ant} + 59 \times 10\, C_{dip} + 70$$

for which the standard deviations of the constants in sequence are 6, 64, and 60, respectively. Thus, for equal concentrations, 9,10-diphenylanthracene contributes a signal at 400 nm that is about 2.5-fold that for anthracene.

The analogous equation at 428 nm is

$$I_{428} = 14.3 \times 10^2\, C_{dip} + 52\, C_{ant} + 21$$

for which the standard deviations in sequence are 99, 10, and 92. The contribution of anthracene to the signal at 428 nm for equal concentrations is only about 3.7% of that of 9,10-diphenylanthracene.

DISCUSSION

Results for perylene and tetracene (Figs. 3 and 4) illustrate the principal advantage of the approach illustrated herein, namely the ability to select whatever pairs of excitation/emission wavelengths are appropriate to provide the highest degree of selectivity for a particular group of compounds. Although synchronous spectra were presented for these components (Fig. 5), it is important to note that the actual calibration data correspond to the emission at a single wavelength-resolution element for a single excitation resolution element. Thus, in practical applications in which there are no interactions, time spent in this study recording all the spectral data could be spent integrating or making repetitive measurements at the particular $\lambda_{ex}/\lambda_{em}$ pairs of interest.

Other data, such as those involving one-way and two-way interactions reflect some limitations in the data obtained in this study. It is important to recognize which of these limitations are representative of the general approach and which are representative of the way it was implemented here. The two principal limitations of the instrumental system used were the short-wavelength cutoff of the detector and the relatively poor spectral resolution of the optical system. The reduced sensitivity below 400 nm forced the use of relatively broad values of $\Delta\lambda$ for anthracene and 9,10-diphenylanthracene, which contributed to interactions between these and other components. These interactions were further aggravated by spectral bandwidths of about 15 nm.

The principal limitation of the general approach described is the stray light that results from continuous illumination of the sample with all excitation wavelengths simultaneously. Some preliminary studies indicated that the detection limits reported above can be improved by using longer integration times. However, the lower limit is imposed by stray light. We are investigating alternative approaches intended to reduce effects of stray light.

Although it is expected that most of the interactions described above can be reduced or eliminated with alternative instrumental characteristics (better short-wavelength response and improved spectral resolution), the data for interactive pairs illustrate an important point. Because the combined signals tend to be additive (see Fig. 2), it should be possible to use either single equations for one-way interactions or simultaneous equations for two-way interactions to resolve mixtures. An alternative and potentially better approach would be to use multiwavelength methods analogous to those used for absorption data [6].

These and other options are being investigated.

REFERENCES

1 M. J. Milano and H. L. Pardue, Anal. Chem., 47 (1975) 25.
2 D. E. Goeringer and H. L. Pardue, Anal. Chem., 51 (1979) 1054.
3 H. L. Felkel, Jr. and H. L. Pardue, Clin. Chem., 24 (1978) 602.
4 H. L. Felkel, Jr. and H. L. Pardue, Anal. Chem., 50 (1978) 602.

5 Y. Talmi, Anal. Chem., 47 (1975) 658A.
6 H. L. Pardue, in J. K. Foreman and P. B. Stockwell (Eds.), Topics in Automatic Chemical Analysis, Horwood, Chichester, 1979, Ch. 6.
7 T. Vo-Dihn, Anal. Chem., 50 (1978) 396.
8 E. L. Inman, Jr. and J. D. Winefordner, Anal. Chim. Acta, 141 (1982) 241.
9 A. Jurgensen, E. L. Inman, Jr. and J. D. Winefordner, Anal. Chim. Acta, 131 (1981) 187.
10 Y. Talmi, Anal. Chem., 50 (1978) 936A.

Analytica Chimica Acta, 152 (1983) 83—93
Elsevier Science Publishers B.V., Amsterdam — Printed in The Netherlands

A STUDY OF THE INTERACTIONS OF BENZO[f]QUINOLINE, QUINOLINE AND PHENANTHRENE BY INFRARED AND REFLECTANCE SPECTROSCOPY AND THE RELATIONSHIP TO ROOM-TEMPERATURE PHOSPHORESCENCE

S. M. RAMASAMY[a] and R. J. HURTUBISE*
Chemistry Department, University of Wyoming, Laramie, WY 82071 (U.S.A.)
(Received 21st February 1983)

SUMMARY

Reflectance spectroscopy is used to provide evidence for the forms of benzo[f]-quinoline and quinoline adsorbed on filter paper, silica gel chromatoplates, and 0.5% polyacrylic acid—NaCl mixture. Infrared data suggest several hydrogen bonding interactions for benzo[f]quinoline and phenanthrene with polyacrylic acid—salt mixtures. With the reflectance and infrared data, a partial model for phosphor/solid surface interaction was developed for the compounds; this model should be useful in room-temperature phosphorescence work.

Little work has been reported on the interactions responsible for room-temperature phosphorescence (r.t.p.) from compounds adsorbed on solid surfaces. The effects of moisture and oxygen on the r.t.p. of sodium 4-biphenylcarboxylate and sodium 1-naphthoate adsorbed on filter paper were investigated [1]; it was suggested that hydrogen bonding of ionic organic molecules to hydroxyl groups of the filter paper was the primary mechanism of providing the rigid matrix for r.t.p., and that moisture helps to disrupt hydrogen bonding and to transport oxygen to the sample matrix. The interactions responsible for r.t.p. of *p*-aminobenzoic acid adsorbed on sodium acetate were also investigated [2]; reflectance spectroscopy indicated that the main interactions involved the formation of sodium *p*-amino-benzoate (the phosphor) and hydrogen bonding with sodium acetate. The resulting data also indicated that the molecule was adsorbed flatly on sodium acetate. It has been postulated that nitrogen heterocycles are held rigidly by hydrogen bonding interactions on silica gel chromatoplates which contain an acidic polymer binder [3]. In a recent study, the dianion of terephthalic acid adsorbed on the sodium salt of polyacrylic acid gave a relatively high phosphorescence signal [4]; with this system no hydrogen bonds could be formed. The phosphorescence lifetime of 2-naphthalenesulfonate on filter

[a]Present Address: Department of Chemistry, Gobi Arts College, Gobichettipalayam 638453, India.

0003-2670/83/$03.00

paper with various nonphosphorescent compounds added individually to the filter paper has been measured [5]. It appeared that packing the solid matrix with materials such as salts or sugars inhibited the internal motion of the phosphor. In addition, the added compounds could clog the channels and interstices of the matrix, decreasing oxygen and moisture permeability. The importance of various salts and solvents used to adsorb the phosphor on solid surfaces was reported [6]; both the salt content and the adsorbing solvent were important in obtaining optimal r.t.p., and the importance of the initial wet solid-surface chemistry was demonstrated.

Nonluminescent techniques have been used rarely to study interactions responsible for r.t.p. Reported here are the results from infrared and reflectance experiments. Evidence is given for several interactions that appear to be important for the r.t.p. of model nitrogen heterocyclic compounds and phenanthrene.

EXPERIMENTAL

Apparatus and reagents

All infrared spectra were obtained with a Beckman IR-10 spectrometer. The spectra were stored on floppy disks using a Bascom-Turner (model 4120) data system. Two sampling intervals (758 ms and 532 ms) were used with the data system to record the 4000—2000 cm^{-1} and 2000—6000 cm^{-1} regions of the infrared spectra. Reflectance spectra were recorded with a Cary model 14R spectrophotometer, using a Cary 1411 diffuse-reflectance accessory. Solution ultraviolet absorption spectra were obtained with a Hitachi 100-80 spectrophotometer.

Ethanol was purified by distillation. The nitrogen heterocyclic compounds and phenanthrene were recrystallized from ethanol. Polyacrylic acid (PAA), secondary standard, was used as received (Scientific Polymer Products, Ontario, NY). Silica gel chromatoplates (EM Laboratories, Elmsford, NY) and Whatman No. 1 paper (Whatman, Clifton, NJ) were used.

Procedures

Infrared spectra. Polyacrylic acid was ground with potassium bromide in a ball-mill to give a 1% (w/w) mixture as a homogeneous powder. An ethanolic or ethanolic 0.1 M hydrobromic acid solution of the phosphor (2 mg) was added to 200 mg of the mixture and then dried at 80°C for 30 min. A 100-mg sample of the dried mixture was pelleted in the usual die at a pressure of 20 000 lbs for 15—20 min. A beam attenuator was used in the reference beam of the infrared spectrometer, if necessary. All stored spectra were smoothed once or twice by averaging over a moving group of 5 points (as described by the manufacturer) before the first-derivative spectra were obtained.

Reflectance spectra. Ethanolic or ethanolic 0.1 M hydrobromic acid solutions containing 200 ng of phosphor were spotted onto filter paper, silica

gel chromatoplate or 0.5% (w/w) PAA—NaCl mixture and dried at 80°C for 30 min. The paper and chromatoplate samples were directly loaded into the sample port of the diffuse reflectance accessory. The PAA—NaCl mixture was added to the cavity of a blackened plexiglas plate and covered with a quartz plate before loading into the sample port. Ethanol-treated and dried samples of the carrier material were used in the reference port.

RESULTS AND DISCUSSION

Reflectance spectroscopy

Reflectance spectroscopy has been used to show that *p*-aminobenzoate is the phosphor adsorbed on sodium acetate giving r.t.p. [2], and that the protonated form of benzo[f]quinoline (B[f]Q) is the adsorbed phosphor on a silica gel chromatoplate [3]. In this work, reflectance spectra were obtained for B[f]Q and quinoline adsorbed on filter paper (Whatman No. 1), 0.5% PAA—NaCl, and EM silica gel chromatoplates under neutral and acidic conditions. Solution absorption spectra were also obtained for B[f]Q and quinoline. Table 1 gives the absorption wavelengths for B[f]Q in solution and on three different solid surfaces under several conditions. Comparison of the absorption wavelengths from the reflectance data with those from the solution data indicates if the neutral form of B[f]Q, the cation of B[f]Q, or

TABLE 1

Absorption wavelengths of benzo[f]quinoline and quinoline in ethanolic solutions and on different surfaces

Conditions	Absorption wavelengths (nm)[a]	
	Benzo[f]quinoline	Quinoline
Solutions[b]		
Ethanol	346, 330, 316, 267, 234	314, 300, 277
Ethanol, 0.1 M HCl	364, 280, 235, 229	314
Ethanol, 0.1 M HBr	364, 280, 236, 229	314
Solid surfaces[c]		
Filter paper, ethanol	347, 331	314, 300, 275
Filter paper, 0.1 M HCl	365, 293	314
Filter paper, 0.1 M HBr	365, 293	312—314
Silica gel chromatoplate, ethanol	345	313, 298, 285
Silica gel chromatoplate, 0.1 M HCl	364	312
Silica gel chromatoplate, 0.1 M HBr	364	314
0.5% PAA—NaCl, ethanol	367, 347, 330, 278	313
0.5% PAA—NaCl, 0.1 M HCl	367	314
0.5% PAA—NaCl, 0.1 M HBr	363	314

[a]Maximum absorption wavelength underlined. [b]The reproducibility was ±0.4 nm based on manufacturer's specifications. [c]The reproducibility was ±2 nm based on duplicate runs.

both, are adsorbed on the solid surfaces in the ground state. As expected, fewer absorption bands were obtained with the reflectance spectra than with the absorption spectra. Comparison of the reflectance wavelengths for B[f]Q adsorbed on filter paper from ethanol with the absorption wavelengths in ethanol shows that the neutral form of B[f]Q is the predominant form adsorbed on filter paper. For the 0.1 M acid solutions of B[f]Q adsorbed on paper, the data indicate that the cation of B[f]Q is adsorbed in relatively large amounts on the paper.

For B[f]Q spotted from neutral ethanol onto the silica gel chromatoplate, Table 1 shows that the neutral form of B[f]Q is adsorbed. With B[f]Q spotted from either 0.1 M HCl or 0.1 M HBr, one strong band appeared at 364 nm in the reflectance spectra. These results show that the cation of B[f]Q is adsorbed on the surface. For a discussion of the binder in these chromatoplates and its effect on the r.t.p. of B[f]Q, earlier reports can be consulted [3, 7].

Benzo[f]quinoline adsorbed from an ethanolic solution onto 0.5% PAA—NaCl gave, in addition to the bands at 347 nm and 330 nm, one at 367 nm (Table 1), indicating that both the cationic and neutral forms of B[f]Q were adsorbed on the surface. The results indicated that PAA protonated some of the B[f]Q in the initial "wet" state and thus the cation of B[f]Q appeared on the surface. Polyacrylic acid undergoes reactions characteristic of carboxylic acids and aqueous solutions of the polyacid are readily neutralized by sodium hydroxide [8]. Thus, it would be expected that PAA would donate protons to B[f]Q in ethanolic solution. In addition, an aqueous solution of B[f]Q has a pK_b of about 9.2 [9]. For the samples adsorbed from the 0.1 M HCl and HBr solutions, the data in Table 1 indicate the B[f]Q cation was adsorbed on the surface.

Identical experiments were run with neutral and acidic ethanolic solutions of quinoline adsorbed onto filter paper, silica gel chromatoplates, and 0.5% PAA—NaCl (Table 1). The conclusions for quinoline were essentially the same as for B[f]Q. The solution absorption spectrum and the reflectance spectrum (Fig. 1) from filter paper for ethanolic solutions of quinoline showed three similar major bands (Table 1). The acidic ethanol solutions of quinoline, however, gave one major band centered at 314 nm as did the corresponding reflectance spectrum. Table 1 shows that the cation of quinoline is adsorbed on 0.5% PAA—NaCl from ethanol because of the absence of bands around 300 nm and 277 nm. This is in contrast to B[f]Q similarly adsorbed for which bands appear for the cation and neutral species (Table 1). Thus, it was important to use the shapes and the position of the bands in the spectrum for quinoline to establish if the cation or neutral molecule was adsorbed on the surfaces.

Table 2 gives the results obtained for B[f]Q in ethanol with varying HCl concentration. By comparing the absorption wavelengths in Table 1 for the ethanolic solution of B[f]Q with the absorption wavelengths for the 10^{-4} M HCl solution of B[f]Q in Table 2, it can be concluded that a large fraction of the neutral form of B[f]Q exists in the 10^{-4} M HCl solution. The data in

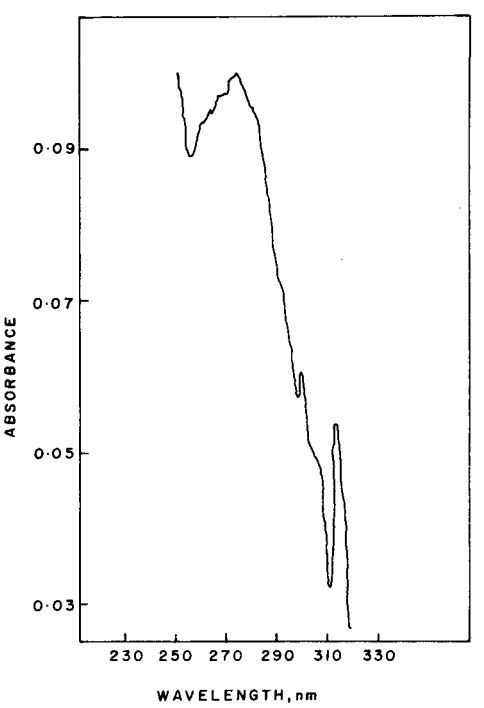

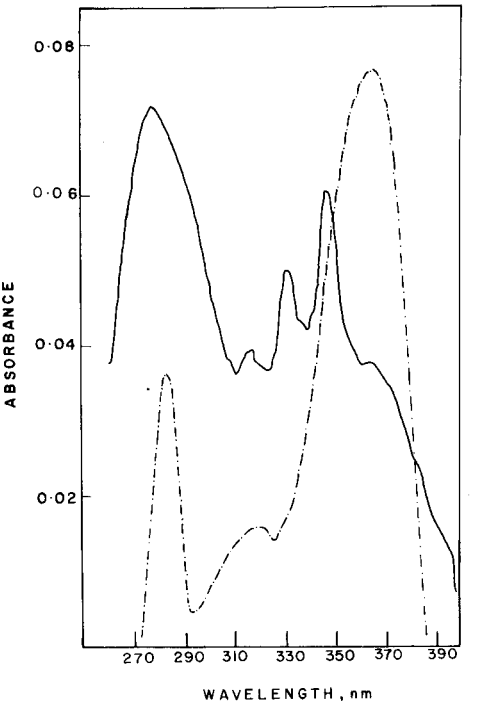

Fig. 1. Reflectance spectrum of quinoline adsorbed from an ethanolic solution onto filter paper.

Fig. 2. Reflectance spectra of B[f]Q adsorbed onto an EM silica gel chromatoplate from: (—·—) a 0.1 M HCl solution; (——) a 0.01 M HCl solution.

Table 2 for the B[f]Q samples (10^{-4} M HCl) adsorbed onto filter paper and silica gel compared to the B[f]Q sample in ethanolic 10^{-4} M HCl shows that predominantly the neutral form of B[f]Q was adsorbed on these surfaces. For the samples from 10^{-3} M HCl, the data in Table 2 for filter paper and silica gel show again that the neutral form was adsorbed. For filter paper with the 10^{-2} M HCl, mainly the cation was adsorbed, but with the silica gel at the same acid concentration, the neutral and cationic forms of B[f]Q were adsorbed. The results for the silica gel can be explained by the presence of a polyacrylate as a binder in the chromatoplates [3]. Apparently a large portion of hydrochloric acid at 10^{-2} M preferentially neutralized the polyacrylate and thus both the neutral and cationic forms of B[f]Q were adsorbed. In addition, it is possible that the B[f]Q cation in the initial "wet" state on the surface reacts by donating a proton to the polyacrylate and thus the neutral form of B[f]Q appears on the surface. As shown by the data in Table 2, the B[f]Q cation is adsorbed on the filter paper and the silica gel at 10^{-1} M HCl. Figure 2 compares the reflectance spectra for B[f]Q on a silica gel chromatoplate adsorbed from 10^{-2} and 10^{-1} M HCl solutions. It is evident

TABLE 2

Absorption wavelengths for B[f]Q in ethanolic solutions and on different surfaces with various concentrations of hydrochloric acid

Conditions	Absorption wavelength (nm)
Solutions[a]	
Ethanol, 10^{-1} M HCl	364, 280, 235, 229
Ethanol, 10^{-2} M HCl	364, 281, 236, 228
Ethanol, 10^{-3} M HCl	365, 280, 236, 228
Ethanol, 10^{-4} M HCl	365[b], 347, 331, 315, 247, 234
Solid surfaces[a]	
Filter paper, 10^{-1} M HCl	365, 293
Filter paper, 10^{-2} M HCl	367
Filter paper, 10^{-3} M HCl	346, 331, 295
Filter paper, 10^{-4} M HCl	337, 322, 305, 285
Silica gel chromatoplate, 10^{-1} M HCl	365, 283
Silica gel chromatoplate, 10^{-2} M HCl	365, 346, 330, 317, 277
Silica gel chromatoplate, 10^{-3} M HCl	346, 330, 316, 288, 275
Silica gel chromatoplate, 10^{-4} M HCl	343, 328, 314, 282, 273
0.5% PAA—NaCl, 10^{-1} M HCl	367
0.5% PAA—NaCl, 10^{-2} M HCl	366
0.5% PAA—NaCl, 10^{-3} M HCl	366, 280
0.5% PAA—NaCl, 10^{-4} M HCl	366, 280

[a]The reproducibility of the wavelengths was as indicated in Table 1. [b]Relatively weak band.

that the band from 10^{-2} M HCl at 365 nm is for the cation and the bands at 346 nm, 330 nm, and 317 nm are for the neutral form of B[f]Q. The results for 0.5% PAA—NaCl in Table 2 show that the cation is adsorbed for the 10^{-1} and 10^{-2} M HCl samples, but with the 10^{-3} and 10^{-4} M HCl samples the data show that some of the neutral form of B[f]Q is also present on the surface. Data in Table 2 for the ethanolic 10^{-4} M HCl solution show that the neutral form of B[f]Q predominates in solution. Thus, after the 10^{-4} M HCl is deposited on the 0.5% PAA—NaCl, the PAA in the initial "wet" state can protonate some of the B[f]Q to form the cation (cf. data in Table 1). More experiments would be necessary to establish the relative amounts of the cation and neutral form of B[f]Q on the 0.5% PAA—NaCl surface.

The reflectance data indicate which forms of B[f]Q and quinoline are adsorbed in the ground state on the various surfaces investigated. In addition, the data provide insight into the initial "wet" chemistry for the filter paper, silica gel, and PAA—NaCl surfaces. For quantitative purposes, it is important to know what form or forms of the phosphor are adsorbed so that conditions can be adjusted to provide only one form of the phosphor for adsorption, preferably the form giving the largest phosphorescence yield. Also, an understanding of the surface chemistry of phosphors would be useful for mixtures because conditions could be adjusted to enhance or diminish a particular phosphor signal.

Infrared spectroscopy

Infrared (i.r.) spectroscopy has been little used in the study of phosphor interactions on solid surfaces [2, 3]. Infrared spectroscopy is particularly important in studying hydrogen bonding. In this work, the interactions of milligram amounts of B[f]Q and phenanthrene with 1% PAA—KBr were investigated. By taking the first derivative of the spectra, it was possible to detect relatively small spectral shifts. For example, Fig. 3 shows the first-derivative and the normal i.r. spectrum over 1440—2000 cm^{-1} for a $B[f]QH^+$/PAA—KBr sample.

Hydroxyl group. For the PAA sample, and for the PAA—HBr sample, one of the strongest absorption bands appeared at about 3122 cm^{-1} (Table 3); this represents the OH stretching frequency for hydrogen-bonded carboxyl groups in PAA [10]. Table 3 shows that the OH stretching frequency for the B[f]Q—PAA sample appeared at 3033 cm^{-1}, corresponding to a 89 cm^{-1} shift compared to the PAA sample. With the PAA—HBr sample, the maximum absorbance appeared at about 3122 cm^{-1} as shown in Table 3. For the $B[f]QH^+$—PAA—HBr sample, the maximum frequency was at 3060 cm^{-1}, which represents a 62 cm^{-1} shift to lower frequencies compared to the PAA—HBr sample (Fig. 4) and indicates disruption of carboxyl group interactions.

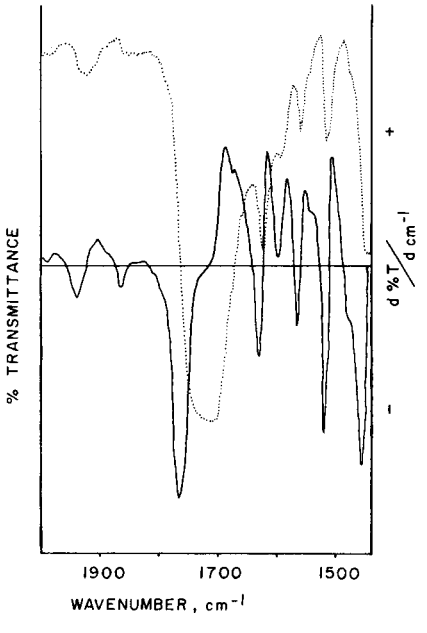

Fig. 3. First-derivative i.r. spectrum (—) and the normal i.r. spectrum (····) for a $B[f]QH^+$—PAA—KBr sample with hydrobromic acid.

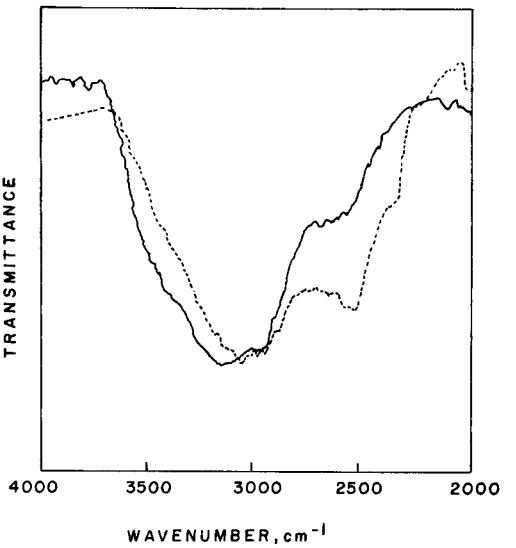

Fig. 4. Infrared spectra of 1% PAA—KBr treated with: (—) ethanolic 0.1 M HBr; (---) a similar sample with 1% B[f]Q present.

TABLE 3

Infrared peak positions for B[f]Q and B[f]QH$^+$ with polyacrylic acid—KBr mixtures[a]

Material[b]	Peak position (cm^{-1})											
	OH	NH^+				C=O	CO/OH		COOH	C—C, C—N		
PAA	3122	—				1704	1402, 1232		1167	—	—	— —
B[f]Q—PAA	3033	2538, 1930				1717	1386,	—[c]	1166	—	—	— —
PAA—HBr	3122	—				1710	1400, 1232		1165	—	—	— —
B[f]QH$^+$—PAA—HBr	3060	2525, 1984, 1918				1710	1399, 1230		1162	1620, 1587, 1555, 1508		
B[f]QH$^+$—HBr	—	2520, 1992, 1919, 1851				—	—	—	—	1617, 1583, 1552, 1506		
B[f]Q	—	—	—	—	—	—	—	—	—	—	—	1566, 1488
Reproducibility (cm^{-1}) based on duplicate runs	±10		±5					±4	±1		±1	

[a]All frequencies determined from first-derivative spectra except the 1992 cm^{-1} value for the B[f]QH$^+$—HBr sample and the 1587 cm^{-1} value for the B[f]QH$^+$—PAA—HBr sample. [b]All samples originally dissolved in ethanol. [c]Band not well defined.

The above-mentioned shifts to lower frequencies suggest that the hydroxyl groups from PAA interact with the π-electrons of the B[f]Q samples. With the B[f]QH$^+$—PAA sample, the NH$^+$ group could also interact with the oxygen in the hydroxyl groups and cause a shift to lower frequency. In addition, with the B[f]Q—PAA sample, a band appeared at 2920 cm^{-1}. Infrared experiments with the PAA anion showed a strong band at 2932 cm^{-1} from carboxylate groups. As shown in Table 3 for the B[f]Q—PAA sample, NH$^+$ vibration bands were detected [11]. These results suggest that some of the carboxyl groups from PAA protonated the nitrogen of B[f]Q, probably while B[f]Q and PAA were mixed with ethanol in the initial preparation of the sample. The dried B[f]Q—PAA mixture used in the infrared work would contain PAA, the anion of PAA, B[f]Q, and B[f]QH$^+$.

NH$^+$ group. As mentioned above, with the B[f]Q—PAA sample, new bands appeared at 2538 cm^{-1} and 1930 cm^{-1} indicating that the B[f]Q cation was present. For the B[f]QH$^+$—PAA—HBr sample, three bands appeared with maxima at 2525, 1984, and 1918 cm^{-1} (Table 3). The shift of the 1984 cm^{-1} band to a lower frequency compared to the 1992 cm^{-1} in the B[f]QH$^+$—HBr sample indicated that the cation was interacting with PAA; the most likely interaction of the NH$^+$ group was with the carbonyl groups and hydroxyl groups of PAA. The neutral sample of B[f]Q mixed with PAA showed two frequencies (2538 and 1930 cm^{-1}) shifted to higher values compared to the two cation samples (Table 3). This suggests interactions different from the B[f]QH$^+$—PAA—HBr sample; however, this sample contained a mixture of B[f]Q and B[f]QH$^+$ which complicates the interpretation of the i.r. data. Generally, the data from the NH$^+$ region did not allow simple interpretation based on frequency shifts.

C=O group. Table 3 shows that the carbonyl stretching frequency (1717 cm^{-1}) for the B[f]Q—PAA sample is shifted to a higher frequency relative to

the PAA (1704 cm^{-1}). For the PAA—B[f]QH^+—HBr sample, there is no frequency shift compared to the PAA—HBr sample. However, the carbonyl bands were sharper in both cases than those from the PAA samples. For the B[f]Q—PAA sample, the shift to higher frequency and sharpening of the carbonyl band imply that the hydroxyl groups of PAA interact with the π-electrons of B[f]Q (see also below). Also the hydroxyl groups of PAA can donate hydrogen to the basic nitrogen of B[f]Q. It was assumed for the B[f]Q—PAA sample that some of the carbonyl groups were freed from interaction with hydroxyl groups or if other hydrogen bonds were formed with the carbonyl groups the hydrogen bonds were not as strong as those in the PAA carboxyl dimeric groups. These situations would cause sharpening of the carbonyl band.

Nakanishi and Solomon [12] have discussed the general i.r. shifts observed for the carbonyl group when a carboxylic acid dimer is disrupted and forms hydrogen bonds with various solvents. With an ether solution, the hydroxyl group of the acid can form a hydrogen bond with the oxygen of the ether group and the carbonyl band exhibits a 25 cm^{-1} higher shift than the dimer because the carbonyl group is freed from interaction with the hydroxyl group. With an alcoholic solution, the carbonyl group of the acid can form a hydrogen bond with the hydroxyl group of the alcohol and the carbonyl group exhibits only a 10 cm^{-1} higher frequency shift compared to the dimer [12]. For the B[f]Q—PAA sample, the shift was 14 cm^{-1} higher than for the PAA sample. These results are analogous to a carboxylic acid dimer interacting with an ether. The 14 cm^{-1} frequency shift indicates that the hydroxyl group of PAA interacts with the nitrogen or with the π-electrons of B[f]Q. The results from the PAA—B[f]QH^+—HBr sample can be considered as similar to an alcohol interacting with a carbonyl group. The sharpening of the carbonyl band implies that the NH^+ groups interact with the PAA carbonyl groups. It is also possible that the sharpening of the carbonyl band is due to the NH^+ group interacting with the oxygen of the hydroxyl group from PAA which would free carbonyl groups to form other bonds or remain unbonded.

CO/OH, COOH groups. For coupled C—O stretching and OH bending in plane (hydrogen-bonding carboxyl group) at 1402 cm^{-1} for the PAA sample [10], a shift to 1386 cm^{-1} was observed for the B[f]Q—PAA sample (Table 3). This indicated that the hydrogen bonds to carboxyl groups were broken and other bonds such as donation of hydrogen to the nitrogen of B[f]Q were formed. For the B[f]QH^+—PAA—HBr sample, only a 2 cm^{-1} shift was detected. The C—O stretching and OH bending in plane also appear at 1223 cm^{-1}. For the B[f]Q—PAA and B[f]QH^+—PAA samples, the bands broadened showing interaction of carboxyl groups with both forms of B[f]Q. Interestingly, the bands around 1167 cm^{-1} for the COOH group [13] showed small shifts and little broadening for the B[f]Q—PAA and B[f]QH^+—PAA—HBr samples.

C—C, C—N groups. The skeletal ring stretching bands for B[f]QH^+—HBr

and B[f]Q samples are indicated in Table 3. For the B[f]Q—PAA samples, these bands were not well defined because of CO/OH and COOH bands. Comparison of the bands for the B[f]QH^+—HBr and B[f]QH^+—PAA—HBr samples shows little or no frequency shifts. However, the band at 1587 cm^{-1} for the B[f]QH^+—PAA—HBr sample almost disappeared which indicated interaction of PAA with the ring system.

Interaction model for B[f] Q based on reflectance and infrared results

For the B[f]Q—PAA sample, a mixture of B[f]Q, B[f]QH^+, PAA, and the anion of PAA are present. It would be necessary to perform more experiments to establish the relative amounts of different components in the mixture. However, it has been shown by us that nanogram amounts of the B[f]Q species, adsorbed from ethanolic solution, can be detected readily by r.t.p. from 0.5% PAA—NaCl, 1% PAA—NaBr, and 1% PAA—KBr. For the neutral form of B[f]Q, the carboxyl groups of PAA can form hydrogen bonds with the π-electrons of B[f]Q to hold the phosphor tightly. The interactions of B[f]QH^+ with PAA are discussed below.

It has also been shown by us that a solution of B[f]Q with 0.1 M HBr in ethanol yields r.t.p. from B[f]QH^+ adsorbed on 0.5% PAA—NaCl, 1% PAA—NaBr, and 1% PAA—KBr at the nanogram level. The infrared results suggest several interactions of PAA with B[f]QH^+. The hydroxyl groups of PAA interact with the π-electrons of B[f]QH^+, and also, the NH^+ group can form bonds with either the oxygen of either the carbonyl group or the hydroxyl group. The i.r. data did not indicate which interaction was more important. Because B[f]QH^+ forms more bonds and presumably stronger bonds than B[f]Q does, it should be held more rigidly than B[f]Q by PAA.

Because hydrobromic acid solutions of B[f]Q were adsorbed onto the PAA—salt mixtures, B[f]Q hydrobromide was adsorbed on the surface. (Table 3 shows the infrared frequencies for the NH^+ group). It was found previously that salts of phosphors can yield strong r.t.p. [2—4]. Thus, the interactions of the hydrobromide are an important consideration. Because B[f]Q exists as the hydrobromide on the surface, one has to consider the interaction of the bromide ion in the solid matrix. The i.r. data did not provide direct evidence on bromide, but it appears that the positive charge of the NH^+ group could be shared by bromide, carbonyl and hydroxyl groups.

Phenanthrene

The hydrocarbon analog of B[f]Q, phenanthrene, which also yields r.t.p., was studied by infrared spectroscopy. With phenanthrene, the main interactions should be with the π-electrons of phenanthrene and the carboxyl groups of PAA. Table 4 shows that the hydroxyl stretching frequencies were shifted to lower values for both the neutral and acidic samples of phenanthrene—PAA; the hydroxyl band was also broadened in both cases. These facts show that the carboxyl dimers in PAA were perturbed and most likely some hydroxyl groups interacted with π-electrons of phenanthrene.

TABLE 4

Infrared peak positions for phenanthrene with polyacrylic acid—KBr mixtures

Material	Peak positions (cm^{-1})			
	OH	C=O	CO/OH	COOH
PAA	3122	1704	1402, 1232	1167
PAA—HBr	3122	1710	1400, 1232	1163
Phenanthrene—PAA	3043	1708	1412, 1238	1170
Phenanthrene—PAA—HBr	3045	1716	1410, 1237	1171
Reproducibility (cm^{-1}) based on duplicate runs	±5	±2	±3	±1

This is supported by the carbonyl shift to higher frequencies for the corresponding neutral and acidic samples of phenanthrene. Also, the CO/OH and COOH bands were shifted to higher frequencies for both phenanthrene—PAA samples (Table 4). Some of the frequencies corresponding to aromatic ring vibrations and out-of-plane bending modes of phenanthrene were detected in the phenanthrene—PAA spectra, but no significant changes were found in this portion of the spectrum. The infrared data support the model that carboxyl groups interact with π-electrons of phenanthrene which would help to anchor phenanthrene to the surface. This appears to be an important factor in allowing r.t.p. to be observed from this compound.

This work was supported by the Department of Energy (Office of Basic Energy Sciences) under contract No. DE-AC02-80ER10624.

REFERENCES

1 E. M. Schulman and R. T. Parker, J. Phys. Chem., 81 (1977) 1932.
2 R. M. A. von Wandruszka and R. J. Hurtubise, Anal. Chem., 49 (1977) 2164.
3 C. D. Ford and R. J. Hurtubise, Anal. Chem., 52 (1980) 656.
4 R. J. Hurtubise and G. A. Smith, Anal. Chim. Acta, 139 (1982) 315.
5 G. J. Niday and P. G. Seybold, Anal. Chem., 50 (1978) 1577.
6 S. M. Ramasamy and R. J. Hurtubise, Anal. Chem., 54 (1982) 2477.
7 R. J. Hurtubise, Talanta, 28 (1981) 145.
8 K. J. Saunders, Organic Polymer Chemistry, Chapman and Hall, London, 1973, p. 121.
9 G. Favaro, F. Masetti and U. Mazzucato, Spectrochim. Acta, Part A, 27 (1971) 921.
10 J. Ostrowska and A. Narebska, Colloid Poly. Sci., 257 (1979) 128.
11 K. Kiss-Eross, in G. Svehla (Ed.), Comprehensive Analytical Chemistry: Analytical Infrared Spectroscopy, Vol. 6, Elsevier, Amsterdam, 1976, p. 367.
12 K. Nakanishi and P. H. Solomon, Infrared Absorption Spectroscopy, 2nd edn., Holden-Day, San Francisco, CA, 1977, pp. 214–216.
13 J. C. Leyte, L. H. Zuiderweg and H. J. Vledder, Spectrochim. Acta, Part A, 23 (1967) 1397.

Analytica Chimica Acta, 152 (1983) 95—104
Elsevier Science Publishers B.V., Amsterdam — Printed in The Netherlands

COLUMN CEMENTATION ON ALUMINIUM POWDER AS A PRECONCENTRATION TECHNIQUE FOR TRACE ELEMENT DETERMINATIONS BY SPARK-SOURCE MASS SPECTROMETRY
Part 1. Copper, Lead, Ruthenium and the Noble Metals[a]

B. FU[b], A. M. URE* and T. S. WEST

The Macaulay Institute for Soil Research, Craigiebuckler, Aberdeen, AB9 2QJ (Gt. Britain)

(Received 11th April 1983)

SUMMARY

The technique of column cementation on aluminium metal powder for preconcentration from solution of copper, lead, ruthenium and the noble metals is shown to be quantitative over a wide range of concentrations. Optimum conditions of pH, temperature and solution flow rate are established. In conjunction with final measurements by spark-source mass spectrometry of the aluminium powder concentrate, detection limits are below 1 $\mu g\ l^{-1}$ and concentration factors of >1000-fold are readily obtainable. Interference effects are discussed; the principal interference, that of iron, can be masked with fluoride.

Spark-source mass spectrometry (s.s.m.s.) is a valuable technique for simultaneous, multi-element, trace analysis and has been used quantitatively for the comprehensive analysis of soils and rocks [1]. Although s.s.m.s. is a sensitive technique with detection limits in the range 0.01—1 ppm, there remain some elements, such as the noble metals, whose abundance in natural samples is generally too low to be directly measurable. In addition, solutions, such as natural waters or soil extracts, cannot be analysed directly. For these reasons, pre-concentration procedures are sometimes necessary before the s.s.m.s. measurements. Because the final sample for spectrometry must be a conducting solid electrode, only four methods of concentration are suitable, viz. co-precipitation, electrochemical deposition, absorption on activated carbon and cementation. A preconcentration technique based on cementation, or spontaneous electrochemical displacement and deposition, on aluminium metal powder has recently been developed [2—4]. Cementation on aluminium metal has already been used for the removal of copper from pot ale and other copper-rich effluents [5]. A detailed investigation of column cementation on aluminium powder as a preconcentration technique for trace element determinations by s.s.m.s. is described in this paper.

[b]On leave from: Beijing (Peking) Mining and Metallurgical Research Institute, People's Republic of China.

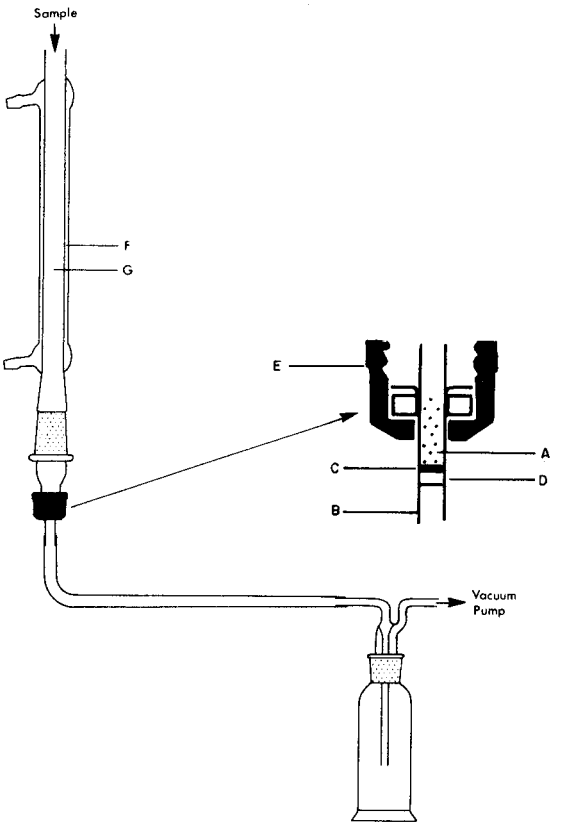

Fig. 1. Schematic diagram of column cementation apparatus, showing the aluminium powder column, A, supported in a PTFE tube, B, on a disc of (Whatman) glass-fibre paper, C, which itself is held in position by the ring of polyethylene tube, D. The column assembly is attached to the apparatus by a connector (Quickfit No. ST51/13), E. Sample solution, G, is drawn through the column from a 25-ml condenser with a hot-water jacket, F, by a vacuum pump and collected in a Drechsel bottle.

EXPERIMENTAL

Apparatus

A diagram of the cementation apparatus is shown in Fig. 1. A column (50 mg) of aluminium powder, A, is placed in a short PTFE tube, B, of length 30 mm and internal diameter 3 mm. A circular piece (4 mm diameter) of Whatman glass microfibre paper, C, is placed on a ring of polyethylene tubing, D, and supports the aluminium powder. The top of the column is connected by means of a connector, E (Quickfit No. ST51/13, cone 14/23), to a 25-ml condenser (Quickfit No. C1/11, socket 14/23), containing the sample solution, G. The water jacket, F, surrounding the condenser is connected to a circulating pump which is installed inside a controlled-temperature water-bath (Grant Instruments) and hot water, at a preselected temperature, is

circulated through the condenser jackets. The sample solution is drawn through the column by gentle suction from a water pump and collected in a Dreschel bottle. Three percolation columns can be connected with their heating jacket water supplies in series, and run from a single water pump by connecting the outlets of the Dreschel bottles with plastic T-joints.

Reagents

All solutions were prepared from analytical reagent-grade chemicals, redistilled acid and glass-distilled water. Stock solutions were prepared as follows. Gold solution (1000 mg l^{-1}) was prepared by dissolving Specpure gold sponge in aqua regia; copper solution (1000 mg l^{-1}) by dissolving copper sulfate in distilled water; lead solution (1000 mg l^{-1}) by dissolving lead nitrate in distilled water; palladium solution (1000 mg l^{-1}) by dissolving ammonium chloropalladite in distilled water; and ruthenium solution (500 mg l^{-1}) by dissolving tris(acetylacetonato)ruthenium, $Ru[(CH_3CO)_2CH]_3$, in nitric acid. The platinum (480 mg l^{-1}) and rhodium (1000 mg l^{-1}) solutions were commercial atomic absorption standards. The stock solutions of gold, lead and ruthenium were further treated to remove nitrate and nitric acid before a mixed standard solution was prepared; i.e., a portion of stock solution was evaporated to dryness on a water bath and a triple evaporation was then done by using each time 30 ml of 6 M hydrochloric acid. A mixed stock solution containing 50 mg l^{-1} copper, lead, palladium, rhodium, and ruthenium and 20 mg l^{-1} of gold and platinum in 5% hydrochloric acid was then prepared.

Cementation procedure

A 50-ml volume of a mixed standard solution containing 5 mg l^{-1} Cu, Pb, Pd, Rh and Ru and 2 mg l^{-1} Au and Pt was prepared and its pH was adjusted to the required value by dropwise addition of purified ammonia, water and 6 M redistilled hydrochloric acid using an EIL Model 2320 pH-meter. A short column containing 50 mg of aluminium powder (Aldrich Chemical Company, 99.999%) was prepared and connected to each cementation device. The aluminium in the column was amalgamated by drawing through 50 ml of 0.004% mercury(II) chloride solution in 0.03 M sulphuric acid. The mixed standard solution, pre-heated in a hot water bath for 15 min, was added immediately to the condenser and drawn through the column. When the solution had passed through the column, the column was removed and dried overnight at room temperature.

For s.s.m.s., an electrode was prepared as follows: the aluminium powder was pushed out of the column with a perspex rod and mixed in an agate mortar with an equal weight of aluminium powder containing indium (125 or 12.5 $\mu g\ g^{-1}$) as an internal standard. Electrodes were prepared from this mixture for s.s.m.s.

The recoveries were calculated from atomic-absorption spectrometric analysis of solutions prepared from the aluminium powder concentrates and verified by analysis of initial and residual solutions, or from s.s.m.s. of the

above electrodes. Atomic absorption spectrometry was done with an IL751 instrument with a flame or IL555CTF furnace atomiser. For s.s.m.s., an AEI 702R instrument was operated under the conditions prescribed earlier [1].

RESULTS AND DISCUSSION

Optimization of experimental parameters

The cementation reaction can be represented by the equation

$$3M^{n+} + n\mathrm{Al} \leftrightarrow 3M + n\mathrm{Al}^{3+} \quad (1)$$

where M^{n+} is the ion of a metal which is more electropositive (noble) than aluminium. Aluminium is thus used to reduce the ions of more noble elements, such as gold and copper, to the elements, which are deposited on the aluminium powder surface. Aluminium is such a very electronegative element, standard potential −1.67 V, that it can reduce ions of many elements and its use in powder form for cementation allows sample electrodes to be pressed directly for s.s.m.s.

The differences of standard electrode potential between aluminium and ruthenium, lead, copper, rhodium, palladium, platinum or gold, range from 0.87 V to 2.66 V. For many metals, such as lead and copper, the difference between the electrode potentials of the amalgamated metal and pure metal is very small (less than 0.1 mV) [6]. However, the hydrogen overvoltage on mercury is very great (about 1 V) and this means that amalgamation of the cemented metal has the advantage that there is very little evolution of hydrogen, and also that competition between the reaction of hydrogen ions and those of metal ions with the aluminium is minimized. Because only a very small portion of the aluminium is amalgamated in this procedure, reduction of hydrogen ion to atomic hydrogen cannot always be inhibited completely. The principal function of amalgamation is to remove the adherent oxide film which readily forms on the metal surface and to provide a more reactive aluminium electrode.

According to electrochemical theory, the electrode potential for a cementation reaction can be derived by applying the Nernst equation:

$$E = E^0_{M/M^{n+}} - E^0_{Al/Al^{3+}} + (RT/nF)\ln(a[M^{n+}]/a[Al^{3+}]) \quad (2)$$

where $E^0_{M/M^{n+}}$ and $E^0_{Al/Al^{3+}}$ are the standard electrode potentials of reactions $M^{n+} + ne^- \rightleftharpoons M$ and $Al^{3+} + 3e^- \rightleftharpoons Al$, respectively. If E for the cementation reaction is positive then the reaction in Eqn. (1) will proceed to the right, i.e., the cementation reaction is thermodynamically feasible. Even though a reaction is thermodynamically feasible however, it may proceed at a very slow rate because of the reaction mechanisms involved. Most cementation reactions are first-order processes and the kinetics are usually diffusion-controlled, i.e., the rate of reaction depends mainly on the rate of diffusion of M^{n+} to the surface of the aluminium or of Al^{3+} from the surface.

The main factors which govern the cementation rate with an amalgamated metal are generally the pH of the solution, the temperature, the stirring rate,

the concentrations of analyte and concomitant ions in the solution, and the electrode potential of the cemented element. In the process of column cementation, the effect of flow rate corresponds to the stirring rate in conventional systems.

The effect of pH

The pH of the solution can influence the redox potential because hydrogen or hydroxide ion often participates in the redox reactions of metal electrodes, and increasing H^+ concentration leads to an enhanced potential. Hydrogen ions are readily reduced by aluminium, producing an accumulation of hydroxide ions near the metal surface and the formation of metal hydroxide films which can slow down or even stop the cementation reaction. In addition, pH is an important factor in producing precipitation of metal ions.

The effect of pH on the cementation was investigated by varying the pH from 1 to 12 with a column temperature of 55°C (hot tap water). The solutions were filtered before being poured into the cementation apparatus and the metal content of any precipitate formed was measured. The extent of precipitation is allowed for in calculating the recoveries, but in general, for the group of elements studied precipitation was not a significant factor at pH < 6. The aluminium powder was considerably dissolved at pH < 2 and the precipitation of metal hydroxide occurred at pH $\geqslant 6$. However, copper, palladium and platinum, which have soluble salts in alkaline medium, can be quantitatively collected by cementation from alkaline solution; the recovery of copper was 98% at pH 10 and 11 in 1 M ammonia medium, while the palladium recovery was 96% and the platinum recovery 88% at pH 12 in sodium hydroxide medium. The cementation recoveries for pH values in the range 2—6 are shown in Table 1.

Although gold, copper, palladium, platinum and rhodium were completely reduced at pH 2, a small fraction was unfortunately reduced by hydrogen produced by reaction between aluminium and hydrogen ion and deposited on the walls of the condenser. Table 1 shows that lead and ruthenium gave maximum recovery at pH 2; the maximum recovery of gold, copper and palladium was at pH 3, while that of platinum and rhodium was at pH 4.

TABLE 1

Percentage recoveries of elements at different pH values

Element	pH 2	pH 3	pH 4	pH 5	pH 6
Au	50	100	96	85	84
Cu	87	92	89	86	72
Pb	88	87	80	77	70
Pd	66	97	94	87	78
Pt	76	87	90	78	63
Rh	84	84	85	83	77
Ru	94	90	89	77	73

TABLE 2

Changes in pH solutions after cementation

Initial pH	2.0	3.0	4.0	5.0	6.0
Final pH	2.6	3.3	3.3	3.5	3.7

However, recoveries of 80—100% were obtained for all the tested elements from pH 3 to 4. It seems that the optimum pH for group recovery was 3.

The pH values of the solutions were changed by passage through the cementation column (Table 2); the pH values of solutions with initial pH $\geqslant 3$ were reduced and those with initial pH < 3 were increased, but all solutions tended to pH 3.3. In consequence, when the cementation is done at pH 3, there is no problem of pH altering in the absence of a buffer.

The effect of temperature

Higher temperature can speed up the reaction at the electrode, and enhance the rate of ion diffusion from the bulk of the solution to the electrode surface and the transport rate of metal atoms from the electrode surface to the inner zones. The rate of reaction will thus be increased as the temperature is raised. A preliminary study of the effect of temperature had previously been made at 25 and 60°C [2].

The effect of temperature was further investigated here, by passing the solutions (at pH 3) through cementation columns at 25, 50, 75 and 95°C. Table 3 shows that raising the temperature of the sample solution above 25°C resulted in a quite substantial increase in the recoveries of Au, Cu, Pb, Pd, Pt, Rh and Ru, but the increase was barely significant when the temperature exceeded 50°C. Too high a temperature made aluminium so active that hydrogen ion was reduced, with the production of hydrogen gas. As a result, a small amount of metal, reduced by hydrogen, was deposited on the wall of the condenser with a slight decrease of recovery at 95°C compared with 75°C. A temperature of 70°C was selected as the optimum.

TABLE 3

Percentage recoveries of elements at different temperatures

Element	Recovery (%)			
	25°C	50°C	75°C	95°C
Au	88	100	100	85
Cu	63	98	99	98
Pb	63	91	92	90
Pd	78	98	98	98
Pt	66	90	94	85
Rh	74	95	98	98
Ru	78	85	88	95

The effect of flow rate

The time during which the ions in solution are in contact with the amalgamated aluminium powder depends on flow rate and will influence the cementation efficiency. The typical flow rate is usually about 50 ml h^{-1} but is dependent on the suction of the water pump and the amount of metal which has been deposited in the column. The effect of flow rate on recovery was investigated over the range 30—250 ml h^{-1}. It was found that for flow rates less than 100 ml h^{-1} there was no significant variation in recovery with flow rate.

The effect of flow rate became obvious, however, when a narrower PTFE tubing with an internal diameter of 2 mm was used for the column. This extended the aluminium powder column to a length of 12.0 mm instead of the normal 5.3 mm (Table 4), for the same weight of aluminium powder. It can also be seen from Table 4 that the recovery obtained from the narrower column was lower than that from the wider column, at the same flow rate, probably because the linear flow velocity of solution is greater in the narrower column than in the wider one. The linear flow velocity of solution, v, can be expressed by $v = R/A$, where R is the volumetric flow rate (i.e., solution volume per unit time) and A is the cross-sectional area of the column. Thus v is inversely proportional to the cross-sectional area of the column. If flow rates are too great, some metal ions will have insufficient time to diffuse to the surface of the aluminium and to react. When the volumetric flow rate through the column of 2-mm diameter was reduced to 29 ml h^{-1} (i.e., v = 154 mm min^{-1}) the recovery was improved almost to that of the column of 3-mm diameter at a flow rate of 55 ml h^{-1} (i.e., $v = 130$ mm min^{-1}).

Recovery at different concentrations

Five solutions at different concentrations, in the range 0.004—5 mg l^{-1}, were cemented. The recoveries for the three most concentrated solutions (Table 5) were measured by a.a.s., and those for the two other solutions were measured by s.s.m.s. It can be seen from Table 5, that the effect of concentration on recovery is in general small and for the elements Pb, Pd,

TABLE 4

The effect of flow rate on recovery of the metals

Diameter of column (mm)	Height of aluminium column (mm)	Flow rate (ml h^{-1})	Recovery (%)					
			Au	Cu	Pb	Pd	Rh	Ru
2.0	12.0	81	71	35	31	43	43	56
2.0	12.0	55	99	60	60	77	65	79
2.0	12.0	29	100	89	79	93	80	89
3.0	5.3	55	100	99	97	98	99	91

TABLE 5

Recovery at the different concentrations of metal ions listed

Metal	Recovery (%)				
	5 ppm	1 ppm	0.2 ppm	0.1 ppm	0.01 ppm
Cu	100	96	100	ND[a]	ND
Pb	96	93	100	80	80
Pd	100	100	100	88	100
Rh	100	100	100	65	63
Ru	95	84	100	ND	ND
	2 ppm	0.4 ppm	0.08 ppm	0.04 ppm	0.004 ppm
Au	100	100	100	84	80
Pt	90	ND	ND	120	120

[a]ND = not determined.

Au and Pt is barely significant in view of the precision of the measurements, viz., about ±5% for a.a.s. and ±15—20% for s.s.m.s. at the lowest concentrations. The lower results for rhodium probably reflect inadequate standardisation (bias) in s.s.m.s., especially as no trend of reduced recovery is found as the concentration is reduced from 0.1 to 0.01 ppm.

Interference by oxidizing agents

It is known that nitrate interferes with cementation reactions because of the passivation of aluminium which occurs readily when the metal comes into contact with oxidising agents, nitric acid or even sulphuric acid solutions. When it is necessary to use nitric acid for preparing sample solutions, the nitric acid must be removed before cementation by successive evaporations to dryness with hydrochloric acid [2].

The dissolved oxygen in solution unavoidably takes part in the electrode reaction during the process of cementation because of its highly electro-

TABLE 6

The effect of dilution on recovery[a]

Volume of solution (ml)	Recovery (%)			
	Cu	Pb	Rh	Ru
25	98	96	99	96
50	100	98	100	97
100	82	76	87	94
150	87	72	96	96
200	75	66	90	92
250	73	59	80	88

[a]The total amount of metal ion was 250 μg for each element.

positive nature. Oxygen can be reduced on the aluminium column in competition with metal ions. The cementation efficiency can also be affected by the reaction of oxygen with the metal being reduced, with a resulting decrease of the cementation rate; in some cases, it can even cause the redissolution of metal already cemented.

Two pieces of experimental evidence point to the depressive interference effects of dissolved oxygen on the cementation process. Firstly, when solutions containing a fixed total amount of a metal ion were diluted, the cementation recovery was reduced for rhodium and ruthenium and especially for copper and lead, as shown in Table 6. This is consistent with the increased total amount of dissolved oxygen in the diluted solution, an amount proportional to the increased solution volume. Secondly, when solutions that had been passed once through the cementation column were again passed through the column, significant losses of the non-noble metals copper and lead occurred (Table 7). Again this can be attributed to re-oxygenation of the solution on standing exposed to air after the first passage through the column. Similar losses were also observed when attempts were made to wash the column with hydrochloric acid (pH 3) after cementation. Table 7 also shows that the lower the solution concentration, the poorer is the recovery after two passes through the column. Obviously, at the lower concentration the total amount of metal deposited was less but it was attacked by the same amount of oxygen in the solution as the higher concentrations.

Interelement interference effects

When the concentration of copper or lead (i.e., of an element capable of cementation on aluminium) in solution was too high, the columns were blocked by the copper or lead cemented on the aluminium. A maximum concentration of 100 mg l^{-1} was permissible for both copper and lead without the column blocking or a reduced recovery of the other elements.

When the concentration of iron(III) ion in solution was more than 10 mg l^{-1}, the column became blocked not by cemented iron but by a precipitate of hydrated iron oxide. The masking of iron(III) with complexing agents such as citric acid, tartaric acid and ammonium fluoride was investigated. Although

TABLE 7

The losses of copper and lead after two passages through the column compared with a single passage

Element	No. of passes	Recovery (%)		
		5 ppm	1 ppm	0.2 ppm
Cu	1	100	96	100
	2	82	39	20
Pb	1	96	93	100
	2	75	40	25

TABLE 8

The masking of iron(III)

Fe(III) added (mg l^{-1})	Volume of 5% NH_4F added (ml)	F^- added (mg l^{-1})	Recovery (%)				
			Au	Cu	Pb	Pd	Rh
0	0.15	38	100	100	100	99	100
10	0.15	38	100	100	100	100	100
100	0.75	190	100	100	100	98	99
1000	5.0	1280	96	100	96	97	99

the first two reagents can mask iron(III) effectively, they also form complexes with Cu, Pb and Rh and reduce their recovery. Fluoride is an effective complexing agent for iron(III).

Standard solutions containing different concentrations of iron(III) were adjusted to pH 3 and a solution of 5% ammonium fluoride in distilled water was added dropwise until the brown colour of hydrated iron(III) disappeared. Two extra drops of the ammonium fluoride solution were then added and the pH was re-adjusted to 3. The masking efficiency can be seen from Table 8; as much as 1000 mg l^{-1} iron(III) can be masked without significant effect on the cementation of the other elements.

Conclusion

For copper, lead, ruthenium and the noble metals, column cementation on amalgamated aluminium powder provides a pre-concentration technique which is quantitative over a wide range of element concentrations. Optimum conditions of pH, temperature and flow rate were established and the principal interference, that of iron(III), obviated by fluoride masking.

Concentration factors of more than 1000 times can readily be obtained from solutions and, in conjunction with s.s.m.s., detection limits well below 1 $\mu g\ l^{-1}$ concentrations in solution can be obtained. The method is not confined only to the elements studied here [2—4]. Part 2 of the series will present the results of a similar study of other elements, including As, Bi, Co, Cr, Fe, Mo, Sb, Se and Tl, together with examples of the application of the technique in the analysis of natural waters and soil extracts.

REFERENCES

1 A. M. Ure and J. R. Bacon, Analyst, 103 (1978) 807.
2 K. H. Welch and A. M. Ure, Anal. Proc., 17 (1980) 8.
3 K. H. Welch, Ph.D. Thesis, Aberdeen University, Gt. Britain, 1981.
4 A. M. Ure, The Analysis of Soils, Geological Materials and Natural Waters by Spark Source Mass Spectrometry, in Proc. VIth Czechoslovak Spectrosc. Conf., Nitra, 1980, p. 61.
5 A. M. Ure and K. H. Welch, J. Sci. Food Agric., 33 (1982) 711.
6 G. Svehla (Ed.), Comprehensive Analytical Chemistry, Vol. III, Elsevier, Amsterdam, 1975, p. 240.

Analytica Chimica Acta, 152 (1983) 105—112
Elsevier Science Publishers B.V., Amsterdam — Printed in The Netherlands

GRADE DETERMINATION OF IRON ORE USING PAIR PRODUCTION

R. J. HOLMES* and A. F. ROCZNIOK

CSIRO Division of Mineral Physics, P.O. Box 124, Port Melbourne, Victoria 3207 (Australia)

P. T. RAFTER and B. D. SOWERBY

CSIRO Division of Mineral Physics, Lucas Heights Research Laboratory, Private Mailbag 7, Sutherland, N.S.W. 2232 (Australia)

(Received 2nd March 1983)

SUMMARY

The electron—positron pair-production technique previously developed for the determination of ash in coal can be applied to the determination of the iron content of iron ore fines of —6 mm particle size. Bulk samples of about 80 kg are irradiated with ^{226}Ra γ-radiation which interacts with the ore by a combination of pair-production, Compton scattering and photoelectric absorption. By measuring the intensity of the resultant 0.511-MeV annihilation radiation and the Compton-scattered radiation, the iron content can be determined with an accuracy (1σ) better than 0.6% iron. This accuracy improves to better than 0.4% iron if corrections are made for water content, preferably with a neutron moisture gauge.

Quality control in the mining industry is based on measurements of various chemical constituents of the ore being mined. Conventional analytical techniques rely on accurate sampling and sample preparation followed by a wet chemical procedure which must be done by skilled personnel in a well equipped laboratory. Not only are these procedures time-consuming and costly, they rely on the final small sample ($\approx$0.5 g) being representative of the ore as a whole. This may not always be the case in routine analyses because of errors in sample preparation, particularly when unskilled labour is used for the latter work.

Bulk analysis techniques based on penetrating neutron and γ-radiation eliminate most of the sample preparation errors and reduce the delay between sample collection and receipt of assay data. Their greatest advantage, however, is that they can be adapted to the continuous analysis of ore on conveyor belts, in chutes or in hoppers. Information on ore grade is then rapidly made available to plant operators and it is possible to automate blending and quality control operations.

Neutron [1—7] and γ-ray backscatter [8] techniques have been used for bulk and on-stream analysis of iron ores. The present work uses the "pair-production" method recently developed by Sowerby and Ngo [9—11] for

0003-2670/83/$03.00

measurement of ash in coal. The method involves irradiation of samples with γ-rays of energy greater than 1.022 MeV, which results in the production of electron—positron pairs. The positron loses most of its energy by collisions with electrons and ions, and finally annihilates by colliding with an electron. This process produces annihilation radiation of energy 0.511 MeV, which can be monitored with a γ-ray detector. Because the probability of pair production per unit weight is proportional to $\Sigma_i w_i Z_i^2/A_i$, where w_i, Z_i, and A_i are the weight fraction, atomic number and atomic weight of element i, the intensity of the annihilation radiation is dominated by the presence of any heavy elements in the ore sample. Thus, in high-grade iron ore, the intensity of the annihilation radiation is strongly correlated with the iron concentration.

DEPENDENCE OF ANNIHILATION RADIATION ON IRON CONTENT

An investigation of the dependence of the calculated intensity of the annihilation radiation on iron content, by means of complete chemical analyses of the iron ore samples used in this work, shows that the correlation coefficient (R) is 0.999 and the r.m.s. deviation is 0.22% iron. The latter is effectively the theoretical limit on accuracy. Here, as in the remainder of this paper, accuracy is defined as the r.m.s. deviation between the chemical and predicted iron contents. The above calculation assumes that the bulk density is constant and that the ore samples are absolutely dry. In practice, measurements of the Compton-scattered radiation and moisture are required to compensate for variations in bulk density and moisture, which may result in poorer accuracy.

Calculation shows that a change in iron content of 1% (w/w) at 60% iron produces a change in $\Sigma_i w_i Z_i^2/A_i$ of 0.8%. This compares with a change in $\Sigma_i w_i Z_i^2/A_i$ of 0.6% for a change in moisture content of 1% (w/w) at low levels of moisture. Thus, unless corrections are made, an increase of 1% (w/w) in free moisture content will result in an error of about —0.7% (w/w) iron in the determination of iron content on a dry basis. This error arises mainly because chemical assays are always expressed on a dry basis regardless of free moisture content, while the pair-production gauge measures concentrations approximately on an as-received basis. Variations in the combined water content of the ore can also cause difficulties, but only when ores having vastly different amounts of combined water are analysed, e.g., hematite and goethite.

EXPERIMENTAL

The intensities of annihilation and Compton-scattered radiation were measured on 16 different samples of iron ore, representative of those presently mined in the Pilbara district of Western Australia. The samples were either natural fines or crushed lump nominally of —6 mm particle size. In

order to obtain a good estimate of the accuracy of the pair-production technique, accurate chemical assays of the samples were required for comparison. Each ore sample, weighing between 200 and 300 kg, was first divided into two halves, and then each half was reduced to between 3 and 6 kg by using a rotary divider. Duplicates were taken in order to estimate the errors in the chemical procedure. The resultant 32 samples were then crushed to —2 mm and finally pulverized, in accordance with ISO 3083 (Iron ores — Preparation of samples). The samples were analyzed on a dry weight basis for Fe, SiO_2, Al_2O_3, MnO and LOI (loss-on-ignition or combined water) by using wet chemical and x.r.f. methods. From the duplicate determinations, the r.m.s. error arising from sampling, sample preparation and the chemical procedure was found to be 0.26% iron, which reduces to 0.18% iron for the average of the duplicates.

A cross-section of the pair-production gauge used in the present work is shown in Fig. 1. About 80 kg of each ore sample is placed in a wooden box and irradiated with a 3.9-GBq (105-mCi) ^{226}Ra γ-ray source. The resultant γ-radiation is detected with a 150 × 100 mm NaI(Tl) crystal. The front face of the detector is covered by a disc (5.4 mm thick) of lead to attenuate the low-energy γ-radiation incident on the detector. The gauge is designed to ensure that scattering angles are greater than about 100° so that the Compton backscatter peak is well separated from the 0.511-MeV annihilation radiation peak.

Data were collected with a Canberra-80 multichannel analyser. Gain stability was maintained with a Harshaw model NA-22 gain stabilizer locked on the 0.511-MeV γ-ray peak. Any small residual gain variations were subsequently corrected by using the ratio of the counts recorded in a small window located on each side of the 0.511-MeV peak displayed on the multichannel analyser.

A typical pulse-height spectrum for a high-grade iron ore sample is shown in Fig. 2. Windows for the Compton-scattered and annihilation radiation were established at 0.06—0.45 MeV and 0.46—0.58 MeV, respectively. The count rates recorded in these windows over the 5-min counting period were

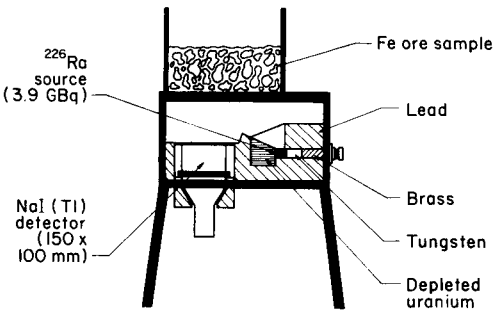

Fig. 1. Schematic diagram of the pair-production gauge.

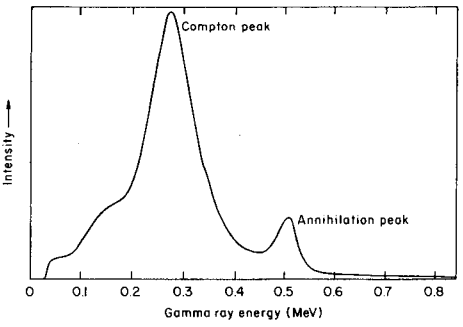

Fig. 2. Typical γ-ray spectrum for high-grade iron ore showing annihilation and Compton peaks.

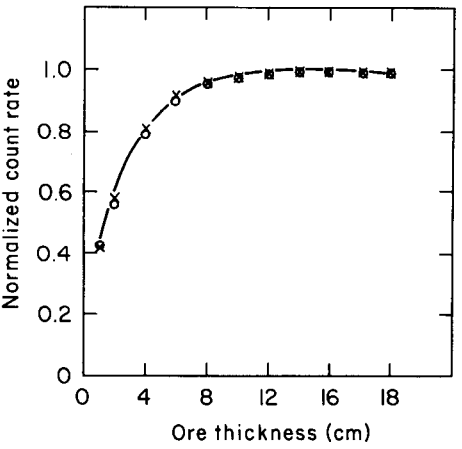

Fig. 3. Variation of (×) annihilation and (○) Compton count rates with ore thickness.

about 53000 cps for the Compton peak and about 5000 cps for the annihilation peak.

The optimum sample thickness was determined by measuring the intensities of Compton-scattered and annihilation radiation over a range of sample thicknesses. As for coal [9], the results in Fig. 3 show that the effective volume of iron ore contributing to each type of radiation is approximately the same. Errors which could arise from sample inhomogeneities are therefore minimized. Figure 3 also shows that there is no significant increase in count rates above a thickness of about 15 cm. In the following measurements, a sample thickness of 20 cm was used.

RESULTS AND DISCUSSION

Annihilation and Compton-scattered radiation counts, sample mass and free moisture content were measured in duplicate for each of the 16 ore samples. Stepwise regression analysis [12] was used to fit the chemical assays for iron against the measured variables. The accuracy of the pair-production technique was calculated in each case. It should be pointed out, however, that the accuracy calculated in this manner includes the sampling, sample preparation and chemical assay error of 0.18% iron as well as the error inherent in the pair-production technique. Allowance for the former must be made if the "intrinsic" accuracy of the pair-production technique is required.

When only the annihilation radiation count rate γ_1 (10^5 counts per 300 s) is used to predict iron concentration, the following calibration equation is obtained (R = 0.969):

$$Fe = 5.68\,\gamma_1 - 30.43 \quad (1)$$

The accuracy in this case is 1.15% iron. However, when the Compton-scattered radiation count rate γ_2 (10^6 counts per 300 s) is also included, the accuracy improves to 0.59% iron. The calibration equation in this case is ($R = 0.992$)

$$Fe = 18.63 + 10.50\,\gamma_1 - 7.88\,\gamma_2 \quad (2)$$

A comparison of the results of chemical determination of iron with those of the pair-production determinations by means of Eqn. (2) is shown in Fig. 4. The Compton-scattered radiation count rate is therefore an important parameter. Its good correlation with the sample mass, which is proportional to bulk density for constant volume samples, is shown in Fig. 5. It is noteworthy, however, that the accuracy is only 0.72% iron when the sample mass is substituted for the Compton count rate in the regression equation. This is attributed to the fact that the latter is a measure of the density of the same effective volume of ore that produces the 0.511-MeV annihilation radiation, while sample mass is a measure of average bulk density.

Effect of water content

The sensitivity of the pair-production technique to variations in free moisture content was tested by adding water to one of the samples. Increasing the free moisture content from 0.6 to 3.1% reduced the predicted grade obtained from Eqn. (2) from 59.9 to 58.1% iron. This corresponds to an error of —0.72% (w/w) iron for every 1% (w/w) increase in free moisture content, which agrees with the calculated value of —0.7% (w/w) iron. Cor-

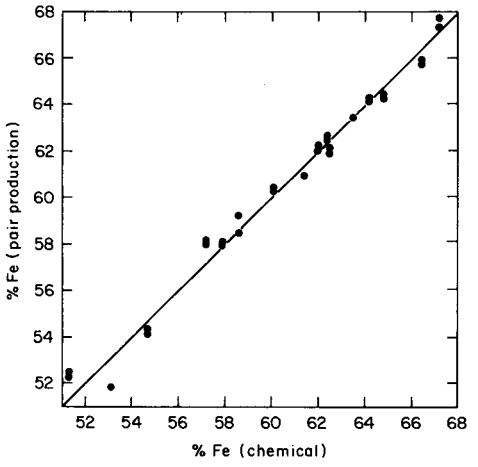

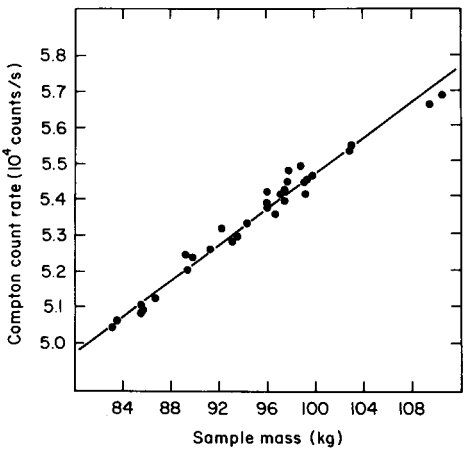

Fig. 4. Comparison of results of dry-basis chemical assays with those of iron determinations based on annihilation and Compton count rates. The r.m.s. deviation corresponds to 0.59% Fe.

Fig. 5. Comparison of Compton count rate with sample mass.

rections for free moisture variations are therefore required to obtain the best accuracy.

A close inspection of Fig. 4 and the experimental data shows that the relatively large errors in the predicted grade of several of the low grade samples is due to natural variations in free moisture content. Most samples contained about 0.5% free moisture, but the three lowest grade samples, namely 51.3, 53.1 and 54.7% iron, contained 1.1, 2.3 and 1.0% free moisture respectively. This was confirmed by including the measured free moisture content (F) in the regression analysis, which produced the following calibration equation (R = 0.996):

$$\mathrm{Fe} = 16.72 + 12.63\gamma_1 - 9.95\gamma_2 + 1.65F \qquad (3)$$

The accuracy of the iron determination is significantly improved to 0.41% iron. The free moisture values used to establish Eqn. (3) were determined by oven-drying in accordance with ISO 3087 (Iron ores — Determination of moisture content). Obviously this method is too cumbersome and time-consuming for use with a bulk analyser. However, infrared moisture gauges are available which respond to free moisture in iron ores [13], although only the surface moisture is detected and the accuracy is poorer than that of the oven-drying method. As a consequence, the accuracy of iron determination, using an infrared moisture gauge for moisture correction, may be slightly poorer than that given above. The infrared moisture measurement would also need to be made on a freshly exposed surface to avoid problems with evaporation of surface moisture.

An alternative method of monitoring moisture is to measure the total moisture content (free plus combined) with a neutron moisture gauge [14]. The effect of using this measurement as a correction term was investigated by including the total moisture content (T), determined by conventional means, in the regression analysis. In this case, the accuracy improves to 0.33% iron when the calibration equation (R = 0.998) used is

$$\mathrm{Fe} = 6.47 + 12.91\gamma_1 - 9.64\gamma_2 + 0.49T \qquad (4)$$

The intrinsic accuracy of the pair-production technique, obtained by making allowance for the error of 0.18% iron in the chemical assay, is only slightly better at 0.28% iron. A comparison of iron determinations based on Eqn. (4) with the wet chemical results is shown in Fig. 6. Once again, additional errors contributed by the neutron moisture gauge may result in a slight deterioration in accuracy.

The combination of the pair production with the neutron moisture gauge is therefore the best proposition. The gauges can be mounted on a conveyor belt to provide continuous measurements of iron content. The integration time is about 5 min, which is much faster than present methods. Because the depth penetration of the method is about 10 cm, the technique also has potential for the analysis of lump ore of −30 + 6 mm particle size. The only precautions required are to ensure that the depth of ore on the conveyor

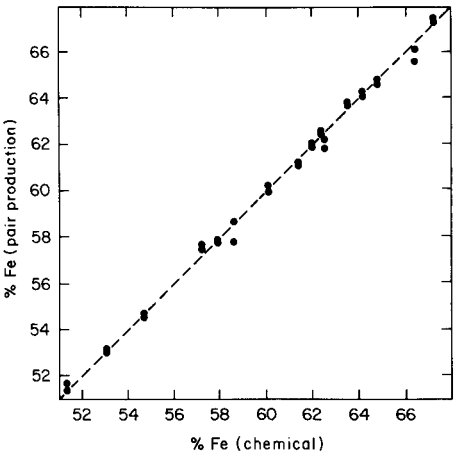

Fig. 6. Comparison of results of dry-basis chemical assays with those of iron determinations based on annihilation and Compton count rates together with corrections for total moisture content. The r.m.s. deviation corresponds to 0.33% Fe.

exceeds about 15 cm and that the ore is not high in manganese. Because manganese and iron have similar atomic numbers, the presence of significant amounts of manganese would increase the measured iron content.

Conclusions

The pair-production technique developed initially for the determination of ash in coal is also applicable to the accurate determination of the grade of iron ore fines. If corrections are made for variations in moisture content, an accuracy of better than 0.4% iron can be obtained.

The technique has potential for the continuous analysis of iron ore on conveyor belts, in chutes or in hoppers, provided that the ore thickness exceeds about 15 cm. In order to achieve the above accuracy, an infrared or preferably a neutron moisture gauge is also required to correct for free or total moisture variations respectively. However, even if moisture corrections are not made, the accuracy is about 0.6% iron, which is adequate for many applications.

The authors thank Hamersley Iron Pty. Ltd. for providing the assayed samples and for permission to publish this paper.

REFERENCES

1 K. Ljunggren and R. Christell, in Proc. Panel on Nuclear Techniques in Geochemistry and Geophysics, IAEA, Vienna, 1974, pp. 181—186.
2 M. Borsaru and R. J. Holmes, Anal. Chem., 48 (1976) 1699; 50 (1978) 296.
3 R. J. Holmes, M. Borsaru and A. W. Wylie, in Proc. North Queensland Conf., Australasian Institute of Mining and Metallurgy, Melbourne, 1978, pp. 235—244.
4 R. J. Holmes, A. J. Messenger and J. G. Miles, Proc. Australas. Inst. Min. Metall., 274 (1980) 17.

5 F. B. W. Woodbury, U.S. Bur. Mines Rep. Invest. No. 8460 and 8461 (1980).
6 A. M. Hassan, A. El-Kady and B. El-Ezaby, Nucl. Instrum. Methods, 192 (1982) 595.
7 M. Borsaru, R. J. Holmes and P. J. Mathew, Int. J. Appl. Radiat. Isot., 34 (1983) 397.
8 R. J. Holmes, Anal. Chem., 48 (1976) 1155.
9 B. D. Sowerby and V. N. Ngo, Nucl. Instrum. Methods, 188 (1981) 429.
10 B. D. Sowerby, V. N. Ngo and W. K. Ellis, Proc. 2nd Appl. Phys. Conf., Melbourne, December, 1981, p. 370.
11 B. D. Sowerby, Aust. Pat. Appl. 650048/80 (1980).
12 N. R. Draper and H. Smith, Applied Regression Analysis, Wiley, New York, 1968.
13 B. Sjoberg, J. Bak, B. Fagerberg, O. Lofgren and H. Ornstein, Proc. 12th Int. Miner. Process. Cong., Sao Paulo, 1977, Vol. 1, p. 66.
14 K. Papez, J. F. Cameron and B. Machaj, Proc. Symp. on the use of Nuclear Techniques in the Basic Metal Industries, Helsinki, 1972, p. 183.

Analytica Chimica Acta, 152 (1983) 113—122
Elsevier Science Publishers B.V., Amsterdam — Printed in The Netherlands

A DETECTOR SYSTEM FOR OXALIC ACID BASED ON THE DETERMINATION OF CARBON DIOXIDE AS METHANE AFTER DEGRADATION OF OXALATE WITH GLASS-BOUND OXALATE DECARBOXYLASE

ANDERS O. LINDBERG

Department of Analytical Chemistry, University of Umeå, S-901 87 Umeå (Sweden)

(Received 18th March 1983)

SUMMARY

A system for the determination of oxalate with glass-bound oxalate decarboxylase (E.C. 4.1.1.2) is described. The sample is pumped through an enzyme reactor and the carbon dioxide which is generated is dialyzed through a porous teflon membrane, methanated and detected with a flame ionization detector. The optimum gas flows for the detector and optimum temperature for methanation were studied. The system was used for the determination of oxalate in a few vegetables. The precision for 1 μmol l^{-1} oxalate was 1%.

In the early paper of Shimazono and Hayaishi [1] the possibility of using oxalate decarboxylase for the determination of oxalate was suggested. This proposal has been examined by several other workers. The first technique used for the determination of liberated carbon dioxide was Warburg manometry [2—5], a method which is simple but insensitive. A widely used technique based on the change in pH of an alkaline trapping medium was introduced by Hallson and Rose [6] for the determination of oxalate in urine. Their procedure has been evaluated [7] and adapted to other matrices [8, 9]. It has also been used with oxalate oxidase [10]. The method is simple and needs no expensive equipment, but it is time-consuming and tends to underestimate the oxalate content [11]. Other methods like conductometry [12], colorimetry [13] and the carbon dioxide electrode [14] have also been used. Unfortunately these methods are insensitive and the risk of endogenous carbon dioxide contamination is high. A radioenzymatic method, described by Bennett et al. [15, 16], is time-consuming (up to two days) which makes it less suitable for routine use. A major improvement was introduced by Kobos and Ramsey [17] who immobilized oxalate decarboxylase on a carbon dioxide electrode. The enzyme can then be used for many assays and is therefore cost-efficient. However, the system has limited sensitivity and precision; for the determination of oxalate in urine, the non-linear portion of the calibration curve had to be used.

A sensitive detector system for enzymatically produced carbon dioxide

0003-2670/83/$03.00

which was based on coulometric titration with photometric end-point detection [18, 19] was recently described [20]. Carbon dioxide was liberated in an enzyme reactor with glass-bound urease, expelled by boiling, dried and determined coulometrically. Compared with other methods based on immobilized enzymes for the determination of compounds as carbon dioxide the sensitivity attained (5% relative standard deviation for 1 μmol l^{-1} urea) constituted an improvement of about two orders of magnitude. Unfortunately, the described system gave unacceptable blanks when tested with samples of biological origin (e.g., urine and extracts of vegetables) which probably arose from the decomposition of compounds to carbon dioxide during the boiling. Without boiling the blank was quite small but the time for expulsion was impractically long. For this reason, work was started to find an alternative way to determine the enzymatically produced carbon dioxide. It was desirable to construct a convenient and reliable system which could be used with an enzyme reactor. For convenience, the system should be of the continuous flow type, and the detector should be sensitive but also robust.

In this paper a system is described, in which a fraction of the carbon dioxide generated is dialyzed through a porous teflon membrane and detected with a flame ionization detector (FID). To detect carbon dioxide with a FID, the gas has to be converted to methane in an oven filled with a catalyst. The system was used for the determination of oxalate in a few vegetables.

EXPERIMENTAL

Reagents

Methane and carbon dioxide standards. Gas mixtures of methane and carbon dioxide were prepared in calibrated glass flasks (0.5 l) which were equipped with special stoppers with rubber septa. The flasks were immersed in a water-bath (25 ± 0.1°C) and filled with dried (Dehydrite) nitrogen (99.99%) from a gas cylinder via a coil of thermostated copper tubing. Methane (99.5%) and carbon dioxide (99.8%) taken from gas cylinders were thermostated in the same way as nitrogen. Samples were withdrawn (calibrated gas-tight Hamilton syringes) through rubber septa attached to the copper tubes.

Oxalate standards. Sodium oxalate (oxidimetric standard, NBS, 99.95%) was dried for 1—2 h at 105° C and dissolved in a buffer (HCl, pH 2.0; 0.1 mM EDTA, p.a.).

Ruthenium catalyst. Silica gel (Grace Chromatographie, Type 58, 0.2—0.4 mm) was sieved with a 45-mesh net. The retained portion (10 g) was soaked in an aqueous solution of Ruthenium Red (Degussa, p.a.; 1 g in 10 ml). The treated silica gel particles were air-dried overnight (120°C) and the ruthenium oxide was reduced with flowing hydrogen in a quartz tube.

Apparatus

Choice of nitrogen and hydrogen flows. Figure 1A is a schematic diagram of the equipment used. It consists of a flask (50 ml) filled with dilute hydrochloric acid (pH 2.0) which was purged with a mixture of nitrogen and hydrogen. The flask was directly connected to the FID with a stainless steel tube. Methane standards were injected through a septum of the flask.

The gases, taken from cylinders, were passed through tubes packed with Ascarite and 13A molecular sieve. Compressed air from the house supply was purified with a tube of 13A molecular sieve. The gas flows were regulated with needle valves and measured with rotameters. The FID of a Perkin-Elmer 881 gas chromatograph was used to detect the methane. The chromatograph was slightly modified; the column was removed and the column inlet to the receiver was plugged. The gas mixture of nitrogen and hydrogen was fed to the detector through the receiver opening which is ordinarily used for venting restrictors. The peak area was determined with a home-built integrator and recorded with a strip-chart recorder.

Choice of temperature for methanation of carbon dioxide. The equipment used was the same as above. A methanation oven with ruthenium catalyst was included. The oven was clamped directly to the outside of the chromatograph. The temperature of the oven was calibrated with a thermocouple embedded in the catalyst and with hydrogen and nitrogen flows of 50 ml min^{-1}. The catalyst was packed in a quartz tube (3.8 mm i.d., 20 cm long). The catalyst bed in the tube was 10 cm long and was heated by an electrical oven (±0.5 °C, 15 cm length). Deviations greater than 0.5 °C caused fluctuations of the baseline. The peak height and area were recorded when methane and carbon dioxide standards were injected through the septum of the flask.

Determination of oxalate. Figure 1B is a schematic diagram of the equipment used. The buffer reservoir, fitted with a special stopper, was made from a 2-l extraction funnel. The buffer (pH 2.0, HCl, 0.1 mM EDTA, p.a.) was purged with purified (Ascarite) synthetic air (hydrocarbons <0.1 ppm) from a gas cylinder. The sample was purged with purified and moist synthetic air (Ascarite and a gas dispersion bottle) before it was injected into the buffer

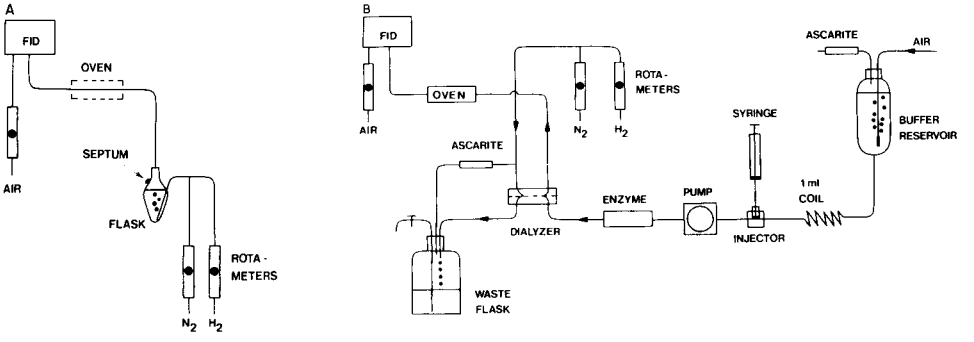

Fig. 1. Schematic diagrams of the experimental arrangements: A, for selection of nitrogen and hydrogen flows and methanation temperature; B, for determination of oxalate.

stream. The buffer was pumped with a peristaltic pump (Gilson Minipuls 2, Elkay acid flexible pump tubing). The sample was injected with a syringe through a septum placed between the buffer reservoir and the pump. The injector was placed at this position in order to obtain a constant flow rate through the enzyme reactor, which connected the pump with a plexiglas dialysis block. Carbon dioxide, formed in the oxalate decarboxylase reactor, traversed a teflon membrane in the block and was swept by a stream of nitrogen (50 ml min^{-1}) and hydrogen (50 ml min^{-1}) into the catalyst oven. The carbon dioxide was there reduced to methane and was then detected with the FID.

The buffer passed through the dialysis block to a 2-l bottle with a rubber stopper. A stainless steel tube through the stopper was connected via a small Ascarite tube to the gas inlet of the dialysis block. This arrangement was vital, because it compensated the over-pressure on the membrane caused by the gas flow. The rubber stopper also held a second stainless steel tube to which a stopcock was fitted.

The enzyme reactor consisted of a stainless steel tube (i.d. 3.4 mm, length 45 mm) tightly packed with enzyme-coated porous glass beads (CPG-10, pore diameter 49 nm, diameter 75—125 μm; Corning Glass) which were held in place by frits cut from a stainless steel screen (Supelco, 10 μm mesh size). The reactor was equipped with a water jacket, which was connected to a thermostat (20 ± 0.05°C). Oxalate decarboxylase (10 U; Sigma Chemical Co., 2—6 U mg^{-1}) was dissolved in 1.5 ml of buffer and coupled to 0.5 g of alkylamino glass (aqueous silanization by glutaraldehyde) [21]. The time for the coupling was extended to 24 h [22].

The dialysis block, made of plexiglas, consisted of two halves (length 150 mm, breadth 65 mm, thickness 11 mm) clamped together by 12 screws. The buffer was pumped through a U-formed groove in one half of the block (total length 230 mm, width 6 mm, depth 0.1 mm); the mixture of nitrogen and hydrogen passed through a corresponding groove (depth 1.0 mm) in the other half. The gas phase and the liquid phase were separated by a porous teflon membrane (pipe thread tape with a thickness of 0.08 mm or Gore-Tex S-10 633, pore size 0.02 μm, thickness 0.08 mm, porosity 50%).

The peak height and area of the sample were recorded by a strip-chart recorder.

Analytical procedure

The buffer was poured into the reservoir and degassed with air for about 30 min. Before a sample was introduced, it had to be purged for about 5 min with air to remove dissolved carbon dioxide. The sample was introduced with a syringe in the buffer flow and carbon dioxide produced was then dialyzed, methanized and detected. The time for one determination was about 4 min. The waste flask had to be emptied once a day; this was simply accomplished by opening the stopcock of the waste flask; the over-pressure in it forced the buffer out through the tube.

Extraction of oxalic acid from food. Essentially the same acid extraction procedure as described by Kasidas and Rose [9] was used. Their method comprises homogenization (here Ultraturrax, Type 45), extraction with 2 M hydrochloric acid and centrifugation of cell debris. In addition, the extract was then filtered (Millipore, 0.6 μm) and appropriately diluted and the acidity was adjusted to pH 2. EDTA was added to a final concentration of 0.1 mM. The following samples were used: spinach (frozen, stewed), rhubarb (frozen, stewed), beetroot (whole, bottled) and tea (Ceylon; 1 g was extracted with 100 ml of hot water for 6 min).

RESULTS AND DISCUSSION

Choice of nitrogen and hydrogen flows

The FID signal depends strongly on the gas flow rates [23]. It has been shown by McWilliam [24] that the optimum hydrogen—nitrogen ratio depends on the compound to be detected. In gas chromatography where several compounds are detected, the gas flow ratio must therefore be chosen as a compromise. Here, however, where methane is the only compound which is determined, the gas flows can easily be optimized. This optimization has received little attention in papers where FID has been used to detect carbon dioxide as methane [25—33]. The flow rate of air, above a certain minimum value (for the chromatograph here used, 400 ml min^{-1}), has little or no effect on the response [34].

Figure 2 depicts the peak area and baseline level as functions of nitrogen flow. As can be seen, the peak area/baseline ratio has its highest value, about 6.8, for a nitrogen flow of 50 ml min^{-1} and a hydrogen flow of 50 ml min^{-1}. These flows were subsequently used throughout this investigation. A further increase in the nitrogen flow was not favourable; a nitrogen flow of 60 ml min^{-1} and a hydrogen flow of 50 ml min^{-1} resulted in a peak area/baseline ratio of 3.5.

Methanation of carbon dioxide

Theoretical calculations. These calculations were done to simulate the methanation of carbon dioxide when it is liberated from water. Figure 3 shows the results obtained when a computer program called SOLGASMIX [35] was used to calculate the methane yield (percentage of input carbon found as methane) at equilibrium for varying hydrogen/carbon ratios. It is assumed that a 1:1 mixture of hydrogen and nitrogen is saturated with water vapour.

It can be seen that the highest methane yield which can be achieved at 600°C is 89.8%. If the temperature is decreased to 500°C the methane yield increases markedly; for an H/C ratio of 100 it is 99.3% and for an H/C ratio of 10 000 it is 99.8%. For a temperature of 400°C the methane yield is 100.00% for all the H/C ratios used. No significant amounts of carbon or C_2-compounds exist under the conditions used.

The conclusion drawn from these calculations is that quantitative methan-

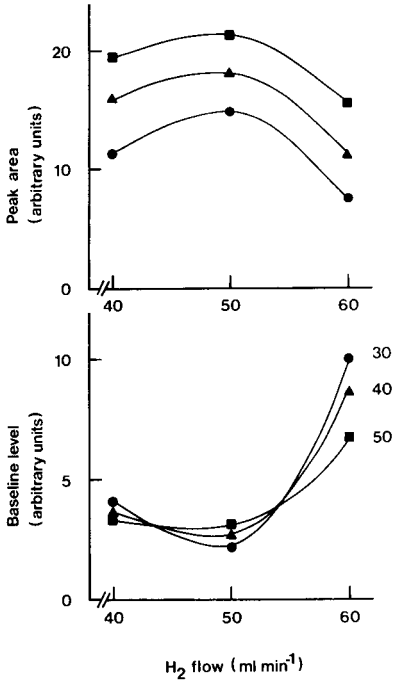

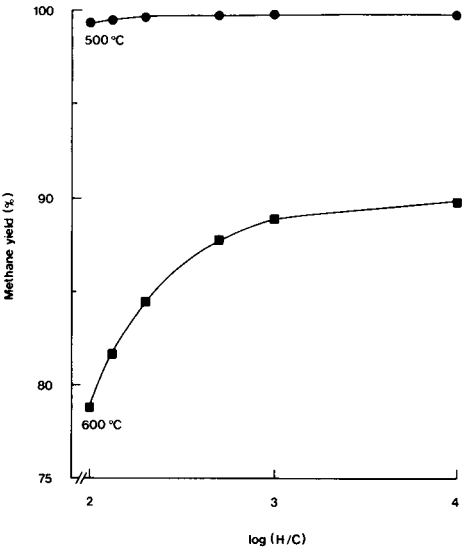

Fig. 2. Peak area and baseline level as a function of nitrogen and hydrogen flows. Sample: 25.4 μl of 1680 μl l^{-1} methane in nitrogen. The numbers in the figure indicate the nitrogen flows (ml min^{-1}).

Fig. 3. Theoretical calculation of carbon conversion to methane in a mixture of nitrogen and hydrogen saturated with water vapour. Methane yield as a function of the hydrogen/carbon ratio. Carbon dioxide was assumed to be added.

ation is thermodynamically feasible even if considerable amounts of oxygen are introduced as water. However, the methanation temperature should be near 400°C.

Selection of catalyst and conditions. Ruthenium was selected as the catalyst because it is regarded as the most effective metal for methanation of carbon oxides, particularly carbon dioxide [36]. Figure 4 depicts the effect of temperature on methanation; the methane yield was calculated from the peak areas for the methane and carbon dioxide standards. It can be seen that the conversion was high (85%) at the lowest temperature used (225°C). The conversion increased with increasing temperature and was quantitative at 375°C. The peak height was affected more severely than the area by the temperature; at 225°C the height was reduced to about 25% of the value at 425°C. The peaks showed a pronounced broadening and tailing at the lower temperatures used. These effects have also been observed by Colket et al. [32]. They found that the conversion to methane was quantitative with ruthenium as the catalyst at a temperature of only 290°C. Of course, the gas

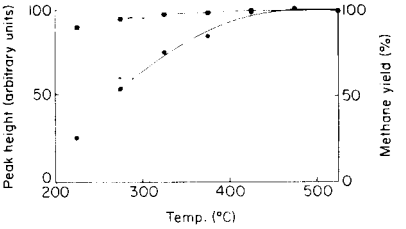

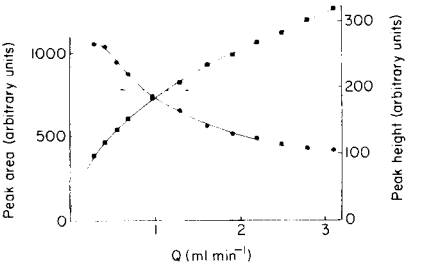

Fig. 4. Methanation of carbon dioxide; peak height and recovery as a function of temperature. Samples (253 μl) were taken of a carbon dioxide standard (8270 μl l^{-1}) and a methane standard (8300 μl l^{-1}). The recovery was calculated from the peak areas.

Fig. 5. Influence of buffer flow rate on peak area and height when 9.8 μl of a carbonate standard (8.09 mmol l^{-1}) was injected into the buffer flow (pH 2.0). The membrane was a teflon thread tape.

velocity and the area of the catalyst are of importance, but the support material and the sintering conditions also affect the catalyzing properties [37]. It is therefore to be expected that the temperature for quantitative methanation will show variation. However, generally speaking, a temperature near 400°C can advantageously be used, because this will result in a quantitative conversion and reasonably fast kinetics. The theoretical calculations for methanation do not take into account kinetic effects. Unfortunately, mechanistic and kinetic studies of carbon dioxide hydrogenation are very limited. Work in this field has been described in two reviews [38, 39]. The effects found in Fig. 4 can therefore not be discussed from a kinetic point of view.

Influence of buffer flow rate on peak area and height

Figure 5 shows the influence of the buffer flow rate on peak area and height when small amounts of a carbonate solution were injected with a syringe into the buffer flow. It can be seen that the peak area decreases with increasing buffer flow rate whereas the peak height increases.

Straight lines were obtained when the peak heights from Fig. 5 were plotted against the square root of the buffer flow rate and when the peak areas were plotted against the reciprocal of the square root of the buffer flow rate. The results obtained can be explained with the theories of Levich [40], who has given an extensive treatment of convective diffusion in liquids.

Straight lines were also obtained when standard solutions of carbonate (0—100 mmol l^{-1}; 10 μl) were injected and the peak area and height were plotted against carbonate concentration. The influence of temperature on peak height was tested; the height increased by 1.5%/°C. This value is to be expected for a diffusion-limited process.

Choice of sample volume and buffer flow rate

The influence of sample volume (up to 1 ml) on peak height was tested. The peak height was a nearly linear function of the sample volume, which indicates that the peak height would have increased for sample volumes even larger than 1 ml. However, an excessive sample volume would decrease the sample throughput; 1 ml was considered a suitable volume for general use.

The pump rate affects two processes, the diffusion in the dialyzer and the kinetics of the enzyme in the reactor. As has been shown earlier, it is advantageous to pump quickly because this results in a thin diffusion layer and sharp peaks. In the enzyme reactor, however, a high pump rate leads to a short residence time and decreased conversion of the substrate. When the pump rate was varied, it was found that the peak height increased with increasing pump rate. However, it was unnecessary to pump faster than 3 ml min^{-1} because the positive effect levelled off.

Determination of oxalate standards and of oxalic acid in vegetables

A straight line was obtained (1-ml samples) when the peak height (arbitrary units) was plotted against oxalate concentration (0—75 μmol l^{-1}). The line had a slope of 46.08 l mol^{-1} (s.e. = 0.089 l mol^{-1}), and an intercept of 5 (s.e. = 3.2). The relative standard deviation was about 1% (n = 5) for an oxalate concentration of 1 μmol l^{-1}, which was the lowest used. The blank was not detectable and the time for one determination amounted to about 4 min.

It was desired to test the system with the determination of oxalate in a complicated matrix. The determination of oxalate in vegetables was chosen; the oxalate content of food is of importance to human health [41]. Vegetable homogenates were spiked with oxalate and the recovery and the content were determined from a standard curve of oxalate in buffer. It can be seen from Table 1, that the recovery of added oxalate was quantitative for the vegetables used. The oxalate content of rhubarb (463 mg/100 g) falls within the limits (260—620 mg/100 g) given by Zarembski and Hodgkinson [42]. Spinach was found to have an oxalate content of 312 mg/100 g which falls outside the interval (356—780 mg/100 g) given by Hodgkinson [41]. However, it is questionable to conclude that the value given here is significantly lower than the values presented by Hodgkinson, as the interval for spinach in his compilation is very wide. The oxalate content of beetroot was found to be 110 mg/100 g, which is close to the value (121 mg/100 g) given by Zarembski and Hodgkinson [42] but much lower than the value (600 mg/100 g) given by Kasidas and Rose [9]. It has been pointed out that their high values should be confirmed in other laboratories [43]. Tea infusion was found to contain 6.3 mg/100 g of oxalate. This value is reasonable in comparison with the values given by Kasidas and Rose [9].

There are still considerable differences of opinion about the true oxalate content of certain foods. Possible reasons for this include the wide natural variation of the oxalate content and the use of inaccurate analytical procedures.

TABLE 1

Determination of oxalate in vegetables

Sample	Oxalate added to sample[a]	Recovery (%)	Oxalate found in sample[a]
Rhubarb	361	101.0	463
Spinach	322	99.2	312
Beetroot	92	101.0	110
Tea infusion	11.2	98.4	6.3
Mean		99.9	
S.d.		1.3	

[a]mg/100 g (anhydrous oxalic acid).

Different varieties may contain different amounts of oxalate; the concentration of oxalate also exhibits seasonal variations and is affected by the nature and the conditions of the soil, the climate and the age of the plant. The practice of expressing the oxalate content per wet weight is also likely to be of importance.

Earlier methods for the determination of oxalate used techniques for the extraction of the analyte resulting in either generation of oxalate from other food constituents or losses by incomplete extraction. By adapting the enzymatic method of Hallson and Rose [6], Kasidas and Rose [9] succeeded in developing a method which was specific and mild yet obviated any preliminary isolation of the oxalate following homogenization of the plant material. Limitations of the method are, however, that fairly large amounts of enzyme are required and each flask can only be sampled once. The use of immobilized decarboxylase in a reactor, as described in this paper, enables the enzyme to be used repeatedly with a concomitant reduction in the cost. The reactor allows a sensitive and closed flow system to be constructed which can be run continuously.

Conclusions

The method described above offers a detection limit which is unmatched by other methods for the determination of carbon dioxide produced by immobilized enzymes such as oxalate decarboxylase. The high concentration of carbon dioxide in air places extensive demands on the equipment and procedure when compounds are determined as carbon dioxide. In spite of this, the system described here can be regarded as comparatively simple and convenient to use. With minor modifications it should moreover be useful for the determination of oxalate in matrices like urine and blood serum. The system should also be of interest in connection with the use of enzymes like oxalate oxidase and decarboxylases for amino acids as lysine, ornithine and phenylalanine [20].

The diffusion technique proposed is an alternative to stripping. Its appli-

cation to other determinations where the analyte is transferred from an aqueous to a gaseous phase, should therefore be of interest.

REFERENCES

1 H. Shimazono and O. Hayaishi, J. Biol. Chem., 227 (1957) 151.
2 G. J. Haas and A. I. Fleischman, Agric. Food Chem., 9 (1961) 451.
3 J. C. Crawhall and R. W. E. Watts, Clin. Sci., 20 (1961) 357.
4 G. G. Mayer, D. Markow and F. Karp, Clin. Chem., 9 (1963) 334.
5 M. E. Ribeiro and J. S. Elliot, Invest. Urol., 2 (1964) 78.
6 P. C. Hallson and G. A. Rose, Clin. Chim. Acta, 55 (1974) 29.
7 P. O. Schwille, M. Paulus, D. Scholz and A. Sigel, Urologe A, 17 (1978) 217.
8 T. Akcay and G. A. Rose, Clin. Chim. Acta, 101 (1980) 305.
9 G. P. Kasidas and G. A. Rose, J. Hum. Nutr., 34 (1980) 255.
10 G. Kohlbecker, L. Richter and M. Butz, J. Clin. Chem. Clin. Biochem., 17 (1979) 309.
11 W. G. Robertson and A. Rutherford, Scand. J. Urol. Nephrol., (Suppl.) 53 (1980) 85.
12 J. D. Sallis, M. F. Lumley and J. E. Jordan, Biochem. Med., 18 (1977) 371.
13 C. F. Knowles and A. Hodgkinson, Analyst, 97 (1972) 474.
14 S. J. Yao, S. K. Wolfson and J. M. Tokarsky, Bioelectrochem. Bioenerg., 2 (1975) 348.
15 D. J. Bennett, F. E. Cole, E. D. Frohlich and D. T. Erwin, J. Lab. Clin. Med., 91 (1978) 822.
16 D. J. Bennett, F. E. Cole, E. D. Cole and D. T. Erwin, Clin. Chem., 25 (1979) 1810.
17 R. K. Kobos and T. A. Ramsey, Anal. Chim. Acta, 121 (1980) 111.
18 A. O. Lindberg, Anal. Chim. Acta, 96 (1978) 319.
19 A. O. Lindberg and A. Cedergren, Anal. Chim. Acta, 96 (1978) 327.
20 A. O. Lindberg, Anal. Chim. Acta, 131 (1981) 133.
21 H. H. Weetall, in K. Mosbach (Ed.), Methods in Enzymology, Vol. 44, Academic Press, New York, 1976, pp. 134—48.
22 J. A. Osborn, R. M. Ianniello, H. J. Wieck, T. F. Decker, S. L. Gordon and A. M. Yacynych, Biotechnol. Bioeng., 24 (1982) 1653.
23 J. Sevcik, Detectors in Gas Chromatography, Elsevier, Amsterdam, 1976, p. 95.
24 I. G. McWilliam, J. Chromatogr., 51 (1970) 391.
25 U. Schwenk, H. Hachenberg and M. Förderreuther, Brennst. Chem., 42 (1961) 37.
26 R. A. Dobbs, R. H. Wise and R. B. Dean, Anal. Chem., 39 (1967) 1255.
27 F. R. Cropper, D. M. Heinekey and A. Westwell, Analyst, 92 (1967) 436.
28 R. P. W. Scott and J. G. Lawrence, J. Chromatogr. Sci., 8 (1970) 65.
29 F. W. Williams, F. J. Woods and M. E. Umstead, J. Chromatogr. Sci., 10 (1972) 570.
30 Y. Takahashi, R. T. Moore and R. J. Joyce, Int. Lab., 2 (1972) 21.
31 R. Villalobos, R. Rowland and R. Roggenkamp, ISA Trans., 15 (1976) 197.
32 M. B. Colket, D. W. Naegeli, F. L. Dryer and I. Glassman, Environ. Sci. Technol., 8 (1974) 43.
33 R. F. Weiss, J. Chromatogr. Sci., 19 (1981) 611.
34 R. Schill, in R. L. Grob (Ed.), Modern Practice of Gas Chromatography, Wiley, New York, 1977, p. 337.
35 G. Eriksson, Chem. Scr., 8 (1975) 100.
36 G. C. Bond, Catalysis by Metals, Academic Press, London, 1962, p. 369.
37 J. H. Sinfelt, Catal. Rev., 3 (1969) 175.
38 V. M. Vlasenko and G. E. Yuzeforich, Russ. Chem. Rev., 38 (1969) 728.
39 G. A. Mills and F. W. Steffgen, Catal. Rev., 8 (1973) 159.
40 V. G. Levich, Physicochemical Hydrodynamics, Prentice Hall, Englewood Cliffs, CA, 1962.
41 A. Hodgkinson, Oxalic Acid in Biology and Medicine, Academic Press, London, 1977, Ch. 7.
42 P. M. Zarembski and A. Hodgkinson, Brit. J. Nutr., 16 (1962) 627.
43 A. Hodgkinson, J. Hum. Nutr., 35 (1981) 136.

Analytica Chimica Acta, 152 (1983) 123—131
Elsevier Science Publishers B.V., Amsterdam — Printed in The Netherlands

ENZYMATIC DETERMINATION OF OXALATE IN URINE BY HEADSPACE SAMPLING OF CARBON DIOXIDE AND FLAME IONIZATION DETECTION

ANDERS O. LINDBERG
Department of Analytical Chemistry, University of Umeå, S-901 87 Umeå (Sweden)
(Received 18th March 1983)

SUMMARY

A method for the determination of oxalate in urine is described. Oxalate is decarboxylated with oxalate decarboxylase (E.C. 4.1.1.2) in vials equipped with rubber septa. Carbon dioxide generated is sampled with a gas-tight syringe, injected into a methanation oven and detected with a flame ionization detector. A simple one-point kinetic method is suggested because enzyme inhibition from sulphate and phosphate may cause incomplete conversion of oxalate. The choice of pH for the method described is discussed in the light of the effect of pH on the Michaelis constant, on the maximum velocity and on inhibition constants. It was estimated that 50 μmol l^{-1} oxalate can be determined with a precision of 10%.

Various pathological conditions give rise to increased excretion of oxalic acid in body fluids, which explains the great interest of clinical chemists in oxalate determinations. Such determinations are of particular interest in studies on stone formation. A vast number of methods for the determination of oxalate in biological fluids has been published. The literature up to 1977 has been reviewed by Hodgkinson [1]. It is evident that the measurement of small amounts of oxalate represents a major problem.

Unspecific procedures like permanganate titration and colorimetry are widely used; some method of separation is therefore usually included in order to avoid interferences, e.g., precipitation, solvent extraction and anion exchange. Unfortunately, substances in complex biological matrices tend to cause co-precipitation, increased solubility or decreased rate of crystallization. This might explain the wide variation in the reported recoveries for oxalate. The isotope dilution technique has been recommended in order to avoid the problems of quantitative separation. This is an advantage, but the method requires sophisticated equipment and is time-consuming. Several papers have also been published utilizing gas chromatographic separation and enzymatic degradation.

During recent years, work has been directed towards the use of various modern separation techniques without isolation of oxalate prior to derivatization [2—5]. A few methods do not need any derivatization [6—9] and

0003-2670/83/$03.00

among these high-performance liquid chromatography (h.p.l.c.) and ion chromatography (i.c.) seem to be most promising.

Larsson et al. [7] described the use of h.p.l.c. in the reversed-phase mode with u.v detection. Interfering compounds were eliminated with a C_{18} cartridge. Applications of reversed-phase h.p.l.c. in biochemistry have been reviewed [10]. Robertson et al. [9] used i.c. with conductivity detection. This technique gave a correlation coefficient of 0.989 compared with a standard colorimetric method; the corresponding figure for reversed-phase chromatography [7] was 0.77.

Many enzymatic methods have recently emerged for determining the oxalate content in urine [11—18], serum [19, 20], food and beverages [21—25]. These methods allow the separation step to be eliminated because their selectivity facilitates their use in complicated matrices. Enzymatic procedures using two [13, 15, 17, 20, 22—25] and even three enzymes [16] have been described for the determination of oxalate. Difficulties encountered in the determination of carbon dioxide liberated by oxalate decarboxylase ((E.C. 4.1.1.2); $(COOH)_2 = CO_2 + HCOOH$) or oxalate oxidase ((E.C. 1.2.3.4); $(COOH)_2 + O_2 = 2CO_2 + H_2O_2$) have made it necessary to increase the complexity of the method by using coupled enzymatic reactions for the determination of formic acid and hydrogen peroxide, respectively. The design of simple methods for the determination of carbon dioxide would therefore be of value.

A serious drawback is that methods based on oxalate decarboxylase tend to underestimate the oxalate content in urine by 10—20% [26]. This is caused by a combination of incomplete degradation of oxalate (by competitive inhibition from sulphate and phosphate) and losses of the carbon dioxide produced. To circumvent this problem of incomplete conversion, a kinetic one-point method is suggested which comprises headspace sampling and determination of carbon dioxide as methane with a flame ionization detector.

Theory

Michaelis and Menten [27] proposed a model for the simplest enzyme kinetics $E + S \underset{k_{-1}}{\overset{k_1}{\rightleftarrows}} ES \overset{k_2}{\rightarrow} E + P$. An enzyme-substrate complex, ES, is formed and decomposes irreversibly to the enzyme and a product. A steady-state rate equation can be derived

$$d[P]/dt = -d[S]/dt = V = V_{max}[S]/(K_M + [S]) \quad (1)$$

where V_{max} is the maximum rate and $K_M = (k_2 + k_{-1})/k_1$ is the Michaelis constant. These two parameters are often determined with a Lineweaver—Burk plot [28] ($1/V$ vs. $1/[S]$). If $[S] \ll K_M$, the reaction obeys first-order kinetics; when $0.1\ K_M < [S] < 10\ K_M$ the reaction is intermediate between first and zero order. If the enzyme is competitively inhibited, the rate equation is

$$V = V_{max}[S]/\{K_M(1 + [I]/K_I) + [S]\} \quad (2)$$

where K_I is the dissociation constant for the inactive enzyme—inhibitor complex. For a first-order enzymatic reaction, the change in substrate concentration between the times t_1 and t_2 will be [29]

$$\Delta[P] = -\Delta[S] = [S]_0 [\exp(-V_{max} t_1/K_M) - \exp(-V_{max} t_2/K_M)] = [S]_0 a(t_1, t_2) \quad (3)$$

If the times t_1 and t_2 are fixed, $\Delta[S]$ will be linearly proportional to the initial substrate concentration, $[S]_0$, regardless of the extent of the reaction. The constant of proportionality, $a(t_1, t_2)$, depends only on V_{max}, K_M and measurement times.

The fundamental requirement for the determination of a substrate from the rate of an enzyme-catalyzed reaction is that the reaction obeys first-order kinetics. This restricts the use of simple kinetic enzymatic methods to enzymes with high K_M values compared with the substrate concentration to be determined. If K_M is too low it can, however, be increased apparently by the addition of a competitive inhibitor [30].

EXPERIMENTAL

Reagents

Oxalate standard. Sodium oxalate (oxidimetric standard, NBS, 99.95%) was dried for 1—2 h at 105°C and dissolved (0.1000 mol l^{-1}) in buffer (HCl, pH 2.0, 0.1 mmol l^{-1} EDTA, p.a.).

Enzyme. Oxalate decarboxylase (20 units; Sigma Chemical Co.; 0—3500, 1.3 U mg^{-1} solid, lot 51F-6806) was dissolved in 1.5 ml of buffer (1 mmol l^{-1} malonic acid, 1 mmol l^{-1} EDTA, pH 3.2). The enzyme solution was stored in the freezing compartment of a refrigerator.

Preliminary experiments

Enzyme measurements. The Michaelis constant (K_M) and the maximum velocity (V_{max}) as a function of pH were determined spectrophotometrically. This is possible because the absorptivity of oxalate is higher than the sum of the absorptivities for formic acid and carbon dioxide. A Unicam SP1800 ultraviolet spectrophotometer equipped with a Unicam AR25 linear recorder was used. All experiments were done in a thermostated room (25 ± 0.5°C). The quartz cuvettes (10 mm light path, 0.6 ml volume) were thermostated in the spectrophotometer to 25 ± 0.05°C. The wavelength was 216 nm and the buffer used served as a blank. Oxalate solutions (600 µl; 0.4, 0.5, 0.7, 1.0 mmol l^{-1}) were pipetted into the cuvette and the temperature was allowed to equilibrate for 10 min. Then 1.0 µl of the oxalate decarboxylase solution was added with a 5-µl Hamilton syringe. The decrease of absorbance vs. time was recorded and the initial reaction rates were estimated from the slopes at the starting points of the curves. K_M and V_{max} were obtained from a Lineweaver—Burk plot. The substrate concentrations were chosen in such a way that the values on the x-axis were evenly spaced and K_M and V_{max} were

evaluated from the intercepts of the axes with straight-line fitting (least squares).

The buffers used were 10 mmol l^{-1} lactic acid (pH 3.50 and 4.00), 10 mmol l^{-1} monochloroacetic acid (pH 3.00) and 10 mmol l^{-1} glycine (pH 2.00). No organic acid was added to the buffer of pH 1.50. All the buffers contained EDTA (0.1 mmol l^{-1}). Sodium hydroxide and hydrochloric acid were used to adjust the pH. A fivefold increase in buffer concentration did not affect the enzyme decarboxylation rate. The initial decarboxylation rate (in the range used for determination of V_{max} and K_M) was a linear function of enzyme concentration.

The following differences at 216 nm between the molar absorptivity (in l mol^{-1} cm^{-1}) for oxalate and the products of the enzymatic decarboxylation were used: 520 (pH 1.50), 630 (pH 2.00), 695 (pH 2.50), 660 (pH 3.00), 615 (pH 3.50), 520 (pH 4.0). To obtain these figures, oxalate (1 mmol l^{-1}) was enzymatically decarboxylated and the total absorbance change was noted. Corresponding figures obtained with absorbance measurements of oxalate and formate solutions gave values which were about 5% higher than the values given above. The difference is probably due to the small u.v.-absorbance of carbon dioxide and hydrogencarbonate [31].

Enzyme inhibition. The decarboxylating rates of 0.1 mmol l^{-1} oxalate were determined as described above with and without the presence of sulphate and phosphate. The sulphate concentrations were 0.1 (pH 1.50), 1 (pH 2.00), 2 (pH 2.50), 10 (pH 3.00), 20 (pH 3.50), 100 (pH 4.00) mmol l^{-1}. The phosphate concentrations were 10 (pH 1.5 and 2) and 3 (pH 2.5, 3.0, 3.5, 4.0) mmol l^{-1}. The inhibition constants for sulphate and phosphate were then calculated from the combination of Eqns. (1) and (2) and with K_M previously determined. This simple method for the determination of the inhibition constants was regarded as justified for the present purpose.

Completeness of enzymatic decarboxylation in the presence of phosphate and sulphate. The completeness of decarboxylation of 0.6 mmol l^{-1} oxalate was spectrophotometrically determined at 40° C and pH 3.50 (10 mmol l^{-1} lactic acid, 0.1 mmol l^{-1} EDTA) in the presence of 25 mmol l^{-1} sulphate and 32 mmol l^{-1} phosphate. To a thermostated quartz cuvette (10 mm light path, 3.0 ml volume) was added 10 and 20 μl of the enzyme solution and the absorbance was recorded for 24 h at 216 nm. From the total absorbance decrease obtained and the known molar absorptivity decrease (615 l mol^{-1} cm^{-1}) the completeness of the decarboxylation was calculated.

Choice of pH for kinetic one-point determination of oxalate. The decarboxylation of oxalate (0.1, 0.2, 0.4, 0.6, 0.8 mmol l^{-1}) was recorded spectrophotometrically (216 nm) at pH 2.0 (10 mmol l^{-1} glycine, 0.1 mmol l^{-1} EDTA) and at pH 3.5 (10 mmol l^{-1} lactic acid, 0.1 mmol l^{-1} EDTA) in the presence of 20 mmol l^{-1} sulphate and 20 mmol l^{-1} phosphate. To a thermostated (40° C) quartz cuvette (10 mm light path, 3.0 ml volume) was added 10 μl of an enzyme solution (13.3 U ml^{-1}) and the absorbance decrease after 30 min was noted.

Apparatus for carbon dioxide determination

Figure 1 is a schematic diagram of the equipment used. The sample was injected with a syringe through a septum and was swept by a stream of nitrogen and hydrogen into a catalyst oven. The methane produced in the oven was then detected with a flame ionization detector (FID); the peak height was recorded with a strip-chart recorder. Details regarding methanation, gas purification and modification of the gas chromatograph are given in the preceding paper [32].

Procedure for determination of urine oxalate

Fresh urine samples were diluted (1:1) with deionized water (Millipore) and concentrated hydrochloric acid was added to adjust the acidity to pH 2.0. The urine samples were diluted in order to decrease the influence of the natural variation of sulphate and phosphate concentration. Glass tubes (9 ml) were filled with 5.0 ml of the diluted samples and with 0.5 ml of a solution containing sulphate (220 mmol l^{-1}, Na_2SO_4, pH 2.0) and phosphate (110 mmol l^{-1}, $NaH_2PO_4 \cdot 2H_2O$). To 5 tubes were added 0, 5, 10, 15 and 20 μl, respectively, of an oxalate standard (0.1 mol l^{-1}, pH 2.0). The screw caps of the tubes were provided with rubber septa through which one long and one short injection needle were inserted. With this arrangement the samples were purged with purified synthetic air [32] (Ascarite) for 15 min to expel dissolved carbon dioxide and other volatile substances. After the purging, the needles were removed and 25 μl of the solution of oxalate decarboxylase were injected with a syringe. The five tubes and a blank tube with no oxalate and no enzyme added were then incubated upside down for 4—5 h in a water-bath (40 ± 0.1° C). The tubes were then shaken vigorously for 2 min with a mechanical shaking apparatus, 5 μl of the gas phase in the tubes was injected with a syringe (Precision Sampling, LC-210) through the septum of the apparatus (Fig. 1) and the peak height was recorded. Ten replicates were taken from each tube.

RESULTS AND DISCUSSION

Determination of K_M *and* V_{max}

Figure 2 describes the influence of pH on V_{max} and K_M. As can be seen, V_{max} is fairly constant between pH 1.5 and pH 3.0 but shows a moderate decrease for higher pH. The enzyme had no activity at pH 1.0. K_M has its minimum value at pH 2.0 and shows an increase at higher pH but has a plateau between pH 3.0 and pH 3.5. The values of V_{max} and K_M are represented in semilogarithmic plots as is usual. An interpretation in terms of ionizable groups in the substrate, enzyme or enzyme–substrate complex is beyond the scope of this paper. The original paper on oxalate decarboxylase by Shimazono and Hayaishi [33] is the only source available regarding the influence of pH on the activity of the enzyme. Unfortunately, their experiments were done with buffers containing phosphate, which is known to

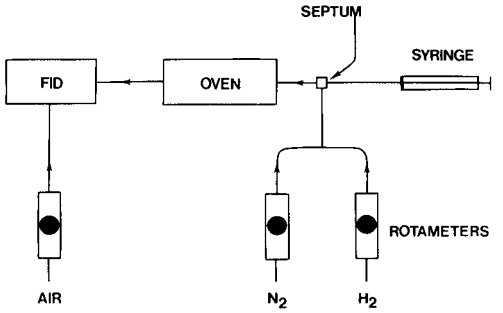

Fig. 1. Schematic diagram of the experimental arrangement.

inhibit the enzyme [26]. No meaningful comparison between their data and the present results can therefore be made.

Determination of K_I *and the completeness of enzymatic decarboxylation in presence of phosphate and sulphate*

Figure 3 describes the influence of pH on K_I for sulphate and phosphate. As can be seen, the inhibitory effect of sulphate increases with decreasing pH, whereas phosphate gives a maximum inhibitory effect at about pH 2.5. It must be stressed that the kinetic results presented here were obtained with a crude enzyme preparation; contaminants in the preparation may affect the kinetic properties of the enzyme. It is therefore highly desirable that methods for the preparation of the pure enzyme be investigated.

Spectrophotometric investigation of the enzymatic decarboxylation was done at pH 3.5, because this pH was the most favourable under conditions of inhibition. The temperature was maintained at 40° C; a temperature of 50° C caused slow denaturation of the enzyme. A sulphate concentration of 25

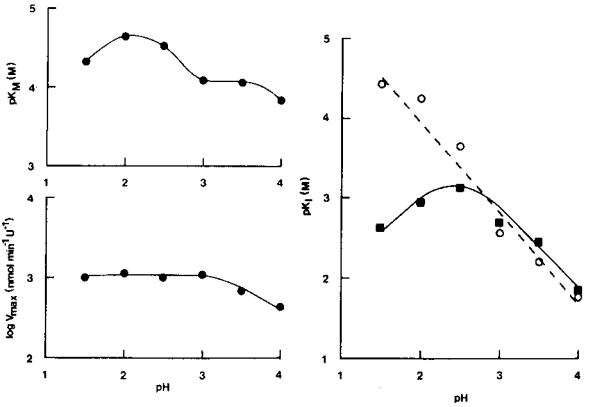

Fig. 2. K_M and V_{max} as a function of pH.

Fig. 3. Inhibition constants for sulphate (○) and phosphate (■) as a function of pH.

mmol l^{-1}, a phosphate concentration of 32 mmol l^{-1} and an oxalate concentration of 0.6 mmol l^{-1} were chosen, because these values approximately represent the highest levels likely to be encountered in human urine [9, 34]. It was found for both the enzyme concentrations used (20 units/1.5 ml buffer with 10- and 20-μl injections) that only 81% of the oxalate was decarboxylated. In urine samples with lower sulphate and phosphate concentrations than used here, a larger fraction than 81% is of course decarboxylated. The ranges for sulphate and phosphate have been reported as 8—25 and 17—32 mmol l^{-1}, respectively [34]. The consequence is that the recovery will show unpredictable variations for various urine samples.

From the recorder tracing, it could be seen that for the higher of the two enzyme concentrations used, 90% of the total absorbance decrease was achieved after about 3.5 h. It seems unlikely that moderately increased enzyme concentrations should result in a considerably higher degree of substrate decarboxylation than reported here. If sulphate and phosphate were removed from the sample, this would result in complete enzymatic conversion, which implies that some kind of separation step is desirable. However, such a step adds complexity to the method and there is always a risk for a poor recovery in a complicated matrix like urine. An alternative to the separation is the use of a simple kinetic method.

Choice of pH for kinetic one-point determination of oxalate

When the absorbance decrease after 30 min at pH 2.0 was plotted against oxalate concentration, it was found to be directly proportional to the oxalate concentration over the range 0—0.6 mmol l^{-1} (slope = 283 l mol^{-1}, s.e. = 7.0 l mol^{-1}, intercept = 0.0004, s.e. = 0.0024). However, the same plot at pH 3.5 showed a pronounced curvature. The reason for this is that the apparent K_m value ($K_M(1 + [I]/K_I)$) is larger at pH 2.0 than at pH 3.5 because of more marked inhibition at the lower pH value (see Fig. 3). It is of course vital that the calibration curve be linear; the concentration of oxalate in urine must be evaluated by a standard addition technique because of the varying concentration of sulphate and phosphate in urine samples. Moreover, it cannot be excluded that other components of varying concentrations may affect the enzyme activity. Thus, oxalate in urine was subsequently determined at pH 2.0 with the one-point kinetic method. The low pH chosen has also the advantage that it prevents any possibility of precipitation of calcium oxalate [35].

Determination of oxalate as carbon dioxide

Initial determinations of carbon dioxide generated from a standard carbonate solution were done. Small amounts of a carbonate standard (10—80 μl) were injected into the vials which contained the buffer of pH 2. The amounts of carbonate injected corresponded well with the concentrations of oxalate likely to be found in urine [9]. The peak height (arbitrary units) was directly proportional to the carbonate concentration in the buffer over the range

TABLE 1

Determination of oxalate in urine

Found in sample (μmol l^{-1})	Recovery[a] (%)
199	95.9
182	94.1
244	93.0
196	100.7
61	102.8
Mean value =	97.3%
S.d. =	4.3%

[a]Oxalate added: 90.8 μmol l^{-1}.

0—0.8 mmol l^{-1} (slope = 815 l mol^{-1}, s.e. = 8.5 l mol^{-1}, intercept = —4, s.e. = 3.7). It was estimated that a 0.05 mmol l^{-1} solution of carbonate could be determined with a precision of 10%.

It can be seen from Table 1 that the recovery of oxalate added to a few urine samples from healthy persons was quantitative. The original oxalate concentration had a range of 60—240 μmol l^{-1}. These data agree reasonably well with the results achieved with ion chromatography [9].

Probably the most widely used technique for the enzymatic determination of oxalate is the trapping of carbon dioxide in an alkaline buffer and subsequent measurement of the pH change [36]. This method has the advantage that no sophisticated equipment is needed and only one enzyme is used. However, it is a disadvantage that it takes a long time, 16 h, [12] even for carbon dioxide generated from carbonate to diffuse from the sample into the trapping medium because the flasks cannot be shaken. There is also a risk of losses of carbon dioxide because the flasks must be opened when the pH change is measured. Moreover, each flask can be sampled only once.

The technique described here has the advantage that the vials can be shaken; the carbon dioxide in the buffer is therefore rapidly and efficiently transferred to the gas phase. Moreover, the vials can be sampled several times. The risk of losses is also reduced, because the vials are not opened during the sampling procedure. In another method for the determination of oxalate [32], immobilized oxalate decarboxylase and a dialysis unit are used in combination with the FID [32]. Compared with that approach, the technique described here needs considerably more technical skill and the risk of contamination from carbon dioxide in air is higher. Work is therefore in progress to develop a method for the determination of oxalate in urine which employs a decarboxylase reactor.

The author thanks Prof. Anders Cedergren for assistance in preparing the manuscript and Dr. Michael Sharp for linguistic revision.

REFERENCES

1 A. Hodgkinson, Oxalic Acid in Biology and Medicine, Academic Press, London, 1977.
2 G. Charransol, C. Barthelemy and P. Desgrez, J. Chromatogr., 145 (1978) 452.
3 H. A. Moye, M. H. Malagodi, D. H. Clarke and C. J. Miles, Clin. Chim. Acta, 114 (1981) 173.
4 J. F. Murray, Jr., H. W. Nolen, III, G. R. Gordon and J. H. Peters, Anal. Biochem., 121 (1982) 301.
5 H. Hughes, L. Hagen and R. A. L. Sutton, Anal. Biochem., 119 (1982) 1.
6 W. Tschöpe, R. Brenner and E. Ritz, J. Chromatogr., 222 (1981) 41.
7 L. Larsson, B. Libert and M. Asperud, Clin. Chem., 28 (1982) 2272.
8 C. J. Mahle and M. Menon, J. Urol., 127 (1982) 159.
9 W. G. Robertson, D. S. Scurr, A. Smith and R. L. Orwell, Clin. Chim. Acta, 126 (1982) 91.
10 B. L. Karger and R. W. Giese, Anal. Chem., 50 (1978) 1048A.
11 P. O. Schwille, M. Paulus, D. Scholz and A. Sigel, Urologe Ausg. A, 17 (1978) 217.
12 G. Kohlbecker, L. Richter and M. Butz, J. Clin. Chem. Clin. Biochem., 17 (1979) 309.
13 J. Yriberri and S. Posen, Clin. Chem., 26 (1980) 881.
14 R. K. Kobos and T. A. Ramsey, Anal. Chim. Acta, 121 (1980) 111.
15 M. F. Laker, A. F. Hofmann and B. J. D. Meeuse, Clin. Chem., 26 (1980) 827.
16 G. Kohlbecker and M. Butz, J. Clin. Chem. Clin. Biochem., 19 (1981) 1103.
17 D. M. Obzansky and K. E. Richardson, Clin. Chem., 28 (1982) 1648.
18 M. Bishop, H. Freudiger, U. Largiadèr, J. D. Sallis, R. Felix and H. Fleisch, Urol. Res., 10 (1982) 191.
19 T. Akcay and G. A. Rose, Clin. Chim. Acta, 101 (1980) 305.
20 M. Sugiura, H. Yamamura, K. Hirano, Y. Ito, M. Sasaki, M. Morikawa, M. Inoue and M. Tsuboi, Clin. Chim. Acta, 105 (1980) 393.
21 G. P. Kasidas and G. A. Rose, J. Hum. Nutr., 34 (1980) 255.
22 P. Anderegg, F. Schur and H. Pfenninger, Brau.-Rundsch., 91 (1980) 133.
23 H.-O. Beutler, J. Becker, G. Michal and E. Walter, Fresenius Z. Anal. Chem., 301 (1980) 186.
24 F. Drawert, H. Paul and W. Hagen, Brauwissenschaft, 34 (1981) 57.
25 H.-O. Beutler, Flüss. Obst., 49 (1982) 62.
26 W. G. Robertson and A. Rutherford, Scand. J. Urol. Nephrol., (Suppl.) 53 (1980) 85.
27 L. Michaelis and M. L. Menten, Biochem. Z., 49 (1913) 333.
28 H. Lineweaver and D. Burk, J. Am. Chem. Soc., 56 (1934) 658.
29 P. W. Carr and L. D. Bowers, Immobilized Enzymes in Analytical and Clinical Chemistry, Wiley, New York, 1980, p. 78.
30 E. J. Sampson and M. A. Baird, Clin. Chem., 25 (1979) 1721.
31 A. L. Underwood and L. H. Howe III, Anal. Chem., 34 (1962) 692.
32 A. O. Lindberg, Anal. Chim. Acta, 152 (1983) 113.
33 H. Shimazono and O. Hayaishi, J. Biol. Chem., 227 (1957) 151.
34 C. F. Knowles and A. Hodgkinson, Analyst, 97 (1972) 474.
35 A. Hodgkinson, Clin. Chim. Acta, 109 (1981) 239.
36 P. C. Hallson and G. A. Rose, Clin. Chim. Acta, 55 (1974) 29.

Analytica Chimica Acta, 152 (1983) 133—139
Elsevier Science Publishers B.V., Amsterdam — Printed in The Netherlands

EFFECTS OF ORGANIC ACIDS AND SOLVENTS IN INDUCTIVELY-COUPLED PLASMA EMISSION SPECTROMETRY

JINRUI XU, HIROSHI KAWAGUCHI* and ATSUSHI MIZUIKE
Faculty of Engineering, Nagoya University, Chikusa-ku, Nagoya 464 (Japan)
(Received 10th January 1983)

SUMMARY

Spectral interferences of the CN band emissions with the analytical lines of rare earths and yttrium were examined in the presence of organic acids or solvents in aqueous sample solutions. The CN band intensity varied with the organic substances as well as with plasma operating conditions. Spectral line intensities of rare earths and yttrium were enhanced by the presence of ethanol, acetone or acetic acid, but suppressed by citric acid. The effects of organic substances on sample uptake rates and intensity distributions along the plasma axis were also investigated.

Inductively-coupled plasma emission spectrometry (i.c.p.e.s.) has been widely accepted as a versatile technique for the analysis of a variety of samples. Although the samples are usually introduced into the i.c.p. as aqueous solutions, there are occasions where the introduction of an organic solvent is preferred or the presence of organic substances in aqueous solutions is inevitable. For example, solvent extraction has often been used as a preconcentration technique in i.c.p.e.s. [1—3]; wear metals in used lubricating oil have been determined by directly introducing the samples diluted by an organic solvent into the i.c.p. [4—6].

Relatively few investigations, however, have been reported on the effects of organic substances in i.c.p.e.s. [7—10]. Truitt and Robinson [7] studied the emission spectra of the plasma after introduction of organic compounds, but their plasma was unlike the i.c.p.'s now commonly used. Greenfield et al. [8] reported enhancement effects in a nitrogen-cooled, high-power i.c.p. when organic acids or solvents were added to aqueous sample solutions. Ito et al. [9] measured the effects of ethanol on the plasma impedance and also reported enhancement of some spectral lines. Recently, Boorn and Browner [10] reported a more detailed investigation on the effects of organic solvents in i.c.p.e.s. They measured the tolerance of a low-power i.c.p. to various organic solvents in terms of the limiting aspiration rates, finding a good correlation between the limiting aspiration rates and evaporation factors for pure organic solvents.

The present paper deals with the effects of organic solvents and acids in aqueous sample solutions on the CN band emissions and analytical signals.

0003-2670/83/$03.00

Wavelength scans around the analytical lines of rare earths and yttrium were obtained by using a high-resolution echelle monochromator to evaluate spectral interferences of the CN bands. A shift of the axial distributions of spectral line intensities was observed in the presence of small amounts of ethanol in the samples.

EXPERIMENTAL

The instruments and their operating conditions used in this work are summarized in Table 1. The optical configuration of the echelle spectrometer was reported previously [11]. Derivative spectrometry with wavelength modulation by a quartz refractor plate was employed to correct continuum background. Wavelength scans were obtained by d.c. amplification. To measure axial profiles of spectral line intensities, a spectrometer with a horizontal scanning slit in front of the entrance slit described previously [12] was employed.

Stock solutions (1000 μg ml^{-1}) of the elements were prepared by dissolving oxides in hydrochloric or sulfuric acid or dissolving salts in deionized water. The solutions were stored in polyethylene bottles. All the reagents used were reagent grade.

RESULTS AND DISCUSSION

CN band interferences

Spectral interferences from molecular band systems are not generally significant in i.c.p.e.s. when aqueous solutions of samples are introduced. When organic solvents are introduced, however, molecular bands such as CN (violet), C_2 (Swan) and NH appear in the wavelength region higher than 330 nm [10]. Rare earth elements and yttrium have their strong lines

TABLE 1

Instruments and operating conditions

Spectrometer	Yanaco model UOP-1, echelle grating monochromator, focal length 0.8 m, grating 79 grooves/mm blazed at 75° 58′, reciprocal linear dispersion 0.058 nm mm^{-1} at 370 nm (66th order), slit width 50 μm, slit heights 0.5 mm entrance and 1.0 mm exit
RF generator	27.12 MHz, incident power 1.4 kW, reflected power < 5 W
Argon flow rate	Outer gas 16 l min^{-1} unless otherwise stated, intermediate gas 0.8 l min^{-1}, carrier gas 0.5 l min^{-1}
Observation height	15 mm above the load coil
Nebulizer	Glass concentric with spray chamber, uptake rate of aqueous solution 1.6 ml min^{-1}
Wavelength (nm)	La II 408.67 Ce II 413.77 Pr II 390.84 Nd II 401.22 Sm II 359.26 Eu II 381.97 Y II 371.03

in this wavelength region, so that the CN bands often interfere with measurements of these elements. These molecular bands cannot be resolved completely with the commonly used spectrometers of moderate resolution and are observed simply as a background shift. Direct overlaps of the analytical lines with molecular bands are observed, however, when a high-resolution spectrometer is applied. In Fig. 1, the wavelength scans around the Y II 371.03-nm line are shown for pure water, aqueous 5% (v/v) ethanol and the same mixture containing 0.05 μg ml^{-1} yttrium. At the lower outer-gas flow rate, the strong CN band emissions in the spectrum of the ethanol solution interfere seriously with the yttrium line. These CN bands can be suppressed by increasing the outer-gas flow rate and almost disappear at 16 l min^{-1} (Fig. 1B).

Wavelength scans around some other spectral lines of rare earths are shown in Fig. 2 for solutions containing 0.5% ethanol. These lines are the strongest in the table of prominent i.c.p. lines reported by Winge et al. [13]. Even at this low content of ethanol, the CN bands interfere with the rare-earth lines when the outer-gas flow rate is low, but again interferences are suppressed at the higher flow rate. The CN molecules are produced by reactions between organic compounds in sample solutions and atmospheric nitrogen. When the flow rate of the outer gas is increased, the plasma is more effectively shielded from the atmosphere, entrainment of air is reduced, and the CN bands are suppressed. Tests showed that, as the outer-gas flow rate was increased from 10 to 18 l min^{-1}, the intensity of the CN 388.34-nm line was reduced to 5% of its initial value. Obviously, entrainment of air also increases with the distance from the torch, and the CN band intensity increases with observation height. The intensity of the CN 388.34-nm line increased by ten times as the observation height was increased from 4 to 20 mm at an outer-gas flow rate of 10 l min^{-1}.

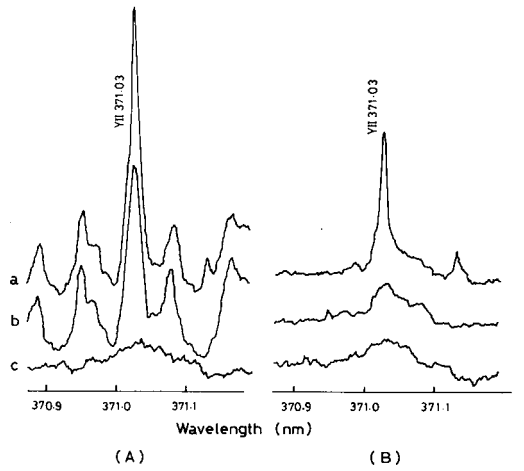

Fig. 1. Wavelength scans around the Y II 371.03 nm-line showing the effects of ethanol and outer-gas flow rate on background. Solutions: (a) 0.05 μg Y ml^{-1} in aqueous 5% (v/v) ethanol; (b) aqueous 5% (v/v) ethanol; (c) water. Outer-gas flow rate: (A) 10 l min^{-1}, (B) 16 l min^{-1}.

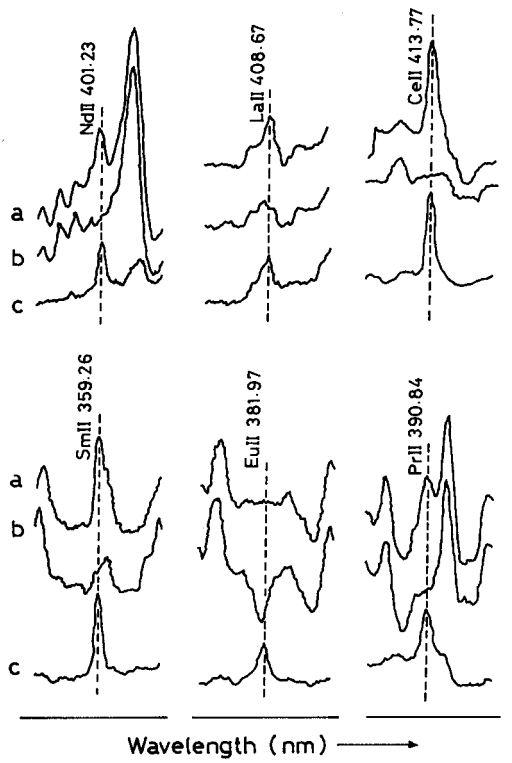

Fig. 2. Wavelength scans around some lines of rare earths showing the effects of ethanol and outer-gas flow rate on background spectra. Outer-gas flow rate: (a, b) 10 l min^{-1}; (c) 16 l min^{-1}. Solutions: (a, c) rare earth element in aqueous 0.5% (v/v) ethanol; (b) aqueous 0.5% ethanol. Concentration ($\mu g\ ml^{-1}$): Nd 0.5; La 0.075; Ce 1.0; Sm 0.5; Eu 0.05; Pr 1.0.

Variation of intensities of the CN bands as a function of the concentration of various organic substances are shown in Fig. 3; this experiment was done at an outer-gas flow rate of 10 l min^{-1} to observe the effects explicitly. The CN band intensities increased almost linearly with the concentration of the organic substance. As can be seen, the CN band emissions for acetone/water mixtures were the highest among the substances examined and about six times higher than for ethanol/water mixtures of the same concentration; this effect may be correlated with the boiling points of the solvents. Boorn and Browner [10] suggested that the tolerance of the i.c.p. to organic solvents could be interpreted in terms of the evaporation factor, a function of solvent properties such as vapor pressure and diffusion coefficient of the solvent vapor. The plasma used in this experiment was extinguished when solutions containing >1% acetone were aspirated, while up to 5% (v/v) ethanol or methanol solutions could be introduced without difficulty. Two organic acids, acetic and citric acids, showed much smaller effects on the CN band intensity. Inorganic carbonates did not produce CN band emissions, as was shown by aspirating up to 5% (w/v) sodium carbonate solutions.

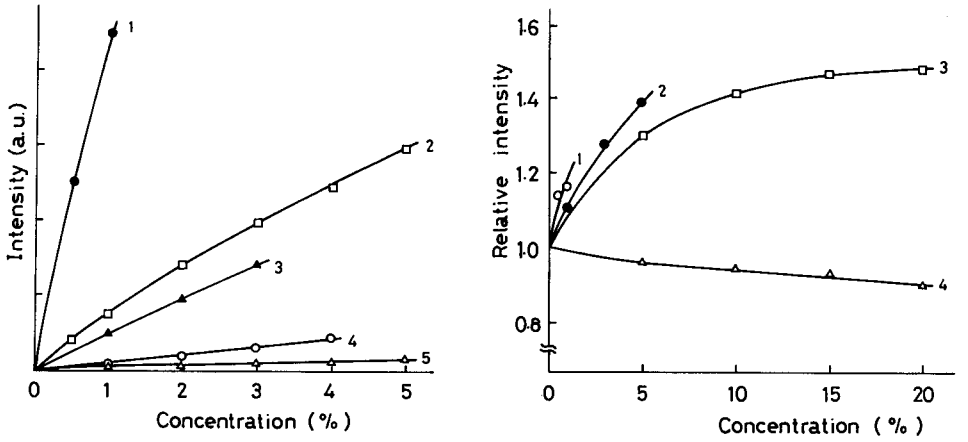

Fig. 3. Variation of intensity of the CN 388.34-nm line as a function of the concentration of organic substances in water: (1) acetone; (2) ethanol; (3) methanol; (4) acetic acid; (5) citric acid (expressed in % (v/v) for 1—4 and in % (w/v) for 5). Outer-gas flow rate of 10 l min^{-1}.

Fig. 4. Variation of the La II 408.67-nm line intensity as a function of the concentration of organic substances in water: (1) acetone; (2) ethanol; (3) acetic acid; (4) citric acid (expressed in % (v/v) for 1—3 and in % (w/v) for 4).

Effect of organic substances on the analyte line intensities

Greenfield et al. [8] reported enhancement effects in the high-power i.c.p. when aqueous solutions of organic acids or methanol were aspirated. Boorn and Browner [10] measured line intensities of three analytes in six pure solvents and reported both enhancement and suppression effects. The effects were attributed variously to changes in the aspiration rate, in the transport efficiencies via changing droplet diameters, and in the plasma temperature because of large vapor loading.

In the present experiments, effects of organic substances in aqueous solutions on the spectral line intensities of rare earths and yttrium were investigated. Variations of the intensity of the La II 408.67-nm line as a function of the concentration of organic substances are shown in Fig. 4. Acetone, ethanol and acetic acid enhanced the emission whereas citric acid suppressed it. Similar results were obtained for the lines of other rare earth elements. The relative uptake rate of these solutions decreased as the concentration of organic substances increased (Fig. 5), and this should lead to decreased signal intensities. Thus the increases in signal intensity for acetone, ethanol and acetic acid solutions must be due to a change in transport efficiency and/or plasma properties which outweighs the change in the uptake rate.

Greenfield et al. [8] obtained the following empirical equation for the signal intensities of analytes in aqueous solutions of organic compounds:

$$I = I_w\ [\eta/(\sigma\rho)^{1/2}]\,[(7.055/\eta) + 1.245] \qquad (1)$$

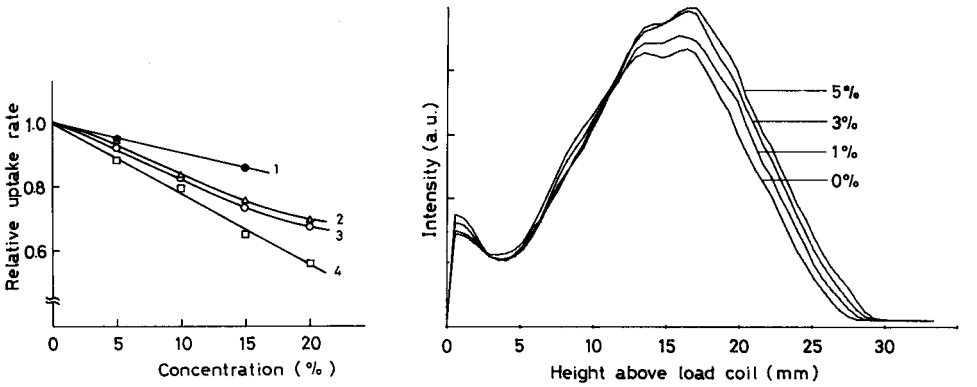

Fig. 5. Variation of uptake rate of solutions as a function of the concentration of organic substances in water: (1) acetic acid; (2) acetone; (3) methanol; (4) ethanol (expressed in % (v/v) for all).

Fig. 6. Effect of concentration of ethanol in water on the axial intensity distribution of the La II 408.67-nm line.

where I_w is the signal obtained from an aqueous solution, η is the viscosity in poises, σ is the surface tension in dyn cm^{-1}, and ρ is the liquid density in g ml^{-1}. The term $\eta/(\sigma\rho)^{1/2}$ in this equation occurs also in Nukiyama and Tanasawa's expression for droplet size [14]. Thus the change in droplet size or transport efficiency may play a major role in the signal enhancement. The enhancement effects calculated by using Eqn. (1), however, were approximately half those obtained experimentally for acetone, ethanol and acetic acid solutions. Though acetone showed a greater effect than ethanol in Fig. 4, the enhancement effects calculated for these solutions were almost the same. Probably the volatility of the solvent, which is not considered in Eqn. (1) also affects the transport efficiency and so the enhancement effects. Boorn and Browner [10] reported signal reductions in certain cases rather than the enhancements predicted by Eqn. (1), which suggests that a more detailed explanation is needed.

Effects of ethanol on the axial distribution of the intensity of the La II 408.67-nm line are shown in Fig. 6. Enhancements are obtained at observation heights more than 11 mm above the load coil, whereas slight suppression appears below 11 mm. These results correspond well to those obtained by Boorn and Browner [10] for pure organic solvents. Temperature decreases caused by the larger vapor loading may explain the suppression observed in the lower region of the plasma.

Conclusions

Molecular bands such as the CN bands produced by the presence of organic substances in aqueous solutions often interfere significantly with analytical lines even when a high-resolution spectrometer is used. The band intensities

depends on the concentration and properties of the organic substances, as well as on the operating conditions of the plasma; the latter can be chosen appropriately to eliminate the interference. Signal enhancements by organic substances can be ascribed mainly to the increased transport efficiency caused by decreased droplet size. The magnitude of these effects, however, is affected by various factors in a complicated way which needs further investigation.

REFERENCES

1 J. M. Motooka, E. L. Mosier, S. J. Sutley and J. G. Viets, Appl. Spectrosc., 33 (1979) 456.
2 R. Shue, T. Ito, H. Kawaguchi and A. Mizuike, J. Chem. Soc. Jpn., 1981 (1981) 172.
3 A. Miyazaki, A. Kimura and Y. Umezaki, Anal. Chim. Acta, 138 (1982) 121.
4 V. A. Fassel, C. A. Peterson, F. N. Abercrombie and R. N. Kniseley, Anal. Chem., 48 (1976) 516.
5 R. N. Merryfield and R. C. Royd, Anal. Chem., 51 (1979) 1965.
6 K. Fujimatsu, T. Iino, H. Uchida, K. Iwasaki, T. Kogane and Y. Matano, Bunseki Kagaku, 30 (1981) T11.
7 D. Truitt and J. W. Robinson, Anal. Chim. Acta, 49 (1970) 401; 51 (1970) 61.
8 S. Greenfield, H. M. McGeachin and P. B. Smith, Anal. Chim. Acta, 84 (1976) 67.
9 T. Ito, H. Kawaguchi and A. Mizuike, Bunseki Kagaku, 28 (1979) 648.
10 A. W. Boorn and R. F. Browner, Anal. Chem., 54 (1982) 1402.
11 J. Xu, H. Kawaguchi and A. Mizuike, Appl. Spectrosc., 37 (1983) 123.
12 H. Kawaguchi, T. Ito and A. Mizuike, Spectrochim. Acta, Part B, 36 (1981) 615.
13 R. K. Winge, V. J. Peterson and V. A. Fassel, Appl. Spectrosc., 33 (1979) 206.
14 S. Nukiyama and Y. Tanasawa, Trans. Soc. Mech. Eng. Jpn., 5 (1939) 63.

Analytica Chimica Acta, 152 (1983) 141—147
Elsevier Science Publishers B.V., Amsterdam — Printed in The Netherlands

CALCIUM MATRIX EFFECTS IN MULTI-ELEMENT ANALYSIS OF ANIMAL BONE BY INDUCTIVELY-COUPLED PLASMA EMISSION SPECTROMETRY

JULIAN LEE

Applied Biochemistry Division, D.S.I.R., Palmerston North (New Zealand)

(Received 16th February 1983)

SUMMARY

Major and minor trace elements including copper, iron, molybdenum and zinc are determined in animal bone by using inductively-coupled plasma emission spectrometry. Copper and molybdenum are determined after preconcentration and separation from matrix elements on the strong cation-exchange resin BioRad AG-MP-50. Calcium causes a spectral interference on the S I 180.73-nm emission line and suppresses the signal intensity of many ion and atom lines. The Cu I 324.75-nm emission line is affected by scattered Ca II 317.93-nm emission. Analytical data are given for the IAEA reference bone material, H-5.

Bones act as important stores in animals for both essential and inessential elements. Recent interest and the recognition of the role of these elements in animal nutrition and related trace element disorders has stimulated concern in establishing reliable concentration values. A recent International Atomic Energy Agency (IAEA) laboratory intercomparison of minor and trace elements in an animal bone reference material (H-5) highlighted the variability of results, particularly for those elements present at sub-$\mu g\ g^{-1}$ levels.

In this study, inductively-coupled plasma emission spectrometry (i.c.p.e.s.) is used for the simultaneous determination of several elements in animal bone. Full advantage of the excellent detection characteristics of i.c.p.e.s. has often been limited in practice by the restrictions imposed by matrix effects. Aerosol production, line intensities and background structure may be modified by changes in the concentration of major constituent elements, particularly by excesses of easily ionizable elements [1, 2]. Matrix interferences are encountered in the analysis of bone extracts where the combined effects of high calcium, phosphate and sodium levels along with residual organic material result in plasma fluctuations and suppression or enhancement of analyte signals. These are of special concern where the analyte is present at low levels. Attempts to minimize matrix effects by dilution often result in lowering the original analyte concentration below its detection limit.

0003-2670/83/$03.00

Quantitative preconcentration and separation of certain trace elements from the calcium phosphate matrix is therefore required. The solubility properties of calcium orthophosphate necessitated extraction from strongly acidic media. After consideration of several liquid—liquid extraction and ion-exchange techniques, a cation-exchange method described by Strelow [3] was used selectively to remove large amounts of calcium from acidified bone extracts on a column of macroporous resin. The preconcentration and separation of trace elements by ion-exchange and elution with methanolic hydrochloric acid is followed by evaporation of the methanol and subsequent determination by i.c.p.e.s.

EXPERIMENTAL

Instrumentation and reagents

An Applied Research Laboratories 34000 system (polychromator, Paschen-Runge mount) with a movable primary slit enabling the near vicinity of any line to be scanned for possible spectral interferences, was used. The experimental facility and argon plasma operating parameters have been described [4]. The analyses were done under compromise conditions for simultaneous multi-element analysis. Wavelength data are given in Table 1.

Chemicals used were of analytical grade or better. Multi-element standards for calibrating the spectrometer were prepared from 100 μg ml^{-1} stock solutions of the potassium salt for phosphorus and sulphur or of the metal chloride in 2 M hydrochloric acid made from redistilled constant-boiling acid. Three standards per decade of analyte concentration for each element were used for calibration.

The analytical-grade macroporous cation resin, AG-MP-50 (50—100 mesh, H^+ form, BioRad Laboratories, Richmond, CA) was used in borosilicate glass columns (200 mm × 50 mm). The resin was washed repeatedly in 5 M nitric acid to remove impurities.

TABLE 1

Wavelength data

Element	Line (nm)	Detection limit (ng ml^{-1})[a]	Interferences	Element	Line (nm)	Detection limit (ng ml^{-1})[a]
B	249.68	12	Fe 249.653 nm, Fe 249.649 nm	Mn	257.61	2
				Mo	202.03	15
Ca	317.93	—		Na	589.59	50
Cr	267.72	8	P 267.712 nm, Mg	Ni	231.60	10
Cu	324.75	6	Ca 317.93 nm, stray light	P	214.91	100
				Sr	407.77	—
Fe	259.95	4	Ca 180.74 nm	Zn	213.86	15
S	180.73	30				
K	766.49	500				
Mg	279.08	50				

[a] 3σ value obtained from an analyte concentration of 5 μg ml^{-1} in 2 M HCl in the presence of 2000 μg ml^{-1} of calcium.

Procedures

Sample preparation. Bone material, freeze-dried and dried over phosphorus(V) oxide (0.5—1.0 g), was accurately weighed into a 150-ml Erlenmeyer flask and 5 ml of re-distilled nitric acid added. The mixture was left overnight and, subsequently, heated carefully on a hot plate at 80°C. When oxidation was complete, the nitric acid was removed by increased heating and the resulting yellow residue was dissolved in 2 M hydrochloric acid. Appropriate dilutions were made for direct multi-element analysis or removal of calcium by ion-exchange.

Calcium removal. A column was filled with 10 g of washed AG-MP-50 resin and 25 ml of bone solution (about 2 g of freeze-dried bone material) was washed onto the resin with 0.1 M hydrochloric acid. Phosphate ions passed through the column with the solvent front. Trace elements (Cu, Zn, Mo) were eluted in one fraction with 3 M hydrochloric acid: methanol (1:1, v/v) at 2 ml min^{-1}. Calcium was removed with 200 ml of 5.0 M nitric acid and the column was washed with deionized water in preparation for the next sample. The fraction containing copper and zinc was evaporated to near dryness and the residue dissolved in 5 ml of 2 M hydrochloric acid. The sample solution contained less than 20 ppm each of calcium and phosphate.

RESULTS AND DISCUSSION

Spectral interferences

In simultaneous multi-element analysis by i.c.p.e.s., spectral and matrix interferences cannot always be avoided [5]. In bone digests, calcium and phosphorus are present at concentrations sufficiently high to require on-line spectral corrections where interferences on analyte emission lines occur. Those of analytical significance, i.e., those that produce a change in signal greater than that given by the analyte at its detection limit, are given in Table 1. The nature of these spectral interferences and others pertinent to this system have been described elsewhere [4, 6]. Boumans [7] has described the methodology for expressing the magnitude of spectral interference factors in terms of critical concentration ratios. These are used for on-line spectral corrections of matrix elements.

The spectral overlap of the Ca II 180.739-nm emission line on S I 180.735 nm produces a particularly large increase in intensity at the sulphur wavelength. For example, in the determination of sulphur in a typical digest solution containing 2 mg ml^{-1} calcium and 25 μg ml^{-1} sulphur, an apparent sulphur concentration equivalent to 51 μg ml^{-1} was found, i.e., 50% of the total emission signal at the S I 180.735-nm line is derived from concomitant calcium. A correction factor of 0.013 μg ml^{-1} "apparent S" for every μg ml^{-1} calcium in solution is therefore incorporated automatically during routine analysis.

The spectrometer system used in this study uses narrow bandpass filters. However, when solutions containing calcium are aspirated into the plasma an apparent emission is recorded at the Cu I 324.75-nm line even when the

Cu I 324.75-nm line exit slit is blocked. When the Ca II 317.93-nm exit slit is blocked, and a calcium solution is aspirated into the plasma, no signal is observed at the Cu I 324.75-nm line. The signal therefore results from scattering and reflection of calcium ion line radiation in the secondary optics after passage of this emission through the Ca II 317.93-nm exit slit. The contributions at the Cu I 324.75-nm line from 1 μg ml^{-1} calcium at viewing heights of 10, 14, 18, 22 and 26 mm above the r.f. coil are 0.033, 0.031, 0.019, 0.012 and <0.001 ng ml^{-1} copper, respectively. This indicates the different ionization stages for the Ca II 317.93-nm and Cu I 324.75-nm lines. Although at the optimum viewing height of 18 mm used in this study for multi-element analysis the effect of stray light from Ca II 317.93-nm emission is small, the contribution from calcium to the total copper signal is large. Dilution of the sample to lower the calcium concentration decreases the copper concentration to below its detection limit. In the analysis of bone digests of sufficient concentration so as to detect copper (>0.1 μg ml^{-1}), calcium is present at levels too high to allow accurate copper determination. The problem may be avoided, apart from eliminating any stray light altogether, by determining copper at 26 mm above the load coil where the contribution of calcium ion emission to the copper signal is negligible.

Matrix effects

The unavoidable presence of large concentrations of calcium and phosphorus in the bone solutions prompted a study of their effect on all analyte signal intensities. Phosphorus, apart from a weak spectral interference on the chromium line, does not cause any severe effects, owing to its weak emission in the plasma. Calcium, however, at high concentrations exhibits a marked effect on many of the emission lines. Table 2 shows the effect of increasing calcium and phosphorus concentrations (simulated bone matrix) on the net emission intensity of various analytes (grouped into ion and atom emission lines) compared with the intensity obtained in the absence of the matrix elements. The effect on the ion emissions is on average twice as great

TABLE 2

Effect of a simulated bone matrix on the line intensities of atom and ion emission lines

Calcium conc. (μg ml^{-1})	Change in signal to background ratio (%)[a]	
	Atom lines (I)	Ion lines (II)
500	−0.7 ± 1.2	−3.5 ± 1.1
1000	−2.7 ± 0.9	−5.5 ± 1.4
2000	−4.0 ± 0.8	−8.5 ± 1.8
10000	−9.7 ± 3.3	−20.0 ± 3.4

[a]Intensities at 5 μg ml^{-1} in the presence of calcium and phosphate (mole ratio 1.5) in 2 M HCl. Results are the mean and standard deviation of the individual matrix effects on (I) atom lines of Cu, Zn, B, S; (II) ion lines of Fe, Mn, Ni, Mo, Cr, Mg. Height above load coil, 18 mm. Plasma conditions as in Fig. 1.

as that on atom emissions. It has previously been shown that, using forced sample delivery, ground-state atom populations are little affected by the matrix, which eliminates nebulization and transport factors as important contributors to the observed changes [8]. Figure 1 illustrates this matrix effect as a function of height above the load coil for several individual analytes. Only sodium shows an enhancement in signal intensity at heights in the plasma greater than 14 mm. Magnesium shows the greatest depression. Appropriate dilutions of the bone matrix need to be made for the accurate determination of sodium and magnesium, in particular, by direct i.c.p.e.s.

The selection of a single internal standard to correct for matrix effects is clearly inappropriate, although the overall standard deviation within each group of elements (Table 2) indicates that a representative element from each group, viz. ion and atom emission lines, could be used.

The method of standard additions was used for the determination of manganese, where excellent sensitivity and the absence of spectral interferences permitted direct measurements but where variable matrix and background fluctuations were encountered. Regression lines were linear with correlation coefficients greater than 0.998.

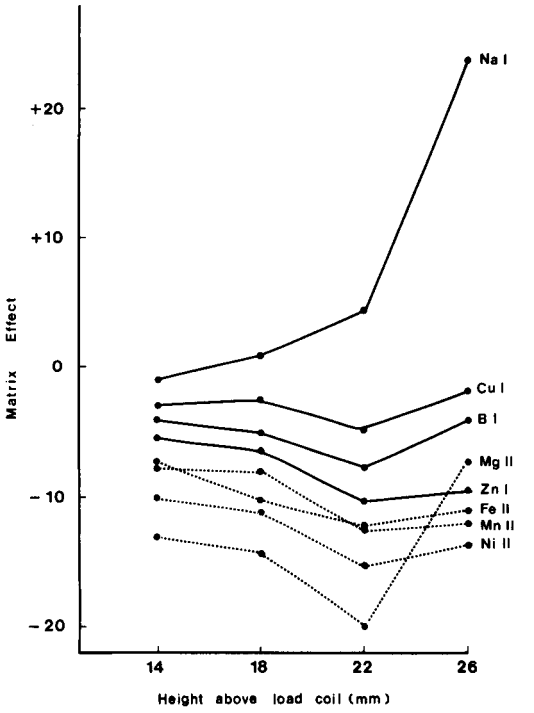

Fig. 1. Matrix effects plotted as a function of height above the load coil while aspirating 5 μg ml^{-1} solutions of various elements. (Matrix effect is the % difference in the net line intensities measured with and without 2 mg Ca ml^{-1} in 2 M HCl. Aerosol gas flow 0.8 l min^{-1}; pump rate 2.0 ml min^{-1}; forward power 1600 W.)

Ion-exchange separation of matrix elements on AG-MP-50

The adverse effect of high calcium concentrations and the low levels of some trace elements of interest, e.g., copper and molybdenum, prevented direct measurements. Trial separations on AG-MP-50 resin indicated that copper, molybdenum and zinc (also lead, aluminium and nickel but the data are not reported here) could be consistently recovered quantitatively as a group in the 3 M hydrochloric acid—methanol fraction free from the matrix elements. Calcium was strongly retained whilst phosphate passed freely through the column. Trace element spikes were added to bone digests before separation on AG-MP-50. Separation conditions outlined by Strelow [3] were followed as closely as possible. Cobalt, iron and manganese could not consistently be recovered under the conditions used. Data on the recovery of copper, the element of most interest here, from three bone digests are presented in Table 3. Recoveries between 91 and 97% were obtained. Although good recoveries of zinc were also found, this element may be determined directly after an appropriate dilution of the original bone digest.

IAEA reference material (H-5)

The IAEA animal bone reference material (H-5) was used to assess the overall performance of the technique and digestion procedure in terms of recovery and precision for the simultaneous determination of major and trace elements. Results are presented in Table 4. For those elements present at concentrations at least an order of magnitude greater than the detection limit, an overall precision of the complete procedure of 1—2% is readily achieved. The higher r.s.d. for sulphur is derived in part from possible losses during digestion and from added error arising from the calcium spectral interference correction. Although the IAEA standard H-5 is not yet certified, the results in Table 4 are in accordance with the information values given in the first progress report [9].

Well-proven techniques have been used in this study of analysis by i.c.p.e.s. of animal bone digests to overcome various spectral and matrix interferences. Further studies will be made with real sample matrix calibration and more extended use of standard bone reference materials.

TABLE 3

Determination of copper and zinc in animal bones following removal of calcium and phosphate by ion-exchange on AG-MP-50

Sample	Recovery of added copper ($\mu g\ ml^{-1}$)			Total ($\mu g\ g^{-1}$)	
	0	0.1	0.2	Cu	Zn
Sheep ulna/radius	<0.005	0.096	0.192	<0.07	73
scapula	0.044	0.141	0.232	1.95	109
IAEA animal bone (H-5)[a]	0.022	0.113	—	0.61	100

[a]For accepted concentration ranges of Cu and Zn, see Table 4.

TABLE 4

Analysis of IAEA H-5 bone reference material

Element	Conc. found[a] ($\mu g\ g^{-1}$)	IAEA values[b]
Ca	247 120 ± 1.4	202 980—220 430
Cu	0.6[c]	0.47—0.82
Fe	82 ± 4.9	76.7—84.8
K	680 ± 3.3	563—706
Mg	3763 ± 1.7	3430—3640
Mn	0.5[d]	0.63—0.89
Mo	0.67[c]	0.04—0.86
Na	5164 ± 1.8	4400—5130
P	104 342 ± 1.8	73 740—117 810
S	2337 ± 5.2	1070—3630
Zn	89 ± 1.7	85—94

[a]Mean and r.s.d. of 6 determinations, referred to dry weight. [b]95% confidence limits for mean of population. [c]Preconcentrated and separated on AG-MP-50 resin (2 determinations). [d]Method of standard additions (2 determinations).

REFERENCES

1 M. W. Blades and G. Horlick, Spectrochim. Acta, Part B, 36 (1981) 881.
2 F. J. M. J. Maessen, J. Balke and J. L. M. de Boer, Spectrochim. Acta, Part B, 37 (1982) 517.
3 F. W. E. Strelow, Anal. Chim. Acta, 127 (1981) 63.
4 J. Lee, ICP Inf. Newsl., 10 (1983) 1.
5 P. W. J. M. Boumans and F. J. de Boer, Spectrochim. Acta, Part B, 30 (1975) 309.
6 J. Lee and M. W. Pritchard, Spectrochim. Acta, 36 (1981) 591.
7 P. W. J. M. Boumans, Spectrochim. Acta, Part B, 35 (1980) 57.
8 J. P. Rybarczyk, Coleen P. Jester, D. A. Yates and S. R. Koirtyohann, Anal. Chem., 54 (1982) 2162.
9 R. M. Parr, Intercomparison of Minor and Trace Elements in IAEA Animal Bone (H-5), Progress Report No. 1, International Atomic Energy Agency, 1982.

Analytica Chimica Acta, 152 (1983) 149—161
Elsevier Science Publishers B.V., Amsterdam — Printed in The Netherlands

MOLEKÜLABSORPTIONSSPEKTROMETRIE BEI ELEKTROTHERMISCHER VERDAMPFUNG IN EINER GRAPHITROHRKÜVETTE

Teil 8. Untersuchung der GeS-Molekülabsorption und Bestimmung von S-Species durch Lichtabsorption von GeS-Molekülen

KLAUS DITTRICH* und BERND VORBERG

Sektion Chemie der Karl-Marx-Universität Leipzig, WB Analytik, Liebigstr. 18, 7010 Leipzig (D.D.R.)

(Eingegangen den 11 April 1983)

SUMMARY

(Molecular absorption spectrometry with electrothermal volatilization in a graphite tube. Part 8. A study of molecular absorption of GeS and determination of sulphur species via GeS)

The molecular absorption of germanium sulphide, generated by volatilization in a graphite tube, is described. The absorption bands of the *D*-system at 285 nm are identified and a new band at 215.2 nm is described. The conditions of the determination of sulphur-containing ions (sulphate, sulphide, sulphite, thiocyanate) are optimized. Sulphide and sulphate can be determined in the same solution by variation of the pH. The influence of other ions on the GeS absorption is discussed. The reciprocal sensitivity for a 60-μl sample giving 0.01 absorbance is 5×10^{-5} M sulphate.

ZUSAMMENFASSUNG

Es wird die Molekülabsorption von GeS-Molekülen, die durch Verdampfung in einer Graphitrohrküvette erzeugt wurden, untersucht. Die Molekülbanden des *D*-Systems bei 285 nm wurden identifiziert. Eine neue Bande bei 215,2 nm wird beschrieben. Die Bedingungen für die Bestimmung S-haltiger Ionen (SO_4^{2-}, S^{2-}, SO_3^{2-}, SCN^-) wurden optimiert. Bestimmungen von S^{2-}- und SO_4^{2-}-ionen sind durch Variation des pH-Wertes in einer Lösung möglich. Der Einfluß anderer Ionen auf die GeS-Molekülabsorption wird diskutiert. Die reziproke Empfindlichkeit bei Einsatz einer 60-μl Probe bezogen auf eine Extinktion von 0,01 beträgt z.B. $5 \cdot 10^{-5}$ Mol $SO_4^{2-}\,l^{-1}$.

Ausgehend von den bisherigen Untersuchungen zur Molekülabsorption halogenhaltiger Species [1] und deren erfolgreichen Anwendung zur Bestimmung von F^-- [2], Cl^-- [3—5], Br^-- [6] und I^--Spuren [7] in Mikroproben, sollte untersucht werden, ob entsprechende Bestimmungen auch für S bzw. S-haltige Ionen möglich sind. Da direkte S-Bestimmungen durch Atomabsorptionsspektrometrie (AAS) zwar möglich sind [8—10], aber wegen der Lage der Resonanzlinie im VUV bei 180,7 nm experimentell schwierig sind, wäre eine solche Bestimmungsvariante nützlich. Moleküle wurden bereits zur

0003-2670/83/$03.00

S-Bestimmung bei anderen Methoden herangezogen. Viele Methoden wurden z.B. auf der Basis der Lichtemission des S_2 bei 384 nm mit der MECA-Technik [11—16] erarbeitet. Ein besonderer Vorteil dieser Methoden besteht darin, daß man auf Grund der zeitabhängigen Verdampfung S-haltiger Anionen wie S^{2-}, SO_3^{2-} und SO_4^{2-} aufeinanderfolgende Emissionssignale erhält, die es gestatten, diese Ionen sequentiell in einer Probe zu bestimmen [14, 15]. Weiterhin wurde die Gasphasenmolekülabsorption für die Bestimmung gasförmiger S-Verbindungen wie H_2S und SO_2 bei Zimmertemperatur eingesetzt [17—20].

Über die Molekülabsorption S-haltiger Moleküle in der Graphitrohrküvette gibt es bis jetzt keine Veröffentlichungen, obwohl bekannt ist, daß die Gegenwart von Schwefelsäure in einigen Fällen zur Depression von AA-Signalen führen kann. Beispiele für eine derartige Verhaltensweise sind die Metalle Germanium und Zinn (Abb. 1), deren AA-Signale in Gegenwart von Schwefelsäure steigender Konzentration erheblich reduziert werden. Die Ursachen dieser Signaldepression wurden bisher nicht exakt untersucht, die allgemein verbreitete Annahme besteht darin, daß eine Erhöhung der Flüchtigkeit der Metalle bewirkt wird. Unsererseits lag die Vermutung nahe, daß auch die Bildung stabiler Moleküle die Depressionsursache sein könnte.

Gegenstand dieser Arbeit soll die Untersuchung der Lichtabsorption stabiler S-haltiger Moleküle in heißen Graphitrohrküvetten und deren mögliche Anwendung zur Bestimmung S-haltiger Ionen sein. Dabei sollten selbstverständlich besonders stabile Moleküle im Vordergrund stehen. In der Tabelle 1 ist eine Übersicht über die Dissoziationsenergien (E_D) stabiler 2-atomiger, S-haltiger Moleküle gegeben. Aus der Tabelle 1 geht hervor, daß

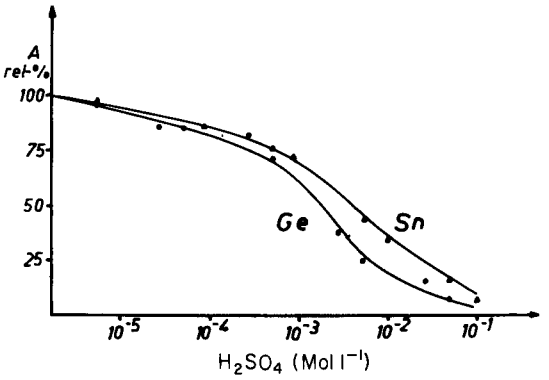

Abb. 1. Abhängigkeit der Ge- und Sn-AA-Signale von der H_2SO_4-Konzentration.

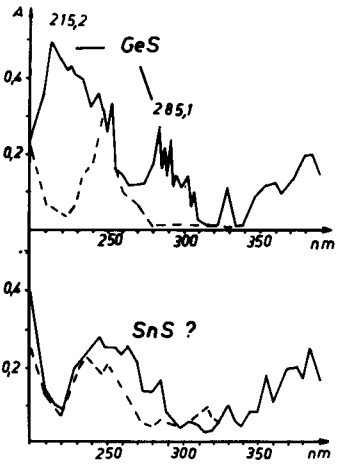

Abb. 2. Molekülabsorptionsspektren von Ge- und Sn-Species: (—) in Gegenwart; und (---) Abwesenheit von sulfidischem Schwefel (Ge = Sn = S^{2-} (Na_2S) = 5 μg/10μl).

TABELLE 1

Dissoziationsenergien (E_D) einiger S-haltiger Moleküle [21]

Molekül	E_D in		Molekül	E_D in	
	kJ Mol^{-1}	eV		kJ Mol^{-1}	eV
CaS	334,5	3,5	SiS	619,6	6,4
BaS	421,2	4,4	GeS	547,6	5,7
AlS	360,1	3,7	SnS	463,9	4,8
InS	284,3	2,9	S_2	422,9	4,4
LaS	575,7	6,0	CuS	280,1	2,9

vor allem die Elemente der IV. Hauptgruppe des Periodischen Systems stabile 2-atomige Moleküle mit Schwefel bilden.

EXPERIMENTELLES

Apparatur und Reagenzien

Zweikanal-Zweistrahl-AA-Spektrometer, Typ 811, (Jarrell-Ash) mit Graphitrohrküvette, Typ 1268 (Beckman; H_2-Hohlkathodenlampe, 35 mA; spektrale Bandbreite 400—250 nm = 0,2 nm, 250—200 nm = 0,4 nm; Untergrundkompensation durch Zweilinienmethode möglich.

Reagenzien zur Spektrenaufnahme. Na_2SiO_3-, Na_2SnO_3-, Na_2GeO_3-Lösungen, Metallkonzentration 2,5 mg ml^{-1} (Stammlösung); Na_2S-Stammlösung 10 mg S ml^{-1}; Na_2SO_4-Stammlösung 10 mg S ml^{-1}.

Reagenzien für analytische Bestimmungen. GeO_2 in Wasser gelöst, mit wenig NaOH stabilisiert, 2,5 mg Ge ml^{-1}; Na_2SO_4-, Na_2SO_3-, Na_2S- und NaSCN-Stammlösungen mit 10 mg S ml^{-1}; einige Metallnitrate in Wasser gelöst mit 10 mg ml^{-1} Metall zur Matrixeinflußüberprüfung. Aus den Stammlösungen wurden die entsprechenden Analysenlösungen durch Verdünnen mit Wasser hergestellt.

Verfahrensweise

Verfahrensweise bei der Spektrenaufnahme. Die Aufnahme der Spektren erfolgte durch punktweises Messen der Extinktion zwischen 200 und 400 nm. Die Probelösung (10 µl) wird in die Graphitrohrküvette gegeben, wo sie getrocknet, verascht und verdampft wird. In Bandengebieten wurde mit einem Wellenlängenvorschub von 0,2 nm nach jeder Messung gearbeitet. In anderen Bereichen betrug dieser Wert 5—10 nm. Es wurden Lösungen eingesetzt, die ein Metall:S-Atomverhältnis von 1:1 besaßen. Die S-Konzentration betrug 0,5 mg ml^{-1}.

Verfahrensweise bei analytischen Bestimmungen. Mikrovolumina von 10—60 µl der entsprechenden Lösung, die aus der Analysenlösung und der Ge-haltigen Zusatzlösung hergestellt wurden, wurden in die Graphitrohrküvette dosiert, dort getrocknet und verascht, d.h. thermisch überarbeitet,

und verdampft. Das bei der ausgewählten Wellenlänge erhaltene Molekülabsorptionsignal wird der Konzentration der S-Komponente gegenübergestellt.

UNTERSUCHUNG DER SPEKTREN DER S-HALTIGEN MOLEKÜLE

Aufnahme der Spektren

Zunächst wurde die Absorption der S_2-Moleküle durch Verdampfen von Na_2SO_4- und Na_2S-Lösungen in der Graphitrohrküvette untersucht. Es konnte keine nennenswerte Lichtabsorption im Gebiet zwischen 380 und 405 nm ermittelt werden. Dies bedeutet jedoch nicht, daß diese Lichtabsorption nicht möglich ist, sondern nur, daß sich das S_2-Molekül unter den angewendeten Bedingungen in unzureichender Konzentration bildet. Auf die Untersuchung der Moleküle der 3. und 2. Hauptgruppe wurde wegen deren verhältnismäßig niedrigen Dissoziationsenergien (Tab. 1) verzichtet.

Untersuchungen unter Anwendung von Lanthansalzen führten, offensichtlich wegen der infolge Carbidbildung schlechten Verdampfbarkeit, zu keinem Ergebnis. Ebenso wurden keine intensiven Absorptionen bei der Verdampfung Si-haltiger Lösungen gefunden. Lediglich im Falle von Ge- und Sn-haltigen Lösungen konnten Spektren erhalten werden, die sich in Gegenwart von S-Komponenten von denen der S-freien Lösungen unterschieden. In der Abb. 2 wurden diese Spektren dargestellt.

Diskussion der Spektren

Es sind vom GeS-Molekül folgende Absorptionsbanden bekannt: $X^1\Sigma^+$—D zwischen 380 und 277 nm und $X^1\Sigma^+$—E zwischen 277 und 214 nm [21], wobei die Absorptionsmaxima zwischen 280 und 300 nm bzw. 240 und 255 nm zu erwarten waren. Aus der Abb. 2 geht hervor, daß das D-System der GeS-Moleküle gefunden wurde (Abb. 3). Eine eindeutige Bestätigung des E-Systems konnte nicht erfolgen. Die im Spektrum intensivste Bande bei 215,2 nm ist noch nicht beschrieben worden. Deshalb mußte zunächst eine Identifizierung ihrer Zugehörigkeit (s.u.) erfolgen. Ausgehend von der Breite

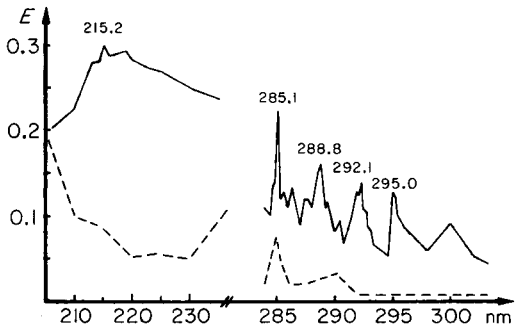

Abb. 3. Feinstruktur der GeS Banden bei 215 und 285 nm: (—) mit S-Komponente; (---) ohne S-Komponente (Ge = 7,5 µg/10 µl; S^{2-} = 2 µg/ 10 µl).

der Bande und dem Vergleich der Energiewerte des Bandenmaximums von 556,4 kJ Mol^{-1} und der Dissoziationsenergie des GeS-Moleküls von 547,6 kJ Mol^{-1} könnte man annehmen, daß es sich um die Dissoziation des Moleküls durch Lichtabsorption handelt.

Vom SnS-Molekül sind ebenfalls zwei Banden bekannt [21]: $X^1\Sigma^+$—D zwischen 402 und 320 nm und $X^1\Sigma^+$—E zwischen 332 und 250 nm. Es ist zu vermuten, daß die gefundene breite Bande zum E-System gehört. Ein exakter Beweis liegt jedoch nicht vor. Wegen der nur geringen Absorptionsintensität des SnS-Systems wurden die weiteren Untersuchungen auf das GeS-System konzentriert.

Dabei wurde auch von der Tatsache ausgegangen, daß offensichtlich beim Germanium die günstigsten Relationen zwischen MO- und MS- Molekülen vorliegen (Tab. 2). Berücksichtigt man, daß in der Graphitrohrküvette ein, wenn auch geringer O_2-Partialdruck vorliegt, so ist die sehr große Stabilität des SiO-Moleküls für die SiS-Bildung ungünstig, hingegen ist der E_D-Wert des SnS-Moleküls für die gegebenen Temperaturen von etwa 3000 K schon wieder verhältnismäßig niedrig. Somit könnte das Germanium für die Bildung einer hohen MS-Konzentration im Plasma tatsächlich am günstigsten sein. Diese Rückschlüsse sind jedoch nur qualitativer Art.

Zuordnung der im Ge-S-System gefundenen 215,2-nm Bande

Da die Bande bei 215,2 nm wegen ihrer großen Intensität für analytische Bestimmungen wahrscheinlich am günstigsten sein konnte, sollte ihre Herkunft zunächst eindeutig bestimmt werden. Es wurde festgestellt, daß diese Bande nur in Gegenwart von Ge^{4+}- und S-haltigen Ionen in den zu verdampfenden Lösungen auftrat. Daraus konnte geschlußfolgert werden, daß entweder eine Ge-S-Species die Ursache der Absorption ist oder daß eine der beiden Komponenten durch die Gegenwart der anderen thermisch stabilisiert wird. Bei Verdampfung dieses stabilisierten Teiles in der Verdampfungsphase könnte dann das absorbierende Teilchen im Plasma gebildet werden. Auf der Basis dieses Vorganges wäre es denkbar, daß entweder ein Ge- oder ein S-haltiges Teilchen für die Absorption verantwortlich ist.

Eine Stabilisierung von Ge durch die leichter flüchtigen S-haltigen Substanzen ist nicht zu erwarten, jedoch wäre die thermische Stabilisierung

TABELLE 2

Dissoziationsenergien (E_D) einiger MO- und MS-Moleküle

Metall	Dissoziationsenergien E_D in			
	kJ Mol^{-1}	eV	kJ Mol^{-1}	eV
	MO		MS	
Si	765,3	7,9	619,6	6,4
Ge	654,8	6,8	547,6	5,7
Sn	526,3	5,5	463,9	4,8

S-haltiger Ionen durch Ge denkbar. Aus diesem Grund wurden Untersuchungen zur SO_2- und SO-Molekülabsorption durchgeführt, denn die Bildung dieser Moleküle war unter den reduzierenden Bedingungen der Graphitrohrküvette am wahrscheinlichsten. Beide Moleküle konnten durch ihre Lichtabsorption nachgewiesen werden (SO_2-Bande zwischen 200 und 250 nm und SO-Bande bei 240 nm). Das Maximum der SO_2-Bande liegt unterhalb 210 nm. Weiterhin wurde festgestellt, daß die Absorptionsintensität der SO_2-Bande mit zunehmender Graphitrohrküvettentemperatur abnimmt, die der SO-Bande jedoch zunimmt. Die Verdampfung in Gegenwart von Ge erfolgte jedoch bei den höchstmöglichen Temperaturen der Graphitrohrküvette (etwa 3000 K). Bei diesen Temperaturen konnte keine SO_2-Bande mehr gemessen werden. Da das SO-Bandenmaximum nicht mit dem bei 215,2 nm gefundenen Bandenmaximum übereinstimmt, konnten somit beide Moleküle nicht die Ursache für die neue Bande sein.

Aus dem gleichartigen Verhalten der Banden bei 215,2 nm und bei 285 nm bei Einsatz von Ge(IV)-haltigen Lösungen und SO_2-haltiger Ar-Atmosphäre konnte durch Variation der Graphitrohrküvetten-Temperature geschlußfolgert werden, daß es sich bei beiden Banden um die Lichtabsorption ein und desselben Teilchens handelt, welches sich aus dem gasförmigen SO_2 bzw. seiner Zersetzungsprodukte SO oder S und den verdampfenden Ge-haltigen Species im Plasma der heißen Graphitrohrküvette bildet.

Wie schon aus der Abb. 3 hervorgeht, besitzt die Bande bei 285 nm eine Struktur. Der Vergleich der Bandenmaxima mit Literaturwerten [21] (Tab. 3) führt zu dem eindeutigen Schluß, daß die Bande bei 285 nm und somit auch bei 215,2 nm vom GeS-Molekül verursacht wird. Zu vermuten ist, daß das *E*-Banden-System dabei in den Dissoziationsbereich übergeht.

UNTERSUCHUNGEN ZUR OPTIMIERUNG DER EXPERIMENTELLEN BEDINGUNGEN FÜR ANALYTISCHE BESTIMMUNGEN

Zur Nutzung der GeS-Molekülabsorption für Spurenbestimmungen von S-haltigen Ionen waren Untersuchungen zur Optimierung der thermischen Parameter der Graphitrohrküvette und der Zusammensetzung der Lösungen

TABELLE 3

Vergleich der beschriebenen [21] und experimentell ermittelten Bandenmaxima des *D*-Systems des GeS

Übergang $v'—v''$		Wellenlänge (nm)	
		Angegeben	Gefunden
3	0	294,9	295,0
4	0	291,8	292,1
5	0	288,7	288,8
6	0	285,8	285,1

mit der Zielstellung einer möglichst hohen GeS-Konzentration im Plasma durchzuführen.

Optimierung der thermischen Parameter und Auswahl der optischen Bedingungen

Die hohe Stabilität des GeS gestattete es und die schlechte Verdampfbarkeit des Ge (K_p = 2830°C) erforderte es, in der Verdampfungsphase die maximal möglichen Temperaturen des Graphitrohrküvetten-Systems anzuwenden. Problematisch dabei ist die Vermeidung der vorzeitigen Verflüchtigung von leicht flüchtigen S-Komponenten. Diese Untersuchung wurde unter Einsatz der am leichtesten flüchtigen S-Verbindung, dem Sulfid, durchgeführt. In der Abb. 4 ist die Abhängigkeit des GeS-Absorptionsignals von der Veraschungs- und von der Verdampfungstemperatur dargestellt. Es ist zu erkennen, daß durch S-Verluste verursachte Signaldepressionen bei Veraschungstemperaturen von größer als 1000°C auftreten. Es ist ebenfalls zu sehen, daß die maximalen Signale bei den höchsten Verdampfungstemperaturen erzielt worden sind. Folgende optimale thermische Parameter ergaben sich: Trocknung: 30 s, 120°C, Veraschung: 10 s, 700°C; Verdampfung: 10 s, 3300°C. Nach Überprüfung wurde festgestellt, daß diese thermischen Parameter auch bei Einsatz der S-Komponente in Form von Sulfat, Sulfit oder Rhodanid am günstigsten waren.

Hinsichtlich der optischen Parameter gab es einige Probleme. Sowohl bei 215,2 nm als auch im *D*-Bandensystem bei 285 nm war wegen der Breite der Banden eine effektive Untergrundkompensation mit der Zweilinienmethode nicht möglich.

Einfluß der Metallkonzentration, der Art des S-haltigen Ions und des pH-Wertes auf die GeS-Absorption

Mit der Erhöhung der Germaniumkonzentration steigt auch die Absorption des GeS-Moleküls. Gleichzeitig nimmt aber auch der nichtkompensierbare Untergrund zu. Ein Optimum ergab sich für 7,5 µg Ge/Dosiervolumen. Auch wegen der schlechten Verdampfbarkeit des Germaniums war eine weitere Erhöhung dieser Menge unzweckmäßig.

Fügt man zu neutralen Ge(IV)-Lösungen der oben genannten Konzentration SO_4^{2-}-, SO_3^{2-}, S^{2-}- oder SCN^--ionen hinzu, so erhält man in jedem Fall eine

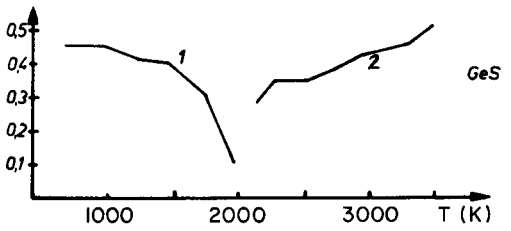

Abb. 4. Abhängigkeit der GeS-Absorption von: (1) der Temperatur der Veraschungsphase; (2) der Verdampfungsphase. (Messung erfolgte in der Verdampfungsphase).

Abhängigkeit der Intensität der GeS-Absorption von der Konzentration des S-haltigen Anions. Allerdings sind die ermittelten Empfindlichkeiten bezogen auf die eingesetzte S-Menge unterschiedlich. Wir führten dieses Ergebnis auf die unterschiedliche Säurestärke und thermische Stabilität der Säuren zurück. Man kann annehmen, daß in der Reihenfolge H_2SO_4—H_2SO_3—HSCN—H_2S beide Eigenschaften abnehmen.

Die Erhöhung des pH-Wertes durch Hinzufügen von 2 M NaOH (bis zum pH-Wert 12) führt zu einer Verbesserung der Empfindlichkeit der GeS-Absorption bei allen genannten Anionen. Ursache dafür ist, daß sich beim Trocknungsprozeß die thermisch relativ stabilen Na-salze bilden, die sich auch bei den genannten (s.o.) relativ niedrigen Veraschungstemperaturen noch nicht zersetzen. Unter diesen Bedingungen werden die Eichkurven für die Bestimmungen dieser Anionen bezogen auf die vorhandene S-Menge identisch.

Erniedrigt man den pH-Wert auf 5, so sinken die Extinktionswerte der GeS-Absorption bei Einsatz von SCN^-- und S^{2-}-ionen stark ab, bei Einsatz von SO_3^{2-}- und SO_4^{2-}-ionen jedoch nur schwach. Diese Resultate sind in der Abb. 5 dargestellt worden. Aus diesem Ergebnis ergeben sich Möglichkeiten für die sequentielle Mehrionenbestimmung (s.u.).

Einfluß anderer Ionen auf die GeS-Absorption

In der Abb. 6 sind die Einflüsse anderer Kationen auf die GeS-Absorption dargestellt worden. Für diese Untersuchungen wurde Sulfat als S-haltige Komponente verwendet. Praktisch alle Kationen haben einen mehr oder weniger starken depressiven Einfluß. Am geringsten ist dieser bei den Alkalimetallen ausgeprägt. Verwendet man als Ausgangslösung eine Na^+-freie, leicht saure Lösung, so ergibt sich bei Zusatz von $NaNO_3$-Lösung sogar ein signalerhöhender Effekt. Dieser ist darauf zurückzuführen, daß während der Trocknung und Veraschung das leichter flüchtige Nitrat vom Sulfat vertrieben wird. Die anderen S-Anionen zeigen diesen Effekt naturgemäß nicht. Stärker

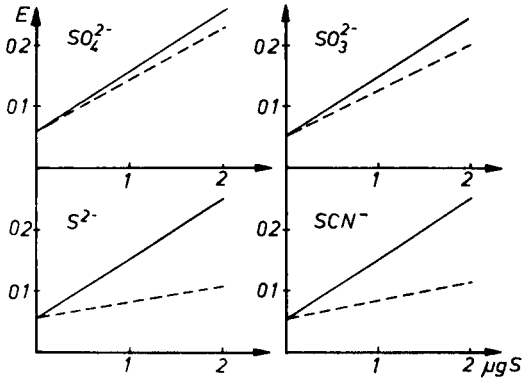

Abb. 5. Abhängigkeit der GeS-Absorption von der Konzentration unterschiedlicher Anionen bei: (—) pH 12; (---) pH 5. (Konzentrationen wurden auf µg S umgerechnet.)

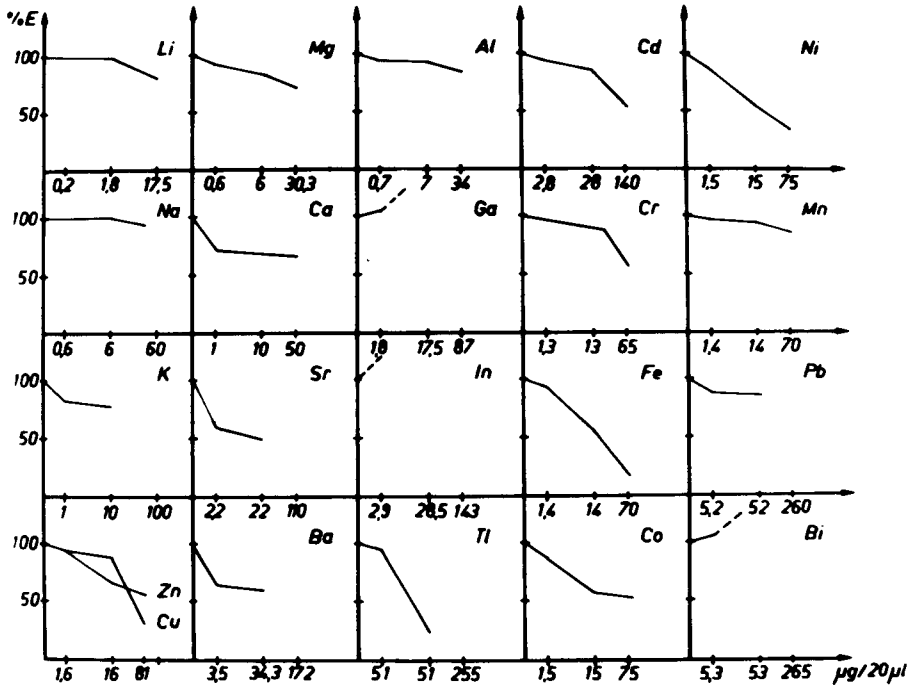

Abb. 6. Abhängigkeit der GeS-Absorption von der Konzentration anderer Kationen (Abszisseneinteilung erfolgte auf der Basis gleicher Atomkonzentration).

depressiv wirken die Erdalkalimetalle. Sie stabilisieren zwar das Sulfat. Offensichtlich ist jedoch der Verdampfungszeitpunkt des Germaniums von dem der Sulfate unterschiedlich. Da die M^{2+}-Konzentration größer als die SO_4^{2-}-ionenkonzentration war, und somit in Gegenwart von Ca^{2+}-, Sr^{2+}- und Ba^{2+}-ionen das gesamte Sulfat als schwerlösliches MSO_4 vorlag, geht aus dieser Untersuchung eindeutig hervor, daß die GeS Bildung über die Gasphase im Plasma erfolgt.

Die Einflüsse der Schwermetallkationen sind ähnlich und vermutlich vorwiegend auf thermische Hydrolyse zurückzuführen.

Wenn Ga^{3+}- und In^{3+}-ionen zugesetzt werden, wächst der Untergrund durch GaO- bzw. InO-Molekülabsorption sehr stark an [1]. Dabei ist zu beobachten, daß die InO-Absorption offensichtlich auf Grund der größeren thermischen Stabilität des In-sulfates gegenüber dem In-nitrat und des damit in der Verdampfungsphase höheren O_2-Partialdruckes mit der Sulfationenkonzentration wächst.

In der Abb. 7 sind die Einflüsse einiger Anionen auf die GeS-Absorption dargestellt worden. Die Halogenide haben einen depressiven Einfluß der auf die partielle Bildung der leichtflüchtigen Germaniumhalogenide and auf die Stabilität der zugehörigen 2-atomigen Moleküle zurückzuführen ist. Phosphat hingegen beeinfluß die GeS-Absorption in dem angegebenen Konzentrationsgebiet nicht.

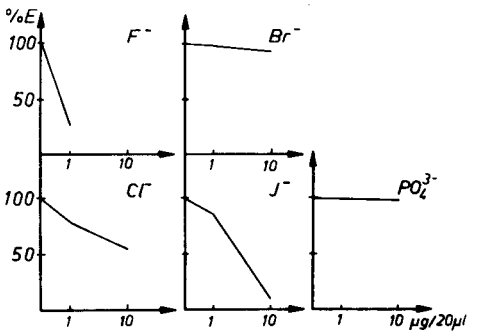

Abb. 7. Abhängigkeit der GeS-Absorption von der Konzentration anderer Anionen.

Insgesamt ist diesem Abschnitt hinzuzufügen, daß, wie bereits in früheren Mitteilungen gezeigt, die chemischen Matrixeffekte sehr umfangreich und vielfältig sind. Im Falle der S-haltigen Anionen kommt hinzu, daß diese in Abhängigkeit vom S-haltigen Ion unterschiedlich sind. Eine vollständige Erfassung aller Einflüsse ist jedoch im Rahmen dieser Arbeit nicht möglich.

ANALYTISCHE BESTIMMUNGEN

Bestimmung von SO_4^{2-}-, SO_3^{2-}, S^{2-}, und SCN^--ionen in wäßrigen Lösungen

Unter Anwendung der optimalen Bedingungen (7,5 µg Ge/10—60 µl Dosiervolumen, pH-Einstellung auf 12 durch NaOH und maximale Verdampfungstemperatur) ist es möglich, die genannten S-haltigen Ionen quantitativ durch GeS-Absorption zu bestimmen. Die analytischen Ergebnisse sind in der Tabelle 4 zusammengefaßt worden. Aus der Tabelle 4 geht hervor, daß die Ergebnisse für die Bestimmung dieser sehr unterschiedlichen Ionen nahezu identisch sind. Zur Verbesserung des relativen Nachweisvermögens wurde untersucht, ob größere Dosiervolumina verwendet werden können. Die Absolutmengen an Ge und NaOH blieben dabei erhalten. Die bei der Sulfatbestimmung erzielten Ergebnisse sind in der Tabelle 5 zusammengestellt worden. Aus der Tabelle geht hervor, daß die Verdünnung keinen

TABELLE 4

Analytische Ergebnisse der GeS-Absorption bei 215,2 nm

Bestimmte Spur	Reziproke Empfindlichkeit (ng)[a]	Lineares Arbeitsgebiet (ng)
SO_4^{2-}	100	100—5000
SO_3^{2-}	110	110—5000
SCN^-	110	110—5000
S^{2-}	110	110—5000

[a]Masseangaben bezogen auf S, Dosiervolumen 10 µl; ng pro 0.01 Extinktion.

TABELLE 5

Analytische Ergebnisse der GeS-Absorption bei Einsatz unterschiedlicher Dosiervolumina für Sulfatbestimmungen

Probevolumen (μl)	Reziproke Empfindlichkeiten[a]	
	(ppm S/H_2O)	(Mol SO_4^{2-} l^{-1})
10	10	3×10^{-4}
20	5	$1{,}5 \times 10^{-4}$
40	2,5	$7{,}5 \times 10^{-5}$
60	1,7	5×10^{-5}

[a] 100 ng S pro 0.01 Extinktion.

negativen Einfluß auf das absolute Nachweisvermögen hat. Somit wirkt sich die Dosierung größerer Volumina insgesamt auf die Verbesserung des relativen Nachweisvermögens aus. Auch der lineare Meßbreich blieb bei dieser Variante erhalten (Tab. 4).

Da keine Möglichkeit für die Untergrundkompensation bestand, wurden zum Zwecke besserer Variabilität auch die anderen Wellenlängen auf ihre analytische Verwendbarkeit hin überprüft. Aus der Tabelle 6 geht hervor, daß beim Bandenmaximum bei 215,2 nm zwar die empfindlichsten Messungen möglich sind, jedoch die anderen Bandenmaxima nicht viel schlechter für die analytischen Bestimmungen geeignet sind.

Aus dem Abschnitt über den Anioneneinfluß (s.o.) ist zu entnehmen, daß die Bestimmung des Sulfates in einem 5-fachen F^--, einem 50-fachen Cl^--, einem 1000-fachen Br^-- und einem 50-fachen I^- Überschuß und in einem 200-fachen PO_4^{3-}-Überschuß möglich ist. Höhere Phosphatkonzentrationen sind wegen des durch Phosphat verursachten unspezifischen, nicht kompensierbaren Untergrundes nicht einsetzbar.

Sequentielle Spurenbestimmung von Sulfid und Sulfat

Durch Ausnutzung der pH-Abhängigkeit der GeS-Absorption (Abb. 5) ist es möglich, S^{2-}- und SO_4^{2-}- oder SCN^-- und SO_4^{2-}- oder S^{2-}- und SO_3^{2-}- oder

TABELLE 6

Analytische Ergebnisse der GeS-absorption bei unterschiedlichen Wellenlängen (Dosiervolumen 20 μl, Sulfat)

Wellenlänge (nm)	Reziproke Empfindlichkeit	
	(ng S)	(ppm S/H_2O)
215,2	100	5,0
288,8	135	6,8
292,1	140	7,0
295,0	140	7,0

TABELLE 7

Analytische Ergebnisse der Bestimmung von SO_4^{2-}- und S^{2-}-ionen in einer Lösung durch GeS-Absorption (Dosiervolumen: 20 µl)

Vorgegebene S-Mengen (µg)		Gefundene S-Mengen (µg)	
Sulfat	Sulfid	Sulfat	Sulfid
0,6	0,6	0,62	0,62
0,4	1,0	0,40	0,98
1,0	0,4	1,00	0,38

SCN^-, und SO_3^{2-}-ionen jeweils in einer Lösung nebeneinander zu bestimmen. Für diese Bestimmungen sind Extinktionsmessungen bei pH 5 und pH 12 erforderlich. Zur Berechnung der jeweiligen Konzentrationen ist es erforderlich, die Absorptionskoeffizienten der einzelnen Ionen bei beiden pH-Werten zu kennen. Deren Ermittlung kann durch die Eichkurventechnik erfolgen. Für die Richtigkeit der Werte ist es jedoch von Vorteil, wenn die Additionstechnik angewendet wird.

Für das Beispiel S^{2-}/SO_4^{2-} erfolgt die Berechnung nach folgenden Formels:

$$[S^{2-}] = \frac{A_5 - A_{12} \cdot k_5(SO_4^{2-})/k_{12}(SO_4^{2-})}{k_5(S^{2-})[k_5(S^{2-}) - k_{12}(SO_4^{2-})]/k_{12}(SO_4^{2-})}$$

$$[SO_4^{2-}] = \frac{A_5 - A_{12} \cdot k_5(S^{2-})/k_{12}(S^{2-})}{k_5(SO_4^{2-})[k_5(S^{2-}) - k_{12}(SO_4^{2-})]/k_{12}(S^{2-})}$$

A_5 ist die Absorbanz für pH 5, usw., und die k-Werte für pH 5 und 12 sind $k_5(SO_4^{2-}) = 0{,}1$, $k_5(S^{2-}) = 0{,}03$; $k_{12}(SO_4^{2-}) = 0{,}103$ und $k_{12}(S^{2-}) = 0{,}09$ ergaben sich für Modellösungen die in der Tabelle 7 zusammengestellten Resultate. Aus der Tabelle 7 ist ersichtlich, daß bei nicht zu großen Konzentrationsunterschieden entsprechende Bestimmungen richtige Werte liefern.

Anwendung der GeS-Absorption zur S-Bestimmung in Flugstaub

Gesamtschwefelbestimmungen sind auf einfache und schnelle Weise in Staubproben möglich. Zu diesem Zweck wird die Substanz mit 0,005 M NaOH in der Hitze behandelt, wobei in den meisten Fällen SO_3^{2-} und SO_4^{2-} vollständig extrahiert werden. Die erhaltene Lösung kann nach Zusatz von Ge(IV) in die Graphitrohrküvette dosiert und vermessen werden. Infolge des alkalischen Extraktionsverfahrens bleibt der größte Teil der Schwermetallkationen im Rückstand. Dadurch werden die Matrixeffekte stark reduziert. Sowohl nach dem Eichkurvenverfahren als auch dem Additionsverfahren werden für S-Mengen zwischen 1 und 0,1% richtige und reproduzierbare Werte erhalten.

LITERATUR

1 K. Dittrich, Anal. Chim. Acta, 97 (1978) 59.
2 K. Dittrich, Anal. Chim. Acta, 97 (1978) 69.
3 K. Dittrich, Anal. Chim. Acta, 111 (1979) 123.
4 K. Dittrich und P. Meister, Anal. Chim. Acta, 121 (1980) 205.
5 K. Dittrich und B. Vorberg, Anal. Chim. Acta, 140 (1982) 247.
6 K. Dittrich und S. Schneider, Anal. Chim. Acta, 125 (1980) 189.
7 K. Dittrich und S. Schneider, Anal. Chim. Acta, 125 (1980) 201.
8 G. F. Kirkbright und M. Marshall, Anal. Chem., 44 (1972) 1288.
9 G. F. Kirkbright, M. Marshall und T. S. West, Anal. Chem., 44 (1972) 2379.
10 P. D. Swain und S. R. Ellebracht, Anal. Chem., 51 (1979) 1605.
11 R. Belcher, S. L. Bogdanski und A. Townshend, Anal. Chim. Acta, 67 (1973) 1.
12 R. Belcher, S. L. Bogdanski, D. J. Knowles und A. Townshend, Anal. Chim. Acta, 77 (1975) 53; 79 (1975) 292.
13 M. Q. Al-Abachi, R. Belcher, S. L. Bogdanski und A. Townshend, Anal. Chim. Acta, 86 (1976) 139; 92 (1977) 293.
14 R. Belcher, S. L. Bogdanski, I. H. B. Rix und A. Townshend, Mikrochim. Acta, II (1977) 71.
15 S. A. Schubert, J. W. Clayton und Q. Fernando, Anal. Chem., 51 (1979) 1297; 52 (1980) 963.
16 T. S. Al-Ghabsha, S. L. Bogdanski und A. Townshend, Anal. Chim. Acta, 120 (1980) 83.
17 L. I. Pleskai, Zhurn. Analit. Khim., 34 (1979) 600.
18 A. Syty, Anal. Chem., 45 (1973) 1744; 51 (1979) 911.
19 M. S. Cresser, Lab. Practice, 27 (1978).
20 K. Fuwa und B. L. Vallee, Anal. Chem., 41 (1969) 188.
21 B. Rosen, International Tables of Selected Constants, Vol. 17, Spectroscopic Data relative to Diatomic Molecules, Pergamon Press, Oxford, 1970, S. 160, 375.

Analytica Chimica Acta, 152 (1983) 163—171
Elsevier Science Publishers B.V., Amsterdam — Printed in The Netherlands

THE ADSORPTION OF COPPER IONS ON THE SURFACE OF COPPER(II) SULPHIDE PRECIPITATE-BASED ION-SELECTIVE ELECTRODES

E. G. HARSÁNYI, K. TÓTH and E. PUNGOR*

Institute for General and Analytical Chemistry, Technical University, 1521-Budapest (Hungary)

(Received 14th March 1983)

SUMMARY

It is shown that one of the factors affecting the detection limit of the copper(II) sulphide precipitate-based electrode is dissolution of the membrane material. The dissolution of copper ions from the membrane can be decreased by suitable treatment of the electrode precipitate with sodium sulphide. The adsorption of the primary ion on the electrode surface in the concentration range below 10^{-4} mol l^{-1} copper ion is also shown to be a significant factor influencing the detection limit of this electrode.

Copper ion-selective electrodes are usually prepared from the sulphide or selenide precipitates of copper(I) or copper(II) as the active material. The salts are precipitated generally in the presence of the appropriate silver salts. Despite the low solubility products of the copper(I) and copper(II) sulphides, K_{so} (Cu_2S) = 10^{-48} and K_{so} (CuS) = 10^{-36} [1], the electrodes exhibit Nernstian response only down to 10^{-5}—10^{-6} mol l^{-1} copper(II) ion in unbuffered solutions. Below 10^{-5} mol l^{-1} copper(II) ion, there is a positive deviation from the Nernstian response, i.e., the electrode indicates higher copper concentrations than the nominal concentrations. The increase in the copper concentration of the test solution is due to dissolution of the membrane material as a consequence of oxidative reactions. Detection limits for copper ion-selective electrodes are reported variously in the literature within the concentration range 10^{-5}—10^{-8} mol l^{-1}.

Numerous papers have dealt with studies of copper ion-selective electrodes; reviews are available [2, 3]. Blaedel and Dinwiddie [4] attempted to measure copper at concentrations below 10^{-5} mol l^{-1}; they found that the surface of the electrode adsorbs copper ions from the test solution, and that lower copper concentrations can be determined only if the adsorbed layer is removed. A memory effect originating from adsorption was investigated by Umezawa et al. [5] who found them to be significant below 10^{-5} mol l^{-1} copper ion concentrations. The memory effect shows up not only in deviation from the Nernstian response but also in increased response times. In earlier work [6], the adsorption of silver and iodide ions on the surface of

0003-2670/83/$03.00

electrodes based on silver iodide was investigated under special circumstances; the silver concentration in the test solution was measured by atomic absorption spectrometry. Adsorption was established at silver concentrations below 10^{-4} mol l^{-1}, and calculations showed that the maximum amount of silver adsorbed corresponded to a monomolecular layer on the surface of the electrode.

The present paper is concerned with the adsorption of copper ions on the surface of a homogeneous copper(II) sulphide electrode membrane. The adsorption of copper ions can be measured only in the concentration range below 10^{-4} mol l^{-1}; therefore to study the adsorption processes, the copper concentration dissolved from the membrane material had to be determined and taken into account. Moreover, the development of an electrode material from which the copper dissolution is low appeared to be advantageous. In the first part of this paper, attempts to decrease the dissolution of copper ions from the electrode membrane are summarized. The measurements and calculations that prove the role of the adsorption of copper ions in the range of the lower detection limit of the sensor are then given.

EXPERIMENTAL

In the earlier paper dealing with the silver iodide electrode [6], it was shown that the dissolution of cations from the electrode membrane material and the adsorption of these ions on the electrode surface can be measured in a suitable cell arrangement consisting of an electrode of relatively large surface area with a small volume of solution. The changes in the cation concentration of these solutions were followed by atomic absorption spectrometry.

The copper(II) sulphide ion-selective electrode and cell arrangement for measuring the electrode potentials

The copper(II) sulphide used for the preparation of the electrode membranes was precipitated from copper sulphate solution with sodium thiosulphate in acidic medium as described earlier [7]. The precipitate was washed with deionized water and dried under nitrogen. Pellets (12 mm diameter) were pressed from the precipitate (1 g each) at a pressure of 10^6 N cm^{-2}. The pellets were glued onto glass tubes of the same diameter. The internal reference electrode was a silver/silver chloride electrode. The internal solution contained 10^{-3} mol l^{-1} copper(II) nitrate and 2×10^{-2} mol l^{-1} potassium chloride. Copper nitrate solutions made by a serial dilution from a 1 mol l^{-1} stock solution were used for electrode calibration.

The arrangement used for measuring the electrode potential is shown in Fig. 1. The ion-selective electrode is inserted into a polyethylene cell (13 mm internal diameter), and connected through an agar salt bridge with the Ag/AgCl double-junction reference electrode (OP-0820-P type, Radelkis, Hungary) immersed in a 10^{-1} mol l^{-1} potassium nitrate solution. The volume of the solution in the cell is 300 μl. The electrode potentials were measured with a

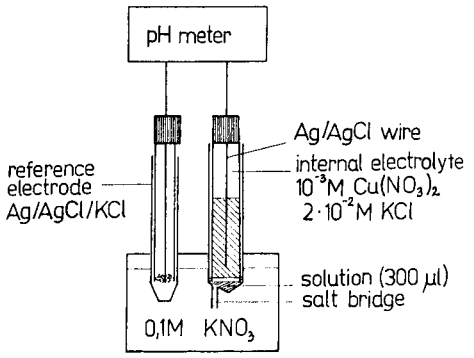

Fig. 1. Arrangement for the measurement of the electrode potential.

Radelkis OP-205 precision pH meter during contact with the test solution every minute for 10 min. The electrode potential stabilized during this period. The test solution in the cell was used afterwards for the atomic absorption spectrometric determination of copper.

Determination of copper in small solution volumes by atomic absorption spectrometry

Copper concentrations were determined by using a Varian AA6 atomic absorption spectrometer with an air—acetylene flame. The hollow-cathode lamp was operated at a lamp current of 3 mA. The absorbances were measured at the 324.7-nm copper resonance line. From the solution volume of 300 µl, 50-µl portions were pipetted into a microfunnel connected to the capillary of the spray chamber. The air carried the solution into the flame at an aspiration rate of 3 ml min^{-1}.

RESULTS AND DISCUSSION

Effect of pretreatment

Electrodes prepared as indicated above showed significant dissolution of copper ions (Table 1). The copper concentrations were determined after immersing an electrode for 10 min in 300 µl of distilled water or in 300 µl of the electrolyte used for adjusting constant ionic strength. The electrodes were conditioned previously in distilled water or in EDTA, copper nitrate or sulphuric acid solutions. One of the copper sulphide pellets was kept for two weeks in 5 ml of distilled water; during this time the colour of the water became blue and a bluish layer could be observed on the surface of the pellet, indicating copper sulphate formation. A scanning electron micrograph shows the surface of this electrode membrane (Fig. 2A); the crystalline coating was identified by electron-diffraction measurement as copper sulphate. For comparison, an untreated surface is shown in Fig. 2B. The formation of copper sulphate on the surface of copper(II) sulphide electrodes was proved by Heijne and van der Linden [8] who used x-ray diffraction. Pungor et al. [9]

TABLE 1

Concentration of copper ions dissolved from CuS electrodes measured in 300-μl solutions[a]

Conditioning of the electrode	Dissolution measured in 300 μl	Cu conc. (mol l^{-1})
Water	Water	1.5×10^{-5}
EDTA (10^{-2} mol l^{-1})	Water	2.7×10^{-5}
$Cu(NO_3)_2$ (10^{-3} mol l^{-1})	Water	3.5×10^{-4}
H_2SO_4 (2.5×10^{-2} mol l^{-1})	10^{-1} mol l^{-1} KNO_3	8.0×10^{-4}
Ascorbic acid (10^{-2} mol l^{-1})	Water	8.0×10^{-6}
Acetate buffer pH 4 with formaldehyde	Acetate buffer	1.6×10^{-4}
KSCN (10^{-1} mol l^{-1})	Water	1.4×10^{-4}
Nitrogen stream through water	Water	3.0×10^{-5}

[a]Distilled water was used for all solutions.

applied x-ray photoelectron spectroscopy to prove formation of copper sulphate on the surface of copper(II) sulphide electrodes as an effect of chemical oxidization.

To decrease the oxidative dissolution of copper ions from the membrane material, the following methods have been suggested in the literature: (a) removal of oxygen from the test solution by a nitrogen stream [10]; (b) application of a buffer solution containing formaldehyde as a weak reducing agent [11]; (c) pretreatment of the electrode in ascorbic acid [7] or other agents (KCN, KSCN). All these pretreatment methods were tried, but no significant decrease in the dissolution of the membrane material could be

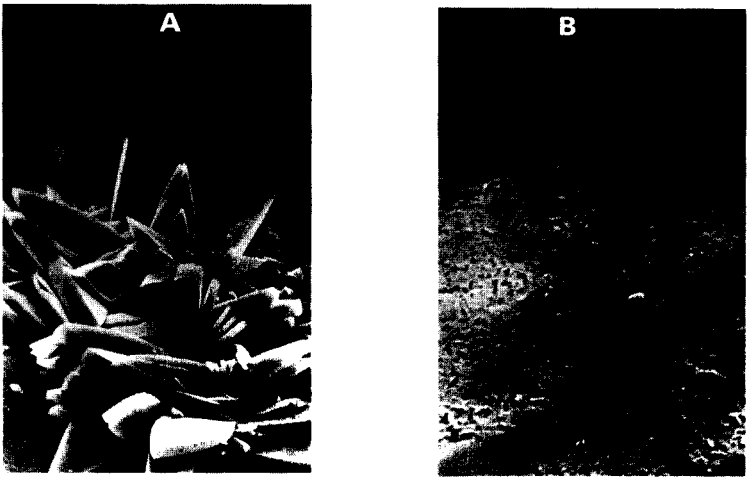

Fig. 2. Electron micrographs of CuS membranes. A, Membrane conditioned in distilled water for two weeks (magnification 500×); B, untreated membrane (magnification 5000×).

achieved; these results are also included in Table 1. However, after pretreatment in ascorbic acid for four days, a calibration curve of increased slope was obtained (Fig. 3A), which is most probably due to formation of copper(I) ions. Copper(I) ions may also influence the electrode potential measured. A similar effect was observed when the electrodes were pretreated in 10^{-1} mol l^{-1} thiocyanate solution; after an electrode had been soaked for four days in the thiocyanate solution, a white coating was observed on the electrode surface. Far-infrared measurements identified the presence of copper(I) thiocyanate. The electron micrograph of this coating is shown in Fig. 4A.

As the use of different reducing agents did not result in a significant decrease in the dissolution of the membrane material, another way of pretreatment was tried. As a conditioning solution, a counter-ion buffer solution (i.e., sulphide ion) was used; this was expected to convert dissolved copper ions to a new copper(II) sulphide coating on the membrane surface, thus preventing further dissolution of copper ions. The electrodes were pretreated in stirred 10^{-2} mol l^{-1} sodium sulphide for an hour, and the calibration curve of the electrode shown in Fig. 3B (curve a) was then obtained. After the conditioning, the electrode was rinsed with distilled water and dried, and the calibration plot was obtained with increasing copper(II) ion concentrations in the range 10^{-6}—10^{-2} mol l^{-1}. Nernstian response was obtained only above 10^{-4} mol l^{-1} copper(II) ion concentration, which means that below this concentration sulphide ions were in excess on the surface of the electrode. This excess of sulphide ion must first be "neutralized" with the copper ions present in the test solution; only when copper ions appear at

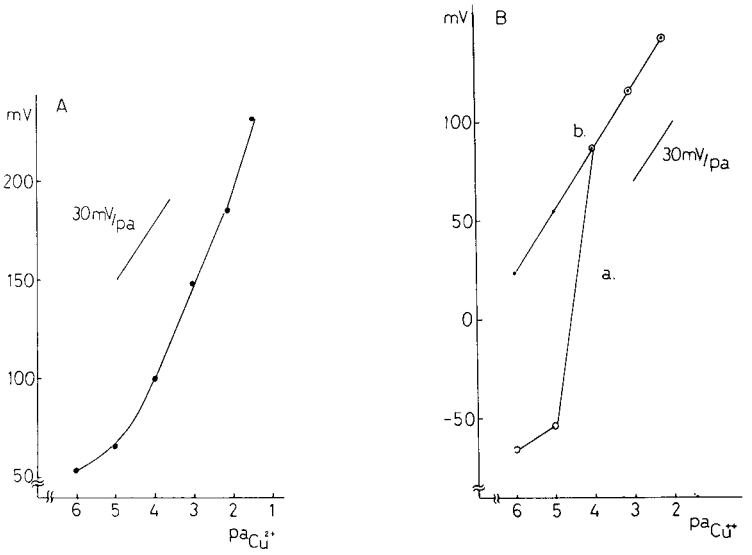

Fig. 3. Calibration curves for electrodes conditioned in (A) 10^{-2} mol l^{-1} ascorbic acid and (B) 10^{-2} mol l^{-1} sodium sulphide solution. Line (a) was measured in the direction of increasing concentrations and line (b) with decreasing concentrations after line (a).

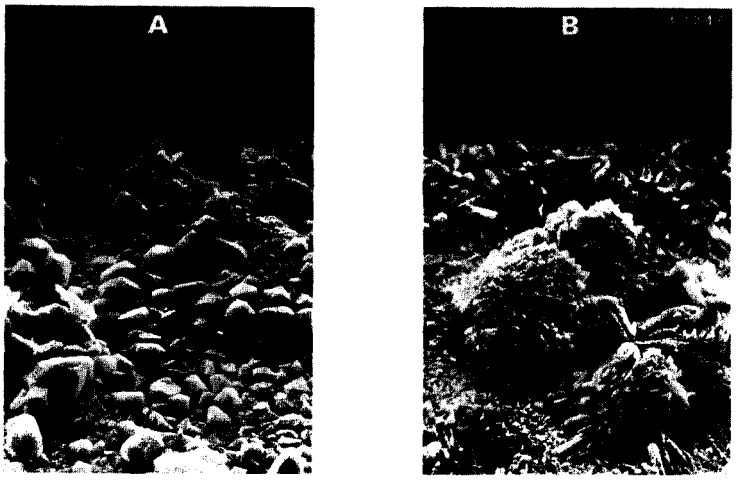

Fig. 4. Electron micrographs of electrode membranes. A, Membrane conditioned in 10^{-1} mol l^{-1} KSCN (magnification 500×); B, membrane conditioned in 10^{-2} mol l^{-1} sodium sulphide (magnification 500×).

the membrane/solution interface will the electrode show the theoretical response to copper ions. Figure 3B (curve b) shows the calibration graph obtained just after the first calibration (curve a) but in the reverse direction, i.e., with decreasing concentrations of copper ion. In this case, Nernstian response was achieved down to 10^{-6} mol l^{-1} copper(II) concentrations.

The dissolved copper ion concentrations were also determined for electrodes pretreated in sodium sulphide solution. The dissolved copper was measured in 300 μl of distilled water after the electrode had been immersed in the water for 10 min. The concentration found was in the range $1.2—5 \times 10^{-6}$ mol l^{-1}, which is a significant decrease compared with the untreated electrodes. The copper concentrations were also measured at different time intervals after a single treatment; the results are summarized in Table 2. Between measurements the electrodes were kept in air, and before measurements they were conditioned for an hour in stirred distilled water. The data show only a slight difference in the dissolution as a function of time.

The electron micrograph of a copper(II) sulphide electrode treated in sodium sulphide solution (Fig. 4B) shows clearly the new crystalline coating on the electrode membrane surface. This coating was identified as copper(II) sulphide by using electron diffraction measurements. The disadvantage of this pretreatment is that the new layer on the surface can be removed by polishing and the dissolution of copper then starts to increase again. This suggests that the release of copper ion may be due not only to surface oxidation of the electrode membrane but also to copper impurities in the membrane material. Buck [12] has already stressed the role of impurities during membrane preparation which can cause leaching of cations.

TABLE 2

Copper ion dissolved from a copper(II) sulphide electrode at different intervals of time after a single treatment with sodium sulphide

Elapsed time	1 h	1 day	1 week	3 months
Cu dissolved (10^{-6} mol l^{-1})	1.2	5	5	7

The above study led to the conclusion that a more reproducible electrode performance would be obtained if the membrane precipitate itself were treated with sodium sulphide solution before the membrane was pressed. To prove this, 10 g of the copper(II) sulphide precipitate was washed with 200 ml of 5×10^{-3} mol l^{-1} sodium sulphide and then with 1 l of distilled water. The precipitate was dried in a nitrogen stream, electrodes were prepared, and the potential response was checked in the concentration range 10^{-7}—10^{-2} mol l^{-1} with 25-ml volumes of solution. The corresponding calibration curve is shown in Fig. 5. The dissolved copper concentrations measured in 300 μl of distilled water for three different electrodes made from the specially treated copper(II) sulphide were found to be 1.0—1.8×10^{-6} mol l^{-1}. These concentrations were unchanged even after three months whether the electrodes were stored in air or in distilled water. Thus adsorption of copper ions could be measured on the surface of the specially prepared electrodes.

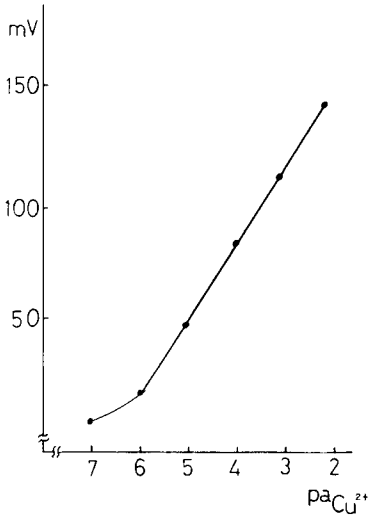

Fig. 5. Calibration curve for an electrode prepared from a precipitate treated with sodium sulphide. The solutions (25 ml) were adjusted to ionic strength 0.1 with KNO_3.

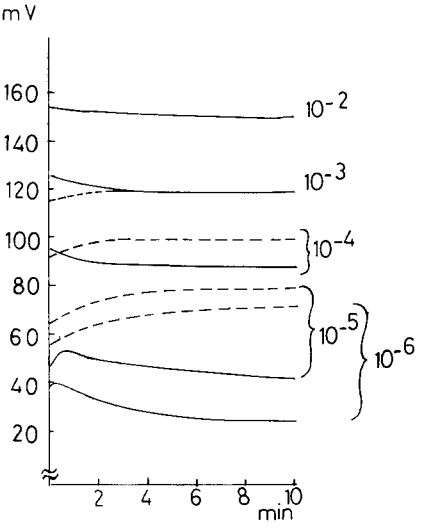

Fig. 6. Electrode potentials measured as a function of time: (—) data obtained by measuring in the direction of increasing concentrations; (---) data obtained by measuring in the direction of decreasing concentrations. The values on the curves are the copper concentrations in mol l^{-1}.

Determination of copper ions adsorbed on the surface of copper(II) sulphide electrodes

The electrodes made from membrane material prepared by the modified method given above were calibrated again after conditioning in distilled water. The solutions (300 μl) covered the concentration range 10^{-6}—10^{-2} mol l^{-1} copper(II) ion. The electrodes were equilibrated for 10 min in the appropriate solution before the potential was read; the copper concentrations of the solutions were then measured by atomic absorption spectrometry. Below 10^{-4} mol l^{-1} copper ion concentrations, the copper concentration measured decreased because of adsorption, and the amount of copper adsorbed on the surface of the electrode could be calculated from this decrease. To prove the adsorption, the Freundlich and Langmuir isotherms were measured and the maximum amount of copper adsorbed was calculated. Similar calculations were made earlier for the silver iodide electrode [6]. Under the given experimental conditions, the maximum amount of copper ion adsorbed on the surface (surface area 1.13 cm^2) was in the range 0.2—0.3 μg. This amount of copper ion corresponds almost to a monomolecular layer. A theoretically calculated monolayer on the given electrode, considering only the geometrical area, would correspond to 0.14 μg of copper.

The processes of adsorption and desorption occurring on the surface of the electrode are supported by the following experiment. An electrode was calibrated in the 300-μl cell with increasing and decreasing copper(II) ion concentrations in the range 10^{-6}—10^{-2} mol l^{-1}. Before measurements the electrode was conditioned in distilled water. The electrode potentials as a function of time are given in Fig. 6. It can be seen that during measurements in the direction of increasing concentrations, the electrode potentials decrease with time whereas they increase with time when decreasing concentrations are used. These measurements support the assumption of adsorption and desorption of copper ions at the electrode/solution interface. When the copper concentration is increased, copper ion adsorption takes place, whereas with decreasing copper concentrations in the test solutions, copper ions desorb from the electrode surface and increase the actual copper concentration in the solution.

Conclusion

Under the experimental conditions described, adsorption and desorption processes play an important role in the operation of precipitate-based electrodes, particularly at low concentrations, in this case below 10^{-4} mol l^{-1} copper ion concentrations. As the copper ion concentration to be measured is decreased, these processes become more and more significant. This can be seen on a linearized Freundlich isotherm (Fig. 7); the adsorbed concentration related to the equilibrium concentration increases as the copper ion concentration of the test solution decreases. This also means that one of the factors affecting the detection limit attainable in unbuffered solution with the given electrodes is adsorption of the primary ion on the surface of the

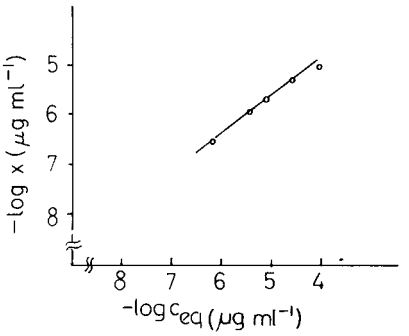

Fig. 7. Linearized graph of the Freundlich isotherm. The logarithm of the adsorbed copper ion concentration is plotted against the logarithm of the equilibrium copper concentration.

precipitate-based electrode. The other important factor is the dissolution of the membrane material.

The authors thank Mrs. Kalló (Polymer Research Institute, Budapest) for taking the scanning electron micrographs.

REFERENCES

1 C.R.C. Handbook of Chemistry and Physics, 62nd edn., CRC Press, Boca Raton, FL, 1981–82.
2 J. Gulens, Ion-selective Electrode Rev., 2 (1980) 117.
3 D. Midgley, Ion-selective Electrode Rev., 3 (1981) 43.
4 W. J. Blaedel and D. E. Dinwiddie, Anal. Chem., 46 (1974) 873.
5 Y. Umezawa, I. Tasaki and S. Fujiwara, in E. Pungor (Ed.), Third Symposium on Ion-selective Electrodes, Mátrafüred 1980, Akadémiai Kiadó, Budapest, 1981.
6 E. G. Harsányi, K. Tóth, L. Pólos and E. Pungor, Anal. Chem., 54 (1982) 1094.
7 J. Pick, K. Tóth and E. Pungor, Anal. Chim. Acta, 61 (1972) 169.
8 G. M. Heijne and W. E. van der Linden, Anal. Chim. Acta, 93 (1977) 99.
9 E. Pungor, K. Tóth, M. K. Pápai, L. Pólos, H. Malissa, M. Grasserbauer, E. Hoke, M. F. Ebel and K. Persy, Anal. Chim. Acta, 109 (1979) 279.
10 D. Midgley, Anal. Chim. Acta, 87 (1976) 7.
11 M. J. Smith and S. E. Manahan, Anal. Chem., 45 (1973) 836.
12 R. P. Buck, Anal. Chem., 48 (1976) 23R.

Analytica Chimica Acta, 152 (1983) 173—190
Elsevier Science Publishers B.V., Amsterdam — Printed in The Netherlands

BIPOLAR PULSE CONDUCTOMETRIC MONITORING OF ION-SELECTIVE ELECTRODES
Part 3. Studies with the Calcium and Fluoride Electrodes in a Continuous Flow System

CHARLES R. POWLEY[a] and TIMOTHY A. NIEMAN*
School of Chemical Sciences, University of Illinois, Urbana, IL 61801 (U.S.A.)
(Received 29th July 1982)

SUMMARY

Bipolar pulse conductometric monitoring of the calcium and fluoride ion-selective electrodes (i.s.e.'s) in a continuous flow system is evaluated. The location and composition of the counter electrode are critical; an electrochemically poised reference electrode is not necessary. The best scheme for conductometric measurements involves making a rapid series of current measurements at various pulse heights, and extrapolating the resulting linear current—voltage (i/V) curve to $V = 0$. For ionic strengths higher than 10^{-3} M, detection limits of about 10^{-6} M were obtained with both the calcium and fluoride electrodes, monitored conductometrically and potentiometrically. Relative standard deviations were about 20% and 12% for calcium and fluoride, respectively, for both monitoring methods. Drift problems observed in previous work with conductometric monitoring of i.s.e.'s were reduced significantly. Flow rates of 20 ml min^{-1} were possible with the calcium electrode. The response time of the calcium electrode is influenced by both diffusion and migration processes. Interfering ions cause the current to overshoot the steady-state current on injection. The conductometric response time of the fluoride electrode is generally faster than the potentiometric response time; both methods have concentration-dependent response times.

Continuous flow systems based on segmented [1, 2] and unsegmented (often termed flow injection analysis) [3—5] streams have become popular in recent years because of their applicability to a wide variety of determinations. Ion-selective electrodes (i.s.e.'s) have frequently been used in continuous flow systems [6—10]. The advantages in using i.s.e.'s in flowing streams, as opposed to static solutions are: (1) the i.s.e. does not alter a low analyte concentration in the sample; (2) a thinner stagnant solution layer exists on the i.s.e. surface, so that response times are shorter; and (3) the reference electrode does not alter the sample, because it is usually placed downstream of the i.s.e. [7]. A problem is encountered when i.s.e. response time is concentration-dependent; response is non-Nernstian if the i.s.e. is not allowed to reach its steady-state response. Therefore, nonlinear calibration plots are often

[a]Present address: Department of Chemistry, University of Georgia, Athens, GA 30602 (U.S.A.).

0003-2670/83/$03.00

obtained in unsegmented flow systems in which steady-state responses are usually not achieved [10]. Also, streaming potentials can interfere with measurements if the flow rate is very high or the solution conductivity is very low [11].

Recently, results obtained with bipolar pulse conductometric monitoring have been reported for the calcium [12, 13] and fluoride [14] electrodes. The quantitative performance of these electrodes with conductometric monitoring was comparable to that obtained potentiometrically with some exceptions. The response time of the calcium electrode is much faster with conductometric monitoring, and the response of the i.s.e. was shown to be concentration-dependent not activity-dependent [13]. Detection limits were in the nanomolar region with the fluoride electrode. Whereas conductometric response time was shown to be independent of fluoride concentration, potentiometric response time had a strong concentration-dependence [14]. Finally, it was observed that an electrochemically poised reference electrode was not necessary in the absence of electroactive interferences. However, problems were encountered in that both electrodes yielded drifting current measurements. Some of the experiments done to circumvent drift problems would not be convenient in a practical situation, and frequent recalibration of the i.s.e. would be necessary.

It was hypothesized earlier that rinsing of the i.s.e. between samples in a continuous flow apparatus might reduce the drift problems [13, 14]. Calcium electrodes are widely used in flow systems for determination of calcium activity in serum and water [15—18]. The fluoride electrode has also been used in slow flow systems [19] as well as in fast flow systems to study i.s.e. response times [19, 20]. This paper reports results of bipolar pulse conductometric monitoring of the calcium and fluoride electrodes in an unsegmented flow system. Method development, aimed at optimizing the quantitative performance of the system, was done with the calcium electrode. The quantitative performance of the calcium and fluoride electrodes was then evaluated. Response times for both electrodes were studied for a variety of conditions.

EXPERIMENTAL

Equipment

Flow cell. The flow cell used for measurements with the calcium and fluoride electrodes is represented in Fig. 1. Electrode 1 is the ion-selective electrode, and electrodes 2—4 are stainless steel counter electrodes; all four electrodes have 1-cm diameters. The calcium i.s.e. is a brass rod, the surface of which is polished and coated with a calcium-selective membrane. This membrane is 70% calcium liquid ion-exchanger (Orion Research, no. 92-20-02) and 30% poly(vinyl chloride) [13]. The fluoride electrode is a commercially available i.s.e. (Orion Research, 74-09). The piece that holds the calcium i.s.e. is made of teflon as is the spacer (1.6 mm thick) which gives the cell a volume of about 300 μl. The teflon holder is replaceable by a similar plexiglas piece

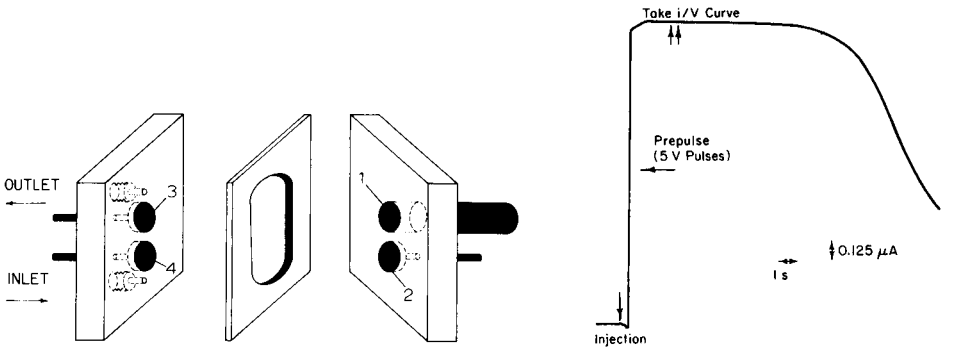

Fig. 1. Diagram of flow cell used. Electrode 1 is the i.s.e. and electrodes 2, 3, and 4 are stainless steel counter electrodes. For details, see text.

Fig. 2. Plot of current vs. time for an injection of Ca^{2+} solution into the flow cell. The *i/V* data collection routine is shown.

when the fluoride electrode is used, and a 12-mm diameter hole is used to hold the fluoride i.s.e. Electrode 2 is then replaced by the end of an 18-gauge platinum wire or 1.6-mm diameter stainless-steel rod. The third piece of the cell (containing two steel counter electrodes) is made from plexiglas, and has 1/4 in.—28 (6.35 mm—1.10) inlet and exit ports through which the solution is pumped.

Flow system. The flow system used consisted of a pump, injector, and flow cell. A high-speed reciprocating pump (Gorman-Rupp Industries, Model Z-12500) was controlled to deliver flow rates of 10—90 ml min^{-1} for experiments with the calcium electrode. This pump was replaced by a syringe pump (Sage Instruments, Model 355) to deliver low flow rates (1—5 ml min^{-1}) without pulsation for measurements with the fluoride electrode. The injector was a pair of slider valves (Altex) and a 1.5-ml sample loop. All tubing was 1.5-mm i.d. teflon. The distance between the injector and the flow cell was kept short (about 10 cm for a volume of 0.18 ml) to minimize dispersion of the injected solution slug [21]. A microswitch in the injector signalled the computer controlling the bipolar pulse conductance (BICON) instrument when an injection was made. The computer then began the specified measurement routine.

Conductometric measurement

Current measurements were made using the BICON technique in the voltage pulse mode [22, 23]. Pulse durations of 100 μs were used throughout. Pulse heights were 0—5 V. The BICON instrument used was an improved version of the instrument described earlier [12], and complete details can be found elsewhere [24]. The instrument is controlled by an INTEL SBC 80/10B microcomputer supplemented by a computer expansion board [13, 24] with extra memory, I/O ports, and a hardware arithmetic unit (Advanced Micro Devices 9511).

Relatively slow (rise time 5 s or greater) conductance changes could be followed by repeatedly applying voltage pulses to the cell while monitoring the output of the sample/hold amplifier in the BICON measurement circuit using a stripchart recorder. This scheme was useful for single pulse-height monitoring of the fluoride electrode. If faster events were to be followed, or current measurements were to be taken over a range of pulse heights, special measurement routines written in 8080 assembly language were used. Two assembly language routines were especially for flow-cell measurements; full details can be found elsewhere [25]. A transient recorder program was written to study the time-dependence of the conductometric signal when a single pulse height is used. This program directs the BICON instrument to collect rapidly a specified number of current measurements following sample injection, and to output their analog equivalents to a stripchart recorder at a slower rate on completion of measurements.

The quantitative capabilities of the calcium and fluoride i.s.e.'s monitored conductometrically in a flow system were studied by using an assembly language program that rapidly takes current measurements over a range of pulse heights. A current measurement at a single, fixed pulse height is influenced by the solution resistance (an unselective entity) and by the membrane resistance, which is changed in the presence of interfering species for both the calcium [13] and fluoride [14] electrodes. Further, the effects of these resistive contributions can be minimized by making current measurements over a range of applied pulse heights to construct plots of current vs. pulse height, or current/voltage (i/V) curves. The i/V curves obtained earlier were linear from 0 to 5 V applied [13, 14], and the current—axis intercept of the line was shown to be related to the short-circuit value of the electrode potential [13]. This intercept, or "zero-pulse current" was not affected by changes in solution or membrane resistance. The i/V data collection program written for flow-cell measurements requires less than 500 ms to obtain a complete i/V curve (7 points at pulse heights of 0—5 V, 256 measurements averaged per point). If offset current [23] is added at the first (highest) pulse height to increase resolution, the amount of offset added at lower pulse heights is decreased at the same relative rate as the pulse height. A least-squares routine is then used to calculate the i/V intercept and slope.

The i.s.e. potential must reach steady-state before collection of i/V data for a particular injection. Otherwise, a nonlinear i/V plot would be obtained with an ill-defined and imprecise intercept. Figure 2 is an example of the current vs. time plot obtained when 10^{-2} M Ca^{2+} is injected into a stream of distilled water at a flow rate of 20 ml min^{-1}. Earlier work [13] demonstrated that the electrode response time decreased as the magnitude of the applied voltage pulse increased. Therefore, to obtain rapid electrode response, 5-V pulses were used to measure the current continuously. It is evident that the voltage pulses force the i.s.e. to respond to the change in Ca^{2+} concentration within 2 s after injection. A i/V plot can therefore be taken about 2.5 s after injection, within the time interval shown in Fig. 2. The i/V collection routine

is preceded by a routine that delivers 5-V pulses to the cell to force the i.s.e. to reach steady-state as quickly as possible.

Potentiometric measurements

When a potentiometric calibration graph or response time was needed a Ag/AgCl reference electrode was placed in the waste reservoir downstream from the flow cell. For the calcium electrode, the resistance between the i.s.e. and reference electrode was reduced by using 0.1 M KCl as the carrier solution; otherwise a steady potential was not achieved. For the fluoride i.s.e., the carrier solution had a low resistance because TISAB was used.

Reagents

All solutions were prepared from reagent-grade chemicals. Distilled deionized water was used throughout. Fluoride standards were prepared in TISAB-IV [14] buffered at pH 8.4 and diluted (1 + 9) with water. The carrier solution for fluoride measurements was TISAB-IV diluted (1 + 9) with water. Calcium standards were prepared in 10^{-3} M KCl and the carrier stream was water.

RESULTS AND DISCUSSION

Development and characterization of the methods

Counter electrode. Development of conditions for conductometric monitoring of the calcium i.s.e. in continuous flow required optimization in relation to the counter electrode and ionic strength. Calibration graphs (i/V intercept vs. log [Ca^{2+}]) were constructed as outlined in the experimental section. The flow rate was 20 ± 1 ml min^{-1}, and 5-V pulses (100 μs in duration) were delivered for 2.5 s before collection of i/V data at pulse heights ranging from 0.5 to 5 V. The slopes of these plots were very shallow when conductometric measurements were taken between the i.s.e. and either stainless steel disk on the opposite side of the flow cell (electrodes 3 and 4, Fig. 1). However, a reasonable slope was obtained over the 10^{-4}—10^{-1} M Ca^{2+} range when the steel disk on the same side of the cell as the i.s.e. (electrode 2) was used as the counter electrode.

It was surprising that use of the counter electrodes (3 or 4) on the opposite side of the flow-cell did not yield a viable working plot. Use of either of these large area electrodes might give the cell an unusually large parallel (geometric) capacitance. However, longer pulse durations also failed to yield viable working curves when electrode 3 was used as the counter electrode. Therefore, the possibility of incomplete parallel capacitance charging was eliminated [13]. Another explanation for the observed dependence on electrode location may be that direct interaction of the electric field of the counter electrode with the i.s.e. affects the membrane potential. The counter electrode that yielded the steepest working curve (electrode 2) did not have a linear current path to the i.s.e. and its electric field is probably weaker at

the i.s.e. surface than anywhere else in the cell. The experiments reported earlier [12—14] involved measurements with the i.s.e. and counter electrode parallel to each other, and gave useful results. However, this flow cell used here has a much smaller volume, and correspondingly higher electric field density, than does the beaker used earlier. Finally, the presence of 1—100 mM KCl in the calcium standards resulted in a lower detection limit (10^{-5} M) than that obtained in the absence of KCl (10^{-4} M); a change in the ionic strength would change the electric field strength.

The counter electrode for most experiments with the calcium i.s.e. was a 1-cm diameter stainless steel disk. Also, 0.16-cm diameter stainless steel and 0.11-cm diameter platinum wires were evaluated. The steel wire yielded the same precision (50% r.s.d. for calcium determinations in the linear range of the working graph) and detection limits (10^{-5} M Ca^{2+}) as the steel disk. However, the r.s.d. became 140% and the detection limit 10^{-4} M when the platinum wire served as the counter electrode. Stainless steel is more passive than platinum, and has a more nearly poised electrochemical potential in solutions lacking electroactive species. A more detailed investigation of the electrochemical potential of the counter electrode is presented elsewhere [25].

Measurement scheme. The calcium electrode system was studied to improve the precision and the detection limit. Precision was poor at Ca^{2+} concentrations below 10^{-3} M, where the working curve had a low slope. The high detection limit and poor precision were attributed to a memory effect arising from earlier passage of high concentrations of Ca^{2+}. The i.s.e. signal returns to baseline rather slowly after injection of a sample, as shown in Fig. 2, which allows for possible interference with the next sample. Voltage pulsing during rinsing restores the signal to baseline more quickly than does rinsing alone; potentiometric signals obtained under similar conditions require close to 30 s to return to baseline, as compared to 10 s for conductometric monitoring. Therefore, the *i/V* prepulsing and data collection routine was also triggered before each injection (while water flowed through the cell), to help eliminate any effects of the previous injection. Two common approaches to elimination of memory effects with potentiometric monitoring of i.s.e.'s in continuous flow have involved longer rinse times between samples [26] and use of segmented streams [9].

Initially, poor precision was also caused by instrumental drift. To correct for this problem, the background signal was measured immediately after collection of *i/V* data by disconnecting the cell and making a current measurement at 0 V applied. The value obtained was then subtracted from the calculated *i/V* intercept to yield the "corrected zero-pulse current."

Figure 3 is a plot of corrected zero-pulse current vs. log [Ca^{2+}] for a flow rate of 20 ml min^{-1} with data collection after 2.5 s of pre-pulsing. All calcium solutions were 10^{-3} M in potassium chloride, with a water carrier solution. The working curve shows the same linear range (3×10^{-5}—10^{-1} M) and detection limit (about 3×10^{-6} M) as the potentiometric and conductometric working curves obtained for static solutions [13] or for a potentiometric

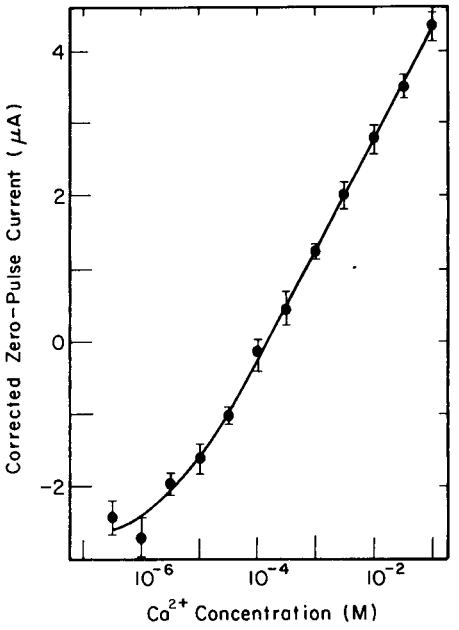

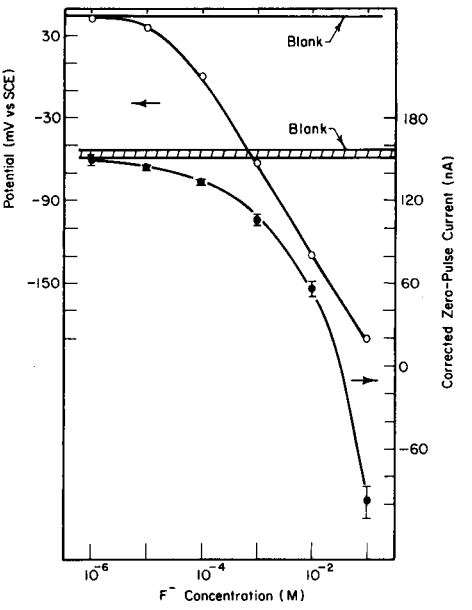

Fig. 3. Plot of i/V intercept minus zero pulse noise vs. Ca^{2+} concentration for fast flow measurements. Current—voltage data were collected 2.5 s after injection.

Fig. 4. Working curves for the fluoride electrode: (•) based on conductometric i/V intercepts; (○) potentiometric. The band for the conductometric blank represents its uncertainty.

working curve in a flowing stream. The error bars represent the standard deviations about each average of 5 injections. The average r.s.d. of Ca^{2+} concentrations determined in the linear range of the working curve is 20% when offset current is added to the cell current to increase the resolution of the measurements [23] and 45% when no offset is used. The long-term drift problems associated with conductometric monitoring of the calcium i.s.e. in still solution have been eliminated, as working curves constructed over a day yield the same absolute values for all the corrected i/V intercepts.

Precision typically obtained for potentiometric monitoring of calcium i.s.e.'s in continuous flow systems is 4—5% r.s.d. for concentration determinations [18, 27, 28]. Working ranges are comparable to those reported here, and flow rates of 0.5—2 ml min^{-1} are most commonly used [27, 29]. Coated-wire i.s.e.'s typically require frequent recalibration [30] or use of a differential measurement technique [28] because their internal potentials drift. Potentiometric working curves constructed with the continuous flow system and coated-brass i.s.e's used here yielded a 20% r.s.d. for concentration values, which is equal to the conductometric r.s.d. value when offset current is used. A major consideration in the choice of coated-metal electrodes was that they are pressure-resistant. The high flow rates used tended to degrade

or destroy the commercially-available i.s.e's with internal reference solutions. Another type of pressure-resistant calcium i.s.e. with a real internal reference is the Selectrode, which has a calomel paste sandwiched between a teflon/graphite conductor and the poly(vinyl chloride) membrane [31]. This electrode may yield better precision than that obtained with the coated-metal electrodes.

Selectivity. Selectivity coefficients for the Ca^{2+} i.s.e. were determined by the method used previously [12, 13] and were calculated from

$$i'_{z.p.} = S \log ([Ca^{2+}] + k\,[I^{j+}])^{2/j} \quad (1)$$

which is the bipolar pulse conductometric analog of the equation recommended for i.s.e. use by IUPAC [32] where $i'_{z.p.}$ is the corrected zero-pulse current, S is the working curve slope, and k is the selectivity coefficient for the interfering species I^{j+}. The resulting values are given in Table 1, with selectivity coefficients obtained in static solutions [13] for comparison. The percent error in measured Ca^{2+} concentration caused by the particular interferent in solution is also reported. Selectivity coefficients for Ba^{2+}, Mg^{2+}, and Sr^{2+} are comparable to those obtained earlier, but selectivity coefficients for Na^+, NH_4^+, and Pb^{2+} are much lower for the flow-cell method than for static solutions. Most of the error attributed earlier to interferences may have been due to drift problems, which were eliminated in the flow-cell method.

Fluoride electrode working curves. The first approach used in making measurements with the fluoride electrode involved continuous monitoring of the cell current at a fixed 5-V pulse height. A platinum wire on the same side of the cell as the i.s.e. was used for the counter electrode, and the flow rate was 1 ml min^{-1}. The deviation of the measured current signal from the

TABLE 1

Selectivity coefficients obtained in continuous flow measurements and in still solution with the calcium electrode. The calcium concentration in all solutions was 10^{-4} M

Interfering species	Conc. (M)	Selectivity coefficient		
		Conductometric method		Potentiometric method (static)[c,d]
		Flow system[a]	Static[b,c]	
Na^+	10^{-1}	0.0015 (150)	0.011	0.014
NH_4^+	10^{-1}	0.0009 (9)	0.0016	0.048
Ba^{2+}	10^{-2}	0.0051 (51)	0.011	0.0016
Mg^{2+}	10^{-2}	0.0068 (39)	0.011	0.0046
Sr^{2+}	10^{-2}	0.032 (240)	0.036	0.0093
Pb^{2+}	10^{-3}	0.025 (25)	0.40	0.77

[a]All solutions 10^{-3} M in KCl. The numbers in parentheses are the percentage errors caused by the interferences. [b]No KCl added to solution. [c]Values from ref. 13. [d]All solutions 0.1 M in KCl.

diluted TISAB-IV carrier solution was measured 30 s after injection. A potentiometric working curve was constructed under similar experimental conditions, but the change in potential from the carrier solution was measured 90 s after injection. Both working curves were quite similar to those shown earlier for still solutions [14]. The conductometric curve again showed anomalous behavior, because of the effects of fluoride on the electrode resistance and potential [14]. Precision of the conductometric curve was poor, so a measurement routine similar to that employed with the calcium electrode was used.

The platinum counter electrode was replaced with a 1.6-mm diameter stainless steel wire. Current—voltage data were taken for each injection of the fluoride standards; the measurement sequence consisted of 30 s of prepulsing (5-V pulses) followed by collection of a 20-point *i/V* curve (256 measurements averaged per point). The corrected zero pulse current was calculated for each *i/V* curve. The flow rate was 5 ml min^{-1} and the volume injected was 1.5 ml. The potentiometric and conductometric working curves obtained are shown in Fig. 4. The most noteworthy feature of the conductometric plot is its curvature. Similar fluoride working plots were linear for static solutions [14]. An explanation for the curvature found for the flow system is that the interference with the electrode potential caused by the electric field of the counter electrode is more severe with the fluoride electrode than with the calcium electrode.

The conductometric *i/V* and potentiometric methods have similar detection limits and practical working ranges. Precision for both methods is good. Precision for fluoride determinations is 12% r.s.d. by conductometric monitoring in the 10^{-3}—10^{-1} M range, increasing to 20% r.s.d. at 10^{-4} M, and 8% by potentiometric monitoring over this entire range. Potentiometric monitoring of fluoride i.s.e.'s in continuous flow systems is usually done at flow rates of 2—8 ml min^{-1}, with precision of 3—5% r.s.d. [10]. The working range is similar to that encountered in still solutions [19] and detection limits are 10^{-6}—10^{-5} M fluoride.

Construction of *i/V* curves eliminates many of the problems encountered in conductometric monitoring of the fluoride electrode. The measurement of the total current at a single pulse height yields a detection limit of about 10^{-9} M fluoride because of changes in the resistance of the surface gel layer at submicromolar concentrations. However, the electrode resistance, while interesting from a fundamental point of view, shows limited quantitative usefulness because of its drift and susceptibility to matrix interferences [14]. The *i/V* curve intercept shows good reproducibility in the flow methods reported here and yielded fluoride results that were relatively free of the matrix interferences reported earlier [14].

Response time studies

Comparison of i.s.e. response time to the time-dependence of the Ca^{2+} concentration. Calcium electrode response times can be studied by using

high flow rates to change the solution concentration rapidly in the cell. Figure 5A is a plot of current through the i.s.e. (for 5-V pulses) vs. time when an injection of 10^{-2} M Ca^{2+} was made at a flow rate of 20 ml min^{-1}. The rise time is very short compared to the time required for return to baseline after the sample leaves the cell. Figure 5B is a similar plot for the current measured between two stainless steel electrodes (electrodes 3 and 4, Fig. 1); this plot has a longer rise time and shorter decay time than Fig. 5A. It must be remembered that the conductance measurements between the two stainless steel electrodes respond linearly to changes in Ca^{2+} concentration (to a first approximation), while the current through the i.s.e. varies logarithmically with $[Ca^{2+}]$.

To verify that the widened peak shown in Fig. 5A was a result of a logarithmic dependence on $[Ca^{2+}]$, the relationship between the i.s.e. current (5-V pulse height) and $[Ca^{2+}]$ was approximated as

$$i = S \log [Ca^{2+}] + C \qquad (2)$$

where S is the slope of the conductometric working curve and C is the current at a calcium concentration of 1 M. Exponentiation of Eqn. (2) yields $[Ca^{2+}] = \exp(-C/S) \exp(i/S)$ which shows that the exponentiated i.s.e. current should be linearly related to $[Ca^{2+}]$ and should show a time dependence in these experiments similar to Fig. 5B. Figure 5C is the resulting plot, which is much more similar to curve B than curve A. These plots indicate that the i.s.e. current must be exponentiated in order to compare the time dependencies of the i.s.e. current and the Ca^{2+} concentration.

Dependence of response time upon pulse height. Table 2 lists the times required for the i.s.e. to reach 95% of its steady-state value (t_{95}) after an injection, as well as the peak full-width-at-half-maximum (f.w.h.m.) values for pulse heights from 0 to 5 V. The f.w.h.m. values were preferred to t_{95} values for the falling edge because they can be measured more precisely and indicate the time required to return to baseline for an asymmetric peak like curve A.

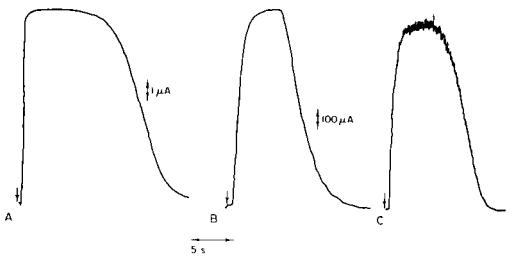

Fig. 5. Current-time profiles for bipolar pulse measurements: (A) between the calcium i.s.e. and the stainless steel counter electrode on the same side of the flow cell; (B) between two steel electrodes on the same side of the flow cell; (C) exponentiated current-time profile of data shown in (A).

TABLE 2

Dependence of response time on pulse height

Pulse height (V)	Rise time and f.w.h.m. (s)			
	Unexponentiated data		Exponentiated data	
	t_{95} ± 0.1	f.w.h.m. ± 0.2	t_{95} ± 0.1	f.w.h.m. ± 0.2
0.00	2.4	12.7	—[a]	—[a]
0.12	2.0	11.7	—[a]	—[a]
0.25	1.3	16.3	4.6	8.8
0.50	1.0	15.6	3.4	9.3
1.00	0.6	14.9	1.3	8.5
2.00	0.4	14.6	0.9	8.5
3.00	0.4	14.0	0.9	7.7
4.00	0.4	14.0	0.9	8.1
5.00	0.4	15.4	1.0	7.6
Solution conductance	1.7	6.9		

[a]Exponentiated current/time profiles were obliterated by noise.

The rise times for unexponentiated data showed the same dependence on pulse height as observed earlier [13]; the response time decreased with increasing pulse height, reaching a minimum at pulse heights $\geqslant 2$ V. The f.w.h.m. value apparently is independent of pulse height. The exponentiated data plots show the same trends in rise times and f.w.h.m. values as the unexponentiated plots. However, the rise times are greater, and compare more favorably with the time dependence of the solution conductance (measured using two stainless steel electrodes) than do the time dependencies of the unexponentiated data. The f.w.h.m. values for exponentiated data also compare more favorably with similar values for the solution conductance.

Random noise in the raw data becomes much more evident when the data are exponentiated, as shown in Fig. 5C. Therefore, it is difficult to make accurate response-time determinations from exponentiated current/time profiles at low pulse heights (less than 2 V) where the signal-to-noise ratio is low.

Flow-rate dependence. The explanation proposed earlier [13] for fast conductometric response times (compared to those obtained in potentiometry) was that Ca^{2+} ions migrated through a stagnant solution layer adhering to the surface of the membrane. Potentiometric response times are thought to be determined by diffusion of ions through this solution layer [33]. Diffusion-based processes are identified in potentiometry by studying response times as a function of flow rate [20, 34]. Solution diffusion processes yield a response time that is inversely proportional to the flow rate [20].

Conductometric response time was studied as a function of flow rate to determine if there were any similarities to the reported potentiometric

behavior. Figure 6 is a plot of the time dependencies of both the rising and falling edges of the current/time profile for an injection of 10^{-2} M Ca^{2+} vs. the reciprocal flow rate. Linear behavior is observed at high flow rates, but at low flow rates, response times are shorter than would be predicted from extrapolation of the linear region. At high flow rates, the adhering solution layer becomes thinner [33] and causes a corresponding decrease in both conductometric and potentiometric response times. However, the conductometric response time is probably both diffusion and migration-dependent, with a relatively large amount of migration dependence at lower flow rates.

Response time dependence on KCl/Ca^{2+} ratio. It was suggested above that the fast conductometric response of the calcium electrode is due to voltage pulsing inducing Ca^{2+} migration through the stagnant layer of solution at the electrode surface. Of course, migration of analyte ions is minimized by a large excess of a supporting electrolyte, which carries virtually all the migration current, so that analyte ions move mainly by diffusion [35]. To investigate the role of analyte migration in conductometric i.s.e. response times, the supporting electrolyte-to-analyte ratio was varied by injecting 10^{-3} M Ca^{2+} solutions and increasing the potassium chloride concentration in the analyte and carrier solutions from 0 to 10^{-1} M. The rise times and f.w.h.m. values for the resulting current/time profiles are shown in the upper half of Table 3. The potentiometric response time for 10^{-1} M KCl is shown for comparison. The presence of the salt increases the response time of the Ca^{2+} i.s.e. The f.w.h.m. values do not show a trend, which indicates that the time required for the i.s.e. to return to a baseline value was not affected.

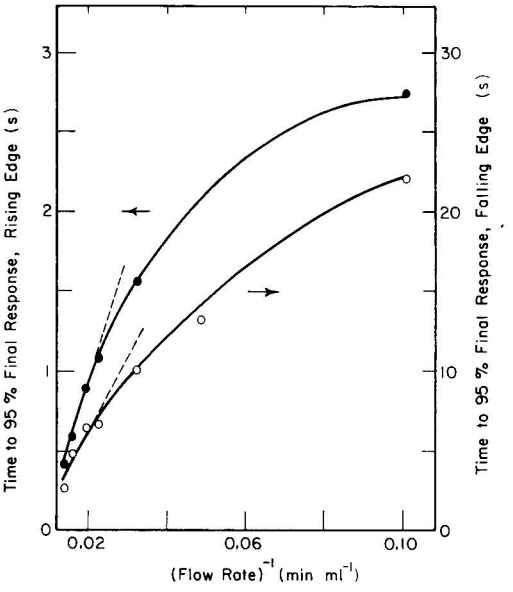

Fig. 6. Response-time dependence on (flow rate)$^{-1}$.

TABLE 3

Response time as a function of KCl/Ca^{2+} ratio for a flow rate of 20 ml min^{-1}

KCl conc. (M)	KCl/Ca^{2+} ratio[a]	Risetime and f.w.h.m. (s)	
		t_{95} ± 0.1	f.w.h.m. ± 0.2
KCl present in both analyte and carrier solutions			
0	0	0.8	10.9
10^{-4}	0.1	0.9	10.4
10^{-3}	1	1.7	10.2
10^{-2}	10	2.0	11.4
10^{-1}	100	2.5	11.4
10^{-1} (potentiometric)	100	3.2	19.4
KCl present in analyte solution only; carrier solution was water			
0	0	0.9	8.5
10^{-4}	0.1	0.3	8.5
10^{-3}	1	0.3	9.3
10^{-2}	10	0.3	11.2
10^{-1}	100	0.3	13.7

[a] Ca^{2+} concentration was constant at 10^{-3} M.

Potentiometric response times are diffusion-dependent, and it is evident that the increase in electrolyte concentration increases the conductometric rise time enough to approach a diffusion-based time scale. The results presented in Tables 2 and 3 for f.w.h.m. values and in Fig. 6 for the t_{95} values of the falling edge of the current/time profile indicate that return of the i.s.e. signal to baseline is not purely diffusion- or migration-based, and is probably a combination of both. A purely diffusion-based time dependence would yield equal potentiometric and conductometric decay times, and the plot of t_{95} (falling edge) vs. $(\text{flow rate})^{-1}$ would be linear. Conversely, a purely migration-based system would yield pulse height and $[KCl]/[Ca^{2+}]$ ratio dependencies of the f.w.h.m. values.

The unusual time dependence of the falling edge was also observed when potassium chloride was present in varying concentrations only in the analyte solution. The t_{95} and f.w.h.m. values for these conditions are summarized in the lower half of Table 3. Addition of the salt to the analyte solution alone decreases the rise time to 300 ms. At 10^{-2} and 10^{-1} M KCl the signal actually overshoots its steady-state value (see below). Apparently, with only water in the carrier solution, the potassium chloride from the analyte solution can retard Ca^{2+} passage out of the membrane, which results in a wider peak with slow return to baseline (see below).

Response time in the presence of interfering species. Response times for interfering species were evaluated by injecting solutions containing 10^{-2} M Ca^{2+} or interfering species into the flow stream. The flow rate of the water carrier solution was 20 ml min^{-1}. The rise time was 0.3 ± 0.1 s for all species

evaluated. The f.w.h.m. value was 11.7 ± 0.2 s for Ca^{2+}, K^+, Na^+, and NH_4^+, increased to 13.0 ± 0.2 s for Ba^{2+}, Mg^{2+}, and Sr^{2+} and was 13.6 ± 0.2 s for Pb^{2+}. Long response times for interfering species have been observed potentiometrically, and were attributed to slow ion-exchange kinetics [36—38]. Apparently, induced migration can overcome such slow kinetics, as the rise times were not affected and the f.w.h.m. values increased only slightly for interfering divalent ions.

Response times and f.w.h.m. values were also determined for solutions which were 10^{-4} M in Ca^{2+} and 10^{-1} M in the interferent. Figure 7 shows typical current—time profiles obtained with and without ammonium ion in the sample. As can be seen, the addition of ammonium ion caused an initial overshoot of the steady-state signal and doubled the width of the peak. Similar effects were observed for 10^{-1} M solutions of other species containing 10^{-4} M Ca^{2+}. The overshoot was less pronounced for divalent species than for monovalent species. Similar overshoots have been observed in potentiometry, when an i.s.e. responds to a high concentration of an interfering species in addition to a low concentration of the primary ion [34, 39, 40]. Two explanations have been suggested. In one, greatly differing selectivities are proposed for surface and bulk ion-exchange sites [41]; if the surface layer adsorbs interfering ions quickly, a fast rise would be expected, followed by a slow decay as the interior equilibrated with the favored primary ion. The second explanation involves fast charging of the space-layer capacitance at the i.s.e./solution interface, followed by slow diffusion of ions and/or exchange sites within the membrane to compensate this charge [42]. The latter explanation would account for the appearance of the overshoot at high ionic strengths and its independence of the identity of the species at the higher concentration.

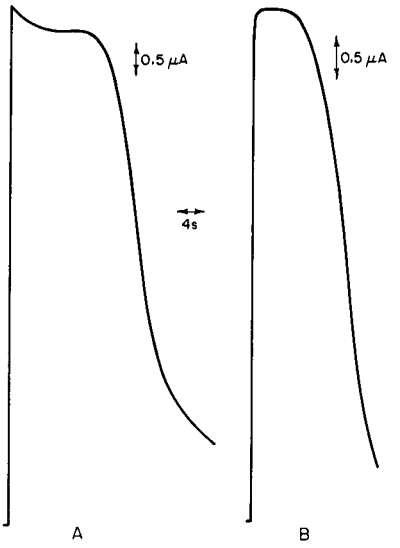

Fig. 7. Current—time profiles for: (A) 10^{-4} M Ca^{2+}/10^{-1} M NH_4^+ injection; (B) 10^{-4} M Ca^{2+} injection.

Table 4 lists the t_{95} values for the rising edge and f.w.h.m. values obtained for seven interfering species added to calcium solutions. The rise time decreases with increasing ionic strength, and overshoots similar to that shown in Fig. 7A were obtained for 0.1 M (and 0.3 M) solutions of all interfering species. Divalent species at 0.1 M concentrations yielded constant f.w.h.m. values that were 2.3—2.5 s higher than those obtained for monovalent ions. The results from the lower part of Table 3 and from Table 4 indicate that the peak width increases with increasing ionic strength. The divalent salt solutions were made with 1:2 electrolytes, so their ionic strengths were 0.3 M. However, 0.3 M solutions of the monovalent species still yielded f.w.h.m. values that were about 1.5 s lower than those obtained for the divalent species (Table 4).

The increase in decay time, which produces the increased f.w.h.m. value with interfering species, is actually caused by the increased ionic strength of the test solution; divalent cations produce a small additional effect. These results support the above hypothesis that high ionic strength retards transport through the solution layer at the membrane surface. The slight increase in f.w.h.m. values for divalent species over monovalent species at equal ionic strengths indicates that interaction with the membrane further retards transport out of the membrane/solution interface. The rapid rise time, possible overshoot, and slow return to baseline all occur at high ionic strength, and may be related. If the rapid rise and overshoot are indeed the result of a space-layer capacitive charging, the delayed return to baseline may be caused by the slow discharge of this capacitance.

Response times at different fluoride concentrations. Potentiometric and conductometric rise times and f.w.h.m. values were measured for the fluoride

TABLE 4

Response times and f.w.h.m. values for injections of mixtures of interfering species and Ca^{2+}. The flow rate was 20 ml min^{-1}. All solutions contained 10^{-4} M Ca^{2+} except where noted otherwise

Species	Conc. (M)	Ionic strength (M)	t_{95} ± 0.1 s (rising)	F.w.h.m. ± 0.1 s
K^+	0.1	0.1003	0.3	15.3
Na^+	0.1	0.1003	0.4	15.0
NH_4^+	0.1	0.1003	0.6	15.7
K^+	0.3	0.3003	0.4	16.3
Na^+	0.3	0.3003	0.4	16.5
NH_4^+	0.3	0.3003	0.3	16.3
Ba^{2+}	0.1	0.3003	0.4	17.9
Mg^{2+}	0.1	0.3003	0.6	17.4
Sr^{2+}	0.1	0.3003	0.4	17.7
Pb^{2+}	0.1	0.3003	0.5	17.6
Ca^{2+}	10^{-4}	0.0003	1.2	8.5
Ca^{2+}	0.1	0.3000	0.5	17.7

electrode at a flow rate of 1 ml min^{-1}. The current was measured during continuous pulsing at a pulse height of 5 V. The results are given in Table 5. Potentiometric rise times showed the same concentration-dependence as observed earlier [14], and fluoride concentrations below 10^{-3} M failed to produce a steady-state signal within 90 s after injection, at which time the injected solution began to leave the cell (the volume injected was 1.5 ml). These response times are longer than those obtained earlier [14] for an addition technique, probably because the concentration changeover was slower. The low flow rate and large post-injector volume (0.48 ml) permit relatively large dispersion in the flow method [21]. The f.w.h.m. values for potentiometric monitoring of the fluoride i.s.e. in the flow method also showed concentration-dependence at low fluoride concentrations, reaching a minimum value at 10^{-3} M.

The conductometric rise times showed concentration-dependence, unlike those obtained in static solution [14], and were always shorter than the potentiometric response times, in agreement with earlier results [14]. The f.w.h.m. values do not show concentration-dependence, but their precision is relatively poor. Continuous pulsing does not, in general, yield good precision for measurements with the fluoride electrode; thus it was necessary to use *i/V* curve extrapolation. The poor reproducibility is attributable to the slowly changing resistance of the gel layer on the surface of the i.s.e. [14].

Conclusion

Bipolar pulse conductometric monitoring of i.s.e.'s in a continuous flow system yields better precision than that obtained earlier with static solutions [12—14]. Detection limits and precision are comparable to those obtained by potentiometry under similar experimental conditions. However, the faster responses obtained conductometrically, as well as the lack of need of a real reference electrode, may make conductometric monitoring attractive in some applications.

TABLE 5

Potentiometric and conductometric response time data with the fluoride electrode for a flow rate of 1 ml min^{-1} (t_{95} is given for the rising edge)

Potentiometric measurements			Conductometric measurements		
F^- conc. (M)	t_{95} (±2s)	F.w.h.m. (±3s)	F^- conc. (M)	t_{95} (±2s)	F.w.h.m. (±10s)
10^{-6}	—[a]	—[a]	10^{-6}	18	110
10^{-5}	—[b]	163	10^{-5}	22	129
10^{-4}	—[b]	126	10^{-4}	—[a]	—[a]
10^{-3}	37	110	10^{-3}	17	136
10^{-2}	24	115	10^{-2}	12	118
10^{-1}	21	108	10^{-1}	5	105

[a]Peak too low to measure t_{95} or f.w.h.m. values. [b]Steady-state signal not achieved.

The response time of the calcium electrode depends on pulse height, flow rate, and ionic strength. The pulse-height and flow-rate dependencies are easily explained; the dependence of the rise times and f.w.h.m. values on ionic strength appears to touch on an area of i.s.e. transient response that has not been fully explored.

One of us (C. R. P.) gratefully acknowledges an American Chemical Society, Division of Analytical Chemistry Fellowship sponsored by FACSS. This research was supported in part by the National Science Foundation (CHE-81-08816).

REFERENCES

1 L. R. Snyder, Anal. Chim. Acta, 114 (1980) 3.
2 H. A. Mottola, Anal. Chem., 53 (1981) 1312A.
3 J. Růžička and E. H. Hansen, Anal. Chim. Acta, 78 (1975) 145.
4 J. Růžička and E. H. Hansen, Anal. Chim. Acta, 114 (1980) 19.
5 J. M. Reijn, W. E. van der Linden and H. Poppe, Anal. Chim. Acta, 114 (1980) 105.
6 K. Tóth, G. Nagy, Z. Feher, G. Horvai and E. Pungor, Anal. Chim. Acta, 114 (1980) 45.
7 E. Pungor, Z. Feher, G. Nagy, K. Tóth, G. Horvai and M. Gratzel, Anal. Chim. Acta, 109 (1979) 1.
8 J. R. Potts, Advances in Automated Analysis, Mediad, Inc., Tarrytown, NY, 1977.
9 P. W. Alexander and P. Seegopaul, Anal. Chem., 52 (1980) 2403.
10 J. Slanina, W. A. Lingerak and F. Bakker, Anal. Chim. Acta, 117 (1980) 91.
11 R. J. Simpson, in A. K. Covington (Ed.), Ion-Selective Electrode Methodology, Vol. I, CRC Press, Boca Raton, FL, 1979, Ch. 3.
12 C. R. Powley, R. F. Geiger and T. A. Nieman, Anal. Chem., 52 (1980) 705.
13 C. R. Powley and T. A. Nieman, Anal. Chim. Acta, 139 (1982) 61.
14 C. R. Powley and T. A. Nieman, Anal. Chim. Acta, 139 (1982) 83.
15 B. Fleet and G. A. Rechnitz, Anal. Chem., 42 (1970) 691.
16 E. H. Hansen, J. Růžička and A. K. Ghose, Anal. Chim. Acta, 100 (1978) 151.
17 D. S. Papastathopoulos, E. P. Diamandis and T. P. Hadjiioannou, Anal. Chem., 52 (1980) 2100.
18 E. J. Fogt, A. R. Eddy, A. H. Clemens, J. Fox and H. I. Heath, Clin. Chem., 26 (1980) 1425.
19 J. Mertens, P. Van den Winkel and D. L. Massart, Anal. Chem., 48 (1976) 272.
20 R. Rangarajan and G. A. Rechnitz, Anal. Chem., 47 (1975) 324.
21 J. Růžička and E. H. Hansen, Anal. Chim. Acta, 99 (1978) 37.
22 D. E. Johnson and C. G. Enke, Anal. Chem., 42 (1970) 329.
23 K. J. Caserta, F. J. Holler, S. R. Crouch and C. G. Enke, Anal. Chem., 50 (1978) 1534.
24 R. F. Geiger, Jr., Ph.D. Thesis, University of Illinois, 1983.
25 C. R. Powley, Ph.D. Thesis, University of Illinois, 1982.
26 Y. Umezawa, I. Tasaki and S. Fujiwara, Nippon Kagaku Kaishi, (1980) 1641.
27 A. U. Ramsing, J. Janata, J. Růžička and M. Levy, Anal. Chim. Acta, 118 (1980) 45.
28 R. W. Cattrall and K. T. Fong, Talanta, 25 (1978) 541.
29 E. H. Hansen, J. Růžička and A. K. Ghose, Anal. Chim. Acta, 100 (1978) 151.
30 J. H. Ladenson and G. N. Bowers, Clin. Chem., 19 (1973) 565.
31 J. Růžička, E. H. Hansen and J. C. Tjell, Anal. Chim. Acta, 67 (1973) 155.
32 G. Guilbault, Ion-Sel. Elect. Rev., 1 (1979) 139.
33 W. E. Morf, E. Lindner and W. Simon, Anal. Chem., 47 (1975) 1596.
34 E. Lindner, K. Tóth and E. Pungor, Anal. Chem., 54 (1982) 202.

35 A. J. Bard and L. R. Faulkner, Electrochemical Methods, Wiley, New York, 1980, Ch. 4.
36 G. J. Moody, R. B. Oke and J. D. R. Thomas, Analyst, 95 (1970) 910.
37 G. A. Rechnitz and Z. F. Lin, Anal. Chem., 40 (1968) 696.
38 B. Fleet, T. H. Ryan and M. J. D. Brand, Anal. Chem., 46 (1974) 12.
39 J. Bagg and R. Vinen, Anal. Chem., 44 (1972) 1773.
40 R. E. Reinsfelder and F. A. Schultz, Anal. Chim. Acta, 65 (1973) 425.
41 W. E. Morf, Anal. Lett., 10 (1977) 87.
42 R. P. Buck, in H. Freiser (Ed.), Ion Selective Electrodes in Analytical Chemistry, Vol. I, Plenum Press, New York, 1978, p. 124.

Analytica Chimica Acta, 152 (1983) 191—202
Elsevier Science Publishers B.V., Amsterdam — Printed in The Netherlands

A STUDY OF COPPER AND CADMIUM IMINODIACETATE COMPLEXES BY ION-SELECTIVE ELECTRODES AND APPLICATION TO CADMIUM MONITORING

R. STELLA* and M. T. GANZERLI VALENTINI

Dipartimento di Chimica Generale and Centro di Radiochimica ed Analisi per Attivazione del C.N.R., Università di Pavia, Viale Taramelli 12, 27100 Pavia (Italy)

(Received 6th March 1983)

SUMMARY

The chelating properties of the iminodiacetate ion (IDA^{2-}) towards copper(II) and cadmium(II) were investigated through pM and pH measurements at constant ionic strength of 0.1 M and at 25°C in the pH range 4—9. The acidity constants found were in good agreement with those already reported but significant differences from reported values were obtained for the stepwise copper complex formation constants, though the overall constant was in good agreement. Evidence is given for the existence of the protonated species CuH $(IDA)_2^-$, which proved helpful in explaining the anomalous complexing capacity of IDA in acidic medium. Practical applications include the use of IDA for lowering the level of copper interference in monitoring cadmium ion with a cadmium-selective solid-state electrode; this provides reliable measurements which are otherwise impossible.

The reported stability constants of complexes of the iminodiacetate ion (IDA^{2-}) with copper(II) and cadmium(II) ions [1—5] are sufficiently different to suggest the possibility that this ligand may be employed as a selective masking agent for copper in the presence of cadmium. Yet measurements conducted on both the Cu—IDA and Cd—IDA systems with ion-selective electrodes (i.s.e.) showed discrepancies from the values calculated from the available constants. For instance, in the acidic region the extent of copper complexation was greater than the calculated value, thus suggesting the presence of a protonated complex. Therefore it seemed worthwhile to investigate these systems by coupling i.s.e.'s to pH measurements; this technique allows a more detailed insight into metal complex equilibria than is possible by previous methods.

A preliminary investigation was also made on iminodiacetic acid dissociation constants and the values obtained were compared with those already reported [1, 2, 6, 7].

0003-2670/83/$03.00

EXPERIMENTAL

Reagents

Sodium iminodiacetate (Fluka) was purified by double recrystallization from methanol and dried at 115°C. The corresponding acid was prepared by passing a 0.1 M disodium salt solution through two columns in series (2 cm i.d., 20 cm high) filled with Dowex 50W-X4 resin converted to the acid form with 0.1 M perchloric acid, and repeatedly washing with deionized and twice-distilled water. Only the central fractions of the eluate were collected and the absence of sodium was checked by atomic emission spectrometry; it is very important to discard all head and tail fractions, as they may contain undesirable ligands. The acid was then diluted and potentiometrically titrated with standard sodium hydroxide or standard copper solution at pH 7 using the corresponding i.s.e. The carbonate-free 0.1 M sodium hydroxide was prepared from a 50% (w/w) solution and standardized against potassium hydrogenphthalate.

A 0.1 M perchloric acid solution was prepared from the 70% acid (Merck, Suprapur) and standardized against sodium carbonate.

A 10^{-2} M copper stock solution was prepared by dissolving a suitable amount of copper(II) perchlorate hexahydrate (ultrapure, Alfa Products) and standardized by titration with EDTA; end-points were detected visually and potentiometrically, with murexide as indicator for the former.

A 10^{-2} M cadmium stock solution was prepared by dissolving a weighed amount of cadmium wire (ultrapure, Alfa Products) in diluted nitric acid (Suprapur, Merck) in a teflon beaker. The excess of nitric acid was evaporated on a hot plate and the residue was taken up with water. The resulting solution was standardized by titration with EDTA; both potentiometric and visual (Calcon indicator) end-points were obtained in ammoniacal medium.

The water used in all experiments was deionized and then twice-distilled in a quartz apparatus.

Instrumentation

A digital millivoltmeter (Orion model 701) was used in all measurements. A combined glass electrode (model 91) was used for pH measurements. The glass electrode was calibrated as suggested by Rajan and Martell [2] by direct titration of acetic acid; the observed readings were compared with the actual hydrogen ion concentrations tabulated by Harned and Owen [8]. In the pH region below 3.5, the meter was calibrated by measurements of solutions with known concentrations of perchloric acid. The concentration of the hydroxide ion was obtained by using a $p(K_w)_c$ value of 13.79 at 25°C in 0.1 M potassium nitrate.

The copper ion-selective electrode (Orion model 94-29A) was used with a single-junction Orion 90-01 reference electrode. The electrode was carefully calibrated at ionic strength 0.1 M with Cu—EDTA buffered solutions as described in a previous paper [9]; a tenfold change in the copper concentration yielded an electrode response change of 29.0 ± 0.5 mV, as expected.

The cadmium ion-selective electrode (Orion 94-48A) was used similarly and calibrated following the analogous procedure for copper: the mV response plotted in a semilog scale versus the free ion concentration was found to be linear down to 10^{-10} M in metal buffer solutions as in the procedure suggested by Růžička and Hansen [10].

Procedure

All experiments were done at 25°C in a constant temperature bath, the ionic strength (I) being adjusted to 0.1 M with potassium nitrate (Suprapur, Merck).

The iminodiacetic acid and its disodium salt were titrated under a nitrogen atmosphere, by first bubbling a nitrogen stream for 30 min and then maintaining the stream in the cell over the solution.

Solutions having the following concentrations were used: $C_A = 4.50 \times 10^{-2}$ M for the acid and $C_B = 8.44 \times 10^{-2}$ M or 9.20×10^{-3} M for the disodium salt. The copper—IDA and the cadmium—IDA systems were separately investigated by simultaneously measuring the free metal ion concentration and the pH in two different sets of experiments. First, titrations of unbuffered IDA (disodium salt) solutions were done with standard copper or cadmium solutions, with $C_{Cu} = 5.82 \times 10^{-2}$ M, $C_{Cd} = 4.38 \times 10^{-2}$ M and $C_B = 4.22 \times 10^{-3}$ M or 9.20×10^{-3} M. Next, solutions of ligand and metal ion in 1:1 and 2:1 molar ratios were titrated with standard 0.1 M sodium hydroxide; here $C_A = 2.11 \times 10^{-4}$ M, 4.22×10^{-3} M and 1.00×10^{-3} M for the copper system, and $C_A = 3.88 \times 10^{-3}$ M, 7.39×10^{-3} M and 3.68×10^{-2} M for the cadmium system. The results in both cases are presented in graphic form with pH and pCu or pCd plotted as a function of the titrant added.

RESULTS AND DISCUSSION

Evaluation of acidity constants

Considering the iminodiacetic acid as a diprotic acid, Chabereck and Martell [1] found $pK_{a1} = 2.54$ and $pK_{a2} = 9.12$ ($I = 0.1$, $T = 30°C$); Rajan and Martell [2] reported $pK_{a1} = 2.50$ and $pK_{a2} = 9.40$ ($I = 0.1$, $T = 25°C$) and Thompson [7] found $pK_{a1} = 2.58$ and $pK_{a2} = 9.33$ ($I = 0.1$, $T = 25°C$). All these values agree well, even with those that may be derived from the results of Liberti and Napoli [6]: $\log \beta_{1,2} = 9.17$ and $\log \beta_{2,2} = 11.73$ ($I = 0.5$, $T = 25°C$). Liberti and Napoli also gave a third formation constant related to a H_3IDA^+ form, which begins to play a significant rôle at pH < 2.5. In this paper, the evaluation of the first two constants was considered sufficient to allow an accurate description of the investigated system.

The acidity constants were calculated by using the well known Bjerrum method which is based on calculation of the complex formation function $\bar{n}$, the average number of moles of hydrogen bound per mole of acid:

$$\bar{n} = ([HIDA^-] + 2\,[H_2IDA])/C_A = (2C_A - aC_A - [H^+] + [OH^-])/C_A$$

where C_A is the analytical acid concentration and a is the number of moles of base added per mole of acid. The plot of $\bar{n}$ as a function of pH is shown in Fig. 1. The pH values for which $\bar{n}$ = 0.5 and 1.5 are taken as equivalent to pK_{a1} and pK_{a2}, respectively. The two acidity constants of iminodiacetic acid, calculated as half integral values were refined by using Bjerrum's convergence method [11]. The results were pK_{a1} = 2.43 ± 0.08 and pK_{a2} = 9.31 ± 0.10, in good agreement with the previously reported values.

Stability constants for the copper—IDA system

In order to evaluate the stability constants of the Cu—IDA system, for which the formation of two mononuclear complexes is reported, it is necessary to find a relationship between the constants and the experimentally determined or calculated variables [M] and [L] (Figs. 2 and 3). The Bjerrum approach, which makes use of the secondary concentration variable $\bar{n}$, the average number of moles of ligand bound per mole of metal, cannot be employed as it does not yield values lower than 0.6 or higher than 1. The relationship may be established by using the secondary concentration variable $\Phi = [M_T]/[M]$, which is called the degree of complex formation [11]. The function Φ finds application in the Leden method which, notwithstanding a number of limitations, is suitable for calculations from potentiometric data. Leden defined a function f(L):

$$f(L) = (\Phi - 1)/[L] = ([M_T] - [M])/[M][L]$$

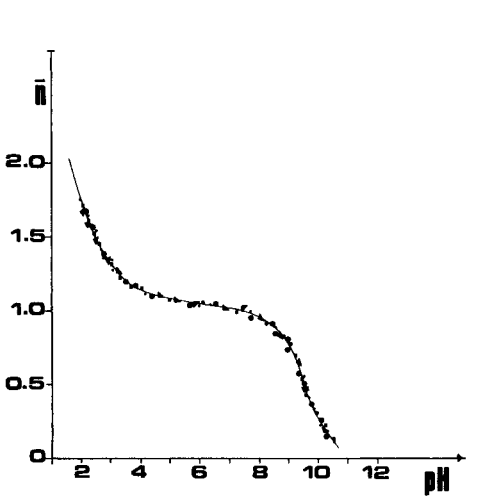

Fig. 1. Formation function $\bar{n}$ of iminodiacetic acid.

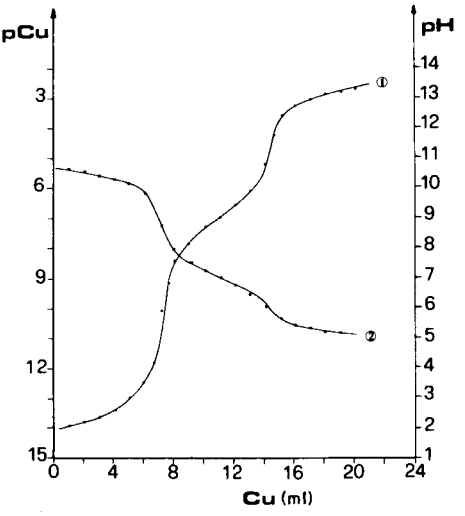

Fig. 2. Titration curves of unbuffered disodium iminoacetate with copper. C_B = 4.22 × 10^{-3} M (100 ml) and C_{Cu} = 5.82 × 10^{-2} M. Curves: (1) pCu; (2) pH. In this and other figures, subscripts A and B are used to indicate IDA in the acid (A) or disodium salt (B) forms when distinction is necessary; otherwise the subscript IDA is used.

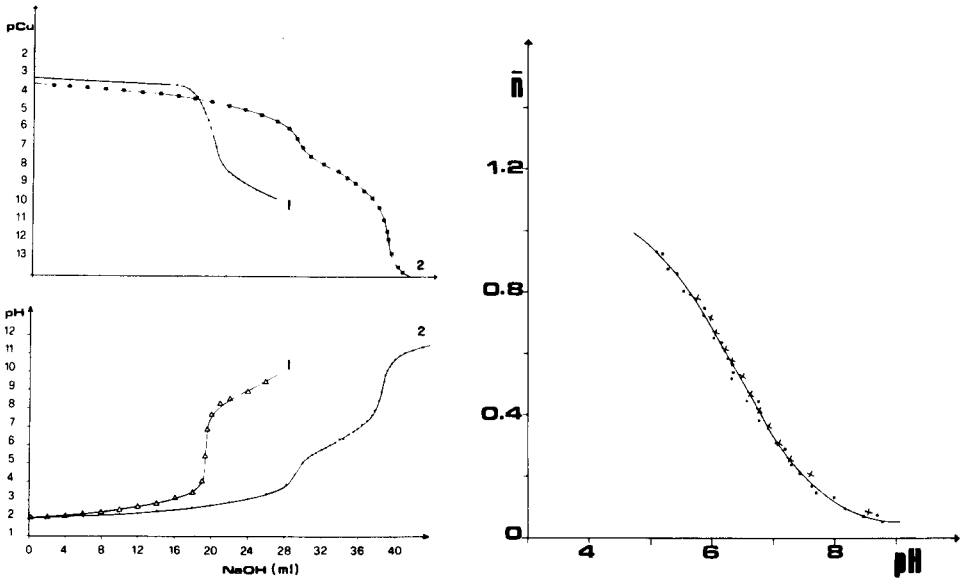

Fig. 3. Titration curves of iminodiacetic acid and copper mixtures with NaOH. C_{NaOH} = 1.03×10^{-2} M; C_{Cu} = 1.00×10^{-3} M (100 ml). Curves: (1) $C_A/C_{Cu} = 1$; (2) $C_A/C_{Cu} = 2$.

Fig. 4. Formation function $\bar{n}$ of the protonated complex $CuH(IDA)_2^-$ considered as a monoprotic acid: (•) direct titration; (×) back-titration.

which, if the number of complexes formed, N, is 2, becomes $f(L) = \beta_1 + \beta_2 [L]$ and if f(L) is plotted versus [L], a straight line is obtained having slope β_2 and an intercept β_1 on the f(L) axis.

The Leden method was applied to the data obtained from both types of titration; a cyclic procedure was adopted to refine the [L] values. Least-square straight line plots were obtained, and the following values were derived for the copper complexes: $\log \beta_1 = 9.32 \pm 0.05$ and $\log \beta_2 = 16.33 \pm 0.12$. The absence of polynuclear species, which are highly improbable, was demonstrated by the fact that β_1 and β_2, calculated from experiments at different concentrations, did not vary within experimental error. Calculations by the Leden method failed to yield straight lines when applied to data obtained at pH lower than 7; this indicates that in acidic media another complex species may be formed. The existence of another copper complex in the acidic region is supported by the difference between the titration with sodium hydroxide of the mixtures with $C_A/C_{Cu} = 2$ and $C_A/C_{Cu} = 1$ (Fig. 3). The latter merely corresponds, as already noted by Chabereck and Martell [1], to the reaction

$$Cu^{2+} + H_2IDA + 2\,OH^- \rightarrow CuIDA + 2\,H_2O$$

In the titration of the mixture containing $C_A/C_{Cu} = 2$, the first equivalence point is obtained when 3/4 of the total acid equivalents are neutralized and

the remaining 1/4 is then neutralized, as shown by the appearance of a second equivalence point. This pattern suggests the existence of a protonated species $CuH(IDA)_2^-$, which does not seem to have been considered by other authors. This species is probably formed during the first titration step in accordance with the reaction

$$Cu^{2+} + 2\ H_2IDA + 3\ OH^- \rightarrow CuH(IDA)_2^- + 3\ H_2O$$

The second acid titration step in Fig. 3 corresponds therefore to

$$CuH(IDA)_2^- + OH^- \rightarrow Cu(IDA)_2^{2-} + H_2O$$

In the pH region 4—9, the Bjerrum method was then applied and the curve reported in Fig. 4 was obtained. The reverse titration was also run by adding standard perchloric acid to a preformed $Cu(IDA)_2^{2-}$ complex solution (C_B = 9.20 × 10^{-3} M and C_{Cu} = 4.60 × 10^{-3} M) and the Bjerrum method was applied; the points thus obtained are also reported in Fig. 4. For $\bar{n}$ = 0.5, the value pK_a = 6.53 ± 0.10 was found.

An interesting trend is shown by the curves reported in Fig. 5, which refer to measurements at constant total ligand concentration and different total copper concentrations: their spacing indicates a well defined dependence, at constant pH in the acidic region, of pCu on the square of C_{Cu} and their slopes are close to +1 for all C_{Cu} values. Further, [Cu(IDA)] and $[CuH(IDA)_2^-]$

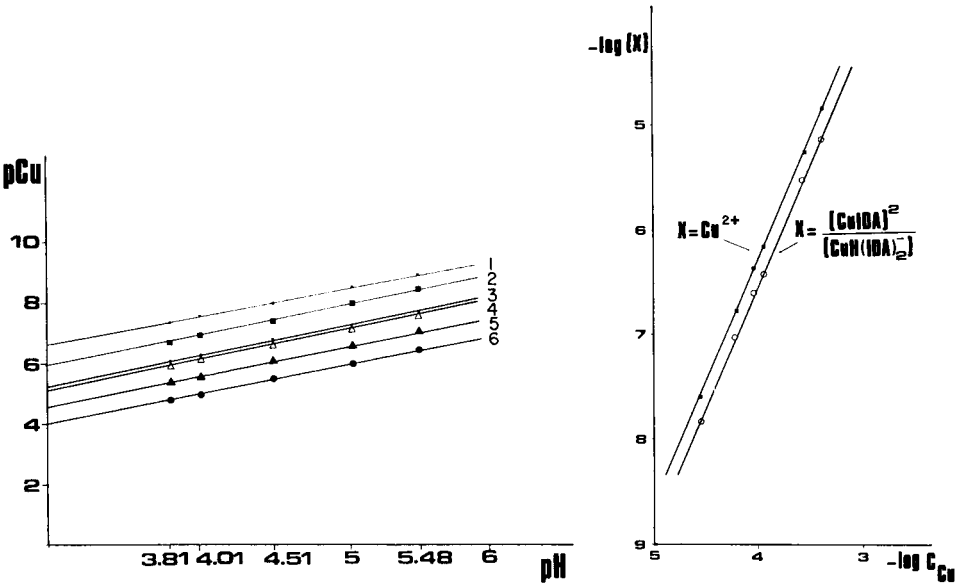

Fig. 5. pCu vs. pH at constant C_A = 1.20 × 10^{-3} M. C_{Cu} (M): (1) 2.76 × 10^{-5}; (2) 5.62 × 10^{-5}; (3) 8.28 × 10^{-5}; (4) 1.12 × 10^{-4}; (5) 2.76 × 10^{-4}; (6) 5.62 × 10^{-4}.

Fig. 6. Calculated log ($[Cu(IDA)]^2/[CuH(IDA)_2^-]$) vs. log C_{Cu} and pCu vs. log C_{Cu} from experimental data. pH 4.01, C_A = 1.20 × 10^{-3} M.

were calculated at constant pH, through the known constants; together with experimentally measured pCu values, these concentrations were used to plot the curves reported in Fig. 6. The trend can only be explained through the existence of the equilibrium

$$Cu^{2+} + CuH(IDA)_2^- \rightleftharpoons 2\,Cu(IDA) + H^+$$

which explains the parallel lines and the slopes of 2.

The distribution of the species formed in the Cu—IDA system were calculated at different pH values; the pattern obtained is reported in Fig. 7.

Stability constants for the cadmium—IDA system

Two stepwise chelate formation constants have been reported in the literature for the Cd—IDA system [1, 5]. The Leden method was again employed to calculate β_1 and β_2 for cadmium complexes. Examples of the results of both kinds of titration are reported in Figs. 8 and 9. The curves of Fig. 9 show that half equivalents of the acid are neutralized before any cadmium chelate is formed.

Only two stepwise complex formation reactions are assumed and this appears to be valid even at pH < 7: all calculated f(L) values, even in the acidic region, fitted a straight line, from which the values $\log \beta_1 = 5.48 \pm 0.04$ and $\log \beta_2 = 9.72 \pm 0.10$ were evaluated for the cadmium complexes. No evidence was found that a species corresponding to $CdH(IDA)_2^-$ is formed.

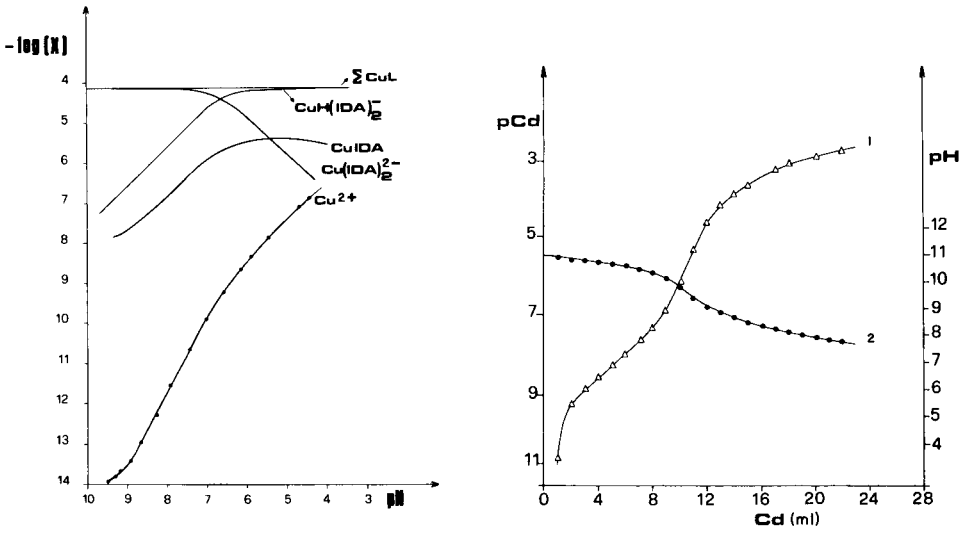

Fig. 7. Cu—IDA complex distribution as a function of pH. $C_B = 1.20 \times 10^{-3}$ M; $C_{Cu} = 7.40 \times 10^{-5}$ M.

Fig. 8. Titration curves of unbuffered disodium iminodiacetate with cadmium. $C_B = 9.20 \times 10^{-3}$ M (100 ml) and $C_{Cd} = 4.38 \times 10^{-2}$ M. Curves: (1) pCd; (2) pH.

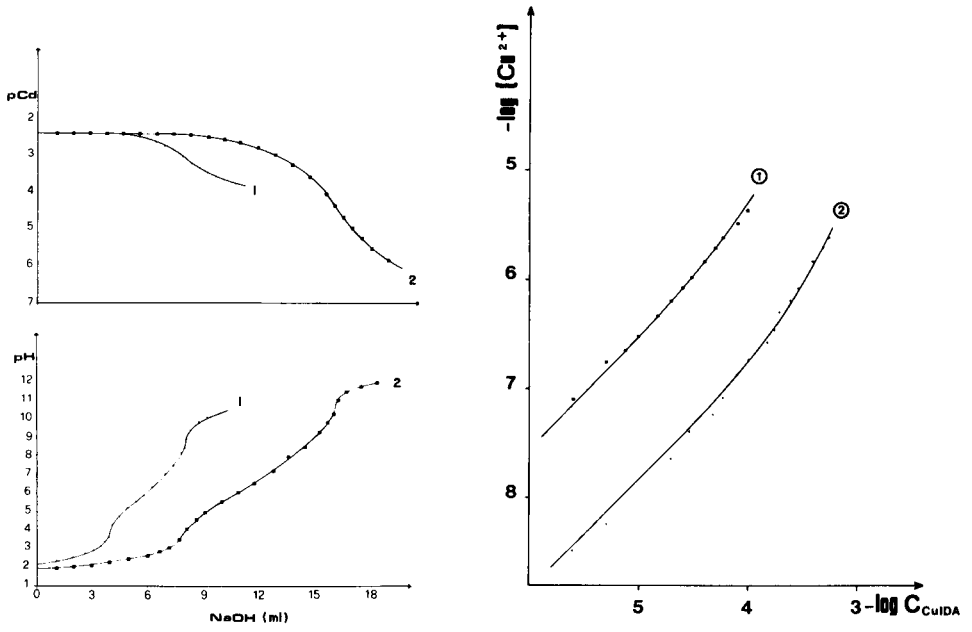

Fig. 9. Titration curves of iminodiacetic acid and cadmium mixtures with NaOH. C_{NaOH} = 9.58 × 10^{-2} M; C_{Cd} = 3.88 × 10^{-3} M (100 ml). Curves: (1) C_A/C_{Cd} = 1; (2) C_A/C_{Cd} = 2.

Fig. 10. Equilibrium Cu^{2+} concentrations in the Cu—IDA system (1) C_{IDA} = 2.53 × 10^{-4} M; (2) C_{IDA} = 1.22 × 10^{-3} M. The solid lines show the calculated values.

APPLICATIONS

It is well known that even low levels of copper cannot be tolerated in any sample for measurement of free cadmium ion with the cadmium-selective electrode. Unfortunately, this interference is commonly encountered and seriously limits the usefulness of the electrode. The present study on copper and cadmium complexes with IDA suggests that the ligand may be successfully exploited to reduce copper interferences in cadmium measurements, most effectively in acidic medium.

In order to check the reliability of the constants found for the Cu—IDA system (Table 1), the copper-selective electrode was calibrated with Cu—EDTA metal buffers and measurements were then made at pH 4.5 on Cu—IDA metal buffers. These Cu—IDA buffers were obtained by adding the preformed CuIDA complex at pH 4.5, to an excess of ligand buffered at the same pH with acetic acid/sodium acetate. Experimental points are compared in Fig. 10 with the values calculated through a multistep computer procedure (solid lines). No set of constants taken from the literature was found to give a better fit.

The effect of free copper ions on the response of the cadmium-selective electrode is evident from the measurements reported in Fig. 11: [Cu^{2+}]

TABLE 1

Acid and chelate equilibrium constants (I = 0.1; T = 25°C)

Cation	Reaction	Logarithmic constant found	Literature values
H^+	$H^+ + IDA^{2-} \rightleftharpoons HIDA^-$	9.31 ± 0.10	9.12 [1]; 9.40 [2]; 9.17 [6]; 9.33 [7]
	$H^+ + HIDA^- \rightleftharpoons H_2IDA$	2.43 ± 0.08	2.54 [1]; 2.50 [2]; 2.58 [7]
	$2\,H^+ + IDA^{2-} \rightleftharpoons H_2IDA$	—	11.73 [6]
	$H^+ + Cu(IDA)_2^{2-} \rightleftharpoons CuH(IDA)_2^-$	6.53 ± 0.10	—
Cu^{2+}	$Cu^{2+} + IDA^{2-} \rightleftharpoons Cu(IDA)$	9.32 ± 0.05	10.55 [1]; 10.63 [3]; 10.42 [4]
	$Cu(IDA) + IDA^{2-} \rightleftharpoons Cu(IDA)_2^{2-}$	—	5.65 [1]; 6.05 [5]; 5.60 [4]
	$Cu^{2+} + 2IDA^{2-} \rightleftharpoons Cu(IDA)_2^{2-}$	16.33 ± 0.12	—
Cd^{2+}	$Cd^{2+} + IDA^{2-} \rightleftharpoons Cd(IDA)$	5.48 ± 0.04	5.35 [1]; 5.54 [5]
	$Cd(IDA) + IDA^{2-} \rightleftharpoons Cd(IDA)_2^{2-}$	—	4.18 [1]; 4.74 [5]
	$Cd^{2+} + 2IDA^{2-} \rightleftharpoons Cd(IDA)_2^{2-}$	9.72 ± 0.10	—

and $[Cd^{2+}]$ were measured with the appropriate i.s.e. after copper had been added to cadmium/IDA mixtures at pH 4.5. In no way can the data trend shown in Fig. 11 be ascribed to any secondary ion effect, which is usually described through the selectivity coefficient in the modified Nikolski equation [12]. An exhaustive investigation of this problem was outside the scope of this work, and interest was restricted to practical applications.

The important considerations are as follows. First, free copper ion, buffered by an excess of IDA, can be tolerated up to a concentration of 4×10^{-7} M (Fig.

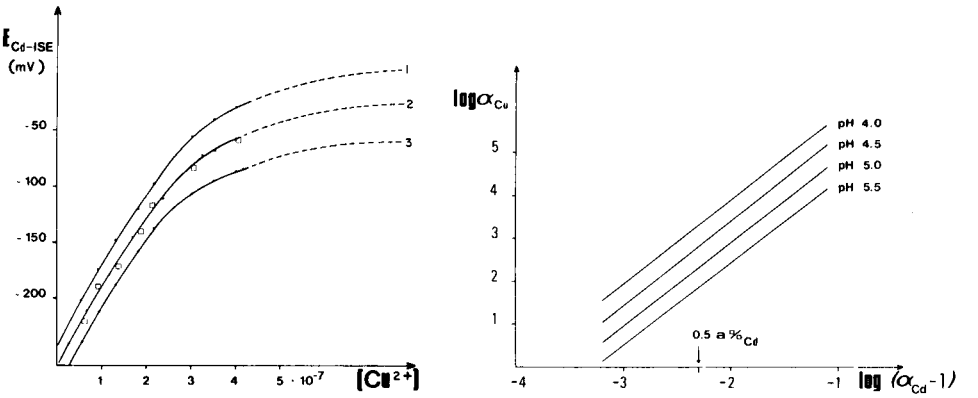

Fig. 11. Response of the cadmium i.s.e. as a function of free copper ion concentration for: (1) $C_{Cd} = 6.85 \times 10^{-5}$ M, $C_{IDA} = 2.50 \times 10^{-4}$ M; (2) $C_{Cd} = 1.37 \times 10^{-5}$ M, $C_{IDA} = 2.50 \times 10^{-4}$ M, and $C_{Cd} = 1.37 \times 10^{-5}$ M, $C_{IDA} = 1.22 \times 10^{-3}$ M; (3) $C_{Cd} = 2.74 \times 10^{-6}$ M, $C_{IDA} = 2.50 \times 10^{-4}$ M. Free $[Cu^{2+}]$ measured with copper i.s.e.

Fig. 12. Corresponding α_{Cd} and α_{Cu} values at selected pHs.

11); the cadmium-selective electrode gives a response proportional to cadmium concentration and equilibrium is attained within reasonable times (≈10 min). Secondly, when the free copper ion concentration exceeds 4×10^{-7} M, equilibration of the electrode response takes such a long time that it becomes analytically useless, and the responses are not obviously correlated to any analytical parameter.

In order to assess the limiting conditions for applicability of the cadmium-selective electrode, the ratios of total metal-to-free ion concentrations, α_{Cu} and α_{Cd}, were calculated; the values are represented logarithmically in Fig. 12. If it is assumed that, under the conditions adopted, copper is complexed predominantly as CuIDA and $CuH(IDA)_2^-$ whereas cadmium is complexed only as CdIDA, then

$$\alpha_{Cu} = ([Cu^{2+}] + [CuIDA] + [CuH(IDA)_2^-])/[Cu^{2+}] = 1 + \beta_{1Cu}[IDA^{2-}] + K_a\beta_{2Cu}[IDA^{2-}]^2[H^+] \quad (1)$$

$$\alpha_{Cd} = ([Cd^{2+}] + [CdIDA])/[Cd^{2+}] = 1 + \beta_{1Cd}[IDA^{2-}] \quad (2)$$

The theoretical error on cadmium measurements can be related to the percentage of complexed cadmium, $a\%$, which is a function of α_{Cd} through the following relationship: $(\alpha_{Cd} - 1) = a\%/(100 - a\%)$. Figure 12 can be used to identify the maximum value of α_{Cu} attainable by IDA addition without affecting the cadmium measurement by a factor higher than $a\%$. The value of α_{Cu} can be related directly to the potential decrease, ΔE, measured with a copper-selective electrode after addition of IDA, to reach the correct conditions for cadmium measurement. The value of ΔE is related to α_{Cu} by the relationship $\Delta E = S \log \alpha_{Cu}$, where S indicates the slope of the electrode response.

This procedure markedly simplifies the problem of adding the correct amount of ligand, which would be difficult to calculate. However, the limiting condition that the free copper be not higher than 4×10^{-7} M implies also that an upper limit for total copper, $C_{Cu}(max)$, be assessed. For a cadmium $a\%$ value of 0.5, $C_{Cu}(max)$ values were derived from α_{Cu} at different pH values (Table 2). Although the cadmium-selective electrode can be used over a wide pH range, hydrogen ions interfere with measurements of low concentrations of cadmium ion, thus pH levels lower than 4 were not considered.

A standard addition procedure was devised for the determination of cadmium in the presence of copper and tested on artificial samples. The linearized Gran plots reported in Fig. 13 refer to samples of $C_{Cd} = 1.37 \times 10^{-5}$ and 1.37×10^{-6} M: the lower concentration may be taken as the limit of determination for the cadmium-selective electrode, at least in the linear response region. The amount of copper added never exceeded the permissible upper limit. Results and related parameters are shown in Table 3.

Samples must be prepared suitably before standard additions and potential measurements can be made with the cadmium-selective electrode. This was

TABLE 2

Maximum allowed copper concentrations in cadmium samples at selected pH for a fixed percentage of complexed cadmium (α%) of 0.5

pH	α_{Cu}	C_{Cu}(max) (mol l^{-1})
4.0	2000	8.00×10^{-4}
4.5	635	2.54×10^{-4}
5.0	210	8.40×10^{-5}
5.5	64.4	2.58×10^{-5}

TABLE 3

Determination of cadmium ion by the standard addition procedure with sample concentrations and main related parameters

Initial conc. ($\times 10^{-5}$ M)		IDA added ($\times 10^{-4}$ M)	Residual [Cu^{2+}]	log α_{Cu}	log ($\alpha_{Cd} - 1$)	α%
Cd^{2+}	Cu^{2+}					
1.37	2.00	4.22	2.57×10^{-7}	1.89	−2.76	0.17
1.37	0.100	0.84	1.60×10^{-7}	0.79	−3.32	0.05
1.37	2.00	8.44	6.45×10^{-8}	2.49	−2.46	0.35
0.137	2.00	4.22	2.63×10^{-7}	1.88	−2.77	0.17
0.137	0.214	1.67	1.25×10^{-7}	1.23	−3.10	0.08
0.137	20.0	50.0	2.27×10^{-8}	3.94	−1.72	1.87

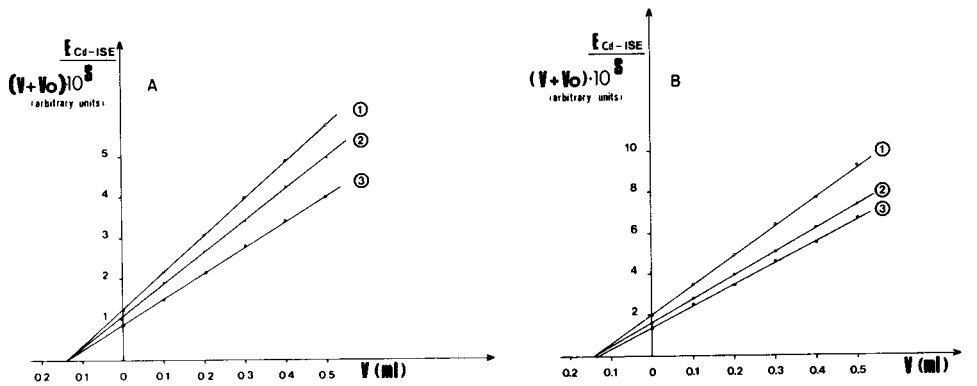

Fig. 13. Gran plots in the standard addition procedure applied to: (A) $C_{Cd} = 1.37 \times 10^{-5}$ M and (B) $C_{Cd} = 1.37 \times 10^{-6}$ M in the presence of different amounts of copper ion and IDA. (A) With additions of 1.00×10^{-2} M cadmium solution: (1) $C_{Cu} = 2.00 \times 10^{-5}$ M, $C_{IDA} = 4.22 \times 10^{-4}$ M; (2) $C_{Cu} = 1.00 \times 10^{-6}$ M, $C_{IDA} = 8.44 \times 10^{-5}$ M; (3) $C_{Cu} = 2.00 \times 10^{-5}$ M, $C_{IDA} = 8.44 \times 10^{-4}$ M. (B) With additions of 1.00×10^{-3} M cadmium solution: (1) $C_{Cu} = 2.00 \times 10^{-5}$ M, $C_{IDA} = 4.22 \times 10^{-4}$ M; (2) $C_{Cu} = 2.14 \times 10^{-6}$ M, $C_{IDA} = 1.67 \times 10^{-4}$ M; (3) $C_{Cu} = 2.00 \times 10^{-4}$ M, $C_{IDA} = 5.00 \times 10^{-3}$ M. $V_0 = 100$ ml.

done by adding the ligand and recording the corresponding potential drop at the copper-selective electrode; the addition was stopped when the reading corresponded to a free ion concentration $[Cu^{2+}] < 4 \times 10^{-7}$ M. The electrode commutator was then switched to the cadmium-selective electrode and standard additions of cadmium ion were made. As shown in Fig. 13, the slopes of the Gran plots vary depending on the residual copper ion activity of the samples but, although the abscissa units may differ, the relative positions of the lines are maintained. The last column of Table 3 shows the $a\%$ values derived from α_{Cu}; they indicate that the percentage of complexed cadmium is very low in all cases, reaching a maximum of 1.87% in the last sample, which was measured with the largest actual experimental error (±12%).

This work was supported by the Consiglio Nazionale delle Richerche as part of the Special Research Project "Environmental Quality Promotion"; the CNR also gave permission for publication. The authors are grateful to S. Meloni for valuable discussions concerning this work.

REFERENCES

1 S. Chabereck, Jr. and A. E. Martell, J. Am. Chem. Soc., 74 (1952) 5052.
2 K. S. Rajan and A. E. Martell, J. Inorg. Nucl. Chem., 26 (1964) 789.
3 G. Anderegg, Helv. Chim. Acta, 47 (1964) 1801.
4 R. P. Bonomo, R. Calì, F. Riggi, E. Rizzarelli, S. Sammartano and G. Siragusa, Inorg. Chem., 18 (1980) 3417.
5 T. Ait-Hamouda and M. J. Schwing-Weill, Analusis, 9 (1981) 93.
6 A. Liberti and A. Napoli, J. Inorg. Nucl. Chem., 33 (1971) 89.
7 L. C. Thompson, Inorg. Chem., 1 (1962) 490.
8 H. S. Harned and B. B. Owen, The Physical Chemistry of Electrolyte Solutions, Reinhold, New York, 1958.
9 R. Stella and M. T. Ganzerli Valentini, Anal. Chem., 51 (1979) 2148.
10 J. Růžička and E. H. Hansen, Anal. Chim. Acta, 63 (1973) 115.
11 See, e.g., F. R. Hartley, C. Burgess and R. M. Alcock, Solution Equilibria, Horwood, Chichester, 1980.
12 G. Eisenman, in R. A. Durst (Ed.), Ion-Selective Electrodes, NBS Spec. Publ. No. 314, Washington, DC, 1969.

Analytica Chimica Acta, 152 (1983) 203–214
Elsevier Science Publishers, B.V., Amsterdam — Printed in The Netherlands

THE INFLUENCE OF VARIOUS METALS ON THE ANODIC OXIDATION OF TRACES OF MERCURY FROM CARBON ELECTRODES IN THIOCYANATE MEDIA

RENATA BILEWICZ and ZENON KUBLIK*
Department of Chemistry, University of Warsaw, 02093 Warsaw, Pasteura 1 (Poland)
(Received 23rd December 1982)

SUMMARY

The influence of traces of Cu(II), Pb(II), Sn(II), Cd(II), Ag(I), Fe(II), Ni(II), Te(IV) and Au(III) on the stripping process of mercury from graphite electrodes was investigated in thiocyanate media. The addition of Pb(II), Cd(II) or Cu(II) usually improves the detection limit for mercury, though copper(II) at certain concentrations has harmful effects. Iron(II) and nickel(II) can cause severe distortion of the mercury stripping peaks if the deposition potential or pH are not selected correctly. The stripping peaks of silver and mercury overlap at low thiocyanate concentration but are quite well separated at high thiocyanate concentrations. In the presence of gold(III) or tellurium(IV), the formation of intermetallic compounds may cause severe distortions of the mercury stripping peak. The nature of the multiple peaks sometimes observed during anodic oxidation of mercury is explained.

Many unexplained phenomena are described in the literature on the anodic oxidation of traces of mercury from graphite electrodes. In some earlier work [1], it was shown that the anodic oxidation was affected by the precipitation of sparingly soluble mercury(I) salts on the electrode surface, but these salts cannot explain the curious phenomena observed in thiocyanate medium, where during dissolution of mercury some authors obtained two [2–5] or even three [2, 3] stripping peaks. From the analytical point of view, the appearance of multiple peaks is harmful. It seemed possible that these multiple peaks could be caused, at least partially, by contaminants present at trace levels in the supporting electrolyte. The aim of the present work was, therefore, to investigate the influence of various substances deposited simultaneously with mercury on the mercury stripping peak.

EXPERIMENTAL

The voltammetric curves were recorded with a Radelkis OH-105 polarograph with a three-electrode arrangement. All potentials are reported relative to the saturated calomel reference electrode used. The counter electrode was a 2-cm^2 platinum foil. The indicator electrode was a paraffin wax-impregnated

0003-2670/83/$03.00

graphite electrode [6] with surface area 3.14 mm^2, or a glassy carbon electrode with surface area 6.15 mm^2. In several tests, a HMDE [7] was used. The gold-plated graphite electrode was prepared by deposition of several monolayers of gold on the graphite electrode from a stirred solution 1 mol dm^{-3} in hydrochloric acid and 3×10^{-3} mol dm^{-3} in gold(III).

All solutions were prepared from reagent-grade chemicals and water purified as described earlier [8]. In some cases, the thiocyanate supporting electrolyte was purified at a large mercury cathode (surface area 20 cm^2) held at −1.0 V by means of a potentiostat (Radelkis OH-404/H). Solutions were deoxygenated with argon prior to measurements. All experiments were done at 25°C.

RESULTS

Preliminary experiments

Figure 1 illustrates the complexity of the processes connected with the occurrence of the multiple peaks. The blank test obtained after a lengthy preconcentration of impurities on the electrode surface (curve 1) shows no peak; such behaviour is usually interpreted as evidence of the high purity of the supporting electrolyte. However, curve 2, obtained after addition of a little mercury(II) to the same solution, has three peaks instead of the expected single peak. These peaks are designated a, b and c in Fig. 1. Peaks b and c were observed by Perone and Kretlov [2] and by Pniev et al. [3], who assumed that they correspond to oxidation of mercury. Both prolongation of the pre-electrolysis time as well as an increase of mercury(II) concentration led to a significant increase of peak b. The heights of peaks a and c increased more slowly under these conditions and at high mercury(II) concentrations they became insignificant compared with peak b. In solutions with lower thiocyanate concentration, all these peaks decreased but simultaneously peak c became better developed and peak b split.

It seems unlikely that peak a corresponds to the oxidation of mercury, though it appeared only after the addition of mercury(II) to the solution. More probably it corresponds to the oxidation of another substance, deposition of which is activated by the simultaneous deposition of mercury. Cyclic voltammetric experiments with higher concentrations of various substances showed that in the potential range around peak a, peaks of lead and copper appeared. In the potential range around peak c, Te and HgTe were oxidized. Anodic stripping at the HMDE showed that the supporting electrolyte used (0.1 mol dm^{-3} NaSCN) contained traces of Cu(II) and Pb(II), but their exact determination was difficult under these conditions because the peaks overlapped. The total concentration of Cu(II) and Pb(II) in the 0.1 mol dm^{-3} NaSCN solution was estimated as 4×10^{-8} mol dm^{-3}.

Strong evidence that peaks a and c on curves 2 and 3 (Fig. 1) do not correspond to oxidation of mercury but to codeposition of other metals

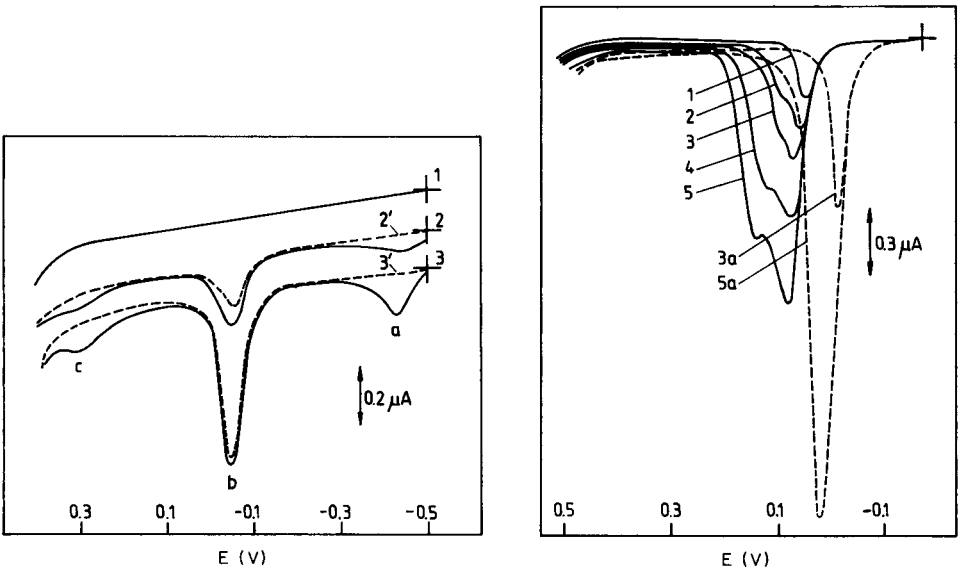

Fig. 1. Anodic stripping curves obtained for Hg(II) in 0.1 mol dm^{-3} sodium thiocyanate at pH 2 after a 20-min deposition at —0.9 V. Concentration of Hg(II): (1) 0; (2,2') 2 × 10^{-7}; (3,3') 6 × 10^{-7} mol dm^{-3}. (- - -) Purified, (——) unpurified supporting electrolyte.

Fig. 2. The influence of thiocyanate ion concentration and deposition time on the anodic stripping curves of mercury. Thiocyanate concentration: (——) 0.02; (- - -) 0.1 mol dm^{-3}. Concentration of Hg(II): 1 × 10^{-6} mol dm^{-3}. Deposition potential —0.9 V. Deposition time: (1) 1; (2) 2; (3,3a) 3; (4) 6; (5,5a) 9 min.

with mercury is shown on curves 2' and 3', which were obtained in purified supporting electrolyte. The addition of a little Hg(II) to the purified thiocyanate solution gave peak b only. Under such conditions, the detection limit for Hg(II), after 30 min deposition, was 4 × 10^{-8} mol dm^{-3} at the impregnated graphite and the glassy carbon electrode.

A decrease in the thiocyanate ion concentration usually affected peak b, as shown in Fig. 2; the peaks obtained at the lower thiocyanate ion concentration were smaller, broader and often split. These effects were better seen on curves obtained for higher Hg(II) concentrations and for longer deposition times. Peak splitting of the type shown in Fig. 2 was observed by Perone and Kretlov [2] who, however, did not explain its origin. The appearance of the split at lower thiocyanate concentrations and longer deposition times suggests that it may be caused by formation of an additional thiocyanate compound of mercury.

The influence of copper(II)

Copper(II) is a common trace contaminant of thiocyanate solutions. It has also been added on purpose to enhance the height of the mercury stripping peak [9—11]. According to Luong and Vydra [12] a tenfold excess of

Cu(II), compared to Hg(II), was not harmful for the determination of traces of mercury by anodic stripping voltammetry in thiocyanate medium. According to Ulrich and Ruegsegger [9], copper is oxidized in thiocyanate medium in two well separated peaks. A comparison of the results of Ulrich and Ruegsegger with the results of Perone and Kretlov [2] and Pniev et al. [3] suggests that the second (more positive) peak of copper oxidation could have been assumed in the latter papers as an additional peak of oxidation of mercury.

Figure 3 presents the stripping curves obtained for small concentration of Cu(II) in the presence of increasing thiocyanate concentrations. As indicated by Ulrich and Ruegsegger [9], the anodic oxidation of copper in thiocyanate medium proceeds in two steps. Bilewicz et al. [13] showed recently that copper(I) thiocyanate is deposited on the electrode in the first step and this deposit is oxidized in the second step. With increasing thiocyanate concentration, the more negative peak shifts to more negative potentials but its height remains unchanged, whereas the more positive peak remains at the same potential but decreases in height. Similar effects were observed when the thiocyanate concentration was kept constant while the copper(II) concentration was increased. At very low Cu(II) concentration (5×10^{-8} mol dm^{-3}), the CuSCN formed in the negative peak partly dissolves; the ratio of the quantity of electricity consumed in the positive and negative peaks, $Q_{pos.}/Q_{neg.}$, is therefore low (0.335). At 5×10^{-6}—10^{-5} mol dm^{-3} Cu(II) concentrations, the deposit of CuSCN is quantitatively oxidized in the positive peak and the ratio $Q_{pos.}/Q_{neg.}$ is 0.99—0.994. At still larger Cu(II) concentrations (2—5×10^{-5} mol dm^{-3}) the ratio $Q_{pos.}/Q_{neg.}$ is more than 1 (1.1—1.38 over the specified range); this can be explained by the occurrence of the chemical reaction

$$Cu(0) + Cu(II) + 2\ SCN^- = 2\ CuSCN \qquad (1)$$

The height of the mercury stripping peak in thiocyanate medium depends in a complex way on the concentration of Cu(II) in solution. In the presence of low concentrations of Cu(II), the mercury stripping peak increases [12, 14] but at higher Cu(II) concentrations it begins to decrease. The increase was explained as a codeposition effect [12], probably correctly. In the presence of a little Cu(II), the detection limit for mercury improves markedly; some curves for very small Hg(II) concentrations in the presence of Cu(II) ions are shown in Fig. 4.

The causes of the decrease in the height of the mercury stripping peak at higher Cu(II) concentrations were not discussed by Luong and Vydra [12]. Two causes seem possible. First, in the presence of Cu(II), some CuSCN may be deposited over the mercury; as this deposit is stable in the potential range where mercury is oxidized, oxidation of the underlying mercury could be difficult. However, this influence cannot be strong because the general shape of the peak remains unchanged. Secondly, a side reaction may occur

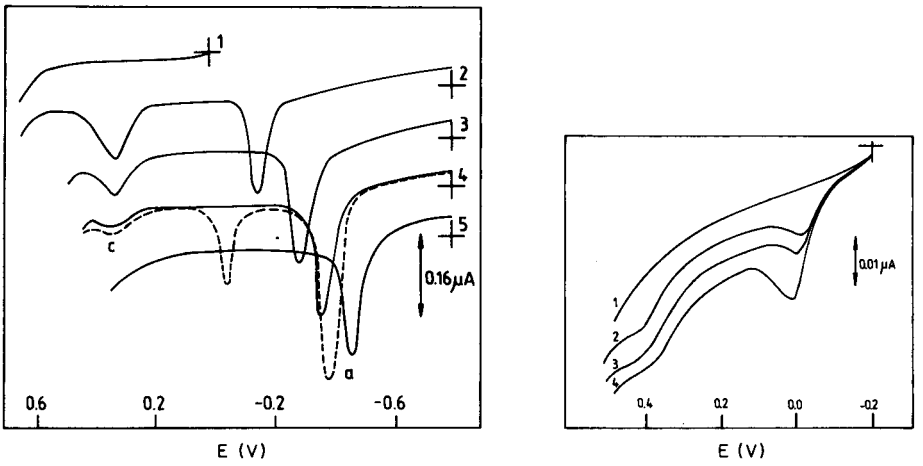

Fig. 3. The influence of thiocyanate concentration on the anodic stripping curves obtained for 2×10^{-7} mol dm^{-3} Cu(II). Deposition time 6 min. Deposition potentials: (1) 0.0 V; (2—5) —0.9 V. Solution: 0.1 mol dm^{-3} $NaClO_4$ with increasing concentrations of thiocyanate: (1,2) 1×10^{-4}; (3) 1×10^{-2}; (4) 0.1; (5) 1 mol dm^{-3}. (---) As (4) but after addition of 1×10^{-7} mol dm^{-3} Hg(II).

Fig. 4. Anodic stripping curves obtained for mercury in 0.1 mol dm^{-3} thiocyanate solution in the presence of 5×10^{-8} mol dm^{-3} Cu(II). Deposition time 20 min; deposition potential —1.0 V. Concentrations of Hg(II): (1) 0; (2) 2×10^{-9}; (3) 4×10^{-9}; (4) 8×10^{-9} mol dm^{-3}.

on the electrode surface:

$$Hg + 2\ Cu(II) + 2\ SCN^- = Hg(II) + 2\ CuSCN \qquad (2)$$

This suggestion is supported by the following results. A graphite electrode covered by a mercury layer about 2 nm thick dipped into 0.1 mol dm^{-3} solution of NaSCN gave voltammograms showing peak b only; when the same electrode was dipped first for 2 min in 0.1 mol dm^{-3} NaSCN solution containing 1×10^{-4} mol dm^{-3} Cu(II) and then transferred to pure NaSCN solution, the voltammograms showed peaks a and c. Evidently, in the presence of sufficient Cu(II), the mercury layer is completely replaced by a CuSCN deposit. At lower Cu(II) concentrations, reaction (2) is slow but its effect can be observed at 5-fold amounts of Cu(II) if the voltammograms are recorded slowly.

The influence of lead(II) and cadmium(II)

The presence of small concentrations of lead(II) [12, 15] and cadmium(II) [15] leads to an increase in the height of the mercury dissolution peak, i.e., these metals enhance the deposition of mercury on the graphite electrode. This was confirmed in the present work for solutions containing 0.1 mol dm^{-3} NaSCN, 1×10^{-6} or 1×10^{-7} mol dm^{-3} Hg(II) and Pb(II) or Cd(II) at concentrations in the range 3×10^{-8}—5×10^{-6} mol dm^{-3}. Lead(II), however, was markedly less effective than cadmium(II). Mercury exerted a positive

effect on the behaviour of cadmium and lead. The width at half height of the peaks obtained for these metals was 38 mV, i.e., the value predicted theoretically [16] for the dissolution of lead or cadmium from homogeneous amalgams, even when the solubilities of lead and cadmium in mercury were markedly exceeded.

The influence of tin(II)

The influence of tin was studied for 0.1 mol dm^{-3} NaSCN at pH 2 containing 1×10^{-7} or 1×10^{-6} mol dm^{-3} Hg(II). The concentration of tin was varied in the range 1×10^{-7}—5×10^{-6} mol dm^{-3}. Special precautions were taken to minimize the reaction between Sn(II) and traces of dissolved oxygen [17]. Under the conditions used, tin(II) neither increased nor distorted the mercury stripping peak. The influence of mercury(II) on the tin stripping peak varied. At 1×10^{-7} mol dm^{-3} Hg(II) (i.e., under conditions where the electrode was not covered uniformly by mercury), the dissolution peak of tin was broad and low. At 1×10^{-6} mol dm^{-3} Hg(II), the tin peak became better developed; its width at half height was 38 mV, indicating a homogeneous amalgam [16], although a heterogeneous amalgam would be expected. At still higher Hg(II) concentrations, the height of the dissolution peak decreased, probably because Sn(II) and Hg(II) reacted in the bulk solution.

The influence of silver(I)

At low thiocyanate ion concentrations, the dissolution peak of silver showed distortions similar to those in Fig. 2 for oxidation of mercury. For more than 1×10^{-6} mol dm^{-3} silver(I) and for deposition times longer than 9 min, these effects, probably caused by deposition of AgSCN, were observed even in 0.1 mol dm^{-3} thiocyanate.

Figure 5 shows the stripping curves obtained for mercury and silver at varying concentrations of thiocyanate, in 0.1 mol dm^{-3} NaSCN the stripping peaks of silver (curve 1) and mercury (curve 2) occur at nearly the same potential, as reported earlier [18]. The single peak obtained after simultaneous deposition of both metals is higher than the sum of the peaks obtained separately for the same concentrations of Ag(I) and Hg(II), which means that the deposition of one metal is enhanced by the presence of the other. At a thiocyanate concentration of 1 mol dm^{-3}, the stripping peaks of silver and mercury were well separated when the concentrations of Hg(II) and Ag(I) were similar. In 3 mol dm^{-3} thiocyanate, separation was good even at a 100:1 ratio of Hg(II) to Ag(I), in accordance with earlier results [18, 19]. Under the conditions used, silver deposited simultaneously with mercury formed the heterogeneous amalgam only; instead of 75 mV predicted by theory [16] for the width of the silver dissolution peak at half height, a value of 50 mV was observed.

The influence of iron(II)

The voltammetric behaviour of iron(II) at the HMDE in thiocyanate medium has been described [20—22], but the influence of iron on the

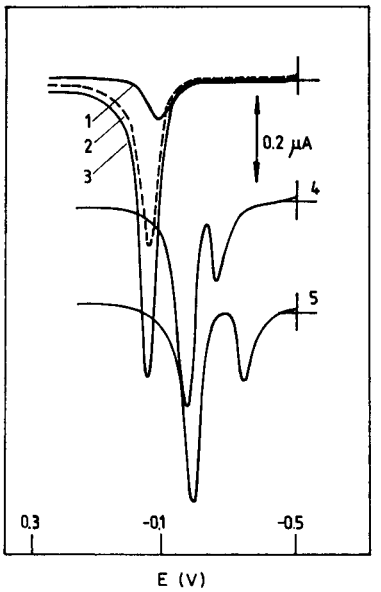

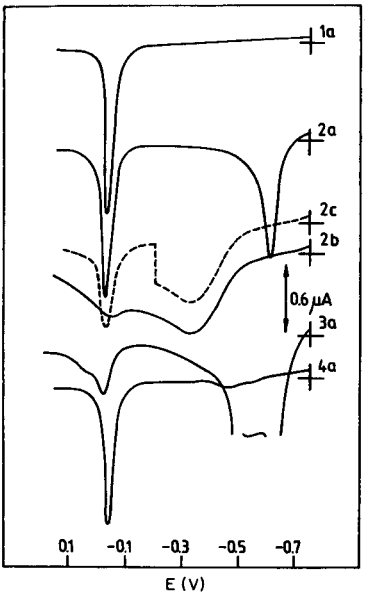

Fig. 5. Mercury stripping curves obtained in the presence of 4×10^{-7} mol dm^{-3} silver(I). Concentration of Hg(II): (1) 0; (2—5) 1×10^{-6} mol dm^{-3}. Concentration of NaSCN: (1—3) 0.1; (4) 1; (5) 3 mol dm^{-3}. Deposition potential —1.0 V; deposition time 3 min; scan rate 1 V min^{-1}.

Fig. 6. Mercury stripping curves obtained in the presence of iron(II) from 0.1 mol dm^{-3} NaSCN at pH 4 containing 3×10^{-6} mol dm^{-3} Hg(II). Concentration of Fe(II): (1) 0; (2) 1×10^{-5}; (3) 3×10^{-5} mol dm^{-3}; (4) as (3) but at pH 2. Deposition time 3 min. Deposition potential: (a) —1.1 V; (b) —1.5 V; (c) at 0.0 V, the scan rate was stopped for 1 min.

mercury stripping peak has not been considered. After deposition on the HMDE at less negative potentials, iron remains on the electrode surface and can easily be re-oxidized during the anodic scan, whereas on deposition at more negative potentials, iron penetrates into the drop and is re-oxidized only with difficulty [20—22].

The present experiments were done with slightly acidic solutions (pH 4 or 2) containing 0.1 mol dm^{-3} thiocyanate, 3×10^{-6} mol dm^{-3} mercury(II) and increasing concentrations of iron(II). For 1×10^{-6} mol dm^{-3} Fe(II), deposition at —1.1 V provided a sharp anodic peak corresponding to oxidation of iron, and the mercury stripping peak was in no way affected; yet, after deposition at —1.5 V, the mercury stripping peak was diminished by about 20%. Figure 6 illustrates the influence of slightly higher concentrations of iron(II). At 1×10^{-5} mol dm^{-3}, iron(II) deposition at —1.1 V provided complete oxidation of iron before the mercury stripping peak started but the mercury peak was slightly lowered (curve 2a). In the same solution but after deposition at —1.5 V, re-oxidation of iron started at less negative potentials, the peak was elongated, and the mercury stripping peak appeared only as a

small hump on the iron dissolution current (curve 2b). The shape of the mercury peak could be improved by stopping the voltage scan to allow most of the iron to re-oxidize before mercury was stripped, but the mercury peak thus obtained was quite small (curve 2c). At 3×10^{-5} mol dm^{-3} Fe(II) (curve 3a), the mercury stripping peak was affected markedly even after deposition at —1.1 V.

The distortions caused by iron(II) could be easily eliminated by appropriate variations of deposition potential or pH. A deposition potential of —0.8 V was convenient because iron(II) is not then reduced, whereas Hg(II) is reduced effectively. The influence of decreased pH is shown by curve 4a.

The influence of nickel(II)

The deposition of nickel on mercury electrodes proceeds in a very complex way. Depending on the conditions used, a homogeneous or heterogeneous nickel amalgam, a surface nickel deposit or an intermetallic compound may be formed. According to Krogulec et al. [23, 24], the deposition of nickel on the mercury surface is a secondary process, preceded by electroreduction of thiocyanate and formation of a nickel sulphide deposit. According to Luong and Vydra [12], the mercury stripping peak is markedly affected by the addition of nickel(II) to the solution.

In the present experiments, the slightly acidic (pH 4 or 2) 0.1 mol dm^{-3} thiocyanate solutions contained 3×10^{-6} mol dm^{-3} Hg(II) and 1×10^{-7}—1×10^{-5} mol dm^{-3} Ni(II). In principle, the effect of Ni(II) was similar to that of Fe(II), i.e., deposition at —1.5 V led to severe distortion of the mercury stripping peak, whereas after deposition at —1.1 V the mercury was affected only slightly or not at all. Similarly, any effect of nickel could be easily eliminated by proper choice of deposition potential or pH.

The influence of gold

Contamination of solutions by gold compounds is unlikely, but thin gold layers may be deposited on graphite electrodes to improve the determination of mercury by anodic stripping [4, 10, 25]. In the present experiment, 0.1 or 0.01 mol dm^{-3} thiocyanate solutions at pH 2 were used with a graphite electrode covered by a layer of gold (0.45—1.2 nm thick). In the supporting electrolyte used, the gold deposit was not dissolved prior to oxidation of thiocyanate. As the curves presented in Fig. 7 show, gold affects the mercury stripping peak significantly. At low Hg(II) concentrations there is only a single diffuse peak, which occurs at markedly more positive potential than the peak obtained at a pure graphite electrode (curve 6). At higher Hg(II) concentrations, an additional peak b appears on the stripping curve; its position is close to that of the peak obtained at a pure graphite electrode. Increasing Hg(II) concentrations affect the height of peak a in a complex manner. Under conditions where the second peak is absent, the height of peak a increases proportionally to increasing Hg(II) concentration. However, after the appearance of peak b, the increase in

height of peak a is no longer proportional. It is evident that peak a represents mercury oxidized from the intermetallic Au—Hg compound whereas peak b corresponds to mercury not bound with gold. For the determination of the higher concentrations of Hg(II), where two stripping peaks appear, the gold-plated electrode is less convenient than the pure graphite electrode, whereas for very low concentrations the gold-plated electrode is advantageous. The detection limit attained at this electrode after a deposition time of 20 min is 2×10^{-8} mol dm^{-3}; this concentration gave no stripping peak at the pure graphite electrode.

The influence of tellurium(IV)

The influence of tellurium(IV) on the mercury stripping peak has not been studied in thiocyanate solutions. In hydrochloric acid solutions, the behaviour of mercury was significantly affected by tellurium(IV) [26]. In the present work, cyclic voltammetry of 0.1 mol dm^{-3} thiocyanate at pH 2 containing 1×10^{-4} mol dm^{-3} Te(IV) showed that the reduction of Te(IV) to tellurium began at —0.35 V and reduction to H_2Te at —0.75 V. Tellurium deposited on the graphite electrode was oxidized at 0.35 V. In stripping experiments done with the same electrolyte, the concentrations of Hg(II) and Te(IV) were varied from 5×10^{-7} to 5×10^{-6} mol dm^{-3} and from 5×10^{-8} to 5×10^{-6} mol dm^{-3}, respectively. Figure 8 shows the influence of increasing concentrations of Te(IV) on the mercury stripping peak. At low Te(IV) concentrations, the peak decreases and when the concentrations of Hg(II) and Te(IV) are equal, the peak disappears completely; the intermetallic compound HgTe must be formed. Further increase of the Te(IV) concentration gives an increase in the positive peak, which corresponds to simultaneous oxidation of tellurium and HgTe. In order to eliminate the effect of Te(IV) on the mercury peak, the deposition potential was changed from —0.7 V to —0.3 V. At the latter potential, Te(IV) was not reduced, but the efficiency of mercury deposition was decreased significantly.

DISCUSSION

Numerous effects must be considered in discussing the influence of substances on the anodic stripping peak of mercury from graphite electrodes in thiocyanate solutions: (1) enhancement of the peak by co-deposition of another metal; (2) formation of heterogeneous amalgams; (3) formation of intermetallic compounds; (4) deposition of the metal or a sparingly soluble salt on the mercury surface; (5) electroreduction of thiocyanate or reactions between Hg(0) and Cu(II).

An essential defect of pure graphite or glassy carbon electrodes, compared with mercury electrodes, is the possible electrodeposition of very small amounts of metals on the electrode surface. Co-deposition of mercury in situ, as in mercury film electrodes, enhances significantly the possibility of deposition of traces of many metals. Conversely, electrodeposition of traces of mercury should be enhanced by the codeposition of other

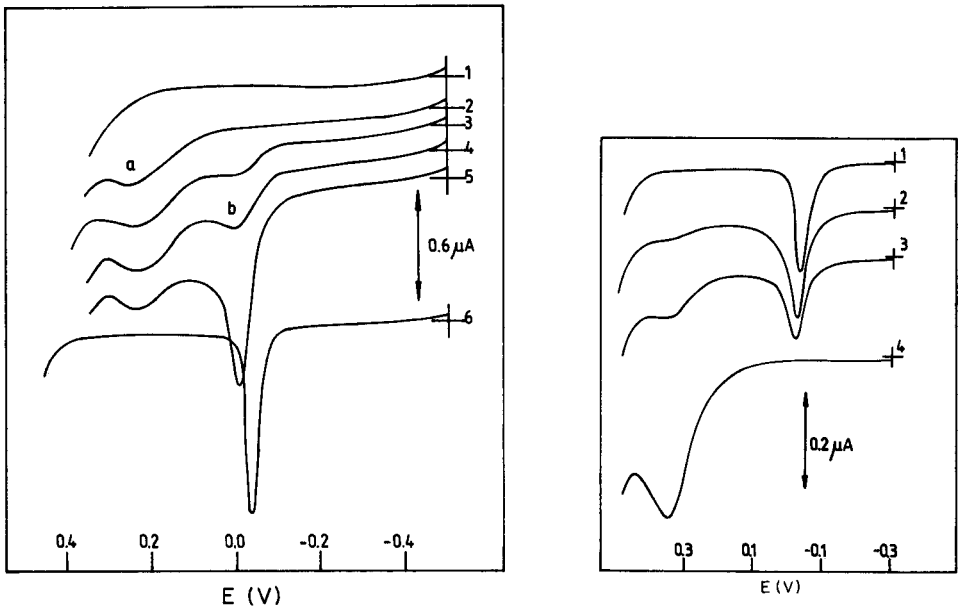

Fig. 7. Mercury stripping curves obtained in the presence of gold in 0.1 mol dm^{-3} NaSCN at pH 2. Hg(II) concentration: (1) 0; (2) 2×10^{-6}; (3) 3×10^{-6}; (4) 5×10^{-6}; (5, 6) 1×10^{-5} mol dm^{-3}. Electrodes: (1—5) graphite electrode with 0.9-nm gold layer; (6) graphite electrode. Deposition for 3 min at —0.9 V.

Fig. 8. Influence of tellurium on stripping curves for 1×10^{-6} mol dm^{-3} Hg(II) in 0.1 mol dm^{-3} NaSCN at pH 2. Concentration of Te(IV): (1) 0; (2) 1×10^{-7}; (3) 3×10^{-7}; (4) 1×10^{-6} mol dm^{-3}. Deposition for 6 min at —0.7 V.

metals. It appears from the above results that the significant discrepancies observed in the literature for the mercury detection limit at graphite electrodes can be satisfactorily explained in terms of codeposition effects exerted by fortuitous contaminants of the solution. The results also show that the codeposition effect can also be responsible for the additional stripping peaks described previously [2, 3] as the second and third peaks of mercury oxidation.

Under the conditions used here (i.e., when similar amounts of mercury and another metal are deposited on the graphite electrode), the solubility of the second metal in mercury is easily exceeded even for metals readily soluble in mercury. The oxidation of heterogeneous amalgams usually proceeds in a complex way [27] and this can cause difficulties in explaining the stripping curves. The above experiments showed that cadmium, lead and tin do not distort the mercury peaks; this may mean that these metals easily form supersaturated amalgams. In contrast, the stripping peaks in presence of silver were distinctly distorted, probably because of the formation of a heterogeneous amalgam. Iron deposited at sufficiently negative potentials easily forms the heterogeneous amalgam, and the mercury stripping peak then obtained is significantly distorted.

During the deposition of several metals on a graphite electrode, the possibility of the formation of intermetallic compounds is significant. The above experiments show that the formation of such compounds does not yield uniform results. When the second constituent of the mercury—metal system is oxidized at a potential more positive than that of mercury, the mercury stripping peak will be affected; such effects were observed for the Au—Hg and Te—Hg systems. When the oxidation potential of the second constituent is more negative than that of mercury, the formation of an intermetallic compound may or may not affect the mercury peak. This effect will depend on the rate of dissociation of the intermetallic compound. In the case of cadmium, the mercury peak was not distorted, possibly because $CdHg_3$ dissociates easily [28]. Severe distortions were caused by nickel, which forms several intermetallic compounds with mercury, but intermetallic compound formation cannot really be blamed because similar effects were observed for iron which does not form intermetallic compounds with mercury. Iron and nickel deposited with mercury could be oxidized completely prior to the mercury stripping peak, which was then affected only slightly or not at all. In contrast, when enough CuSCN was deposited, the mercury stripping peak was affected because the CuSCN deposit remained on the mercury surface during stripping.

According to some authors [23, 24, 29], thiocyanate can be electroreduced in solutions containing certain transition metal ions. Sulphides formed in the electroreduction process may cause additional peaks. Yet, although the stripping curves obtained above for iron and nickel were complex, the observed effects could not be attributed to the reactions of electroreduction products of thiocyanate.

The presence of copper(II) can lead to enhancement of the mercury stripping peaks [9—11]. However, in thiocyanate medium in the presence of excess of copper(II), the opposite effect can be observed, i.e., the mercury stripping peak is decreased owing to oxidation of mercury by copper(II) in forming copper(I) thiocyanate.

REFERENCES

1 R. Bilewicz, Z. Stojek and Z. Kublik, J. Electroanal. Chem., 96 (1978) 29.
2 S. P. Perone and W. J. Kretlov, Anal. Chem., 37 (1965) 968.
3 W. W. Pniev, L. A. Moskovskikh and W. S. Putrova, Zh. Anal. Khim., 28 (1973) 1918.
4 S. Combet and M. Dozol, Electrochim. Acta, 24 (1979) 1283.
5 M. Stulikova and F. Vydra, J. Electroanal. Chem., 42 (1973) 127.
6 Z. Stojek, B. Stepnik and Z. Kublik, J. Electroanal. Chem., 74 (1976) 277.
7 W. Kemula and Z. Kublik, Anal. Chim. Acta, 18 (1958) 104.
8 E. Bednarkiewicz, M. Donten and Z. Kublik, J. Electroanal. Chem., 127 (1981) 241.
9 L. Ulrich and P. Ruegsegger, Z. Anal. Chem., 277 (1975) 349.
10 R. E. Allen and D. C. Johnson, Talanta, 20 (1973) 799.
11 T. Miva and A. Mizuike, Jpn. Analyst, 17 (1968) 448.
12 L. Luong and F. Vydra, J. Electroanal. Chem., 50 (1974) 379.
13 R. Bilewicz, Z. Stojek, Z. Kublik and J. Osteryoung, J. Electroanal. Chem., 137 (1982) 77.

14 Z. Yoshida and Z. Kihara, J. Electroanal. Chem., 95 (1979) 159.
15 E. M. Royzenblat and G. N. Vieretina, Zh. Anal. Khim., 29 (1974) 2376.
16 W. T. de Vries and E. van Dalen, J. Electroanal. Chem., 14 (1967) 315.
17 S. Glodowski and Z. Kublik, Anal. Chim. Acta, 115 (1980) 51.
18 J. Hubmann, J. Buffle and D. Monnier, Anal. Chim. Acta, 62 (1972) 393.
19 E. Ja. Neyman and Kh. Z. Brainina, Zh. Anal. Khim., 28 (1973) 886.
20 W. Haerdi, J. Buffle and D. Monnier, J. Electroanal. Chem., 23 (1969) 81.
21 I. V. Markova, S. I. Sinyakova and V. I. Shirokova, Zh. Anal. Khim., 28 (1973) 2214.
22 Z. Stojek and Z. Kublik, J. Electroanal. Chem., 70 (1976) 317.
23 T. Krogulec, A. Barański and Z. Galus, J. Electroanal. Chem., 57 (1974) 63.
24 T. Krogulec and Z. Galus, J. Electroanal. Chem., 117 (1981) 109.
25 R. W. Andrews, J. H. Larochelle and D. C. Johnson, Anal. Chem., 48 (1976) 212.
26 Yu. A. Figelson, E. Ya. Neyman and V. G. Jakovleva, Zh. Anal. Khim., 30 (1975) 300.
27 Z. Galus, CRC Crit. Rev. Anal. Chem., (1975) 370.
28 L. F. Kozin and M. B. Dergatcheva, Tr. Inst. Org. Katal. Elektrokhim., Akad. Nauk Kaz. S.S.R., 3 (1972) 31.
29 E. Itabashi and S. Ikeda, J. Electroanal. Chem., 27 (1970) 243; 36 (1972) 189.

Analytica Chimica Acta, 152 (1983) 215—222
Elsevier Science Publishers B.V., Amsterdam — Printed in The Netherlands

CATALYTIC—KINETIC DETERMINATION OF THIOUREAS BY A BIAMPEROSTATIC METHOD WITH IODINE—AZIDE AS THE INDICATOR REACTION

SIEGBERT PANTEL

Institut für Anorganische und Analytische Chemie der Universität, D-7800 Freiburg i. Br. (W. Germany)

(Received 23rd March 1983)

SUMMARY

A biamperostat method is described, in which the iodine concentration in the iodine—azide reaction mixture is kept very low and constant by the automatic addition of increments of a potassium triiodide solution. This is used to determine the catalysts thiourea, phenylthiourea, benzoylthiourea and tetramethylthiuram sulphide in the nanomolar range in aqueous as well as in 20% ethanolic solution. The catalytic activities of another fifteen substituted thioureas are measured and listed.

The catalytic influence of compounds with negative divalent sulphur on the iodine—azide reaction was first described by Raschig in 1908 [1, 2] and was used from 1928 onwards for qualitative tests [3, 4]. For quantitative purposes, either the nitrogen development may be measured [5—7] or the iodine consumed may be determined by spectrophotometry [8] or titrimetry [7, 9—13]. The iodine consumption can be measured in closed systems by using a relatively large excess of iodine and back-titrating with thiosulphate or better with phenylarsine oxide to avoid possible interference through the formation of thiohydroxylamine-*S*-sulphonates in nearly neutral solutions (pH 5—7) [13]. Phenylarsine oxide, however, may be carcinogenic.

With the method of competitive reactions [14, 15], a very small excess of iodine is present during the reaction, so that oxidative destruction of the catalyst may be avoided, but the two reactions proceed simultaneously with unknown effects on each other. Another possibility for keeping the iodine concentration constant and very low is to make use of a "stat" method [16], which is also classified as an open system.

Stat methods are especially useful in the examination of catalyzed reactions of the general type, $A + B \overset{K}{\rightleftarrows} X + Y$, in the so-called "initial state" with a rate law of quasi-zero order. This means that the concentrations of reactants A and B can be regarded as constant, resulting in a linear relationship between the concentration of the indicator substance c_X and time. This is achieved, for example, by controlled addition of reactant A to the measuring vessel as it is consumed (reactant B is present in relatively high excess). Any suitable

0003-2670/83/$03.00

physical property of the system which is proportional to the concentration of the substance to be kept constant, may be used to regulate the rate of addition from the burette (after conversion of the measured effect to an equivalent voltage). This is done by comparison of the measured voltage (actual potential) with the preset working potential, equivalent to the preset working concentration of the substance A to be kept constant. The apparatus used is shown schematically in Figs. 1 and 2. The speed of addition, extrapolated as $\Delta \tan \alpha = \tan \alpha_K - \tan \alpha_0$ from a suitable recorder trace (Fig. 3a) is a measure of the catalyst concentration. This principle has been used with different indicating systems to determine catalysts as well as activators, inhibitors and reactivators [17–23].

The main advantage of the stat methods is that it is not necessary to use a large concentration of substance A to maintain the conditions of the initial state. This is of great importance for the determination of rather unstable catalysts, as the substance to be added from the burette is often a strongly oxidizing agent. Thus, in the iodine—azide reaction, the preset concentration of iodine is 0.2 mM or less.

A biamperometric indicator system was chosen because the iodine/iodide pair is very easily measured at a polarisation potential as low as 10 mV; thus, electrode reactions can be avoided as far as possible. Attempts were therefore made to determine organic compounds containing divalent sulphur with the aid of a biamperostat [24] in the usual way, by the $\Delta \tan \alpha$ method (Fig. 3a). Surprisingly, in most cases, a very high reaction speed resulted, exceeding the highest possible addition rate of the burette and independent of the concentration of the catalyst. After a certain period of time, the reaction showed exactly or almost exactly the speed of the uncatalyzed reaction (Fig. 3b; AB and CD represent the uncatalyzed reaction and BC the catalyzed reaction). Different catalyst concentrations produced different step heights; the step heights were reproducible and gave linear or almost linear calibration graphs on plotting the iodine consumption (equivalent to BC) against the catalyst concentration (see below). The step height can be explained on the basis that the catalyst first causes a very high rate of conversion in the indicator reaction, but is quickly deactivated by oxidation; this has already been discussed by Müller et al. [15].

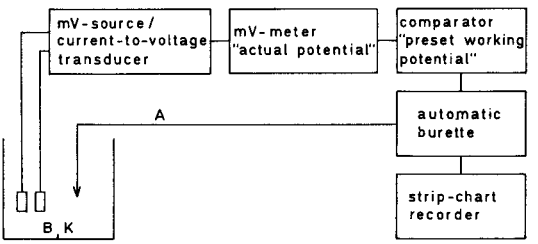

Fig. 1. Schematic design of a biamperostat apparatus: A and B are the reactants for the indicator reaction and K is the catalyst.

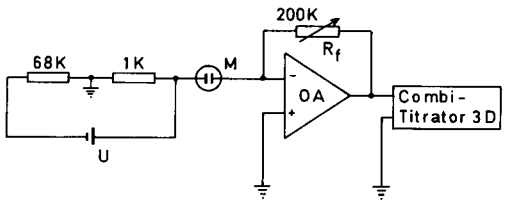

Fig. 2. Current-to-voltage transducer with mV source: OA, operational amplifier (Teledyne-Philbrick type 844 BE); U, mercury battery (1.35-V Mallory RM 42 R); M, microdouble-platinum electrode.

The slope of the calibration graph is a measure of the catalytic activity of the relevant sulphur compound during its lifetime. It may be called the "reactivity number" N_R = I/S, i.e., the ratio of gram-atoms of iodine consumed to gram-atoms of sulphur present. Kurzawa and Krzymien [12] named this quotient the coefficient of induction whereas Schacherl [13] called it the azide factor.

The consumption of iodine is strongly dependent on the pH value (Fig. 4); the effects of the sodium azide and iodide concentrations, as well as of the preset iodine concentration, are much smaller. To eliminate these effects for measurements under slightly different reaction conditions, it may be of advantage to define a "relative molar coefficient of catalytic activity", F, as has been done for iodine-containing organic compounds [22]: $F = c(\text{thiourea})/c(\text{RS})$; $F = N_R(\text{RS})/N_R(\text{thiourea})$. Here $F = 0.025$ means that 1 nmol of thiourea has the same catalytic activity as 40 nmol of the particular sulphur compound RS. The N_R and F values for the compounds examined in this paper are given in Table 1.

Further experiments were done at pH 5.9; at appreciably higher acidities, toxic hydrogen azide was evolved. While sulphide, thiosulphate, cysteine and thioureas formed steps as shown in Fig. 3(b), cystine or a suspension of cadmium sulphide showed the usual addition plot for stat methods (Fig. 3a). The catalytic activity of the more stable substances (e.g., cystine) was less than that of the others. Thus cystine could be determined in the range

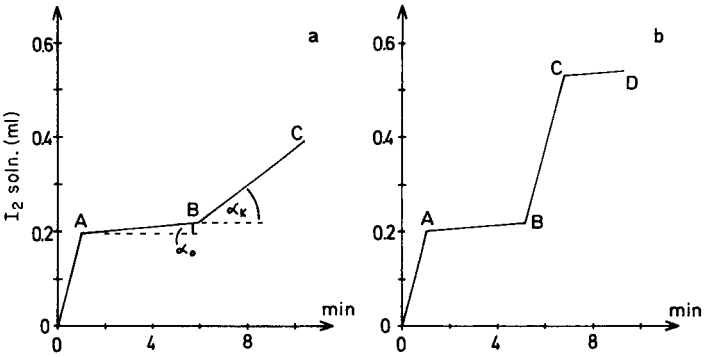

Fig. 3. Recorder plots: (a) for stable catalysts; (b) for short-lived catalysts.

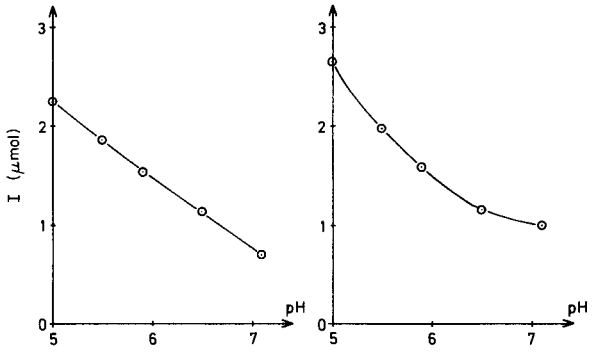

Fig. 4. Iodine consumption as a function of the pH value: (a) for thiourea in aqueous solution (11 nmol/5 ml); (b) for phenylthiourea in aqueous solution (12 nmol/5 ml). Both solutions were 0.6 M in sodium azide and 0.01 M in potassium iodide.

0.4—4 μmol/5 ml and 1 μmol of cystine consumed 27.9 μg of iodine per min under the same conditions as for the determination of nanomolar amounts of thioureas.

The recorder graphs (Fig. 3b) indicate the possibility of determining such substances by direct titration, but this does not give good reproducibility because, in contrast to the stat method where a constant iodine concentration is maintained, the excess of iodine near the end-point is very small and therefore the reaction is very slow. For thioureas, a direct titration method at constant rate with a mixture of iodine and sodium azide has been reported by Suzuki [25] and criticized by Kurazawa and Krzymien [12].

As some of the sulphur compounds were not soluble enough in water to provide measurable catalytic activity, ethanol was added to the indicator reaction mixture in those cases (up to 20%); more ethanol caused precipitation and also lowered the biamperometric current too much. The influence of ethanol on the indicator reaction was small, but different, as can be seen for thiourea and phenylthiourea in Table 1.

EXPERIMENTAL

Samples and reagents

Thiourea, *N*-phenylthiourea, *N*-methylthiourea, *N*-allylthiourea, *N,N'*-dimethylthiourea, *N,N*-diethylthiourea and *N,N,N',N'*-tetramethylthiourea were purchased (Merck, EGA, Riedel-de-Haën). *N,N,N',N'*-Tetraethylthiourea, *N*-(*p*-hydroxyphenyl)-thiourea and *N*-(*p*-nitrophenyl)-thiourea were prepared by reaction of the respective aliphatic or aromatic amines with thiophosgene in diethyl ether and subsequent reaction with ammonia or amine [26, 27]. *N,N'*-diethylthiourea, *N,N,N'*-triethylthiourea, *N*-benzoylthiourea, *N*-benzoyl-*N'*-phenylthiourea, *N*-benzoyl-*N'*-(*p*-hydroxyphenyl)-thiourea and *N*-benzoyl-*N'*-(*p*-nitrophenyl)-thiourea were prepared by reaction of the respective alkyl or benzoyl isothiocyanates with ammonia or amine [28, 29]. *N,N*-Diethyl-

TABLE 1

Reactivity numbers N_R and relative molar coefficients of activity F for substituted thiourea in aqueous medium and in 20% ethanolic medium with iodine—azide as the indicator reaction

S || X—C—Y		M.p. or b.p. (°C)	N_R	F
X—	—Y			
I. Aqueous medium				
H_2N—	—NH_2	179	138	1.00
$(CH_3)HN$—	—NH_2	122	140	1.01
$(C_2H_5)HN$—	—NH_2	112	132	0.96
$(CH_2{=}CH{-}CH_2{-})HN$—	—NH_2	77	133	0.96
C_6H_5HN—	—NH_2	154	142	1.03
$(CH_3)_2N$—	—NH_2	160	112	0.81
$(C_2H_5)_2N$—	—NH_2	103	108	0.78
$(CH_3)HN$—	—$NH(CH_3)$	65	118	0.85
$(C_2H_5)HN$—	—$NH(C_2H_5)$	81	112	0.81
$(C_2H_5)_2N$—	—$NH(C_2H_5)$	48	116	0.84
$(CH_3)_2N$—	—$N(CH_3)_2$	77	78	0.57
$(C_2H_5)_2N$—	—$N(C_2H_5)_2$	$Kp_{2.5}$ = 79—80	155	1.12
II. 20% ethanolic medium				
H_2N—	—NH_2	179	138	1.00
C_6H_5HN—	—NH_2	154	133	0.96
HO—C_6H_4—NH—	—NH_2	Decomp.	41.5	0.30
O_2N—C_6H_4—NH—	—NH_2	Decomp.	19.3	0.14
C_6H_5—C(=O)—NH—	—NH_2	172	7.5	0.05
C_6H_5—C(=O)—NH—	—NHPh	146	9.6	0.07
C_6H_5—C(=O)—NH—	—NH—C_6H_4—OH	203	18.1	0.13
C_6H_5—C(=O)—NH—	—NH—C_6H_4—NO_2	179	7.8	0.06
$(CH_3)_2N$—	—S—C(=S)—$N(CH_3)_2$	106	261	1.89[a]

[a]Referred to one sulphur atom/molecule.

thiourea was prepared from diethylcyanamide and hydrogen sulphide [30]. Tetramethylthiuram sulphide, $(CH_3)_2N{-}\overset{\overset{S}{\|}}{C}{-}S{-}\overset{\overset{S}{\|}}{C}{-}N(CH_3)_2$, was formed as byproduct in the preparation of *N,N*-dimethylthiourea from dimethylthio-

carbamoyl chloride and aqueous ammonia at −10°C. It was isolated as canary-yellow crystals by extraction of the raw reaction product with benzene and by recrystallization.

All substances were recrystallized from water, aqueous ethanol or ethanol/diethyl ether until the catalytic activity remained constant; they were characterized through melting point, boiling point, analysis or spectroscopy.

The sodium azide solution was prepared from sodium azide (p.a.) and adjusted to pH 5.9 with phosphoric acid. The concentration and pH value were determined daily and the latter was adjusted if necessary with phosphoric acid. The solution must be stored in a closed bottle, because the pH rises on contact with air.

Apparatus

The apparatus used has been described in detail [24]. It consists of a Combi-Titrator 3D (Metrohm) with a current-to-voltage transducer and a mV source (Fig. 2). A 7-ml test tube (15-mm i.d.) serves as reaction vessel and is mounted in a thermostated aluminium block (25.0 ± 0.1°C). A home-made double platinum electrode (3-mm o.d. shank, 0.5-mm wire diameter) and the capillary end of the burette (Mikrodosimat, 1-ml) are fitted through a plastic lid on the test tube. The tip of a 100-μl Eppendorf pipette is inserted through a 5-mm hole in the lid to start the reaction by addition of the catalyst solution. The reaction mixture is stirred magnetically at 500 rpm. The recorder speed was 1 cm min^{-1} in all cases.

Procedure

To the measuring vessel are added 2 ml of 1.5 M sodium azide solution (pH 5.9), 0.5 ml of 0.1 M potassium iodide solution, 1 ml of ethanol (extra pure) if necessary and twice-distilled water up to 4.9 ml. After thermostating for 2 min, the measuring device is compensated to zero with the voltage offset null of the operational amplifier and 200 μl of 0.005 N iodine solution (634.5 mg of iodine and 1.0 g of potassium iodide made up with water to 1 l) are added manually from the Mikrodosimat burette. Then the feed-back resistor (R_f, Fig. 2) is immediately balanced so that the millivolt meter shows exactly 600 mV (preset working potential, equal to 127 μg of iodine) and automatic addition of 0.005 N iodine solution from the Mikrodosimat is started. After about 5 min (uncatalyzed reaction, AB in Fig. 3b), 0.1 ml of an aqueous or ethanolic solution of the catalyst standard solution or of the unknown sample solution is added with an Eppendorf pipette.

The recorder traces are similar to that shown in Fig. 3(b). A calibration graph is drawn by plotting micromoles of iodine consumed (extrapolated from the height equivalent to BC in Fig. 3b) versus catalyst concentration. The graphs are linear or almost linear in all cases. The N_R values are extrapolated from the calibration graphs and the F values are calculated.

When not in use, the indicator electrode is stored in 0.1 M potassium triiodide solution for proper conditioning.

RESULTS AND DISCUSSION

Thiourea was determined in aqueous solution; the results for some single determinations are given in Table 2. The reproducibility of the procedure was tested at a thiourea concentration of 13.0 nmol/5 ml by measuring ten replicate samples. The standard deviation, s, was found to be 0.32 nmol/5 ml; the standard error, s.e. ($sn^{-1/2}$), was calculated as 0.10 nmol/5 ml. Phenylthiourea, benzoylthiourea and tetramethylthiuram sulphide were determined in 20% ethanolic solution. Some results for single determinations are given in Table 2.

For the investigation of the iodine—azide reaction, catalyzed by thioureas and similar compounds, the biamperostat method seems to be a good alternative to the method of Kurzawa and Krzymien [12], who back-titrated excess of iodine after a definite induction time, and to the method of competitive reactions, first described by Klockow et al. [14].

From the results given in Table 1, it can be seen that there is little difference in the catalytic activities of monophenyl-, monoalkyl-, dialkyl- and trialkyl-substituted thiourea. A significantly smaller activity is found for tetramethylthiourea and phenyl ring-substituted derivatives of thiourea or benzoylthiourea (Table 1). Tetramethylthiuram sulphide shows a significantly higher activity than any of the other species investigated.

In the interpretation of the results, it must be taken into account, as has been pointed out by Müller et al. [15], that the mechanisms of the iodine—azide reaction as well as of the deactivation reaction have never really been clarified. Therefore statements about a relation between chemical constitution and catalytic activity are difficult. But one thing is clear from the present

TABLE 2

Determination of thiourea and substituted thioureas as catalysts in the iodine—azide reaction

Thiourea (nmol/5 ml)		Phenylthiourea (nmol/5 ml)		Benzoylthiourea (nmol/5 ml)		Tetramethylthiuram sulphide (nmol/5 ml)	
Given	Found	Given	Found	Given	Found	Given	Found
2.60	2.72	2.49	2.63	69.4	68.0	0.61	0.62
5.20	5.07	4.60	4.59	124.8	118.0	1.05	1.10
7.80	7.61	6.96	6.57	183.1	190.0	1.54	1.55
10.40	10.34	8.54	8.87	250.2	260.0	2.09	2.05
13.00	13.04	9.85	10.12	295.2	300.0	2.65	2.60
15.60	15.58	12.87	13.14	374.5	365.0	3.07	3.12
18.20	18.10	16.42	16.29	434.5	440.0	3.65	3.70
20.80	20.65	19.97	19.71	498.8	510.0	4.61	4.59
23.40	23.55	23.12	23.39	568.7	560.0	5.25	5.29
26.00	26.08	26.28	26.28	624.2	634.0	6.14	6.14

work: tetramethylthiuram sulphide seems not to be able to form a resonance structure with thiol character, possesses two C=S double bonds and shows the highest catalytic activity of the whole series. Tetraethylthiourea also shows high activity. Cystine has only a C—S—S—C bridge and no C=S double bonds; it shows only a weak catalytic activity with the conventional recorder plot, equivalent to Fig. 3(a). Cysteine reacts quickly, as in Fig. 3(b), and so does sulphide. Therefore it may be concluded that substances with C=S double-bond character and/or thiol groups show an induction effect, equivalent to Fig. 3(b), and those ones without C=S double-bond character and without thiol groups may react much more slowly (Fig. 3a).

The author is greatly indebted to Professor Dr. Herbert Weisz for his encouragement and helpful discussions.

REFERENCES

1 F. Raschig, Chem. Ztg., 32 (1908) 1203; Ber. Dtsch. Chem. Ges., 48 (1915) 2088.
2 Gmelins Handbuch der Anorganischen Chemie, Vol. 8—Jod, Verlag Chemie, Berlin, 1933, p. 185.
3 F. Feigl, Z. Anal. Chem., 74 (1928) 369.
4 F. Feigl and E. Chargaff, Z. Anal. Chem., 74 (1928) 376.
5 E. Friedmann, J. Prakt. Chem., 146 (1936) 179.
6 H. Holter and S. Lovtrup, C. R. Trav. Lab. Carlsberg Ser. Chim., 27 (1949) 63, 72.
7 R. E. Press and K. A. Murray, J. S.-Afr. Chem. Inst., 5 (1954) 31, 45.
8 A. K. Babko and L. V. Markova, Zavod. Lab., 25 (1959) 1283.
9 G. Russell, Chemical Analysis in Photography, Focal Press, London, 1965, p. 64.
10 Z. Kurzawa, Chem. Anal. (Warsaw), 5 (1960) 551, 741.
11 E. Michalski and A. Wtovkowska, Chem. Anal. (Warsaw), 6 (1961) 365; 7 (1962) 691, 783.
12 Z. Kurzawa and M. Krzymien, Chem. Anal. (Warsaw), 13 (1968) 1047 and references therein.
13 R. Schacherl, Mikrochim. Acta (Wien), II (1978) 141.
14 D. Klockow, J. Auffarth and G. F. Graf, Z. Anal. Chem., 311 (1982) 244.
15 H. Müller, L. Beyer, Ch. Müller and Ch. Schröter, Z. Anorg. Allg. Chem., 446 (1978) 226.
16 K. Møller, Biochim. Biophys. Acta, 16 (1955) 162.
17 J. L. Haining and J. S. Legan, Anal. Biochem., 45 (1972) 469.
18 B. Tan and J. K. Grime, Anal. Lett., 12 B(1979) 1551.
19 J. K. Grime and K. R. Lockhart, Anal. Chim. Acta, 106 (1979) 251.
20 S. Pantel and H. Weisz, Anal. Chim. Acta, 109 (1979) 351 and references therein.
21 S. Pantel, Anal. Chim. Acta, 129 (1981) 231.
22 S. Pantel, Anal. Chim. Acta, 141 (1982) 353.
23 H. Weisz, S. Pantel and G. Marquardt, Anal. Chim. Acta, 143 (1982) 177.
24 S. Pantel and H. Weisz, Anal. Chim. Acta, 70 (1974) 391.
25 S. Suzuki, Jpn. Analyst, 65 (1962) 299, 384.
26 G. M. Dyson and H. J. George, J. Chem. Soc., 125 (1924) 1703.
27 O. Billeter, Ber. Dtsch. Chem. Ges., 20 (1887) 1629; 26 (1893) 1681.
28 A. W. Hofmann, Ber. Dtsch. Chem. Ges., 1 (1868) 25.
29 H. Hartmann and I. Reuther, J. Prakt. Chem., 315 (1973) 144.
30 F. Kurzer and P. M. Sanderson, J. Chem. Soc., (1957) 4461.

Analytica Chimica Acta, 152 (1983) 223—228
Elsevier Science Publishers B.V., Amsterdam — Printed in The Netherlands

CREATININE-SELECTIVE ENZYME ELECTRODES

GEORGE G. GUILBAULT*[a] and PIERRE R. COULET

Laboratoire de Biologie et Technologie des Membranes du CNRS, Université Claude Bernard, Lyon, 43 Boulevard du 11 Novembre 1918, 69622 Villeurbanne Cedex (France)

(Received 15th March 1983)

SUMMARY

Two selective creatinine enzyme electrodes have been developed for the determination of creatinine in the range 1—100 mg dl^{-1}. The electrodes were prepared using a new microbial enzyme (creatinine deiminase) immobilized on collagen and pig intestine membranes, in conjunction with an ammonia electrode. The electrodes are quite stable, have a response time of 2—10 min, and are sufficiently sensitive to detect normal levels of creatinine in blood serum.

Reliable assay of creatinine in serum is better than urea nitrogen for evaluating renal function because it is relatively unaffected by diet or rate of metabolism. Most methods used for creatinine determination are based on the reaction with picric acid in alkaline solution, the well-known Jaffé reaction [1]. This method lacks selectivity and many metabolites and drugs interfere [2, 3]. Many modifications have improved the precision but not the selectivity [4—10]. In order to improve the selectivity, several investigators have proposed the use of creatinine amidohydrolase (E.C.3.5.2.10) from *Alcaligenes*, which cleaves creatinine to creatine. The latter is determined via a creatine kinase—pyruvate kinase—lactate dehydrogenase sequence with spectrophotometric determination of NADH [11, 12]. This system involves four enzymatic reactions and is rather expensive; it is also difficult to locate problems that develop in the procedure [13].

Szulmajster [14] first described the isolation of another enzyme, a creatinine deiminase from *Clostridium* paraputrific cells, that converts creatinine directly to *N*-methylhydantoin and ammonia. Spectrophotometric [15] and fluorimetric [16] methods have been proposed for monitoring this reaction.

Meyerhoff and Rechnitz [17] first tried to design an enzyme electrode for creatinine, by entrapping the soluble creatininase between a cellophane membrane and the gas-permeable membrane of an Orion ammonia gas

[a]On sabbatical leave from the Chemistry Department, University of New Orleans, New Orleans, LA 70148, U.S.A.

0003-2670/83/$03.00

sensor. The activity of the enzyme continuously decreased, and the detection limit (5×10^{-4} M) was too high to be of practical use in serum. Guilbault et al. [18] described an electrode based on chemically bound *Pseudomonas* enzyme. Excellent selectivity and stability, but poor sensitivity, were achieved.

In this paper, the construction of two new types of enzyme electrode, based on microbial creatinine deiminase is described. Collagen and pig intestine membranes are used. The resulting self-contained creatinine electrodes are highly selective, sensitive and reliable.

EXPERIMENTAL

Materials and apparatus

Creatinine deiminase (E.C.3.5.4.21) of microbial origin, highly purified, was obtained as a freeze-dried powder (Farmitalia Carlo Erba, Milan, Italy). The activity was 1.9 U mg^{-1} at 37°C and pH 8. The enzyme has no glutamate dehydrogenase, urease, creatinase or arginase activity, and is stable for 1 year at 5°C.

Aqueous creatinine standards (1, 2, 10, 25, 50 and 100 mg dl^{-1}) were prepared from creatinine (Prolab, France). Solutions of urea, creatinine, arginine, cytosine, guanine and adenine (Prolab, France) were prepared at 100 mg dl^{-1} concentrations in doubly-distilled water. Pyrophosphate buffer (0.1 M, pH 8.5) was prepared from sodium pyrophosphate (p.a.; Merck). Phosphate buffer (0.10 M, pH 8.7) was prepared from potassium hydrogenphosphates (Merck). Clinical standard control serum (Unitrol; Biomerieux, Lyon, France) was used for all assays.

All potential readings were made using a Minisis 6000 pH/mV meter (Tacussel, Lyon) and the readings were displayed on a Servotrace recorder (Sefram, Paris).

The enzyme electrodes were constructed by placing the active enzyme membrane over the end of an ammonia sensor (Universal Sensors, P.O. Box 736, New Orleans, LA 70148) and holding it in position with a rubber O-ring.

Immobilization of enzymes

The creatininase was coupled to collagen films (Centre Technique du Cuir, Lyon) or pig intestine membranes (Universal Sensors, New Orleans, LA) by using the acyl-azide procedure previously applied to the activation of collagen films, followed by coupling [19]. Available carboxyl groups from aspartate and glutamate were esterified by treatment with a mixture of 0.2 M hydrochloric acid/methanol for 3—4 days at 20—22°C. Following a 20-s wash in distilled water, the membranes were soaked overnight in aqueous 1% hydrazine solution, and finally immersed for 3 min in 0.5 M sodium nitrite–0.3 M hydrochloric acid at 4°C prior to coupling. After a quick wash in alkaline buffer, the activated membranes (about 2 × 2 cm) were soaked in 1.5 ml of 0.05 M glycine—sodium hydroxide buffer, pH 9, containing 20 mg

of a lyophilized sample of creatininase, for 3 h. After a 10-min wash in 1 M potassium chloride, the membranes were soaked in buffer at 4°C before use.

Procedure

Place the electrode in a 5-ml beaker containing 2 ml of buffer. Stir, and record the background potential until it becomes constant (less than 1 min). Add 0.5 ml of the calibration standard or serum to be assayed, and record the potential change over 1—2 min. Calculate the concentration of creatinine from a calibration plot of potential vs. log creatinine concentration.

RESULTS AND DISCUSSION

Immobilization of enzyme and characteristics of bound creatininase

Several types of collagen films, prepared with collagen membranes developed by the Centre Technique du Cuir (CTC, Lyon, France), have been used in this laboratory for enzyme immobilization. They have previously been used for enzyme electrodes [20—23] and are very stable.

Binding of creatinine deiminase to collagen as well as to pig intestine membranes was achieved using the acyl-azide process. Electrodes prepared from the membrane gave linear calibration plots of log creatinine vs. potential (Fig. 1) for 1—100 mg dl^{-1} creatinine with both the collagen (curve A) and the pig intestine membranes prepared by the above immobilization

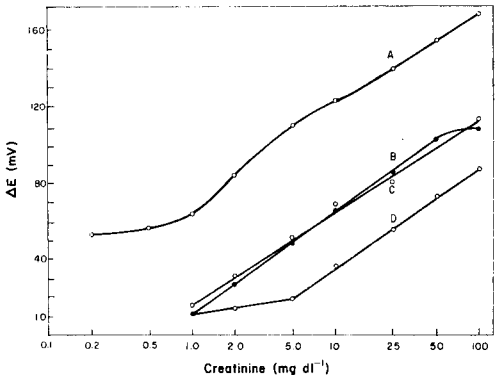

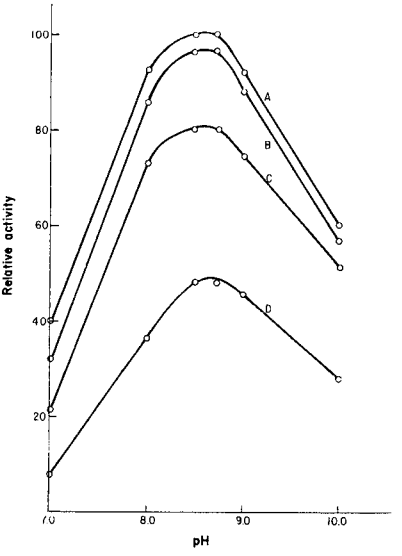

Fig. 1. Calibration plots for several creatinine electrodes: (A) on collagen, day 1 (slope = 55 mV $decade^{-1}$); (B) on pig intestine, day 1 (slope = 60 mV $decade^{-1}$); (C) on collagen, day 2 (slope = 57 mV $decade^{-1}$); (D) on pig intestine, immobilized via glutaraldehyde (slope = 54 mV $decade^{-1}$).

Fig. 2. Effect of pH on relative activity of a creatinine—collagen membrane electrode in various buffers: (A) phosphate; (B) pyrophosphate; (C) Tris; (D) borate.

method (curve B). The enzyme electrode prepared by using the glutaraldehyde coupling procedure on pig intestine showed linearity only for 5—100 mg dl^{-1} creatinine (curve D). As usually noted, the enzyme electrodes became slightly more sensitive after 1 day of storage or use (curve C). As little as 0.6 mg creatinine dl^{-1} could be detected.

The immobilized and soluble creatinine deiminase activity was measured over the pH range 7—10. The response of the creatinine electrode depends on two factors, the optimum conditions for the enzyme reaction and the best conditions for the electrode to sense the ammonia liberated. Because the amount of ammonia present at equilibrium is pH-dependent, the higher the pH, the higher the ammonia concentration, and hence the larger the response. The maximum activity of the enzyme also depends on pH; the optimum pH value has been reported to be 8 for the soluble enzyme and 7 for the nylon-tube immobilized enzyme [24]. Phosphate was reported to be the best buffer, phosphate being an activator for the microbial enzyme [24].

The pH optimum for the creatinine electrode was 8.5—8.7, phosphate and pyrophosphate proving better buffers than Tris or borate (Fig. 2). Hence a 0.1 M phosphate buffer, pH 8.7, which gave slightly greater sensitivity, was used in further studies. Tris gave high backgrounds at the ammonia electrode, so this buffer should be avoided.

The Michaelis constant for the immobilized enzyme was determined from a Lineweaver—Burk plot of $(\text{rate})^{-1}$ vs. $[\text{creatinine}]^{-1}$ and was found to be 5.5 mM, compared with the value of 1.8 mM reported for the soluble enzyme by the manufacturers.

The enzyme electrode was found to be highly selective for the assay of creatinine. No response of the electrode to creatine, urea, arginine, cytosine, guanine or adenine (100 mg dl^{-1}) was observed. The only important interference is ammonia, to which the basic sensor responds (see below).

STABILITY AND RESPONSE TIME OF THE SYSTEM

The ammonia electrode was quite stable once equilibrium was reached, a drift of less than 1 mV was found over several minutes. Only 2—5 min was required for 95% response with the enzyme electrode, and a steady state was usually reached within 10 min for each sample analyzed. In order to speed up the measurement time, the rate of formation of ammonia can be measured; in this case satisfactory results are usually obtained in about 2 min. The long recovery times of commercial ammonia electrodes pose well-known problems. With the ammonia sensor used here, the recovery time was decreased so that only 5—10 min was required to reach a steady baseline after use, depending on the concentration of creatinine to which the electrode had been exposed. Thus, up to 10 samples/hour can be assayed. The detection limit of the electrode is about 0.6 mg dl^{-1}. Thus, serum samples can be diluted and good results still obtained.

The long-term stability of two creatinine electrodes is shown in Fig. 3.

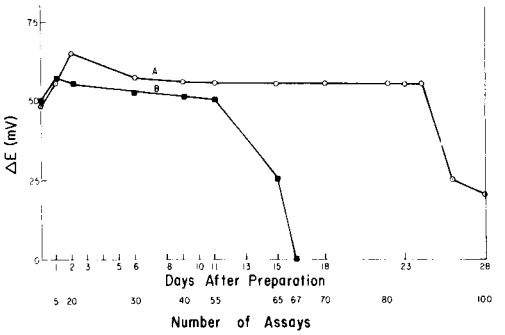

Fig. 3. Long-term stability of creatinine electrodes: (A) collagen membrane; (B) pig intestine membrane.

Between measurements, the electrodes were kept at 4°C. The response of each electrode to a 50-mg dl^{-1} sample of creatinine in pH 8.7 phosphate buffer over 28 days was studied. On each day shown, the electrode was used for at least 5 measurements. As previously observed with enzyme electrodes, the response increased after the first day, reached a maximum, and decreased gradually with storage or use. The electrode could be reliably used over a period of 3 weeks and about 100 assays.

The precision of response was also reasonable. When four replicate creatinine samples (1.0 and 5.0 mg dl^{-1}) were measured, the average within-day relative standard deviation was <2%, and the day-to-day variation about 2.5%.

Serum creatinine measurements

Increasing amounts of creatinine were added to a sample of reconstituted freeze-dried control sera which had a stated creatinine content determined with use of the Jaffé method [1]. These samples were assayed by the creatininase electrode method. The recoveries obtained are shown in Table 1. The mean recovery was 101%.

TABLE 1

Recovery studies for added creatinine

Creatinine concentration (mg dl^{-1})			Recovery (%)
Added	Expected[a]	Found	
0.0	1.54	1.54	100
1.0	2.54	2.60	102
2.0	3.54	3.61	102
5.0	6.54	6.65	102
10.0	11.54	11.6	100.5

[a] 1.54 mg dl^{-1} originally present in serum.

Interference of ammonia. The normal range of ammonia in blood serum is reported to be 40—80 $\mu g\ dl^{-1}$ ($2.4—4.8 \times 10^{-5}$ M) and for a patient with hepatic coma the level can go as high as 400 $\mu g\ dl^{-1}$. The ammonia content of freshly drawn blood rises rapidly on standing (because of enzymatic deamination of labile compounds like glutamine) to two or three times its normal level [25]. In the present method, blood is diluted (1 + 4) with buffer, so that the normal level of ammonia is less than 10^{-5} M, which is not detected by the electrode. No problems were encountered, for example, with the normal control serum sample (Unitrol), which contained about 4×10^{-5} M ammonium ions. In any event, a test for the ammonium level present in serum should first be done, using an ammonia sensor with a layer of inert protein. If the level is higher than normal, a further dilution with buffer can be done (up to 1 + 9). This is possible because of the high sensitivity of the new creatinine probes.

The authors thank Mr. Loic Blum who assisted in preparation of some of the enzyme membranes. G. G. Guilbault thanks CNRS for financial support and Professor D. Gautheron for making his visit possible.

REFERENCES

1 M. Jaffé, Z. Physiol. Chem., 10 (1886) 391.
2 D. S. Young, L. C. Pestanen and V. Gibberman, Clin. Chem., 21 (1975) 2860.
3 S. Narayanan and H. D. Appleton, Clin. Chem., 18 (1972) 270.
4 J. A. Owen, B. Iggo, F. J. Scandrett and C. R. Stewart, Biochem. J., 58 (1954) 426.
5 E. Knoll and D. Stamm, Z. Klin. Chem. Klin. Biochem., 8 (1970) 582.
6 R. J. Mitchell, Clin. Chem., 19 (1973) 408.
7 D. Heingard and G. Tiderstrom, Clin. Chim. Acta, 43 (1973) 305.
8 P. H. Lokha, V. Chantarothipol and A. Wongvibulsin, Clin. Chem., 24 (1978) 1578.
9 J. C. Cook, Clin. Chim. Acta, 32 (1971) 485.
10 E. Knoll, F. Rebel and H. Wisser, J. Clin. Chem. Clin. Biochem., 16 (1978) 239.
11 Boehringer Mannheim Corp. German Patents P2122294.6 and P2122298.0; Biochemica Information, Boehringer Mannheim Corp. Mannheim, 1974, p. 65.
12 G. Moss, R. Bondak and D. Buzzelli, Clin. Chem., 21 (1975) 1422.
13 A. Wahlefeld, G. Herz and H. U. Bergmeyer, Scand. J. Clin. Lab. Invest., 29, suppl. 126 (1972) Abstract 30.1.
14 J. Szulmajster, J. Bacteriol., 75 (1958) 633.
15 F. Lim, Clin. Chem., 20 (1974) 871.
16 S. Chen, S. S. Kuan and G. G. Guilbault, Clin. Chim. Acta, 100 (1980) 21.
17 M. Meyerhoff and G. A. Rechnitz, Anal. Chim. Acta, 85 (1976) 277.
18 G. G. Guilbault, S. P. Chen and S. S. Kuan, Anal. Lett., 13 (1980) 1607.
19 P. R. Coulet, J. H. Julliard and D. C. Gautheron, French Patent 2 235 133 (1973); Biotechnol. Bioeng., 16 (1974) 1055.
20 D. R. Thevenot, R. Sternberg, P. R. Coulet, J. Laurent and D. C. Gautheron, Anal. Chem., 51 (1979) 96.
21 P. R. Coulet, R. Sternberg and D. R. Thevenot, Biochim. Biophys. Acta, 612 (1980) 317.
22 P. R. Coulet and C. Bertrand, Anal. Lett., 12 (1979) 581.
23 C. Bertrand, P. R. Coulet and D. C. Gautheron, Anal. Chim. Acta, 126 (1981) 23.
24 S. Canbiaghi, D. Brassi, E. Murador, G. Aimo, A. Caropresco and G. Rosso, Clin. Chem., 28 (1982) 1461.
25 N. Tietz, Fundamentals of Clinical Chemistry, 2nd edn., W. B. Saunders, Philadelphia, p. 1052.

Analytica Chimica Acta, 152 (1983) 229—237
Elsevier Science Publishers B.V., Amsterdam — Printed in The Netherlands

TWO-PHASE BUFFER SYSTEMS WITH DIPROTIC ACIDS

T. J. JANJIĆ*, E. B. MILOSAVLJEVIĆ, W. NANAYAKKARA and M. K. SRDANOVIĆ
Chemical Institute, Faculty of Sciences, University of Belgrade, P.O. Box 550, 11001 Belgrade (Yugoslavia)

(Received 27th October 1982)

SUMMARY

Possible equilibria in two-phase buffer systems with diprotic acids are discussed and a method for evaluation of the relevant apparent acidity and partition constants is proposed. The mode of action of these buffers is described and equations for the dependence of buffer capacity on pH and for evaluation of dilution effects are derived. These equations were verified for two-phase buffer systems containing 1,2-benzenedicarboxylic acid, morphine hydrochloride or cinchonine dihydrochloride with an appropriate organic solvent. Agreement between theory and actual measurement was excellent.

Two-phase buffer systems containing acid—base pairs of monoprotic acids have already been investigated and it has been shown that these systems have important advantages over classical (single-phase) buffers [1—4]. This paper extends these earlier studies to two-phase buffer systems containing acid-base pairs of diprotic acids.

THEORY

In all the systems considered here the aqueous phase contains 1 M sodium chloride. Depending on the charge of the diprotic acid, a distinction must be made between three types of two-phase buffers.

Buffer type I. This contains the undissociated acid (H_2A), the ampholyte (HA^-), and the base anion (A^{2-}). In this type of buffer, there are protolytic equilibria and partition of the undissociated acid between organic and aqueous phases, and the ion-pairs Na^+HA^- and $Na_2^{2+}A^{2-}$ may also be extracted into the organic phase.

Buffer type II. This contains the acid cation (H_2A^+), ampholyte (HA), and the base anion (A^-). Protolytic equilibria and partition of the ampholyte between two phases must be considered, and extraction equilibria involving the ion-pairs $H_2A^+Cl^-$ and Na^+A^- are possible.

Buffer type III. This contains the acid cation (H_2A^{2+}), ampholyte (HA^+), and uncharged base (A). In addition to the protolytic equilibria and partition of the uncharged base, the ion-pairs $H_2A^{2+}Cl_2^{2-}$ and HA^+Cl^- may also be extracted into the organic phase.

0003-2670/83/$03.00

Other possible equilibria, including the extraction of $H_2A^+A^-$ [5], formation of half salts in type II buffers [6], dissociation of ion-pairs in the organic phase [7], dimerization or oligomerization of any species in the organic phase [7—10], adduct formation between ion-pairs and uncharged ampholyte in type II buffers or any other adduct formation [8, 10], are not considered here, because they are unlikely to occur to a significant extent in the two-phase systems investigated.

The presence of the large concentration of sodium and chloride ions compared to the concentrations of the other species simplifies the treatment of the processes involving the formation and extraction of ion-pairs. These equilibria can therefore be considered as simple partition of the charge-carrying species. In order to unify the mathematical considerations of all three types of buffer, it is necessary to omit the charges of individual ions (except for H_3O^+ and OH^-) and to denote uniformly the species with the same degree of protonation in the organic phase, irrespective of whether they are ion-pairs or neutral molecules. For example, $(H_2A)_o$ is used uniformly to denote the species $(H_2A)_o$, $(H_2A^+Cl^-)_o$ and $(H_2A^{2+}Cl_2^{2-})_o$ in buffers of type I, II and III, respectively (subscript o denotes the organic phase).

The equilibria in all three types of two-phase buffer with diprotic acids can then be summarized as in Fig. 1.

Determination of the relevant equilibrium constants

The acidities of diprotic acids in the aqueous phase of the two-phase medium are given by the apparent acidity constants defined in the following manner:

$$K^{app}_{H_2A} = a_{H_3O^+} C^{app}_{HA}/C^{app}_{H_2A}\,;\; K^{app}_{HA} = a_{H_3O^+} C^{app}_{A}/C^{app}_{HA}$$

where $C^{app}_{H_2A} = \alpha(C_{H_2A})_o + C_{H_2A}$, $C^{app}_{HA} = \alpha(C_{HA})_o + C_{HA}$, and $C^{app}_{A} = \alpha(C_A)_{org} + C_A$. In these definitions, α is the ratio of the organic and aqueous phase volumes ($\alpha = V_o/V_w$). As may be seen, the apparent concentration of a component in the aqueous phase is the concentration that would exist if the total amount of that component, in the entire system, were dissolved only in the aqueous phase. It follows that the apparent acidity constants and the corresponding acidity constants, defined as $K_{H_2A} = a_{H_3O^+} C_{HA}/C_{H_2A}$ and $K_{HA} = a_{H_3O^+} C_A/C_{HA}$, are interrelated by the equations

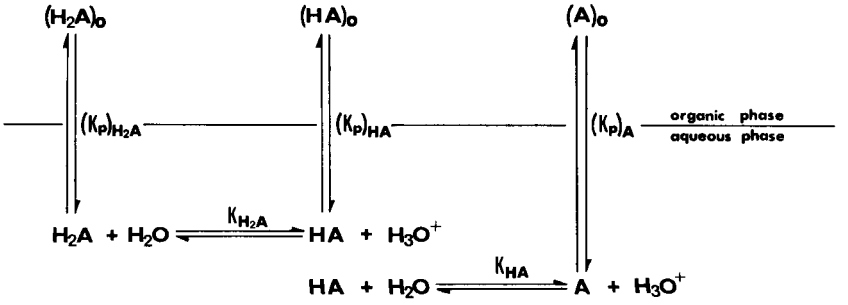

Fig. 1. Equilibria in a two-phase buffer with a diprotic acid.

$$K^{app}_{H_2A} = K_{H_2A}(1 + \alpha(K_p)_{HA})/(1 + \alpha(K_p)_{H_2A}) \quad (1)$$

$$K^{app}_{HA} = K_{HA}(1 + \alpha(K_p)_A)/(1 + \alpha(K_p)_{HA}) \quad (2)$$

where $(K_p)_{H_2A} = (C_{H_2A})_o/C_{H_2A}$, $(K_p)_{HA} = (C_{HA})_o/C_{HA}$ and $(K_p)_A = (C_A)_o/C_A$.

The apparent acidity constants in the corresponding two-phase medium, which are necessary for evaluation of the theoretical buffer curves $\beta = f(\mathrm{pH})$, as well as for calculation of the partition constants $(K_p)_{H_2A}$, $(K_p)_{HA}$ and $(K_p)_A$, are determined in much the same way as acidity constants of diprotic acids in aqueous medium [11]. In the two-phase medium, the apparent formation function $\bar{n}^{app}$ is defined as follows:

$$\bar{n}^{app} = (2C^{app}_{H_2A} + C^{app}_{HA})/C^{app}_{tot}$$

where C^{app}_{tot} is the apparent total concentration of the diprotic acid. This function may be evaluated from the experimental data obtained by pH titration of the diprotic acid in the appropriate two-phase medium. The apparent acidity constants, $K^{app}_{H_2A}$ and K^{app}_{HA}, can be determined for well-separated ionization processes from the equations

$$pK^{app}_{H_2A} = pH - \log[(2 - \bar{n}^{app})/(1 - \bar{n}^{app})] \quad (3)$$

$$pK^{app}_{HA} = pH - \log[(1 - \bar{n}^{app})/\bar{n}^{app}] \quad (4)$$

and for overlapping ionization processes, from

$$\bar{n}^{app}/a_{H_3O^+}(1 - \bar{n}^{app}) = (1/K^{app}_{HA}) + a_{H_3O^+}(2 - \bar{n}^{app})/K^{app}_{H_2A}K^{app}_{HA}(1 - \bar{n}^{app}) \quad (5)$$

The values of the apparent acidity constants depend, of course, on the ratio of the equilibrium phase volumes so that the value of this ratio must be kept constant during a titration.

In order to calculate the dilution effects in two-phase buffers, the values of the partition constants $(K_p)_{H_2A}$, $(K_p)_{HA}$ and $(K_p)_A$ must be known. These constants may be evaluated from the data obtained by titrations of the diprotic acid in two-phase media with various ratios of the equilibrium phase volumes. Transformations of Eqns. (1) and (2) give the following relationships:

$$[1 - \mathrm{antilog}(pK^{app}_{H_2A} - pK_{H_2A})]/\alpha = (K_p)_{HA}\,\mathrm{antilog}(pK^{app}_{H_2A} - pK_{H_2A}) - (K_p)_{H_2A} \quad (6)$$

$$[1 - \mathrm{antilog}(pK^{app}_{HA} - pK_{HA})]/\alpha = (K_p)_A\,\mathrm{antilog}(pK^{app}_{HA} - pK_{HA}) - (K_p)_{HA} \quad (7)$$

The three partition constants can be evaluated from the intercepts and slopes of the straight lines obtained when the left-hand sides of Eqns. (6) and (7) are plotted against $\mathrm{antilog}(pK^{app}_{H_2A} - pK_{H_2A})$ and $\mathrm{antilog}(pK^{app}_{HA} - pK_{HA})$, respectively.

Consideration of Eqns. (1) and (2) shows that for very large values of the three above partition constants, the apparent acidity constants $K^{app}_{H_2A}$ and

K_{HA}^{app} are changed only slightly by variation in α. Accordingly, when this is the case, the above-described method is not applicable for the determination of these partition constants.

The constant $(K_p)_{HA}$ may be evaluated from Eqn. (6) or (7). The agreement between the values obtained from the different equations is an additional criterion for the applicability of the method to a given two-phase system.

Functional dependence of buffer capacity β on pH

In a two-phase system with a diprotic acid, the mass-balance equation is

$$C_{tot}^{app} = C_{H_2A}^{app} + C_{HA}^{app} + C_{A}^{app} \tag{8}$$

The following relationship is also valid:

$$C_b = C_{HA}^{app} + 2\,C_{A}^{app} + C_{OH^-} - C_{H_3O^+} \tag{9}$$

where C_b is the concentration of the strong base added to the two-phase system.

From Eqns. (8) and (9), as well as from the expressions for the apparent acidity constants:

$$C_b = [(K_{H_2A}^{app} C_{tot}^{app} a_{H_3O^+} + 2\,K_{H_2A}^{app} K_{HA}^{app} C_{tot}^{app})/(a_{H_3O^+}^2 + K_{H_2A}^{app} a_{H_3O^+} + K_{H_2A}^{app} K_{HA}^{app})] + C_{OH^-} - C_{H_3O^+} \tag{10}$$

Differentiation, $dC_b/da_{H_3O^+}$, of Eqn. (10) and replacement of $da_{H_3O^+}$ by $-2.303\ a_{H_3O^+}\ dpH$, gives the following relationship for buffer capacity of the investigated diprotic acid in the two-phase medium:

$$\beta = 2.303\{C_{tot}^{app} K_{H_2A}^{app} [(a_{H_3O^+}^3 + 4\,K_{HA}^{app} a_{H_3O^+}^2 + K_{H_2A}^{app} K_{HA}^{app} a_{H_3O^+})/(a_{H_3O^+}^2 + K_{H_2A}^{app} a_{H_3O^+} + K_{H_2A}^{app} K_{HA}^{app})^2] + C_{H_3O^+} + C_{OH^-}\} \tag{11}$$

Dilution effect

The dilution effect $\Delta pH_{1/2}$ is defined as $\Delta pH_{1/2} = pH_{ad} - pH_{bd}$, where subscripts *bd* and *ad* denote the conditions before and after two-fold dilution of the aqueous phase. From the mass-balance equation and from the partition constant expressions:

$$C_{tot}^{app} = C_A\{1 + \alpha(K_p)_A + [a_{H_3O^+}/(K_a)_{HA}] + [\alpha(K_p)_{HA} a_{H_3O^+}/(K_a)_{HA}] + [a_{H_3O^+}^2/(K_a)_{H_2A}(K_a)_{HA}] + [\alpha(K_p)_{H_2A} a_{H_3O^+}^2/(K_a)_{H_2A}(K_a)_{HA}]\} \tag{12}$$

If the terms within curly brackets are denoted by R, Eqn. (12) simplifies to $C_{tot}^{app} = C_A\,R$.

From the charge-balance equation, along with the expressions for $(K_p)_{HA}$ and $(K_p)_A$:

$$C_b = C_A\{[a_{H_3O^+}/(K_a)_{HA}] + [\alpha(K_p)_{HA} a_{H_3O^+}/(K_a)_{HA}] + 2 + 2\alpha(K_p)_A\} + C_{OH^-} - C_{H_3O^+} \tag{13}$$

This expression may be simplified to $C_b = C_A S + C_{OH^-} - C_{H_3O^+}$.

When the aqueous phase is diluted two-fold, then $2(C_{tot}^{app})_{ad} = (C_{tot}^{app})_{bd}$. From this equation, along with the simplified forms of Eqn. (12) and (13):

$$2[(C_b)_{ad} - (C_{OH^-})_{ad} + (C_{H_3O^+})_{ad}]R_{ad}/S_{ad} = [(C_b)_{bd} - (C_{OH^-})_{bd} + (C_{H_3O^+})_{bd}]R_{bd}/S_{bd} \quad (14)$$

The right-hand side of this expression is known. To get the theoretical $\Delta pH_{1/2}$ value it is necessary to find, by iteration, the pH value for which Eqn. (14) is valid, bearing in mind that after two-fold dilution of the aqueous phase, $2(C_b)_{ad} = (C_b)_{bd}$.

EXPERIMENTAL

All titrations were done under a nitrogen atmosphere to exclude the effects of carbon dioxide. For calculations, suitable programs were used with a Texas Instruments TI 59 programmable calculator. The ionic strength of the aqueous phase was kept constant by addition of sodium chloride. Other experimental arrangements were the same as described earlier [1].

To prove the validity of the theoretical considerations, three diprotic acids were investigated: 1,2-benzenedicarboxylic acid (buffer type I), morphine hydrochloride (buffer type II) and cinchonine • 2 HCl (buffer type III). In all the experiments described below, two organic solvents were used: 1-octanol for systems with 1,2-benzenedicarboxylic acid and cinchonine, and tributylphosphate for systems containing morphine.

RESULTS AND DISCUSSION

Determination of the relevant partition constants

The effects of a change in α on the function $\bar{n}^{app} = f(pH)$ for the three diprotic acids studied are presented in Figs. 2 and 3. From Figs. 2 and 3A, it can be seen that for systems with 1,2-benzenedicarboxylic acid and cinchonine, two ionization processes overlap so that Eqn. (5) had to be used for calculating the apparent acidity constants. For the system with morphine (Fig. 3B), the ionization processes are well separated and Eqns. (3) and (4) could be used to evaluate the apparent acidity constants.

The partition constants $(K_p)_{H_2A}$, $(K_p)_{HA}$ and $(K_p)_A$ for the three systems were then evaluated from Eqns. (6) and (7). The fact that the $(K_p)_{HA}$ value could be obtained from one of these equations and then substituted into the other enables one of the acidity constants to be evaluated approximately if the other is obtainable in the usual manner. This method is suitable for evaluating the acidity constant for an ionization process in which the uncharged component of the acid-base pair is practically insoluble in water; as is known, the usual methods based on titration of the given acid in aqueous medium cannot be applied in such cases. An approximate K_{HA} value for cinchonine • 2 HCl was obtained through the above-described method.

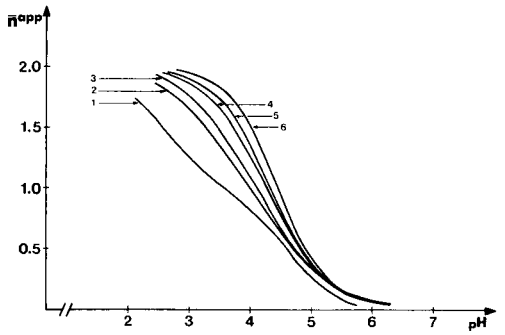

Fig. 2. Apparent formation functions for 1,2-benzenedicarboxylic acid in the two-phase system with 1-octanol; I = 1 (NaCl), T = 25°C. Curve (1) α = 0, C_{tot} = 0.0261 M. For other curves C_{tot}^{app} varied from 0.0236 M to 0.0472 M: (2) α = 0.5; (3) α = 1; (4) α = 2; (5) α = 3; (6) α = 5.

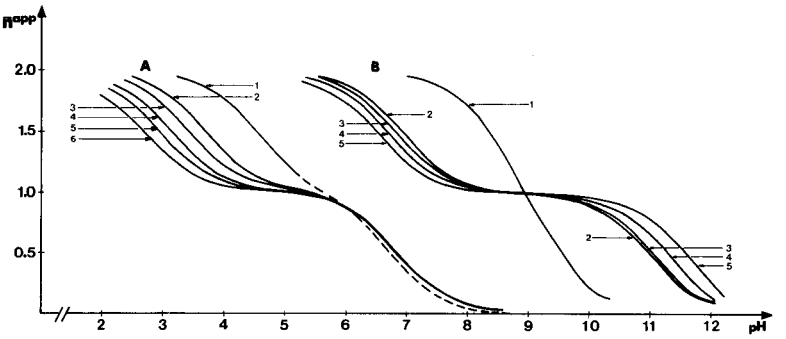

Fig. 3. Apparent formation functions for (A) cinchonine • 2 HCl in the two-phase system with 1-octanol, and (B) morphine • HCl with tributylphosphate; I = 1 (NaCl), T = 25°C. For (A): (1) α = 0, C_{tot} = 0.0099 M (the dashed part of the curve was calculated on the basis of the approximated pK_{HA} value, see text); for other curves C_{tot}^{app} = 0.0494 M and (2) α = 0.5; (3) α = 1; (4) α = 2; (5) α = 3; (6) α = 5. For (B): (1) α = 0, C_{tot} = 0.0010 M; for other curves C_{tot}^{app} varied from 0.0485 M to 0.0570 M: (2) α = 1.7; (3) α = 2.3; (4) α = 3.6; (5) α = 5.1.

The partition constants and other pertinent data for the systems examined are presented in Tables 1 and 2.

Functional dependence of buffer capacity β on pH

In Fig. 4, the functional dependences of buffer capacity on pH for the three two-phase buffer systems studied are presented, along with theoretical buffer curves for classical one-phase buffers with the same acids. It can be seen that the experimental buffer capacity values are in very good agreement with those calculated theoretically from Eqn. (11). Further, the one-phase buffers have smaller buffer capacities because of the poor water solubility of the uncharged component of the acid—base pairs of the corresponding acid

TABLE 1

Values of acidity constants and apparent acidity constants[a] of the diprotic acids studied (I = 1 (NaCl), T = 25°C)

α[b]	1,2-Benzenedicarboxylic		Morphine · HCl		Cinchonine • 2 HCl	
	$pK^{app}_{H_2A}$	pK^{app}_{HA}	$pK^{app}_{H_2A}$	pK^{app}_{HA}	$pK^{app}_{H_2A}$	pK^{app}_{HA}
0.0	2.591 ± 0.004	4.583 ± 0.005	8.477 ± 0.002	9.452 ± 0.006	4.551 ± 0.002	6.7 ± 0.3
0.5	3.319 ± 0.007	4.67 ± 0.01			3.713 ± 0.005	6.872 ± 0.005
1.0	3.549 ± 0.001	4.646 ± 0.006			3.456 ± 0.008	6.839 ± 0.008
1.7			6.938 ± 0.004	11.001 ± 0.006		
2.0	3.839 ± 0.003	4.693 ± 0.009			3.135 ± 0.009	6.825 ± 0.009
2.3			6.825 ± 0.002	11.015 ± 0.009		
3.0	3.995 ± 0.004	4.672 ± 0.009			2.954 ± 0.009	6.84 ± 0.01
3.6			6.685 ± 0.002	11.284 ± 0.007		
5.0	4.238 ± 0.004	4.684 ± 0.005			2.69 ± 0.01	6.85 ± 0.01
5.1			6.506 ± 0.005	11.594 ± 0.007		

[a]The constants are given in the form $\bar{x} \pm t(P;f)\sigma/n^{1/2}$, where $\bar{x}$ is the mean value obtained by the least-squares method, $t(P;f)$ is Student's factor for P = 95%, $f = n - 2$ degrees of freedom and $\sigma/n^{1/2}$ is the standard deviation of the mean [12]. [b]Ratio of phase volumes at equilibrium. When $\alpha = 0$, the acidity and apparent acidity constants are identical.

TABLE 2

Values of the partition constants[a] of the systems studied (I = 1 (NaCl), T = 25°C)

Diprotic acid	$(K_p)_{H_2A}$	$(K_p)_{HA}$	$(K_p)_A$
1,2-Benzenedicarboxylic	8.4 ± 0.7	0	0
Morphine · HCl	$5 \times 10^{-2} \pm 1 \times 10^{-2}$	21 ± 4	0
Cinchonine · 2 HCl	0	11.8 ± 0.5	9.1 ± 0.7

[a]The results are represented in the same way as in Table 1.

(for the systems with morphine and cinchonine, the right-hand ordinate in Fig. 4B, C for the classical buffers is reduced tenfold compared to the left-hand ordinate).

Dilution effect

To prove the validity of the equations derived in the theoretical part, actual dilution effects in the three two-phase buffers were investigated. The results are summarized in Table 3. The agreement between the experimentally measured pH values and those calculated from Eqn. (14) is very good.

Conclusion

It can be concluded that the experimental evidence completely confirms the validity of the mathematical considerations based on the proposed model for two-phase buffers with diprotic acids. It has also been shown that these three diprotic acids can be determined by pH titrations in the appropriate two-phase media.

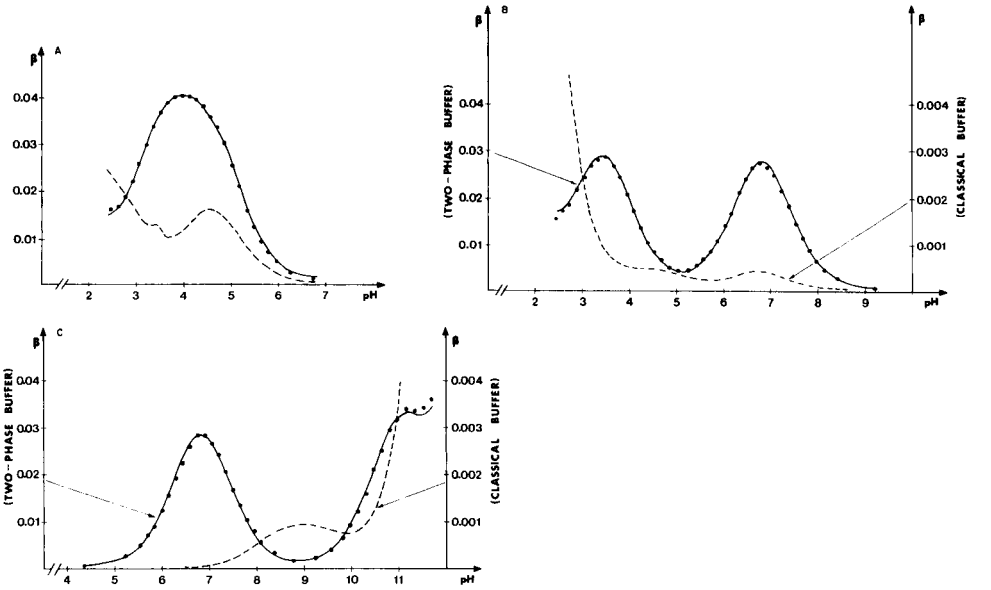

Fig. 4. Functional dependences of buffer capacity β on pH for buffers containing acid–base pairs of (A) 1,2-benzenedicarboxylic acid, (B) morphine hydrochloride, and (C) cinchonine dihydrochloride. (—) Theoretical buffer curve for the two-phase system calculated from Eqn. (11). (···) Experimental data points: (A) α = 1, C_{tot}^{app} = 0.0488 M; (B) α = 2.3, C_{tot}^{app} = 0.0495 M; (C) α = 1, C_{tot}^{app} = 0.0486 M. (---) Theoretical buffer curve for the corresponding classical aqueous buffer (solubilities of 1,2-benzenedicarboxylic acid, morphine and cinchonine in 1 M sodium chloride are about 0.026 M, 1×10^{-3} M, and 1×10^{-4} M, respectively). The data are valid for I = 1 (NaCl), T = 25°C.

TABLE 3

Dilution effects in two-phase buffers with diprotic acids (I = 1 (NaCl), T = 25°C)

Acid	α[a]	pH value				
		Before dilution	On 2-fold dilution of aq. phase[b]		On 2-fold dilution of both phases[b]	
			Measured	Calc.	Measured	Calc.
1,2-Benzenedicarboxylic	1	3.00	2.83	2.84	3.01	3.04
		3.51	3.30	3.31	3.51	3.52
		4.05	3.92	3.91	4.05	4.05
		4.60	4.56	4.56	4.61	4.60
		5.00	5.01	4.99	5.02	5.00
Morphine • HCl	2.3	6.00	6.27	6.29	—[c]	—[c]
		6.41	6.68	6.70		
		6.83	7.10	7.12		
		7.25	7.54	7.54		
		7.69	7.97	7.97		
		10.33	10.01	10.02		
Cinchonine • 2 HCl	1	2.85	3.14	3.12	2.88	2.91
		3.49	3.76	3.76	3.50	3.50
		4.24	4.51	4.50	4.24	4.24
		5.02	5.20	5.18	5.02	5.02
		6.75	6.77	6.74	6.75	6.75
		7.59	7.60	7.58	7.58	7.59

[a]Before dilution. [b]Related to the initial phase volume. [c]These experiments were not done because tributylphosphate contained too much free acid.

The authors are grateful to the Serbian Republic Research Fund for financial support. The paper was presented in part at the 24th Annual Meeting of the Serbian Chemical Society, Belgrade, in January 1982.

REFERENCES

1 T. J. Janjić and E. B. Milosavljević, Anal. Chem., 50 (1978) 597; Bull. Soc. Chim. Beograd, 43 (1978) 553.
2 T. J. Janjić, E. B. Milosavljević and M. K. Srdanović, Anal. Chim. Acta, 107 (1979) 359.
3 T. J. Janjić and E. B. Milosavljević, Anal. Chim. Acta, 120 (1980) 101; Bull. Soc. Chim. Beograd, 46 (1981) 297.
4 T. J. Janjić, E. B. Milosavljević and W. Nanayakkara, Analusis, 10 (1982) 197.
5 R. A. Hux, Su Puon and F. F. Cantwell, Anal. Chem., 52 (1980) 2388.
6 G. Chuchani, J. A. Hernández and J. Zabicky, Nature, 207 (1965) 1385.
7 G. Schill, in J. A. Marinsky and Y. Marcus (Eds.), Ion Exchange and Solvent Extraction, Vol. 6, Dekker, New York, 1974, Ch. 1.
8 K. Gustavii, P. A. Johansson and A. Brändström, Acta Pharm. Suec., 13 (1976) 391.
9 R. R. Grinstead, Solvent Extr. Chem., Proc. Int. Conf., Göteborg, 1966, Wiley, New York, 1967, p. 426.
10 E. Högfeldt, Solvent Extr. Chem., Proc. Int. Conf., Jerusalem, 1968, Wiley, New York, 1969, p. 157.
11 F. J. C. Rossotti and H. Rossotti, The Determination of Stability Constants, McGraw-Hill, New York, 1961, p. 110.
12 J. M. Wilson, R. J. Newcombe, A. R. Denaro and R. M. W. Rickett, Experiments in Physical Chemistry, 2nd edn., Pergamon, Oxford, 1968, p. 364.

Analytica Chimica Acta, 152 (1983) 239—245
Elsevier Science Publishers B.V., Amsterdam — Printed in The Netherlands

DETERMINATION OF ACIDITY CONSTANTS BY A SOLUBILITY METHOD

YOSHIKIYO MOROI* and RYOHEI MATUURA

Department of Chemistry, Faculty of Science, Kyushu University 33, Fukuoka 812 (Japan)

(Received 17th January 1983)

SUMMARY

Details are given of a method for the determination of dissociation constants of acids by simple solubility measurements. The method is particularly useful for dibasic acids whose solubility in aqueous solution of low pH is too low to be determined precisely by normal analytical methods. The dissociation constants of 1-naphthoic acid, 2-naphthol, diphenic acid and terephthalic acid are reported. The values generally agree well with literature data.

The dissociation of chemical species which occurs on its dissolution or by addition of other species to its solution gives rise to important changes in the physico-chemical properties of the solution. To clarify the causes of these changes, a knowledge of the degree of dissociation is essential and many methods have been used to determine such dissociation constants as precisely as possible [1, 2].

The acidity constants (K_a) of acids are usually determined by titrimetric, electrochemical or spectrophotometric methods [3]. Other methods, using colligative properties, are also available. However, these methods have, in general, a disadvantage of requiring fairly high concentrations of acid. In a previous paper [4], an "isoextraction" method was introduced for pK_a determination for acids slightly soluble in water. This method is particularly valuable for studying the association equilibria in dilute solutions [5, 6]. Indeed, the method works well for pK_a determinations but becomes less useful when chemical decomposition or reaction with other species in the organic phase occurs. In contrast, a direct solubility method, which is a variation of the isoextraction method from a thermodynamic point of view, has an advantage over the isoextraction method in that there is no reaction of species in the solid phase present; only its dissolution in the aqueous phase takes place. Thus, the solubility method should be very useful for studying the physico-chemical solution properties of acids too insoluble to be investigated by other methods. Detailed consideration will be given to dibasic acids sparingly soluble in aqueous solutions at low pH. The K_a values of monobasic and dibasic acids thus obtained will be presented and compared with literature data.

0003-2670/83/$03.00

THEORY

Acidity constants K_{ai} are equilibrium constants for reactions of the following stepwise type:

$$AH_n \overset{K_{ai}}{\rightleftharpoons} AH_{n-1} + H^+; \quad AH_1 \overset{K_{an}}{\rightleftharpoons} A + H^+$$

(most charges are omitted for convenience). The dissociation constants are defined as $K_{ai} = a_{AH_{n-i}} a_{H^+} / a_{AH_{n-i+1}}$ where a_j is the activity of species j. The total number of components of this system is $(n + 3)$ including water, the number of phases is one, and the number of equilibrium equations is n. Hence, at constant temperature and pressure, two other intensive variables can be selected to specify the thermodynamic system. However, the electroneutrality of the solution reduces the freedom by one, so that only one intensive variable remains. Even if another two components, hydroxide ion and air, are taken into account, this degree of freedom still remains one because of the presence of the air phase and the dissociation equilibrium equation of water. A hydrogen ion concentration can be selected as the variable which leads to the total acid concentration. Thus, the pK_a value can be determined from the variation of the hydrogen ion concentration with total acid concentration (Ostwald's dilution law). However, when the solubility method is employed, a solid phase of acid coexists with the aqueous phase. It reduces the degree of freedom by one resulting in zero degrees of freedom at constant temperature and pressure, and the concentrations of species AH_j cannot be changed without introduction of other components into the system. Hence, the determination of the pK_a value requires solubility measurements at different pH values by introduction of other chemical species. The key point of the solubility method is that the concentration of undissociated AH_n in the aqueous phase remains constant at constant temperature and pressure, regardless of the introduction of any other chemical species into the aqueous phase, so long as the total ionic strength is kept constant and low, because AH_n in the aqueous phase is in equilibrium with solid AH_n. Thus the solubility method is a variation of the isoextraction method.

For a monobasic acid (AH)

As the concentration of A in the aqueous phase depends on the pH, the total analytical concentration of the acid can be expressed as

$$[A_t] = [AH] + [A] = [AH] + [AH]\, K_{a1}/\gamma_A a_{H^+}$$

where the activity of the nonionic species AH is assumed to be equal to its concentration. Because the AH concentration and γ_A, the activity coefficient of A, remain constant at constant ionic strength, this equation predicts a linear relationship between $[A_t]$ and $1/a_{H^+}$. Dividing the slope by the intercept of the line gives the value of K_{a1}/γ_A.

For a dibasic acid (AH_2)

The total analytical concentration of the acid is

$$[A_t] = [AH_2] + [AH_1] + [A] = [AH_2]\{1 + (K_{a1}/\gamma_{AH})(1/a_{H^+}) + (K_{a1}K_{a2}/\gamma_A)(1/\gamma_A)(1/a_{H^+})^2\} \quad (1)$$

Because every parameter except a_{H^+} of the right-hand side of this equation is constant for the above reason, $[A_t]$ changes inversely with $(1/a_{H^+})^2$. If the K_{a1} and K_{a2} values differ greatly, Eqn. (1) can be divided into two parts, one for $pH \leqslant pK_{a1}$, the other for $pK_{a1} \ll pH < pK_{a2}$. In the first region a dibasic acid can be treated just like a monobasic acid giving the equation already provided [7, 8]. The problem, however, is to evaluate K_{a1} and K_{a2} when K_{a1} is close to K_{a2}. From Eqn. (1) the values of K_{a1} and K_{a2} can be obtained from the three coefficients of the graph $\{A + B(1/a_{H^+}) + C(1/a_{H^+})^2\}$ as

$$K_{a1} = \gamma_{AH}(B/A) \text{ and } K_{a2} = (\gamma_A/\gamma_{AH})(C/B) \quad (2)$$

Thus, the precise determination of the total concentration of the acid $[A_t]$ in aqueous phases of different pH and the successive measurement of the three coefficients are vital requirements for the estimation of K_{a1} and K_{a2}. The activity coefficients γ_{AH} and γ_A can be estimated by the Debye–Hückel approximation [9]. When the solubility of an acid at low pH is relatively high, i.e., $>10^{-4}$ mol dm^{-3}, determination of $[AH_2]$ in Eqn. (1) is not difficult. The problem arises when $[AH_2]$ is too small to be measured precisely by the usual analytical methods.

For dibasic acids with solubilities of $<10^{-4}$ mol dm^{-3} at low pH, therefore, the precise determination of $[AH_2]$ is difficult, but its correct value is indispensable for the determination of K_{a1}. In such a case, the pH of the aqueous phase remains almost constant during dissolution of the dibasic acid, even when the ionic strength of the buffer solution used is less than 10^{-3}. Accordingly, the activity coefficients can be omitted from Eqn. (1), leaving the following equation, which has an accuracy better than 87%.

$$[A_t] = [AH_2]\{1 + K_{a1}(1/a_{H^+}) + K_{a1}K_{a2}(1/a_{H^+})^2\} \quad (3)$$

Even if $[AH_2]$ is very difficult to determine precisely, $[AH_2]K_{a1}$ and $[AH_2]K_{a1}K_{a2}$ values, which are the second and third coefficients of the $(a_{H^+})^{-2}$ graph can be determined with greater ease and precision. Therefore, K_{a2} can be obtained from their ratio. If $K_{a1} = K_{a2}$, this gives

$$[A_t]_0 = [AH_2]\{1 + (K_{a2}/a_{H^+}) + (K_{a2}/a_{H^+})^2\} \quad (4)$$

where $[A_t]_0$ is $[A_t]$ in Eqn. (3) when $K_{a1} = K_{a2}$. Because $K_{a2} < K_{a1}$, as is clear from the initial reaction equation, $[A_t]_0 < [A_t]$. Suppose that K_{a1} can be related to K_{a2} by the equation $K_{a1} = K_{a2}(1 + \Delta)$, where Δ refers to a difference between K_{a1} and K_{a2} values (see Appendix). When Eqn. (4) is subtracted from Eqn. (3) and this expression for K_{a1} is introduced, then

$$[A_t] - [A_t]_0 = [AH_2]\Delta\{(K_{a2}/a_{H^+}) + (K_{a2}/a_{H^+})^2\} \quad (5)$$

The best K_{a1} value, which depends on a correct $[AH_2]$ value, can be tested in two ways, one using Eqn. (2) and the other relying on the difference given by Eqn. (5). That is to say, the correct $[AH_2]$ value can be determined after it has been employed as a parameter. The K_{a1} value can be estimated directly by introducing a probable $[AH_2]$ value into Eqn. (2). However, $[A_t]_0$ at each pH can also be calculated by its introduction into Eqn. (4), because K_{a2} has been determined. Consequently, the difference at each pH between an experimental concentration $[A_t]$ and the calculated concentration $[A_t]_0$ can be plotted against K_{a2}/a_{H^+}, giving a second-order dependence which goes through the origin (Eqn. 5). From the coefficient giving the best fit for the difference, the Δ value can be determined because an $[AH_2]$ value has been given as the parameter, and finally K_{a1} can be determined from the expression $K_{a1} = K_{a2}(1 + \Delta)$. If the $[AH_2]$ value was correct, the K_{a1} values obtained in both ways would be identical. Therefore, the object is to find the concentration of $[AH_2]$ which makes the K_{a1} values obtained by the two procedures coincide.

EXPERIMENTAL

Materials

1-Naphthoic acid (analytical-reagent grade; Wako Pure Chemicals) was recrystallized twice from benzene (m.p. 165.5—166.5°C). 2-Naphthol (guaranteed-reagent grade; Nakarai Chemicals) was recrystallized twice from benzene, once from water/ethanol, and finally from benzene (m.p. 121.5—122.0°C). Diphenic acid (guaranteed-reagent grade; Nakarai Chemicals) was purified by recrystallization once from water/ethanol and once from benzene/ethanol (m.p. 230.5—232.5°C). Terephthalic acid (Nakarai Chemicals) was purified by recrystallization once from ethanol and once from water and was found to be pure by t.l.c. Buffer solutions were made from analytical-reagent grade phosphoric acid, sodium dihydrogenphosphate and disodium hydrogenphosphate for 1-naphthoic acid, 2-naphthol and terephthalic acid and from acetic acid and sodium acetate for diphenic acid. The buffer solutions had an ionic strength of 0.05 for the former three acids and 0.05 and 0.5 for diphenic acid.

Apparatus and procedure

A spectrophotometer (Hitachi 100-50) and pH meter (Horiba F-7, LC) were used. The pH meter was standardized at 25.0°C in a thermostat. A suspension of acid powder in buffer solutions was stirred by a disk rotor in a 10-ml injector tube dipped in the thermostat controlled at 25.0 ± 0.01°C [10]. At hourly intervals, a few milliliters of filtrate was withdrawn through a filter of 0.23-μm pore-size (Millipore; GSTF 01300) by applying a pressure on the injector, and the run proceeded for more than 2 h to reach dissolution

equilibrium. The filtrate was analyzed for its total acid concentration and its pH was determined at 25.0°C.

1-Naphthoic acid, 2-naphthol and terephthalic acid had absorption maxima at 283, 345 and 240 nm, respectively, at pH >11; their molar absorptivities were 6.52×10^3, 2.89×10^3 and 1.255×10^4 dm^3 mol^{-1} cm^{-1}, respectively, at these wavelengths. For diphenic acid, the molar absorptivity used was 1.033×10^4 dm^3 mol^{-1} cm^{-1} at 245 nm and pH >11.

RESULTS AND DISCUSSION

The variation of solubility of 1-naphthoic acid and 2-naphthol with hydrogen ion concentration is illustrated in Fig. 1. The plots are linear, as expected from the equation given for a monobasic acid above. From the ratio of the slope to the intercept, K_{a1} is calculated to be 2.12×10^{-4} for 1-naphthoic acid and 2.80×10^{-10} for 2-naphthol. γ_A is estimated at the ionic strength of 0.05 from the equation [9] $\log \gamma_z = -0.15z^2I^{1/2}/(1 + 1.5I^{1/2})$, where I is the ionic strength and z is the charge on the species. The K_{a1} values can be compared with the literature values of 2.02×10^{-4} at 25°C obtained by a conductimetric method for 1-naphthoic acid and 2.7×10^{-10} at 19.5°C obtained spectrophotometrically for 2-naphthol [11].

The dependence of total diphenic acid concentration on $1/a_{H^+}$ is shown in Fig. 2. As mentioned before, when K_{a1} is much larger than K_{a2}, a dibasic acid can be treated as a monobasic acid at pH $\leqslant K_{a1}$ (see Fig. 2). The linear relationship leads to a K_{a1} value of 5.36×10^{-4}, which compares with a liter-

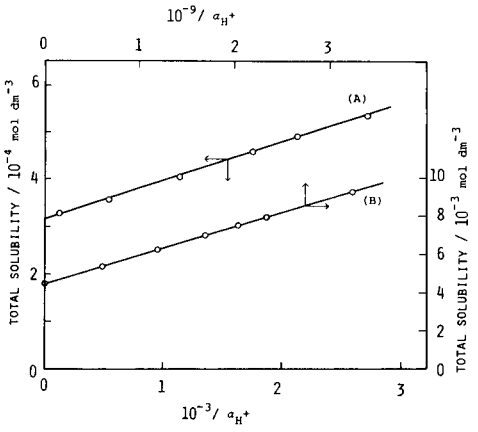

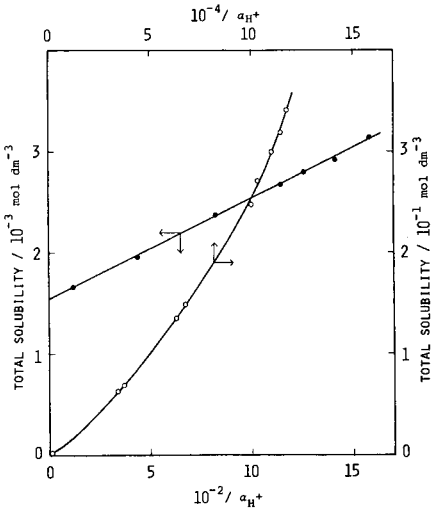

Fig. 1. Plots of total solubility against $1/a_{H^+}$ for: (A) 1-naphthoic acid; (B) 2-naphthol.

Fig. 2. Plots of total solubility of diphenic acid against $1/a_{H^+}$: (•) pH $\leqslant K_{a1}$; (○) pH <5.5.

ature value of 6.8×10^{-4} [12]. From the second-power curve at pH <5.5, the three coefficients ($A = 1.08 \times 10^{-3}$, $B = 1.12 \times 10^{-6}$, $C = 1.43 \times 10^{-11}$) may be obtained by the least-squares method. These coefficients give the values $K_{a1} = 6.76 \times 10^{-4}$ at ionic strength 0.67 and $K_{a2} = 3.48 \times 10^{-6}$ at ionic strength 0.67 ($K_{a2} = 7.05 \times 10^{-6}$ at ionic strength 0.50). The K_{a2} values can be compared with the reported value of 4.5×10^{-6} [12]. The problem was that the ionic strength could not be kept constant in this experiment because of the high solubility of the acid. Therefore, an ionic strength of 0.05 for pH $\leqslant pK_a$ and 0.67 for pH $\leqslant$5.5 was used in order to estimate the activity coefficients, γ_{AH} and γ_A, from the modified Debye—Hückel equation [9]. The disagreement between the present value and the literature data seems to be due mainly to an incorrect ionic strength employed. Thus, the solubility method is not a good way to estimate the dissociation constants of acids whose solubility is relatively high.

Figure 3 shows the total acid concentration of terephthalic acid plotted against $1/a_{H^+}$, which can be fitted to the second-power curve of $1/a_{H^+}$, as expected from Eqn. (3). The three coefficients ($A = 2.53 \times 10^{-5}$, $B = 7.52 \times 10^{-9}$, $C = 4.29 \times 10^{-13}$) were again determined by the least-squares method, and the values $K_{a1} = 2.47 \times 10^{-4}$ and $K_{a2} = 3.16 \times 10^{-5}$ were obtained after estimating γ_A and γ_{AH} as described above. These values can be compared with literature data, $K_{a1} = 2.9 \times 10^{-4}$ and $K_{a2} = 3.5 \times 10^{-5}$ at 25°C obtained spectrophotometrically [11]. One problem is whether the Debye—Hückel approximation, which ideally regards a real charge as a point charge can be applied here, especially to a doubly-charged ion such as terephthalate.

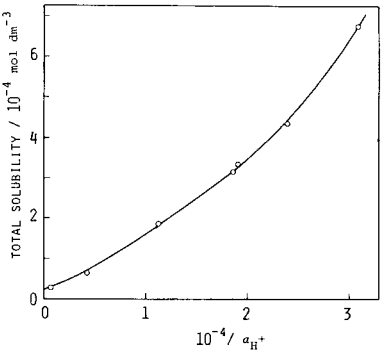

Fig. 3. Plot of total solubility of terephthalic acid against $1/a_{H^+}$.

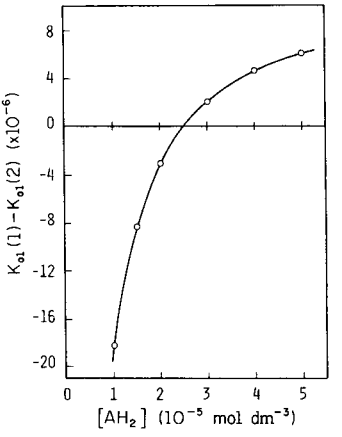

Fig. 4. Variation of the difference between K_{a1} (1) and K_{a1} (2) values with the concentration [AH_2], where K_{a1} (1) is obtained from Eqn. (2) and K_{a1} (2) is obtained from K_{a2} $(1 + \Delta)$ $(1/a_{H^+} = 3.0 \times 10^4)$.

As mentioned above, an accurate K_{a1} value depends on whether or not $[AH_2]$ is correct. As the coefficients of the linear and the square terms of $1/a_{H^+}$ of the curve (Fig. 3) are known, the method involving Eqn. (5) can be used. Figure 4 shows the differences between the K_{a1} values obtained by the two procedures described above. The concentration which gave the best agreement was 2.5×10^{-5} mol dm^{-3}; the K_{a1} value was then 2.5×10^{-4}.

The agreement of the present K_a values with literature data supports the feasibility of the solubility method for a determination of the dissociation constants of organic acids, particularly dibasic acids whose solubility at low pH is too small to be determined precisely.

Thanks are due to the Ito Science Foundation for financial support. The technical help of Mr. H. Noma is gratefully acknowledged.

APPENDIX

A second-power curve can be expressed as $y = A + Bx + Cx^2$. By defining y_0 as $A[1 + (Cx/B) + (Cx/B)^2]$, $y - y_0$ is obtained in the form $A\Delta[(Cx/B) + (Cx/B)^2]$, where Δ satisfies $B/A = (C/B)(1 + \Delta)$. If A is assumed to deviate from the correct value by δ, then y_0 becomes:

$$y_0 = (A + \delta)[1 + (Cx/B) + (Cx/B)^2]$$

From the corresponding change of $y - y_0$,

$$1 + \Delta = [Bx + Cx^2 - \delta]/(A + \delta)[(Cx/B) + (Cx/B)^2]$$

Hence, the difference between K_{a1} (1) and K_{a1} (2) becomes

$$K_{a1}(1) - K_{a1}(2) = \delta/(A + \delta)[x + (C/B)x^2]$$

where K_{a1} (1) and K_{a1} (2) are defined respectively as $B/(A + \delta)$ and $C(1 + \Delta)/B$.

REFERENCES

1 F. J. C. Rossotti and H. Rossotti, The Determination of Stability Constants and Other Equilibrium Constants in Solution, McGraw-Hill, New York, 1961.
2 C. B. Monk, Electrolytic Dissociation, Academic Press, London, 1961.
3 R. A. Robinson and R. H. Stokes, Electrolyte Solutions, 2nd edn., Butterworths, London, 1961.
4 P. Mukerjee and Y. Moroi, Anal. Chem., 50 (1978) 1589.
5 P. Mukerjee and A. K. Ghosh, J. Am. Chem. Soc., 92 (1970) 6403, 6413.
6 A. K. Ghosh and P. Mukerjee, J. Am. Chem. Soc., 92 (1970) 6419.
7 H. A. Krebs and J. C. Speakman, J. Chem. Soc., (1945) 593.
8 H. L. Johnston and H. L. Leland, J. Am. Chem. Soc., 60 (1938) 1439.
9 R. G. Bates, Determination of pH; Theory and Practice, 2nd edn., John Wiley, New York, 1973.
10 Y. Moroi, K. Sato and R. Matuura, J. Phys. Chem., 86 (1982) 2463.
11 G. Kortum, W. Vogel and K. Andrussow, Dissociation Constants of Organic Acids in Aqueous Solution, Butterworths, London, 1961.
12 U. Mazzucato and A. Foffani, Ricerca Sci., 26 (1956) 2474.

Analytica Chimica Acta, 152 (1983) 247—255
Elsevier Science Publishers B.V., Amsterdam — Printed in The Netherlands

DETERMINATION OF NICKEL IN BIOLOGICAL MATERIALS AND SEA WATER BY NEUTRON ACTIVATION AND LIQUID SCINTILLATION COUNTING OF NICKEL-65

H. BEM[a], J. HOLZBECHER and D. E. RYAN*

Trace Analysis Research Centre, Department of Chemistry, Dalhousie University, Halifax, Nova Scotia, B3H 4J1 (Canada)

(Received 18th February 1983)

SUMMARY

A method has been developed for the determination of submicrogram quantities of nickel in biological materials and sea water. Nickel is preconcentrated by coprecipitation with α-benzildioxime followed by neutron activation and liquid scintillation counting of nickel-65. Copper, cobalt, and manganese partially coprecipitate and trace amounts of chlorine and bromine are adsorbed onto the surface of the solid phase; these interferences are removed by washing the chloroform extract of dissolved precipitate with an aqueous solution of citric acid containing inactive carriers of bromide, chloride, copper(II), manganese(II) and sodium ions. Nickel is finally stripped into the aqueous phase with 2 M hydrochloric acid. A new scintillator is described which can tolerate large volumes of water. The detection limit is 5 ng. Precision and accuracy are evaluated by using four standard reference materials.

Nickel is believed to be an essential element to human and animal life but it is also known to be toxic and has been reported to be carcinogenic [1, 2]. There are still many uncertainties about its natural levels in biological samples [3], mainly because of the lack of precise methods for the determination of nickel in submicrogram amounts. Certified values of nickel concentration are given for only two NBS biological standard reference materials: SRM 1571 Orchard Leaves, and SRM 1655 Oyster Tissue. Recently, differential pulse voltammetry has been applied to the determination of nickel in food and environmental and biological materials, including four NBS standard reference materials [4].

Neutron activation methods, because of the poor sensitivity for this element, have been applied for somewhat higher concentrations but only a few attempts have been made to quantify nickel in biological tissues or fluids.

The reaction with fast reactor neutrons, $^{58}Ni(n,p)^{58}Co$, which produces long-lived ^{58}Co ($t_{1/2}$ = 70.8 days), has been mainly used in multielement neutron activation methods [5—11]. However, in order to decrease inter-

[a] On leave from Technical University of Lodz, Poland.

0003-2670/83/$03.00

ference from other nuclides and to obtain better statistics for counting of the 811-keV γ-rays of ^{58}Co, a long waiting period (>3 weeks) after irradiation is necessary. Application of pre-irradiation chromatography on Chelex-100 resin for preconcentration of nickel allows determination in water and sea water by counting of ^{58}Co after 3 months [12].

Activation with thermal neutrons followed by direct γ-spectrometry cannot be applied to these purposes because of the low cross-sections for the (n,γ) reaction of nickel nuclides. In addition, the mainly produced ^{65}Ni($t_{1/2}$ = 2.52 h) radionuclide is a β-emitter with low γ-ray abundances; β-counting by liquid scintillation or Cerenkov techniques is advantageous because ^{65}Ni can be counted with the relatively high efficiency of 20.5% [13].

Calcium, magnesium, nickel and silicon in biological materials have been quantified by using neutron activation and Cerenkov counting [14]. Although the detection limit was 50 ng of nickel, the nickel content in bovine liver could only be estimated to be less than 0.5 μg g^{-1}.

The detection limits in neutron activation (n.a.) methods depend on the detection efficiency of nuclear radiation and the background in the region of interest. Because of poor selectivity and resolution of β-counting techniques, careful separation and purification from other β-radionuclides is necessary. The detection efficiency of ^{65}Ni in the present work was improved by use of a new scintillation mixture instead of Cerenkov counting.

The aim of the present study was to develop a simple and sensitive method for determination of nickel in biological and environmental samples by n.a. and liquid scintillation counting of ^{65}Ni after previous selective preconcentration of nickel. α-Benzildioxime was chosen as a preconcentration reagent; it has low water solubility and has been successfully applied to nickel determination in steel [15] and sea water [16].

EXPERIMENTAL

Reagents and samples

The α-benzildioxime was prepared as described previously [15]. The reagent was 1% (w/v) in dimethylsulfoxide (Fisher, Certified ACS). Standard solutions of manganese, cobalt, copper, and nickel (for atomic absorption; Alfa-Ventron) were used to study the selectivity of coprecipitation. Hydrochloric acid (Ultrex, J. T. Baker), hydrofluoric acid (Fisher Reagent ACS) and hydrogen peroxide 30% (Fisher, Certified ACS) were used for dissolving ashed biological samples.

The ammonium tartrate (Fisher, Certified) solution was 1 M. Two wash solutions containing (a) 0.025 M sodium hydroxide, and (b) 0.1 M citric acid, 0.05 M sodium chloride, 0.05 M sodium bromide, 0.05 M magnesium nitrate and 0.01 M copper nitrate, were prepared from Fisher, Certified ACS salts in distilled water. A dimethylsulfoxide and chloroform (Fisher, Certified ACS) mixture (2:8 v/v) was used for dissolving irradiated precipitate. The scintillation solution was prepared by mixing 600 ml of Triton X-100 (Fisher

Scintanalyzed) with 400 ml of distilled ethanol and addition of 4 g of sodium salicylate (Fisher, Certified).

The sea water was from the Northwest Arm, Halifax, Nova Scotia, taken directly from a tap in the Oceanography laboratories of the University; the water is filtered through sand before entering the building. It was further filtered through a Metricel membrane filter, pore size 0.45 μm (Gelman Sci.).

Samples (0.5 g) of the National Bureau of Standards standard reference materials (SRM 1571 Orchard Leaves, SRM 1575 Pine Needles, SRM 1655 Oyster Tissue, and 2 ml of SRM 1643a Trace Elements in Water) were processed to evaluate the accuracy of the method.

Apparatus

Samples containing ^{65}Ni radionuclide were counted for 30 min in an LKB Rack-Beta II 1215 liquid scintillation counter. A well-type 7.5 cm × 7.5 cm NaI(Tl) detector in conjunction with a Canberra 8100 (4096 channel) pulse-height analyzer was used to check the separation of radioactive impurities from the organic phase.

In preliminary experiments to determine all possible radioactive impurities in irradiated precipitates, a 60-cm^3 Canberra Ge(Li) detector (full width at half maximum of 1.88 keV at the 1332 keV photopeak of ^{60}Co, peak-to-Compton ratio 35:1, and an efficiency of 9.5%) in conjunction with a Tracor Northern TN-11 4096 channel pulse-height analyzer was used.

Samples were irradiated in the inner site of the research reactor (SLOWPOKE) at a flux of 5×10^{11} n cm^{-2} s^{-1} for 3 h.

Procedures

Preconcentration procedure. The preconcentration procedure for sea water was the same as described previously [16]. For SRM 1643a, 2 ml of solution was added to 100 ml of distilled water; 1 ml of 1 M ammonium tartrate was added and the pH was adjusted to 9.5 with concentrated Ultrex ammonia solution. This solution was rapidly stirred and 2 ml of reagent solution was added slowly. The precipitate was filtered after 30 min. The wet precipitate was transferred to small (2/5 dram) polyethylene irradiation vials and then dried in a vacuum oven. The same procedure was applied to nickel, manganese, cobalt, and copper standards.

Solid biological SRM's were ashed by heating at 450°C for 8 h in a porcelain crucible. The remaining residue was partially dissolved by addition of 2 ml of concentrated hydrochloric acid; the suspension was transferred to a teflon vial followed by addition of 0.5 ml of hydrofluoric acid and 0.5 ml of 30% hydrogen peroxide. The solution was evaporated to dryness and the dry residue was dissolved again by addition of 0.1 ml of hydrochloric acid and 5 ml of distilled water. The solution was transferred to a 200-ml beaker containing 100 ml of distilled water. The remainder of the precipitation procedure was as for SRM 1643a.

Separation and measurement of nickel-65. The irradiated precipitate, after

a 10-min waiting period, was quantitatively transferred to a separatory funnel and dissolved by a mixture of 2 ml of dimethylsulfoxide and 8 ml of chloroform. To avoid adsorption losses of nickel-65, 0.1 ml of an aqueous solution containing 100 μg of inactive nickel carrier was added. Excess of organic reagent and the dimethylsulfoxide were removed from the chloroform layer by shaking with 10 ml of 0.025 M sodium hydroxide. The chloroform phase containing nickel benzildioximate was then washed with five 10-ml volumes of 0.1 M citric acid solution containing the inactive carriers, sodium, copper(II), manganese(II), chloride and bromide ions. Finally, nickel was stripped from the chloroform to the water phase by shaking with 5 ml of 2 M hydrochloric acid. The aqueous phase was separated, neutralized to about pH 6, adjusted to a total volume of 10 ml, and transferred to 22-ml glass scintillation vials containing 10 ml of the scintillation solution.

RESULTS AND DISCUSSION

Selectivity of α-benzildioxime for coprecipitation of nickel

It is known that, in addition to nickel, several other elements (Pd, Fe, Co, Cu, and Mn) form stable metal—dioxime complexes [17] and these complexes can be expected to contaminate the nickel α-benzildioximate. The possible adsorption of other ions present in solution must also be considered.

Figure 1 shows the typical γ-ray spectrum of an irradiated precipitate from pine needle samples. It is evident that high activities of copper and manganese nuclides can be detected as well as those of antimony, sodium, and chlorine.

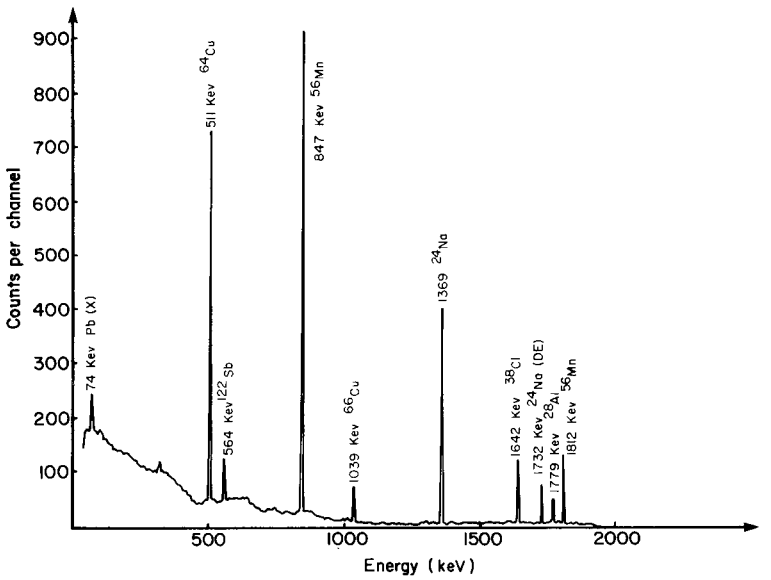

Fig. 1. γ-Ray spectrum of the SRM 1575 Pine Needles (0.125 g, t_{ir} = 3 h, t_d = 7 min, t_c = 10 min).

Table 1 shows that only the nickel chelate quantitatively coprecipitates with α-benzildioxime. The initial concentrations of elements were chosen to approximate the average concentrations of these elements after digestion of 0.5-g biological samples and dilution to 100 ml. The amounts of coprecipitated copper and cobalt dioximates depend strongly on the amount of α-benzildioxime. For example, for 10 mg of precipitated α-benzildioxime, only about 10% of the copper coprecipitates but 100% of nickel is recovered. In order to avoid substantial losses of precipitate during transfer from filter to irradiation vial, 20 mg of α-benzildioxime (2 ml of 1% dimethylsulfoxide solution) was precipitated in routine procedures.

Removal of radioactive impurities

The majority of radioactive impurities, together with excess α-benzildioxime and dimethylsulfoxide, are easily removed from the organic phase by shaking with 10 ml of 0.025 M sodium hydroxide. In contrast to nickel, the copper chelate is decomposed quantitatively in alkaline medium and decomposition of the cobalt complex is nearly quantitative [18]. In addition, antimony impurity that was present in the reagent and most of ^{24}Na and ^{56}Mn are stripped to the aqueous phase. Final separation from the trace amounts of ^{24}Na, ^{56}Mn, ^{64}Cu, ^{38}Cl, and ^{82}Br radionuclides was done by two-phase isotopic exchange with an aqueous 0.1 M citric acid solution containing a large excess of the above-mentioned inactive carriers. Among different nickel dioximates, only α-benzildioxime remains in chloroform phase after extraction with 0.1 M citrate solution [19]. It is not necessary to add a cobalt carrier to the wash solution because of its very low levels ($\sim 0.2\ \mu g\ g^{-1}$) in biological and environmental samples and short half-life of the most active radionuclide produced, ^{60m}Co ($t_{1/2}$ = 10.5 min). Among other potential interferences, iron is completely masked by ammonium tartrate and palladium is unlikely to be present in biological samples. However, palladium can be easily removed from solutions after digestion by preliminary coprecipitation with the same reagent in acidic medium. Under that condition, nickel remains in solution [15].

Extraction with 50 ml of citric acid solution in five 10-ml portions was sufficient to remove all radioactive impurities from the chloroform phase.

TABLE 1

Coprecipitation of nickel, cobalt, copper and manganese with α-benzildioxime

Element	Initial amount in solution (μg)	Amount coprecipitated (μg)	Element	Initial amount in solution (μg)	Amount coprecipitated (μg)
Nickel	0.25	0.245	Cobalt	1.0	0.39
	1.00	0.975	Copper	100	77
	10.0	10.2	Manganese	100	0.1

Moreover, the half-life determined by 30 consecutive counts of 30 min each (total period equal to at least 6 half-lives of ^{65}Ni) ranged from 2.5 to 2.6 h and agreed well with the accepted value of $t_{1/2}$ = 2.52 h for ^{65}Ni [20]. Total recovery of nickel determined for aqueous solutions of nickel standards which contained 0.1—10 μg of nickel was 95% or better.

Choice of detection method

The sensitivity of n.a. for given conditions of irradiation depends on the sensitivity of radiation measurements. For nickel-65, after separation and purification, the total activity can be determined by measurement of γ-radiation by NaI(Tl) detector, by Cerenkov counting of the chloroform phase, or by liquid scintillation with a proper scintillation solution. However, because of the low γ-abundancies or strong yellow colour of chloroform solutions (colour quenching), good sensitivities cannot be expected for the first two methods. Chloroform solution, also, cannot be directly added to a scintillation solution because of its strong chemical quenching properties. However, nickel can be quantitatively stripped into an aqueous phase on shaking the chloroform solution with 2 M hydrochloric acid; the nickel complex is decomposed and nickel(II) moves to the aqueous phase. This colourless solution can be simply measured by Cerenkov counting or, after neutralization, by liquid scintillation. Most commercially available scintillation cocktails can tolerate up to 50% (v/v) of water but detection efficiency is markedly lowered at high water content. Triton X-100/water mixtures with sodium salicylate were recently applied to measurement of β-radiation of phosphorus-32 in aqueous solutions [21, 22]. In the present study, a Triton X-100/ethanol/sodium salicylate mixture was used to measure the nickel-65 in aqueous solution; addition of ethanol makes the solution less viscous and thus easier to handle. Sodium salicylate acts as a wavelength shifter and matches emitted photons to the optimum sensitivity of photomultipliers.

Figure 2 shows the influence of sodium salicylate on the detection efficiency for nickel-65 in the mixture Triton X-100/alcohol/water (3:2:5 v/v). A relatively high detection efficiency (~80%) is achieved for concentrations of sodium salicylate of 2 g l^{-1}.

Figure 3 shows a comparison of the influence of added water on the detection efficiency for nickel-65 with the commercial scintillator Scintiverse II and the Triton cocktail. It is evident that the Triton cocktail is superior above 3 ml of added water. This is important because the total volume of the aqueous phase increases to 10 ml in the proposed procedure. The Triton X-100 mixture shows a stable counting efficiency in the pH range 2—10. A Triton X-100/alcohol mixture containing sodium salicylate (4 g l^{-1}) was finally chosen as the scintillation solution.

A comparison of different counting methods for the determination of nickel is shown in Table 2. The detection limits were calculated on the basis of 3 times the square root of the background. The lowest detection limit of 5 ng of nickel was achieved for liquid scintillation counting with Triton

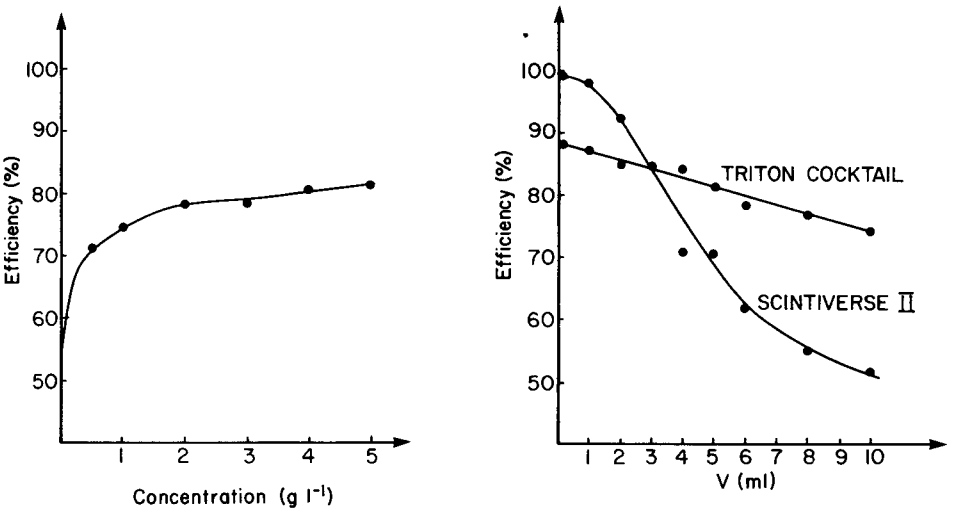

Fig. 2. Influence of sodium salicylate concentration on nickel-65 detection efficiency in Triton X-100/alcohol/water mixture (3:2:5 v/v).

Fig. 3. Influence of added water on detection efficiency for nickel-65.

X-100 cocktail. For blank samples (100 ml of distilled water treated in the same way), a somewhat higher background of 2500 counts/30 min was observed compared to 1650 counts/30 min for scintillation solution only. This is equivalent to about 30 ng of nickel.

TABLE 2

Comparison of different counting methods of nickel-65 for n.a. determination of nickel[a]

Method	Sensitivity (counts/μg/30 min)	Detection limit (μg)	Remarks
Instrumental n.a., Ge(Li) detector	80	2	
NaI(Tl) counting of chloroform phase after purification	6810	0.1	
Cerenkov counting of chloroform phase	9055	0.013	Yellow colour
Back-extraction of Ni to 2 M HCl and Cerenkov counting	16325	0.008	Colourless solution
Liquid scintillation counting with Scintiverse II	20740	0.008	Hazy gel
Liquid scintillation counting with Triton/ethanol mixture	31050	0.005	Transparent solution

[a]Standard condition: irradiation time 3 h, decay time 60 min, counting time 30 min.

TABLE 3

Determination of nickel in different samples

Sample	Concentration (mg kg^{-1})	
	This work[a]	Reported values
SRM 1571 Orchard Leaves	1.23 ± 0.1	1.3 ± 0.2[b]
SRM 1575 Pine Needles	2.88 ± 0.2	2.63 [4]; 3.5[c]
SRM 1643a Trace Elements in Water	0.058 ± 0.005	0.055 ± 0.003[b]
SRM 1655 Oyster Tissue	0.98 ± 0.07	1.03 ± 0.19[b]
Sea Water	$0.55 \times 10^{-3} \pm 0.03 \times 10^{-3}$	

[a]Standard deviations are on the basis of at least three results. [b]Certified values. [c]Non-certified value.

Precision and accuracy

The accuracy of the method for nickel was evaluated with some biological SRM's. To avoid precipitation of calcium tartrate from samples with a high calcium content (orchard leaves and pine needles), only one-half or one-fourth of the total digestion solutions was used. Results are presented in Table 3. The good agreement between the values found and those certified or reported by others proves that recovery of nickel from different samples is quantitative and fully confirms the suitability of this method. The imprecision of the method was found to be better than 10% for as little as 0.1 μg of nickel.

This work was supported by a grant from the Natural Sciences and Engineering Research Council of Canada.

REFERENCES

1 T. D. Luckey and B. Venugopal, Metal Toxicity in Mammals, 2nd edn., Plenum Press, London, 1979, p. 196.
2 M. Costa and J. D. Heck, Trends Pharmacol. Sci., 3 (1982) 408.
3 L. Kosta and A. R. Byrne, J. Radioanal. Chem., 69 (1982) 117.
4 B. Pihlar, P. Valenta and H. W. Nürnberg, Fresenius Z. Anal. Chem., 307 (1981) 337.
5 R. A. Nadkarni and G. H. Morrison, Anal. Chem., 45 (1973) 1957.
6 B. Maziere, J. Gros and D. Comar, J. Radioanal. Chem., 24 (1975) 279.
7 G. F. Clemente, J. Radioanal. Chem., 32 (1976) 25.
8 G. F. Clemente, L. Rossi and G. P. Santoroni, J. Radioanal. Chem., 37 (1977) 549.
9 R. A. Nadkarni and G. H. Morrison, J. Radioanal. Chem., 43 (1978) 347.
10 G. D. Kamas and S. M. Phillana, J. Radioanal. Chem., 46 (1978) 87.
11 N. I. Ward and D. E. Ryan, Anal. Chim. Acta, 105 (1979) 185.
12 R. R. Greenberg and H. M. Kingston, J. Radioanal. Chem., 71 (1982) 147.
13 G. Guzzi, R. Pietra, E. Sabbioni and F. Girardi, J. Radioanal. Chem., 20 (1974) 751.
14 R. Pietra, E. Sabbioni and F. Girardi, Radiochem. Radioanal. Lett., 22 (1975) 243.
15 D. E. Ryan and J. Holzbecher, Can. J. Chem., 53 (1975) 311.
16 O. Liardon and D. E. Ryan, Anal. Chim. Acta, 83 (1976) 421.
17 B. Egneus, Talanta, 19 (1972) 1387.

18 V. M. Peshkova, V. M. Bochkova and B. K. Astakhova, Zh. Anal. Khim., 16 (1961) 596.
19 V. M. Peshkova and V. M. Savostina, Analytical Chemistry of Nickel, Jerusalem, 1967, p. 43.
20 G. Erdtmann and W. Soyka, The Gamma Rays of the Radionuclides, Verlag Chemie, Weinheim, 1979, p. 15.
21 N. P. Chow, in C. T. Peng, D. L. Horrocks and E. L. Alpen (Eds.), Liquid Scintillation Counting, Recent Applications and Development, Vol. 1, Academic Press, New York, 1980, p. 387.
22 T. F. Kellog, Int. J. Appl. Radiat. Isot., 33 (1982) 165.

Analytica Chimica Acta, 152 (1983) 257—263
Elsevier Science Publishers B.V., Amsterdam — Printed in The Netherlands

SIMULTANEOUS THERMOMETRIC COMPLEXIMETRIC TITRATION OF CALCIUM AND MAGNESIUM WITH SULFOSALICYLIC ACID AS AN AUXILIARY REAGENT

HITOSHI YOSHIDA*, TOSHIAKI HATTORI, HIDESHI ARAI and MITSUHIKO TAGA
Department of Chemistry, Faculty of Science, Hokkaido University, Sapporo 060 (Japan)
(Received 5th November 1982)

SUMMARY

Calcium and magnesium are titrated thermometrically with EDTA (tetrasodium salt) solution in the presence of sulfosalicylic acid, which is introduced to change the difference in conditional stability constants between Ca—EDTA and Mg—EDTA, and to increase the apparent endothermic change in the reaction of magnesium with EDTA. Over the Ca:Mg concentration range of 10:1 to 1:10 mM relative standard deviations are <2% for both elements. The method is applied to sea water.

Several methods [1—6] have been developed for the titrimetric determination of calcium and magnesium. In most of these, two titrations are required. However, Jordan and Alleman [7] noted that the heat of complexation of magnesium with EDTA is endothermic and that of calcium with EDTA is exothermic. On this basis they introduced a single, consecutive thermometric titration of calcium and magnesium. Callicott and Carr [8] applied this titration in the determination of calcium and magnesium in serum.

In these methods, when the concentration of calcium is small in comparison with magnesium or vice versa, the calcium end-point may be located only with difficulty, and the precision of the titration suffers. One of the reasons is the small difference between the stability constants of Ca—EDTA and Mg—EDTA ($\Delta \log K \approx 2$). This difference can be improved by introducing an auxiliary complexing agent into the titration system; for example, if the reagent complexes magnesium more strongly than calcium, the calcium end-point would become clearer. Christiansen et al. [4], using this concept, introduced 3,4-dihydroxybenzoic acid and acetylacetone for successive determinations of calcium and magnesium by complexiметric potentiometric titration. Another reason for poor end-points in the original method [7] is the small enthalpy change. If an auxiliary complexing agent is added which gives an exothermic reaction with magnesium, then the formation of Mg—EDTA in the presence of that reagent will be more endothermic than that in the absence of the reagent.

The simultaneous thermometric titration of calcium and magnesium with EDTA in an ammonium—ammonia buffer has been previously investigated

0003-2670/83/$03.00

[9]. The final end-point was sharper in the presence of sodium chloride. In this paper, sulfosalicylic acid is suggested as the auxiliary complexing agent, with sodium chloride also present in the titration system. The method is suitable for application to sea water.

EXPERIMENTAL

Apparatus

As shown in Fig. 1, the differential thermometric titration apparatus consists of a temperature measurement system, reaction cells, titrant addition system, and temperature control and heating systems. The two fast-response glass thermistors (6PA 203K 282-E-type, 20 kΩ at 25°C; TOA Electronics) formed two arms of a Wheatstone bridge. The closest matching pair was selected from a large number of thermistors. The bridge output was amplified and used to drive the Y axis of the X-Y recorder (Model D-51, Riken Denshi Co.). The titrant volume delivered from the burettes (Mettler DV-11) was shown on the X-axis. The reaction cells were two 100-ml Dewar flasks. The solution in each flask was stirred at equal speed by stirrers driven by one belt. Copper—constantan thermocouples were used to indicate the temperatures in each vessel. The heating system was used not only to warm up the sample solutions, but also to calibrate the enthalpy changes of some reactions. These systems were placed in a suitably lined box to eliminate external influences. Measurements of pH were made with a Horiba Model F-7ss pH meter.

Reagents

All chemicals used were of guaranteed reagent grade. The appropriate amount of disodium-EDTA to prepare a 0.5 M solution was dissolved in twice the equivalent molar quantity of 4 M sodium hydroxide diluted with carbon dioxide-free distilled water; the solution was standardized with a

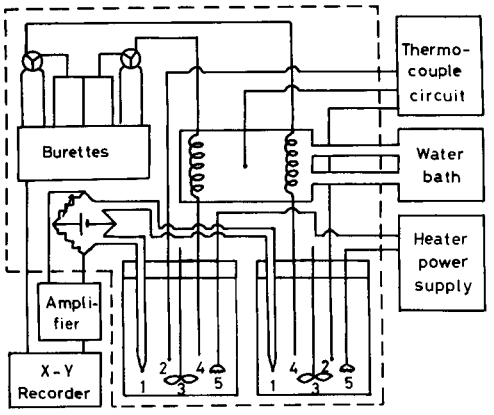

Fig. 1. Differential thermometric titration apparatus: (1) glass thermistor; (2) thermocouple; (3) stirrer; (4) burette tip; (5) heater.

standard zinc solution, using Eriochrome Black T as indicator in the conventional way [14]. Standard solutions of calcium and magnesium were prepared from the nitrates and standardized with the 0.5 M EDTA, using the above indicator. A 63.6-g portion of sulfosalicylic acid dihydrate was dissolved in 6 M ammonia solution, which was adjusted to pH 10 with 1 M sodium hydroxide, and diluted to 500 ml with distilled water, to give a 0.5 M solution.

Procedure and calibration

One burette is filled with 0.5 M EDTA, and distilled water is put into the other as a reference. A sample containing 2.5—25 $\times$ 10^{-4} mol of calcium or magnesium or both is placed in a 250-ml graduated flask, and 50 ml of 0.5 M sulfosalicylate solution and 11.7 g of sodium chloride are added. The solution is diluted to the mark with distilled water, and kept in a thermostat at 25°C for 30 min. A 50-ml portion of the sample is placed in a 100-ml Dewar flask, with 50-ml of distilled water at 25°C added to the reference flask. If required, the temperatures of these two solutions is adjusted to that of the titrant by use of a heater. The two solutions are titrated at the same time, immediately after the temperature has equilibrated, as shown on the recorder. After a titration the enthalpy change of the reaction is calibrated by Joule heating; the electric heater in the sample flask generates the required amount of heat, and draws an analogous straight line to the titration graph. The enthalpy change is calculated by comparison of the slopes of the titration and calibration line.

RESULTS AND DISCUSSION

Titration curves

In Fig. 2, curve 1 represents a simultaneous thermometric titration curve for equimolar concentrations of calcium and magnesium at pH 10 without addition of other salts. The first inflection, indicating the calcium end-point, is very smooth and the inflection for the calcium + magnesium end-point is very indistinct. Curve 2, obtained after adding sodium chloride, has a sharper second end-point because the slope after the end-point is less than that in curve 1. A possible reason for this improvement is that sodium chloride inhibits the reaction of ammonium ions with EDTA; the apparent heat of reaction of ammonium ions with EDTA is —20.0 kJ mol^{-1} (endothermic) [10], which is the same as that of magnesium ions with EDTA, whereas the heat of reaction of sodium ions with EDTA is 5.9 kJ mol^{-1} (exothermic) [11].

In curve 3, where sulfosalicylic acid and sodium chloride are effective, the first end-point is much sharper. The titration curve before and after the first end-point is composed of two straight lines. The heat released during the reaction of magnesium with EDTA is greatly increased. The second end-point is a little more obscure because of the decrease in the conditional stability constant of Mg—EDTA.

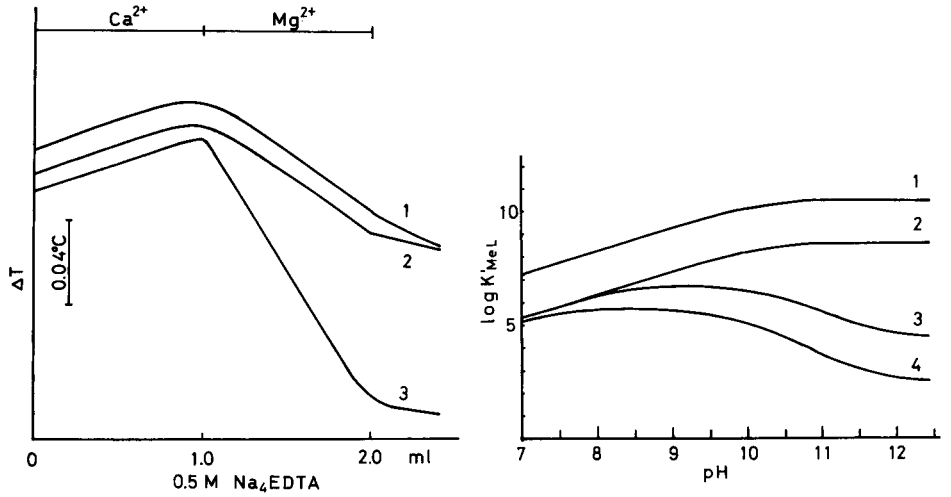

Fig. 2. Typical titration curves for 1×10^{-2} M calcium and 1×10^{-2} M magnesium with EDTA: (1) ammonium—ammonia buffer at pH 10; (2) as (1) but with 0.8 M sodium chloride added; (3) as (2) but with 0.1 M sulfosalicylic acid also added.

Fig. 3. Computed conditional stability constants for Ca—EDTA and Mg—EDTA as a function of pH: (1) Ca^{2+} in pure solution; (2) Mg^{2+} in pure solution; (3) Mg^{2+} in 10^{-2} M sulfosalicylic acid; (4) Mg^{2+} in 0.1 M sulfosalicylic acid.

Conditional stability constants

The conditional stability constants for Ca—EDTA and Mg—EDTA are plotted in Fig. 3 as a function of pH in the presence and absence of sulfosalicylic acid. The curves are calculated on the basis of the stability constants of Ca—EDTA, Mg—EDTA and Mg—sulfosalicylic acid, and the dissociation constants of EDTA and sulfosalicylic acid. These constants were taken from the compilation of Perrin [12], except for the Mg—sulfosalicylic acid constants, which were determined by potentiometric titration [13]. The values found were $\log K_1 \doteq 5.2$ and $\log K_2 = 3.0$ at 25°C, $\mu = 0.1$ (NaCl). Although calcium forms a complex with sulfosalicylic acid, it is weak, and thus its stability constant was not determined. Figure 3 is useful in indicating suitable pH values for the consecutive titration.

Enthalpy changes in sulfosalicylic acid solution

The apparent enthalpy of the reaction of calcium and magnesium with EDTA in the presence of various concentrations of sulfosalicylic acid is shown in Fig. 4. The enthalpy of the calcium reaction decreases slightly with increasing sulfosalicylic acid concentration, as expected from the weak complexing ability of calcium with that ligand. The enthalpy of the magnesium reaction, however, decreases greatly with increasing concentration of sulfosalicylic acid up to about twice the molar concentration of magnesium, and then remains constant up to at least a twenty-fold molar excess. Therefore 0.1 M sulfosalicylic acid, at pH 10, is recommended.

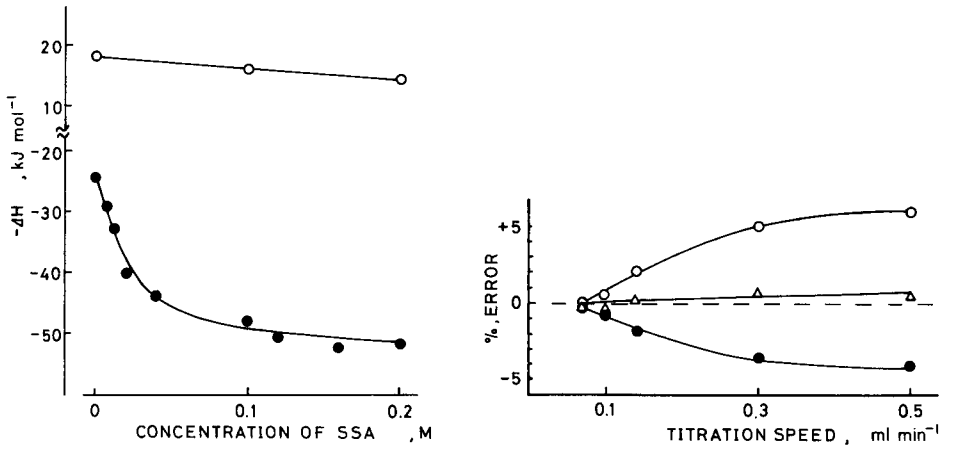

Fig. 4. Apparent enthalpy changes of Ca—EDTA and Mg—EDTA in various concentrations of sulfosalicylic acid: (○) 1×10^{-2} M Ca^{2+}; (●) 1×10^{-2} M Mg^{2+} (0.4 M ammonium buffer, pH 10, titration with Na_4EDTA).

Fig. 5. Effect of titration speed on the simultaneous titration of 5×10^{-3} M calcium and 5×10^{-3} M magnesium at pH 10: (○) Ca^{2+}; (●) Mg^{2+}; (△) $Ca^{2+} + Mg^{2+}$.

When 10^{-2} M magnesium was titrated thermometrically with sulfosalicylic acid at pH 10, the apparent enthalpy change was exothermic and the titration curve did not give a clear end-point. The enthalpy change became nearly constant after addition of sulfosalicylic acid in excess of twice the molar concentration of magnesium. The enthalpy change for the reaction of magnesium ions with sulfosalicylic acid is -14 kJ mol^{-1}. This value is in agreement with the difference in the apparent enthalpy change of the reaction of magnesium ions with EDTA in the absence of sulfosalicylic acid (23 kJ mol^{-1}) and in the presence of two moles of that ligand per mole of magnesium (37 kJ mol^{-1}).

Effect of titration speed

Figure 5 shows the titration errors for calcium and magnesium depending on the titration speed. A positive error for calcium arises with increasing titration speed, in contrast to the negative error for magnesium. But the relative error for calcium + magnesium is within 1% at rates as high as 0.5 ml min^{-1}. When calcium or magnesium alone is titrated, the error is slight at any speed. The reason for these errors is probably the slow exchange reaction between calcium and Mg—EDTA [8].

Determination of calcium and magnesium

The titration curves obtained at Ca:Mg concentration ratios of 1:10 and 10:1 in the presence and absence of sulfosalicylic acid are compared in Fig. 6. Table 1 gives some results; the relative standard deviations are within 2% for calcium and magnesium.

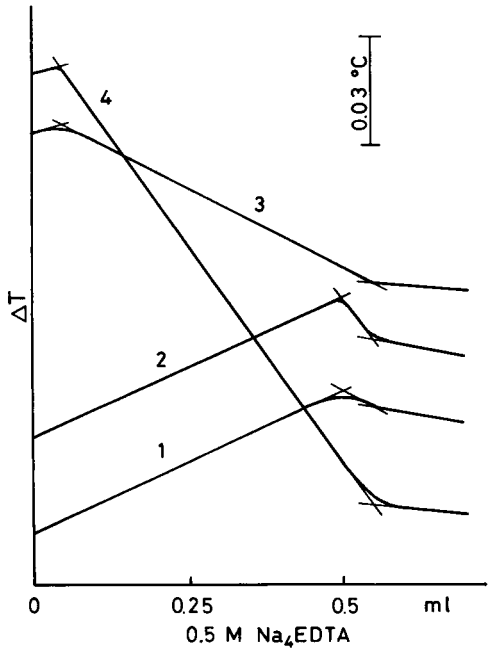

Fig. 6. Thermometric titration curves of Ca:Mg in the following ratios: (1) 10:1; (2) 10:1 in presence of sulfosalicylic acid; (3) 1:10; (4) 1:10 in presence of sulfosalicylic acid.

TABLE 1

Titration of calcium and magnesium

Ca:Mg	Calcium			Magnesium		
	Taken (mM)	Found (mM)	R.s.d.[a] (%)	Taken (mM)	Found (mM)	R.s.d.[a] (%)
10:1	10.03	10.04	0.2	1.01	1.02	1.4
1:1	1.00	1.00	0.9	1.01	1.01	0.7
1:10	1.00	1.01	1.7	10.12	10.09	0.2

[a]5 results.

This method was applied to sea water obtained near Rumoi, Hokkaido. The results (395 ± 1 ppm Ca and 1229 ± 4 ppm Mg) agree satisfactorily with those obtained using an indicator [14] (395 ± 1 ppm Ca, 1238 ± 3 ppm Mg). Each value is the mean ± standard deviation of 5 determinations.

REFERENCES

1 K. Toei and T. Kobatake, Talanta, 14 (1967) 1354.
2 B. Van't Reit and J. E. Wynn, Anal Chem., 41 (1969) 158.

3 H. Sato and K. Momoki, Anal. Chem., 44 (1972) 1778.
4 T. F. Christiansen, J. E. Busch and S. C. Krogh, Anal. Chem., 48 (1976) 1051.
5 K. Ohzeki, E. Schmacher and F. Umland, Fresenius Z. Anal. Chem., 293 (1978) 18.
6 L. L. Jackson, J. Osteryoung, J. O'Dea and R. A. Osteryoung, Anal. Chem., 52 (1980) 71.
7 J. Jordan and T. G. Alleman, Anal. Chem., 29 (1957) 9.
8 R. H. Callicott and P. W. Carr, Clin. Chem., 22 (1976) 1084.
9 H. Yoshida, S. Kusumi, M. Taga and S. Hikime, 19th Annual Meeting Jpn. Soc. Anal. Chem., 2B21 (1970).
10 P. T. Priestley, W. S. Sebborn and P. F. W. Selman, Analyst, 90 (1965) 589.
11 R. G. Charles, J. Am. Chem. Soc., 76 (1954) 5854.
12 D. D. Perrin (Ed.), Stability Constants of Metal—Ion Complexes, Part B: Organic Ligands, Pergamon Press, Oxford, 1979.
13 M. Calvin and K. W. Wilson, J. Am. Chem. Soc., 67 (1945) 2003.
14 Japanese Industrial Standard: "Testing Method for Industrial Water", JIS K0101, 1979.

Analytica Chimica Acta, 152 (1983) 265—269
Elsevier Science Publishers B.V., Amsterdam — Printed in The Netherlands

Short Communication

GLUCOSE-ELIMINATING ENZYME ELECTRODE FOR DIRECT SUCROSE DETERMINATION IN GLUCOSE-CONTAINING SAMPLES

F. SCHELLER* and R. RENNEBERG

Zentralinstitut für Molekularbiologie der AdW der D.D.R., Bereich Angewandte Enzymologie, 1115 Berlin-Buch (E. Germany)

(Received 8th March 1983)

Summary. Direct determination of sucrose in glucose-containing samples is achieved by a multilayer enzyme electrode. The glucose is eliminated by an outer layer containing glucose oxidase and catalase, whilst the sucrose reaches a glucose oxidase—invertase layer, thus producing hydrogen peroxide which is measured by the indicating electrode. Up to 2 mM glucose can be tolerated. Food products were analyzed successfully.

The feasibility of glucose measurements with an enzyme electrode has been firmly established [1—5]. For disaccharides, e.g., sucrose [5—9], lactose [7, 8] and maltose [10], glucose oxidase-based enzyme-sequence electrodes have been developed. In many food processes, combinations of sugars, especially glucose and sucrose, are particularly important. However, the glucose content of samples interferes in the disaccharide electrode measurement because glucose oxidase is a component of the electrode system. In order to eliminate this problem, the values of glucose concentrations before and after enzymatic [11] or acidic [12] hydrolysis can be subtracted in the determination of disaccharides. In addition, the simultaneous measurement of glucose and disaccharides by two differently constituted enzyme electrodes has been described [13]. These procedures suffer from the inaccuracy arising from the subtraction of two large values or from dual measurements.

This communication describes the function of a multilayer electrode comprising a glucose-eliminating layer preceding the disaccharide-reacting layer for the direct measurement of sucrose in glucose-containing samples. This approach was tested in the analysis of standard solutions, instant cocoa powder and sugar beet juice.

Experimental

Chemicals. The enzymes used were lyophilized commercial products: Catalase-free glucose oxidase from *Penicillium notatum* (46 U mg^{-1}; VEB Arzneimittelwerk, Dresden), glucose oxidase from *Aspergillus niger* (100 U mg^{-1}, containing about 320 U mg^{-1} catalase; Boehringer, Mannheim) and

0003-2670/83/$03.00

invertase (100 U mg^{-1}; Serva Biochimica, Heidelberg). The enzymes were entrapped in gelatin [14]. The glucose-eliminating layer contained 1 mg of catalase-containing glucose oxidase. The sucrose-converting layer consisted of co-immobilized catalase-free glucose oxidase (1 mg cm^{-2}) and invertase (0.5 mg cm^{-2}).

Stock solutions of glucose and sucrose were prepared by dissolving the anhydrous substances in 0.1 M phosphate buffer, pH 7.0. The glucose standard was allowed to attain mutarotation equilibrium. The sugar beet were crushed and 26 g of the pulp was extracted with 178 ml of 0.1 M phosphate buffer, pH 7.0. After filtration, a 50-μl aliquot of the solution was added to the measuring cell. At the same time, the sucrose concentration was determined by polarimetry (Polamat; VEB Carl Zeiss Jena). The sucrose concentration of the instant cocoa "Trinkfix" (Trumpf Schokoladenfabrik, Aachen) was directly measured in a suspension of 200 mg of powder in 10 ml of the 0.1 M phosphate buffer.

Apparatus and procedure. The enzyme layers were attached to the tip of a modified oxygen electrode (0.5 mm diameter platinum indicator electrode; VEB Metra Radebeul) as indicated in Fig. 1. The enzyme layers were separated by a dialysis membrane in order to prevent the penetration of catalase into the glucose oxidase—invertase layer. The dialysis membrane used was Nephrophan (17 μm thick; VEB CKB Bitterfeld).

The electrode was dipped into 2 ml of 0.1 M phosphate buffer, pH 7.0, to which 50 μl of sample had been added, in a thermostated cell. Current—time curves were recorded by using a GWP 563 Polarograph (Acad. Sci., G.D.R.). The indicator electrode was polarized at a constant potential of +600 mV vs. Ag/AgCl (0.1 M KCl), thus responding to hydrogen peroxide formation.

Results and discussion

Principle of the multilayer sucrose electrode. Hydrogen peroxide or glucose in the sample first penetrate the glucose oxidase—catalase layer where they are enzymatically converted to non-responsive products (Fig. 1). Sucrose, however, does not react in the first layer. Therefore, the sucrose molecules reach the layer containing glucose oxidase and invertase where they are converted in a reaction sequence to give hydrogen peroxide. Initially, the effectiveness of the immobilized catalase was tested by addition of hydrogen peroxide to the sample. The current was independent of the hydrogen peroxide concentration up to 50 mM, showing that the peroxide was completely destroyed by the catalase. Also, the addition of glucose up to 2 mM did not produce any measurable current increase, indicating complete conversion of glucose in the anti-interference layer. Inhibition of the catalase with 10 mM sodium azide, however, resulted in a linear current increase with increasing glucose concentration at low glucose concentrations (Fig. 2).

The sensitivity of the enzyme sandwich arrangement for sucrose is about 10 times less than for glucose in the presence of 10 mM sodium azide. The

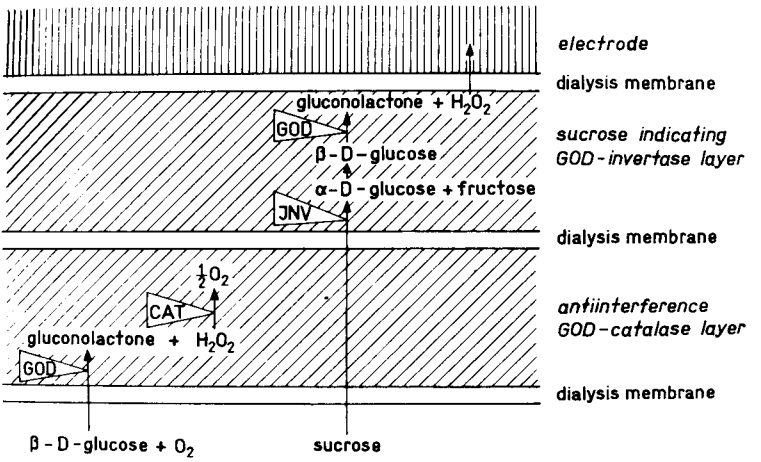

Fig. 1. Cross-section of the enzyme layers.

response time for sucrose was about 6 min compared with 2 min for glucose under conditions of catalase inhibition (Fig. 3). This behaviour might be explained both by the longer diffusion path of sucrose to get to the second enzyme layer and by the delay in the spontaneous mutarotation of the α-glucose formed in the invertase-catalyzed reaction. The linear measuring range extends up to 13 mM sucrose (Fig. 2). The optimum pH for sucrose measurement is 7.0, whereas the optimum value for glucose was found to be

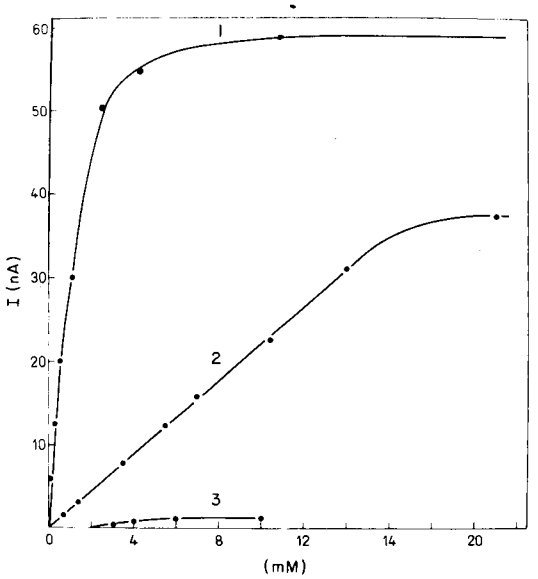

Fig. 2. Concentration dependence of electrode current for glucose and sucrose: (1) glucose with the anti-interference layer inactive; (2) sucrose; (3) glucose with an active anti-interference layer.

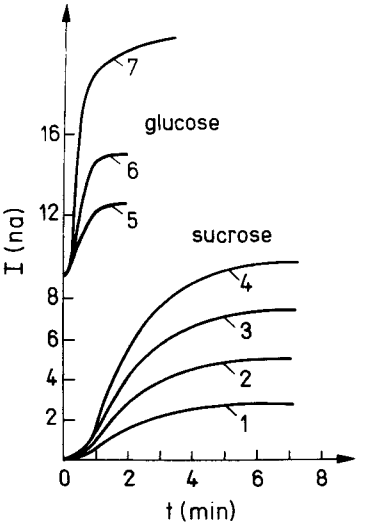

Fig. 3. Responses to sucrose and glucose. Sucrose concentration: (1) 1.4; (2) 2.8; (3) 4.2; (4) 5.6 mM. Glucose concentration: (5) 0.11; (6) 0.22; (7) 0.88 mM (0.1 M phosphate buffer, pH 7.0; 10 mM NaN_3).

pH 5.5. The sandwich electrode retained glucose-eliminating activity for 6 days. The sucrose signal decreased by 50% over 4 days of use, indicating the limited stability of invertase entrapped in gelatin.

Measurement of sucrose in glucose-containing samples. The potential interference of glucose in sucrose measurements was tested for mixtures of 80 mM sucrose and 5—50 mM glucose. The value of sucrose was not influenced significantly by the glucose concentration. The concentration interval studied exceeds the maximal glucose/sucrose ratio of most food samples. Therefore an interference-free sucrose measurement can be expected.

The sucrose content of ten different sugar beets was determined with the enzyme electrode described. In these samples, the glucose concentration is about 0.5%. The results obtained were compared with the values obtained with the Polamat (GDR-standard for sucrose measurement in sugar beets) (Fig. 4). The linear correlation equation is $y = 0.91x + 2.0$, with a correlation coefficient of 0.82. The sucrose content of "Trinkfix" measured by the enzyme electrode was 69.5%. According to the label it contains 10% glucose and 68% sucrose. The coefficient of variation was 3.2% (16 determinations).

Conclusions

The enzyme electrode comprising the glucose-eliminating glucose oxidase—catalase layer and the sucrose-converting glucose oxidase—invertase layer allows the direct measurement of sucrose in glucose-containing samples. A precondition for the functioning of the electrode is a sufficiently high oxygen concentration inside the sucrose-converting layer. Therefore the

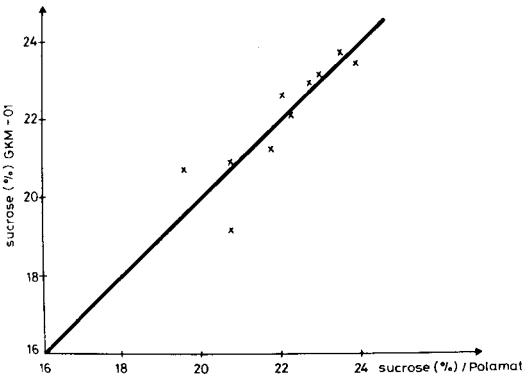

Fig. 4. Correlation between sucrose concentration as measured by enzyme electrode and polarimetry.

glucose content must not be too high compared with the sucrose concentration.

This principle of eliminating an interfering substance might be extended to other amperometric and also potentiometric enzyme electrodes, e.g., for the measurement of other disaccharides or amylase activities and also to substrates of NADH-dependent dehydrogenases.

REFERENCES

1 L. Clark and C. Lyons, Ann. N. Y. Acad. Sci., 102 (1962) 29.
2 G. Guilbault and G. Lubrano, Anal. Chim. Acta, 64 (1973) 439.
3 D. Thevenot, R. Sternberg, P. Coulet, J. Laurent and D. Gautheron, Anal. Chem., 51 (1979) 96.
4 F. Scheller, D. Pfeiffer, M. Kühn, J. Hundertmark, A. Quade, M. Jänchen, G. Lange, H. Holesch and H. Dittmer, Acta Biol. Med. Ger., 39 (1980) 671.
5 D. Pfeiffer, F. Scheller, M. Jänchen, K. Bertermann and H. Weise, Anal. Lett., 13B (1980) 1179.
6 I. Satoh, I. Karube and S. Suzuki, Biotechnol. Bioeng., 18 (1976) 269.
7 M. Cordonnier, F. Lawny, D. Chapot and D. Thomas, FEBS. Lett., 59 (1975) 263.
8 C. Bertrand, P. Coulet and D. Gautheron, Anal. Chim. Acta, 126 (1981) 23.
9 J. Kulys, Anal. Lett., 148 (1981) 377—397.
10 P. Coulet and C. Bertrand, Anal. Lett., 12B (1979) 581.
11 L. Trauberman, Food Eng., 47 (1974) 58.
12 J. Kulys and M. Pesljakene, J. Anal. Chem., 25 (1980) 1168 (in Russian).
13 D. Pfeiffer, F. Scheller, M. Jänchen and K. Bertermann, Biochimie, 62 (1980) 587.
14 F. Scheller, D. Pfeiffer, M. Jänchen, J. Seyer, M. Siepe and R. Pittelkow, GDR-Patent G01N/127 843 (1979).

Analytica Chimica Acta, 152 (1983) 271—274
Elsevier Science Publishers B.V., Amsterdam — Printed in The Netherlands

Short Communication

AMPEROMETRIC DETERMINATION OF ZINC WITH AN APOENZYME-TREATED GRAPHITE ELECTRODE

J. J. JASAITIS, V. J. RAZUMAS and J. J. KULYS*
Institute of Biochemistry, Lithuanian Academy of Sciences, Vilnius (U.S.S.R.)
(Received 21st February 1983)

Summary. Zinc can be determined in the range 0.8—12 μM by activation of apo-alkaline phosphatase immobilized through covalent binding on a graphite electrode. *o*-Hydroxyphenylphosphate is used as substrate. Current is measured at an applied potential of 0.3 V vs. SCE.

Very few studies have been made of the use of enzyme electrodes for the determination of metal ions. Liu et al. [1] constructed a potentiometric enzyme electrode sensitive to mercury(II) and silver(I) ions, based on glucose oxidase and catalase immobilized in a polyacrylamide gel [1]. The lower limits of determination were 5×10^{-4} M Hg^{2+} and 4×10^{-6} M Ag^{+}, respectively. The present communication describes the development of an amperometric method for the determination of zinc ions with use of alkaline phosphatase from *E. coli* immobilized by covalent binding on a graphite electrode. The zinc ions present in alkaline phosphatase may be removed by complexing with EDTA. Selective binding of zinc ions by the resulting apoenzyme reactivates enzyme activity, and allows very sensitive detection [2] and determination [3] of zinc.

Experimental

Reagents. Alkaline phosphatase (E.C. 3.1.3.1) from *E. coli* (All-Soviet Research Institute of Applied Biochemistry, Olaine) had an activity of 7.9 U mg^{-1}. Enzymatic activity was determined spectrophotometrically [4] with disodium *p*-nitrophenylphosphate (Fluka) as a substrate in 0.1 M Tris–HCl—10 mM magnesium sulphate buffer, pH 8.0. Water-soluble carbodiimide-1-cyclohexyl-3-(2-morpholinoethyl)carbodiimide-metho-*p*-toluenesulfate (Serva, G.F.R.) was used. *o*-Hydroxyphenylphosphate was synthesized from phosphorus(V) oxide and catechol [5]. All other reagents were chemically pure or of the highest purity available. Regeneration of the activity of immobilized alkaline phosphatase was studied in 0.1 M Tris—HCl buffer (pH 8.0) containing no magnesium ions. Enzyme immobilization was done in 0.05 M acetate buffer (pH 5.6). All solutions were prepared in twice-distilled water, which was also used for all washings.

0003-2670/83/$03.00

Apparatus. Electrochemical measurements were done with a OH-105 polarograph (Radelkis, Hungary) in a 25-cm^3 glass cell thermostatted at 25 ± 0.1°C, using a three-electrode circuit. A graphite disc (0.6 cm in diameter) pressed into teflon was used as the working electrode. The electrode surface area after activation and immobilization of the enzyme (0.89 cm^2) was determined by the dependence of the limiting current of potassium hexacyanoferrate(III) reduction in 1 M potassium chloride on the electrode rotation speed [6]. A saturated calomel electrode (Radiometer, Denmark) was used as the reference. A platinum plate having a geometrical surface area of 12.4 cm^2 served as the auxiliary electrode. During measurements the solutions were stirred by a disc magnetic stirrer (Radiometer).

A Specord M-40 spectrophotometer and quartz cells (1 cm) were used for spectrophotometric measurements.

Immobilization of alkaline phosphatase on graphite. The enzyme was covalently attached to graphite using the water-soluble carbodiimide [7]. For this purpose, the graphite electrode was polished with fine emery paper, and treated ultrasonically for 5 min (22 kHz, 0.2 A) in absolute methanol and water. It was anodized in 10% nitric acid—2.5% potassium dichromate at 2.2 V vs. SCE for 30 s and washed with water. The activated graphite electrode was kept in 0.05 M carbodiimide solution in 0.05 M acetate buffer (pH 5.6) for 30 min and then immersed in the enzyme solution (alkaline phosphatase, 1 mg ml^{-1}, in 0.05 M acetate buffer, pH 5.6) for 12 h at 4°C The electrode was washed with 1 M sodium chloride solution (30 min) and stored in 0.1 M Tris—HCl buffer (pH 8.0) for 48 h at 4°C to eliminate any adsorbed protein.

Removal of zinc from the immobilized enzyme. Zinc was removed as described previously [8] by immersing the enzyme electrode for 48 h in 0.05 M EDTA solution at pH 5.5. The process was monitored spectrophotometrically by following the hydrolysis rate of *p*-nitrophenylphosphate [4].

Determination of zinc. The enzyme electrode with apo-alkaline phosphatase was placed in a cell containing 0.1 M Tris-HCl buffer (pH 8.0) and kept at +0.3 V vs. SCE until a constant background current was established (about 5 min) [9]. The solution of *o*-hydroxyphenyl phosphoric acid in the same buffer was introduced into the cell to give an overall concentration of 10^{-4} M. Then the buffer solution containing zinc acetate (1—12 μM) was introduced and the value of the constant catalytic current resulting from oxidation of the hydrolysed substrate was recorded.

Results and discussion

When stored in the solution of EDTA (pH 5.5) for 2 days, the enzyme electrode based on covalently attached alkaline phosphatase completely loses its catalytic properties with reference to *p*-nitrophenylphosphate. It is also inactive in the hydrolysis reaction of the synthesized substrate *o*-hydroxyphenylphosphate as indicated by the absence of an electrode current at 0.3 V vs. SCE. The current is generated on platinum or carbon electrodes after catechol ester hydrolysis to catechol, which may be detected at potentials (<0.35 V vs. SCE) lower than that for direct ester oxidation [10].

Introduction of zinc ions at low concentrations into the electrochemical cell containing 10^{-4} M catechol ester and an apo-phosphatase electrode produces a stationary current after about 30 s; the magnitude of the current depends on the concentration of zinc ions in the solution (Fig. 1). The lower limit of determination is 0.8 μM. A plot of inverse current against inverse zinc concentration is linear. Its equation may be expressed as

$$i^{-1}\ (\mu A^{-1}) = (0.051 \pm 0.012) + (2.264 \pm 0.032)\ [Zn^{2+}]^{-1}\ (\mu M^{-1})$$

It has a correlation coefficient of 0.9998 (12 results). The electrode based on immobilized alkaline phosphatase may be re-used if, after a determination, it is immersed in EDTA solution (pH 5.5) for 1 h and stored in 0.1 M Tris—HCl buffer (pH 8.0) at 4°C. Under these conditions, the data in Fig. 1 can be reproduced over three weeks.

The activation of alkaline phosphatase by zinc ions and the catalytic process can be presented in a simplified form:

$$\text{a-E} + Zn^{2+} \overset{K_{Zn}}{\rightleftarrows} \text{E; E} + \text{S} \overset{K_S}{\rightleftarrows} \text{E} \cdot \text{S} \overset{k}{\rightleftharpoons} \text{E} + \text{P}$$

where a-E and E are the apo-enzyme and active enzyme, respectively, S is *o*-hydroxyphenylphosphate, P is catechol, K_{Zn} is the dissociation constant for zinc in the enzyme active site, K_S is the dissociation constant of the enzyme-substrate complex and k is the first-order rate constant for product formation.

From this scheme, if the overall process rate is limited by the catalytic reaction, the stationary rate of catechol formation (R) may be expressed as

$$R = k[E]_0[S]_0/\{K_S(1 + K_{Zn}/[Zn^{2+}]) + [S]_0\} \quad (1)$$

where $[E]_0$, $[S]_0$, and $[Zn^{2+}]$ are the overall concentrations of enzyme, substrate and zinc ions. Under stationary-state conditions, the substrate flow to the electrode surface equals the enzymatic reaction rate because the thickness of the catalytic layer is considerably smaller than that of the diffusion layer δ [11]:

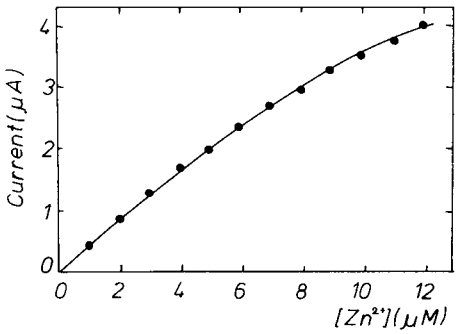

Fig. 1. Dependence of the current in the presence of *o*-hydroxyphenylphosphate on zinc concentration (0.1 mM substrate in 0.1 M Tris—HCl buffer, pH 8.0, E = 0.3 V vs. SCE, 25°C).

$$D([S]_0 - [S]_s)/\delta = V_{max}[S]_s/\{K_S(1 + K_{Zn}/[Zn^{2+}]) + [S]_s\} \quad (2)$$

$$D[P]_s/\delta = V_{max}[S]_s/\{K_S(1 + K_{Zn}/[Zn^{2+}]) + [S]_s\} - k_s[P]_s \quad (3)$$

where $D = D_S \approx D_P$ is the diffusion coefficient for substrate or product, $[S]_0$ and $[S]_s$ are the substrate bulk and surface concentrations, respectively, $[P]_s$ is the concentration of the enzymatic reaction product at the surface, V_{max} is the maximal rate of the enzymatic reaction, and k_s is the heterogeneous rate constant for catechol oxidation. In the derivation of Eqns. (2) and (3), it is assumed that the product concentration outside the diffusion layer is zero. If $K_M = K_S(1 + K_{Zn}/[Zn^{2+}])$ where K_M is the apparent Michaelis constant, $k = V_{max}/K_M$, $\beta = D/\delta$, and if during the experiment $K_M/[S]_0 \gg 1$ the solutions to Eqns. (2) and (3) are $[S]_s = \beta[S]_0/(\beta + k)$ and $[P]_s = k\beta[S]_0/(k + \beta)(k_s + \beta)$. The constant electrode current is $i = nFAk_s[P]_s = nFAk_sk\beta[S]_0/(k + \beta)(k_s + \beta)$, where n is the number of electrons involved in the electrode process, F is the Faraday constant and A is the area of the electrode. Thus the inverse current is directly proportional to the inverse zinc concentration as observed experimentally:

$$i^{-1} = (k_s + \beta)/nFAk_s[S]_0(1/\beta + K_S/V_{max} + K_SK_{Zn}/V_{max}[Zn^{2+}]) \quad (4)$$

This equation indicates that at low zinc concentrations the current is directly proportional to the immobilized enzyme activity and inversely proportional to the product of the dissociation constants.

REFERENCES

1 C. C. Liu, F. M. Fryburg and A. K. Chen, Bioelectrochem. Bioenerg., 8 (1981) 703.
2 A. Townshend and A. Vaughan, Anal. Chim. Acta, 49 (1970) 366.
3 A. Townshend and A. Vaughan, Talanta, 17 (1970) 289.
4 H.-U. Bergmeyer (Ed.), Methods of Enzymatic Analysis, Academic Press, New York, 1965, p. 783.
5 K. J. Humphries and G. Scott, J. Chem. Soc., Perkin Trans. 2, 6 (1973) 831.
6 R. N. Adams, Electrochemistry at Solid Electrodes, Dekker, New York, 1969, p. 89.
7 C. Bourdillon, J.-P. Bourgeous and D. Thomas, Biotechnol. Bioeng., 21 (1979) 1877.
8 M. L. Applebury and J. E. Coleman, J. Biol. Chem., 244 (1969) 709.
9 V. J. Razumas, J. J. Kulys and A. A. Malinauskas, Anal. Chim. Acta, 117 (1980) 387.
10 J. Kulys, V. Razumas and A. Malinauskas, Bioelectrochem. Bioenerg., 7 (1980) 11.
11 V. G. Levich, Physicochemical Hydrodynamics, Prentice-Hall, Englewood Cliffs, N.J., 1962, p. 60.

Analytica Chimica Acta, 152 (1983) 275—280
Elsevier Science Publishers B.V., Amsterdam — Printed in The Netherlands

Short Communication

COULOMETRIC GENERATION OF HYDROGEN ION BY ANODIC OXIDATION OF ASCORBIC ACID AND NAPHTHOHYDROQUINONES IN ACETONITRILE AND IN ACETIC ACID—ACETIC ANHYDRIDE MIXTURES

VILIM J. VAJGAND*

Institute of Chemistry, University of Beograd, Studentski trg 16, Beograd (Yugoslavia)

RANDJEL P. MIHAJLOVIĆ

Institute of Chemistry, University of Kragujevac, Radoja Domanovića 12, Kragujevac (Yugoslavia)

(Received 3rd January 1983)

Summary. Coulometric generation of hydrogen ions by the oxidation of ascorbic acid, 1,4-naphthohydroquinone and 2,6-naphthohydroquinone in anhydrous acetonitrile and in acetic acid—acetic anhydride is described. Current—voltage curves for solvents, indicator, titrated bases and depolarizer show that all three depolarizers are oxidized at potentials more negative than those of bases and other components in the solution. Titrations of sodium acetate and potassium hydrogenphthalate in acetic acid—acetic anhydride (1:6), and of triethanolamine, *p*-toluidine and γ-picoline in acetonitrile, with hydrogen ions generated at a platinum anode by the oxidation of these depolarizers, proved that ascorbic acid and 1,4-naphthohydroquinone are successful. With ascorbic acid, the current efficiency was 100 ± 0.3%.

A problem faced in the titrimetric and potentiometric determination of bases in nonaqueous media is the preparation of non-aqueous titrant solutions. Kolthoff and Ikeda [1] attempted to obtain nonaqueous perchloric acid solution in acetonitrile by the action of 100% sulphuric acid on barium perchlorate, but 0.25 M perchloric acid solution obtained by this method contains at least 0.07% of water. In order to remove water, Coetzee and Kolthoff [2] added acetic anhydride to the solution of perchloric acid in acetonitrile. Other workers have tried to obtain nonaqueous perchloric acid in acetonitrile by electrolyzing silver perchlorate [3] or sodium perchlorate [4].

Unfortunately, perchloric acid solutions obtained by any of these methods are unsuitable for the titration of bases for several reasons. The hydrogen ion activity in acetonitrile decreases on standing, with an abrupt decrease one hour after preparation of the solution; on standing in acetonitrile, perchloric acid may decompose to water and Cl_2O_7 [5] or form a cyclic dimer [6]. On standing with acetic anhydride, the concentration of perchloric acid decreases on account of CH_3COClO_4 formation [7].

To avoid the preparation of perchloric acid solution, Streuli [8] titrated aliphatic and aromatic amines with hydrogen ions generated at a platinum

0003-2670/83/$03.00

anode from the oxidation of water which was introduced as $LiClO_4 \cdot 3H_2O$. These titrations gave 10% low results for aromatic amines, because they were oxidized by oxygen liberated concurrently; this oxidation could be prevented by adding hydroquinone as antioxidant to the anolyte [9].

Mather and Anson [10, 11] applied a mercury anode for titrations of sodium acetate, potassium hydrogenphthalate and sodium fluoride in acetic acid—acetic anhydride. Mercury was thought to be oxidized to mercury(I) ions which react with acetic acid to produce hydrogen ions. However, a study of the electrochemical oxidation of mercury in acetic acid—acetic anhydride mixtures led Durand and Tremillon [12] to conclude that mercury was oxidized quantitatively to mercury(I) which did not react with acetic acid, i.e., hydrogen ions cannot be obtained in this way.

Difficulties connected with titrimetric and coulometric determinations of bases in nonaqueous media can be avoided, as shown earlier [13—16], by generating hydrogen ions at a platinum anode directly by oxidation of dihydric and trihydric phenols and their derivatives, or cyclohexadiene, or thiol compounds. The present paper deals with the application of ascorbic acid and naphthohydroquinones as sources of hydrogen ions in coulometric titrations of bases in nonaqueous acetonitrile and acetic acid—acetic anhydride mixture.

Experimental

Chemicals. All depolarizers examined and bases titrated were of p.a. purity (Merck or Fluka). Before use, acetonitrile was purified as described by Krešković et al. [17]. Acetic acid and acetic anhydride were redistilled and fractions boiling at 116° and 138°, respectively, were collected.

Sodium acetate solution was prepared by weighing directly in a volumetric flask a weighed amount of sodium carbonate (obtained by heating sodium hydrogen carbonate at 270° C), dissolving it in a little acetic acid and diluting the solution to the mark with acetic acid—acetic anhydride mixture. Potassium hydrogen phthalate solution was obtained by weighing the base directly in a volumetric flask and adding the solvent mixture to the mark.

Liquid organic bases were first dried over fused potassium hydroxide and then distilled under reduced pressure. The purity of the bases was checked by titrations with hydrogen ions generated from hydroquinone oxidation [14].

The supporting electrolyte was 0.2 M sodium perchlorate solution in anhydrous acetonitrile or in acetic acid—acetic anhydride (1:6).

Titration end-points were detected by means of a 0.1% solution of either crystal violet in anhydrous acetonitrile or malachite green in acetic acid—acetic anhydride.

Equipment. The equipment used consisted of a current source, an electrolytic vessel, a differential colorimeter and a pen-recorder. The current source was a voltage—current stabilizer (Vinca, Beograd); the current in the generating circuit was measured with a precise milliammeter (Iskra, Kranj).

The electrolytic cell was U-shaped (Fig. 1), the anolyte being separated from the catholyte by means of a sintered glass G-4 disk. The volume of the anolyte was 2—3 cm^3 and that of the catholyte about 10 cm^3 (Fig. 1A), or the volumes of the anolyte and the catholyte were 20 cm^3 and 25 cm^3, respectively (Fig. 1B). The electrodes were platinum wire spirals, each with an area of about 300 mm^2. During electrolysis, the anolyte was stirred strongly with a magnetic stirrer. Titration end-points were detected either visually or with a Lange differential colorimeter (Model VI). In photometric end-point detection, the anode compartment of the electrolytic vessel was placed in front of one photocell, whereas a cuvette containing the supporting electrolyte to which one drop of indicator was added, was placed in front of the other photocell. Changes in the photocurrent intensity during the electrolysis were recorded by a chart recorder (Radelkis, Type OH-102).

Procedure for visual end-point detection. The anode and cathode compartments of the electrolytic cell (Fig. 1A) are filled with the supporting electrolyte to the same level. To the anolyte are added a drop of indicator, about 100 mg of ascorbic acid and a drop of the base investigated. The current is switched on and electrolysis is continued until the indicator colour changes. Then, a weighed amount (about 4×10^{-5} mol) of the base investigated is added to the anolyte. After simultaneous switching on of the current and the chronometer, the titration is continued until the same indicator color is obtained. A new base aliquot is then added to the anolyte and the solution is again titrated. Several samples can be determined successively in the same supporting electrolyte.

Procedure for photometric end-point detection. The supporting electrolyte is poured into the electrode compartments (Fig. 1B) to the same

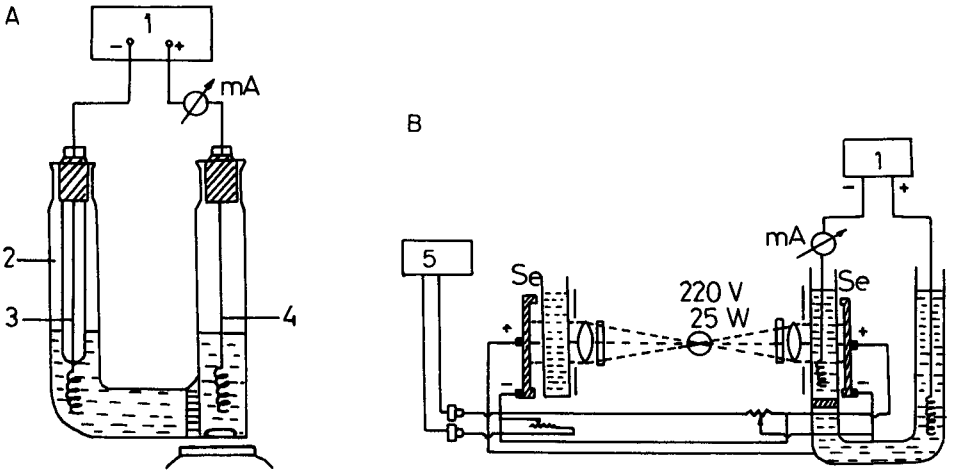

Fig. 1. Schematic diagram of the apparatus for coulometric titration of bases with (A) visual end-point detection, and (B) photometric end-point detection. (1) Current stabilizer; (2) electrolytic cell; (3) Pt cathode; (4) Pt anode; (5) pen recorder; (Se) selenium photocell.

level, and about 100 mg of ascorbic acid, 2—3 drops of the indicator and a small amount of the investigated base are added to the anolyte. The anode compartment is placed in front of one photocell; in front of the other photocell is placed a cuvette with supporting electrolyte containing a drop of the indicator. The platinum electrodes are dipped into the electrolyte chambers, and magnetic stirring is started. The recorder pen is zeroed by widening the colorimeter slit, and the current is switched on. When the base added has reacted with the generated hydrogen ions, the indicator changes colour and so does the photocurrent. The electrolysis is interrupted at the maximum change of photocurrent. Then, to the anolyte is added a weighed amount (about 4×10^{-5} mol) of the base under test and the titration is allowed to proceed to the same photocurrent. Several samples can be titrated successively in the same supporting electrolyte.

Results and discussion

Oxidation of ascorbic acid. Ascorbic acid is readily oxidized by mild oxidants to form dehydroascorbic acid; more powerful oxidants, having oxidation potentials higher than 1.1 V, oxidize ascorbic acid to oxalic and threonic acids, or even to carbon dioxide. Oxidation of ascorbic acid at a platinum microelectrode gives dehydroascorbic acid and produces the usual voltammetric wave [18]. It was assumed here that the anodic oxidation of ascorbic acid at the platinum anode for coulometric purposes in nonaqueous acetonitrile or acetic acid—acetic anhydride (1:6) would also proceed only to the dehydroascorbic acid stage with the production of two hydrogen ions.

From the current—voltage curves 1—6 (Fig. 2A, B) obtained for ascorbic acid, and the indicators, bases and solvents used, it is clear that ascorbic acid in anhydrous acetonitrile and in acetic acid—acetic anhydride (1:6) is oxidized

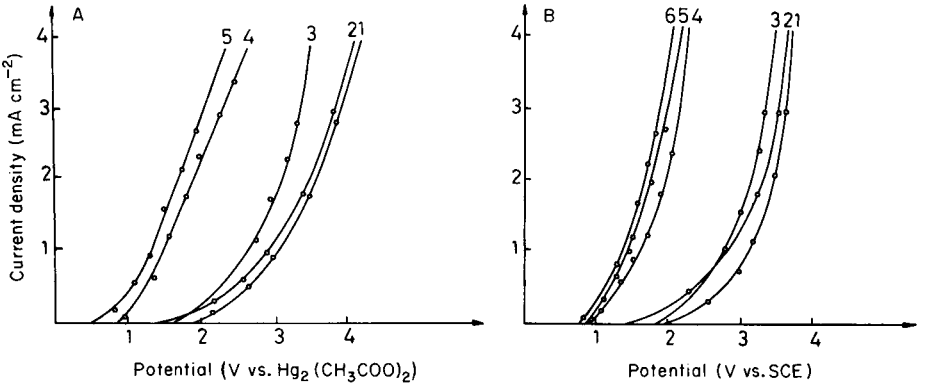

Fig. 2. Change of anode potential with current density. A, In 0.2 M sodium perchlorate in acetic acid—acetic anhydride (1:6): (1) solvent; (2) malachite green; (3) sodium acetate; (4) ascorbic acid; (5) 1,4-naphthohydroquinone. B, In 0.2 M sodium perchlorate in anhydrous acetonitrile: (1) solvent; (2) crystal violet; (3) pyridine; (4) 2,6-dihydroxynaphthalene; (5) 1,4-dihydroxynaphthalene; (6) ascorbic acid.

at potentials which are more negative than the oxidation potentials of the other components present in the solution.

In order to establish whether the oxidation of ascorbic acid is rapid and quantitative, sodium acetate and potassium hydrogen phthalate were titrated in the acetic acid—acetic anhydride mixture, and γ-picoline and *p*-toluidine in anhydrous acetonitrile, with hydrogen ions generated in the oxidation to dehydroascorbic acid; visual or photometric end-point detection was used as in the Experimental part. Percentage current efficiency was calculated from the weighed amount of the base and that found in titration with generated hydrogen ions. In each case, correction was made for the current consumed in neutralization of the solvent in which the base was dissolved. The results obtained in such titrations are given in Table 1.

Oxidation of naphthohydroquinones. Oxidation potentials of naphthohydroquinones in water and aqueous alcohol are about 300 mV more negative than those of benzohydroquinones [19]. Oxidation potentials of anthrahydroquinones in water are about 150 mV, so that they are oxidized to the corresponding quinones by atmospheric oxygen and therefore cannot be applied as sources of hydrogen ions in coulometric titrations. The oxidation potentials of 1,4-naphthohydroquinone and 2,6-naphthohydroquinone in anhydrous acetonitrile and in acetic acid—acetic anhydride (1:6) (Fig. 2B) are more negative than those of the indicator, the titrated base and the solvent. Oxidation of these naphthohydroquinones at a platinum anode proceeds in the usual way to form the corresponding naphthoquinone with production of two hydrogen ions, as in the case of ascorbic acid. Results obtained in the determination of triethanolamine and *p*-toluidine in anhydrous acetonitrile, and of sodium acetate and potassium hydrogen phthalate in acetic acid—acetic

TABLE 1

Current efficiency in titrations of bases with hydrogen ions generated by the oxidation of ascorbic acid or 1,4-naphthohydroquinone (I = 9 mA)

Depolarizer	Solvent	Titrated base	Current efficiency[a] (%)
1,4-Naphthohydroquinone	CH_3COOH—$(CH_3CO)_2O$	Sodium acetate	100.1 ± 0.6
		Potassium hydrogenphthalate	100.0 ± 0.4
	CH_3CN	Triethanolamine	100.0 ± 0.1
		p-Toluidine	100.1 ± 0.6
Ascorbic acid	CH_3COOH—$(CH_3CO)_2O$	Sodium acetate	100.0 ± 0.3
		Potassium hydrogenphthalate	100.0 ± 0.2
	CH_3CN	*p*-Toluidine	99.9 ± 0.3
		γ-picoline	99.9 ± 0.2

[a]Mean and standard deviation for 6—8 measurements.

anhydride, by means of hydrogen ions generated by the oxidation of 1,4-naphthohydroquinone, are given in Table 1.

As the oxidation potentials of ascorbic acid and 1,4-naphthohydroquinone in anhydrous acetonitrile and in acetic acid—acetic anhydride (1:6) are more negative than the oxidation potentials of all the components present in the solution, and as the oxidation of these depolarizers proceeds with 100% current efficiency, it can be concluded that these depolarizers can be applied successfully as sources of hydrogen ions in coulometric titrations of bases in these solvents. Although the oxidation potentials of 2,6-naphthohydroquinone and 1,4-naphthohydroquinone are similar, the former cannot be used because its oxidation product is precipitated at the platinum anode, which decreases the current efficiency.

REFERENCES

1 I. M. Kolthoff and S. Ikeda, J. Phys. Chem., 65 (1961) 1020.
2 J. F. Coetzee and I. M. Kolthoff, J. Am. Chem. Soc., 79 (1957) 6110.
3 A. Schmidt and J. Noack, Z. Anorg. Allg. Chem., 296 (1958) 262.
4 J. Vedel and B. Tremillon, J. Electroanal. Chem., 1 (1959/60) 241.
5 P. T. Cotrell and C. K. Mann, J. Electrochem. Soc., 116 (1969) 1499.
6 D. Clark, M. Fleischmann and D. Pletcher, J. Electroanal. Chem., 36 (1972) 137.
7 G. Durand and B. Tremillon, Bull. Soc. Chim. Fr., (1963) 2855.
8 C. A. Streuli, Anal. Chem., 28 (1956) 130.
9 R. B. Hanselman and C. A. Streuli, Anal. Chem., 28 (1956) 916.
10 W. B. Mather and F. C. Anson, Anal. Chim. Acta, 31 (1959) 468.
11 W. B. Mather and F. C. Anson, Anal. Chem., 33 (1961) 132.
12 G. Durand and G. Tremillon, Bull. Soc. Chim. Fr., (1969) 2867.
13 V. J. Vajgand, R. P. Mihajlović and M. M. Rakočević, Glasnik Hem. Društva, Beograd, 37 (1972) 269.
14 V. J. Vajgand and R. P. Mihajlović, Talanta, 16 (1969) 1311.
15 V. J. Vajgand, R. P. Mihajlović and S. M. Manetović, Glasnik Hem. Društva, Beograd, 38 (1973) 126.
16 R. P. Mihajlović and V. J. Vajgand, Zbornik Radova PMF, Kragujevac, 2 (1981) 121; 3 (1983) 145.
17 P. Kreškov, N. Bikova and A. Kazarjan, Kislotno-osnovnoe Titrovanie v Nevodenih Rastvorah, Himija, Moskva, 1967.
18 E. M. Skobec and N. N. Atamanenko, Zav. Lab., 11 (1949) 1291.
19 J. B. Conant and L. F. Fieser, J. Am. Chem. Soc., 46 (1924) 1858.

Analytica Chimica Acta, 152 (1983) 281—284
Elsevier Science Publishers B.V., Amsterdam — Printed in The Netherlands

Short Communication

POTENTIOMETRIC TITRATION OF PHARMACEUTICAL COMPOUNDS IN FORMULATIONS WITH SODIUM TETRAPHENYLBORATE

E.P. DIAMANDIS* and T. K. CHRISTOPOULOS

Laboratory of Analytical Chemistry, University of Athens, 104 Solonos Street, Athens 114 (Greece)

(Received 29th January 1983)

Summary. Simple potentiometric titrations are described for the determination of various cationic pharmaceutical compounds with sodium tetraphenylborate; end-points are detected with a tetraphenylborate-selective electrode. Satisfactory results were obtained for the active components in various antihistaminic, neuroleptic, antispasmodic, anticholinergic, tranquilizer and antidepressant preparations. The relative standard deviation at the 25-μmol level is typically 0.3—0.7%.

Ion-selective electrodes have been applied successfully to the determination of various pharmaceutical compounds in drugs [1]. Sodium tetraphenylborate has been extensively used for the determination of univalent cations, including various alkaloids, cationic surfactants, quaternary ammonium compounds and amines, by gravimetric or titrimetric methods. In many titrimetric methods, ion-selective electrodes are used for end-point detection [2—9]. Recently, the construction of a liquid-membrane tetraphenylborate electrode was described, along with its application in the potentiometric titration of various organic cations with tetraphenylborate [10]. Here, this electrode is used in the semi-automatic titration of several pharmaceutical compounds with sodium tetraphenylborate. For most compounds, steep titration curves with large potential breaks were observed. The precision of the titrations was better than 1% in all cases (typically 0.3—0.7%). Application of the method to various commercial pharmaceutical preparations gave satisfactory results.

Experimental

Apparatus. The electrodes, the reaction cell and the titration and recording system were as previously reported [10]. Titrant delivery rates were kept constant at 0.36 ml min^{-1}. Titrations were done at ambient temperature (22 ± 2°C) with constant magnetic stirring.

Reagents. Solutions were prepared with deionized distilled water from reagent-grade materials. The standard 0.010 M sodium tetraphenylborate solution was prepared and standardized as reported previously [10]. Standard solutions of the pharmaceutical compounds were prepared from materials of the highest purity available used as received; generally, 10^{-3} M

0003-2670/83/$03.00

solutions were prepared by dissolving the appropriate amount of the hydrochloride (chlorpromazine, promethazine, imipramine, clomipramine, opipramol, amitriptyline) or bromide (prostigmine, pyridostigmine, clidinium) in water. Thioproperazine bismethane sulfonate was also dissolved in water. Medazepam was dissolved in citrate buffer, pH 2.5. Commercial pharmaceutical preparations were purchased from pharmaceutical industries and local drug stores.

All buffers (0.10 M) were prepared as before [10]. Buffers used were citrate (pH 2.5), acetate (pH 3.3 and 5.0), and phosphate (pH 7.0 and 10.2).

Titration of aqueous solutions of pharmaceutical compounds with standard 0.01000 M sodium tetraphenylborate solution. Pipet into a 50-ml beaker a 25.00-ml aliquot of the sample in the range 2.00×10^{-4}—1.00×10^{-3} M for chlorpromazine hydrochloride, promethazine hydrochloride, imipramine hydrochloride, clomipramine hydrochloride, opipramol dihydrochloride, amitriptyline hydrochloride, thioproperazine bismethane sulfonate, medazepam, clidinium bromide, prostigmine bromide and 4.00×10^{-4}—1.00×10^{-3} M for pyridostigmine bromide. Add 5.00 ml of the appropriate buffer solution, start the stirrer and after the potential has stabilized (ca. 1 min) start the constant-rate burette and the recorder simultaneously to obtain the titration curve. Calculate the amount of the pharmaceutical compound present in the sample titrated in the usual way.

Analysis of pharmaceutical preparations. For tablet preparations, 20 tablets are weighed and powdered. An appropriate weighed amount of the powder (equivalent to about 0.5 mmol of active ingredient) is transferred to a 500-ml beaker, and stirred vigorously with about 400 ml of water for 15 min. The solution is diluted to the mark in a 500-ml volumetric flask and a 25.00-ml aliquot is titrated as described above. For injections, drops and syrups, an appropriate volume of the sample (equivalent to 0.2 mmol of active ingredient) is diluted with water to 200 ml in a volumetric flask and a 25.00-ml aliquot is titrated as described above.

Results and discussion

The optimum pH for each titration, selected to provide accurate precise results, small blanks and steep end-point breaks, was found by titrating each compound at various pH values in the range 2.5—10.2. Titrations at pH < 2.5 are not feasible because the electrode misbehaves in strongly acidic solutions and the sodium tetraphenylborate solution decomposes (cf. [10]). The optimum pH values are listed in Table 1, and the results obtained for the drugs in aqueous solutions and in commercial preparations are shown in Tables 1 and 2, respectively. There is fairly good agreement between the amounts of substance calculated by the titrimetric method with the nominal values. The end-point jumps were steep, except for Anafranil, Noveril and Mestinon tablets, but even in these cases the deviations were acceptable (Table 2). The solutions obtained for titration after dissolution of the commercial preparations were usually turbid, coloured or viscous, because of

TABLE 1

Results obtained for various drugs by potentiometric titration with sodium tetraphenylborate[a]

Compound	Optimum pH	Assay (%)	R.s.d. (%)	End-point break (mV)
Chlorpromazine hydrochloride	3.3	101.5	0.7 (4)[b]	230
Promethazine hydrochloride	3.3	99.0	0.4 (5)	180
Thioproperazine bismethane sulfonate	3.3	98.1	0.6 (6)	180
Imipramine hydrochloride	3.3	101.4	0.7 (4)	250
Clomipramine hydrochloride	3.3	99.9	0.6 (3)	250
Opipramol dihydrochloride	5.0	99.4	0.6 (3)	120
Amitriptyline hydrochloride	3.3	97.9	0.4 (4)	250
Medazepam	2.5	99.7	0.4 (3)	190
Clidinium bromide	3—7	99.7	0.5 (4)	110
Pyridostigmine bromide	3—10	100.2	0.2 (4)	95
Prostigmine bromide	5—10	98.5	0.6 (4)	100

[a]Results are based on the titration of a sample containing about 25.0 μmol of compound. [b]The number in parentheses is the number of determinations.

TABLE 2

Determination of active substances in various pharmaceutical preparations by potentiometric titration with sodium tetraphenylborate

Preparation[a]	Content of drug		R.s.d.[c] (%)
	Nominal	Found[b]	
Chlorpromazine injection (Largactil)	5 mg ml^{-1}	5.1	0.2 (4)
Chlorpromazine tablets (Largactil)	100 mg/tabl.	99.5	0.2 (3)
Promethazine injection (Phenergan)	50 mg/2 ml	50.9	0.4 (4)
Promethazine syrup (Phenergan)	1 mg ml^{-1}	1.03	0.4 (4)
Promethazine tablets (Phenergan)	25 mg/tabl.	25.6	0.4 (4)
Promazine injection (Sparine)	50 mg ml^{-1}	49.6	0.3 (3)
Promazine syrup (Sparine)	10 mg/5 ml	10.3	0.3 (3)
Imipramine injection (Tofranil)	25 mg/2 ml	24.8	0.2 (3)
Imipramine tablets (Tofranil)	25 mg/tabl.	25.4	0.1 (3)
Amitriptyline tablets (Amitriptyline)	25 mg/tabl.	25.9	0.4 (3)
Clomipramine tablets (Anafranil)	25 mg/tabl.	25.3	0.9 (3)
Opipramol tablets (Insidon)	50 mg/tabl.	50.1	0.2 (3)
Trifluoperazine tablets (Stelazine)	5 mg/tabl.	5.2	0.4 (3)
Dibenzepin tablets (Noveril)	240 mg/tabl.	239	0.8 (3)
Cyproheptadine tablets (Periactin)	4 mg/tabl.	4.1	0.9 (3)
Propyromazine[d] drops (Diaspasmyl)	100 mg/10 ml	95.7	0.7 (3)
Prostigmine[d] tablets (Prostigmine)	15 mg/tabl.	15.0	0.3 (4)
Pyridostigmine[d] tablets (Mestinon)	60 mg/tabl.	62.7	0.2 (3)

[a]Compound is present as the hydrochloride, except where indicated. [b]Compounds titrated at optimum pH (Table 1) or at pH 3.3 for compounds not included in Table 1. End-point breaks were as listed in Table 1; for unlisted drugs, the breaks were 160—250 mV, except for dibenzepin (125 mV). [c]Number of determinations in parentheses. [d]Present as hydrobromide.

the excipients present. All these solutions could be titrated potentiometrically without difficulty.

Chlorpromazine has been titrated potentiometrically with silver nitrate and a chloride or silver ion-selective electrode, after combustion of the sample to release chloride [2], which is time-consuming. Selig [4] titrated chlorpromazine and other pharmaceutical substances with sodium tetraphenylborate and a fluoroborate ion-selective electrode. The substances listed in Tables 1 and 2 have not previously been determined by potentiometric titrations with sodium tetraphenylborate to a tetraphenylborate-selective electrode end-point.

The proposed procedures are simple, accurate and sensitive and are suitable for quality control. Their main limitation is lack of selectivity, as any ion that precipitates tetraphenylborate at the relevant pH will cause positive errors. Fortunately, many pharmaceutical preparations contain the active ingredient in mixtures with inert excipients.

The authors are grateful to Professor T. P. Hadjiioannou for valuable discussions and Mrs G. Tsoutsoura for technical help.

REFERENCES

1 V. V. Cosofret, Membrane Electrodes in Drug-Substances Analysis, Pergamon Press, Oxford, 1982.
2 Y. M. Dessouky, K. Tóth and E. Pungor, Analyst, 95 (1970) 1027.
3 S. Pinzauti and E. La Porta, Analyst, 102 (1977) 938.
4 W. Selig, Talanta, 27 (1980) 914; Mikrochim. Acta, (1980 II) 133; Frezenius Z. Anal. Chem., 308 (1981) 21.
5 E. P. Diamandis and T. P. Hadjiioannou, Anal. Lett, 13 (B15) (1980) 1317.
6 K. Vytras, M. Dajkova and V. Mach, Anal. Chim. Acta, 127 (1981) 165.
7 A. Gur'ev, G. M. Lizunova, I. M. Korenman and O. N. Medvedeva, Zh. Anal. Khim., 36 (1981) 130.
8 E. P. Diamandis, E. Athanasiou-Malaki, D. S. Papastathopoulos and T. P. Hadjiioannou, Anal. Chim. Acta, 128 (1981) 239.
9 C. E. Efstathiou, E. P. Diamandis and T. P. Hadjiioannou, Anal. Chim. Acta, 127 (1981) 173.
10 T. K. Christopoulos, E. P. Diamandis and T. P. Hadjiioannou, Anal. Chim. Acta, 143 (1982) 143.

Analytica Chimica Acta, 152 (1983) 285—288
Elsevier Science Publishers B.V., Amsterdam — Printed in The Netherlands

Short Communication

VOLTAMMETRIC DETERMINATION OF URANIUM IN SEA WATER AFTER PRECONCENTRATION ON THE TRIOCTYLPHOSPHINE OXIDE-COATED GLASSY CARBON ELECTRODE

KOSUKE IZUTSU*, TOSHIO NAKAMURA and TOSHIYUKI ANDO

Department of Chemistry, Faculty of Science, Shinshu University, Asahi, Matsumoto 390 (Japan)

(Received 23rd March 1983)

Summary. The voltammetric method which determines traces of uranyl ions after preconcentration on a tri-n-octylphosphine oxide (TOPO)-coated glassy carbon electrode was applied in the determination of uranium in sea water. Removal of hydrogencarbonate ions from the sea water by pH adjustment and heating was the only necessary pretreatment.

Recently Izutsu et al. [1, 2] reported a voltammetric method for the determination of trace uranyl ions after preconcentration on the tri-n-octylphosphine oxide (TOPO)-coated glassy carbon (GC) electrode. The method has excellent selectivity and sensitivity, and, among the constituents contained in sea water, only hydrogen carbonate ions would be expected to interfere with the determination of uranium. The present communication reports the use of this method in the determination of uranium in a sample of sea water which was collected in the Sea of Japan. The results were verified by using the spectrophotometric procedure of Ohnishi et al. [3].

Experimental

Voltammetric measurements. For voltammetric measurements, a personal computer (Sol-20; Processor Technology), equipped with 12-bit A/D and D/A converters, was used in combination with a potentiostat, a function generator, and an X—Y recorder. The TOPO-coated GC electrode was prepared and treated as described recently [2], except that 5 μl of ethanolic 0.0025 M TOPO solution was used to coat the GC disk (3.0 mm diameter) electrode. A weighing bottle (80 mm tall, 30 mm diameter) served as the electrolytic cell, and an Ag/AgCl reference electrode and a platinum wire counter electrode were set through a teflon stopper. All voltammetric measurements were at 25°C. Nitrogen was passed through the solution continuously even during the preconcentration and the voltammetric measurement to purge dissolved oxygen as completely as possible. During preconcentration, the solution was stirred magnetically with a Spin-fin (19 mm diameter × 12.7 mm) at 600 rpm. Voltammograms were measured at a scan-rate of 10 V s^{-1}. All reagents were the same as those used previously [2].

0003-2670/83/$03.00

Voltammetric procedure for sea water. The sea water was collected in the Sea of Japan off the coast of Etchu-Miyazaki, Toyama Prefecture, and was filtered through a 0.45-μm Millipore filter. The sample (30 ml) was placed in the electrolytic cell and 120 μl of 0.1 M acetic acid and 120 μl of 1 M hydrochloric acid were added to adjust the pH to about 2.5. It was boiled gently for ca. 5 min to remove dissolved carbon dioxide. After being cooled to room temperature, the solution was adjusted to pH 4.0 with sodium hydroxide and deaerated with nitrogen for about 30 min with the electrodes in position. The voltage of the TOPO-coated GC electrode was then cyclically scanned ten times between 0 V and −1.4 V to remove the uranyl ions concentrated on the electrode surface. The electrode was kept at 0 V for 20 min to preconcentrate uranyl ions, and then the voltammogram was measured between 0 V and −1.4 V. The peak current was measured by the computer and the current–potential curve was also recorded. The amount of uranium was determined by the standard addition method; the addition of known amounts of uranyl ions and the measurement of the peak current after preconcentration was repeated several times.

Spectrophotometric measurements. A Shimadzu multipurpose recording spectrophotometer MPS-50L and a 5-cm cuvette were used. Chelate resin (Dowex A-1; 50–100 mesh, sodium form) was a product of Dow Chemicals Co.; 1,2-cyclohexanediaminetetraacetic acid (CyDTA) and arsenazo-III were Dotite reagents (Dojindo Co.). Other reagents were of analytical-reagent grade (Wako Pure Chemicals Industries) and were used as received.

Spectrophotometric procedure for sea water. The sample (1 l) was acidified with 10 ml of concentrated hydrochloric acid, boiled for 20 min, and then cooled to room temperature. After the solution had been adjusted to pH 3 with aqueous ammonia, 5 ml of 1% (w/v) CyDTA solution and 4 g of Dowex A-1 were added and the solution was stirred for 70 min to collect the uranium onto the resin. The resin was removed to a 50-ml beaker and 20 ml of 3% (w/v) ammonium carbonate solution was added to liberate the uranium. The resin was filtered off, the filtrate was evaporated to dryness, and the residue was dissolved in 12 ml of 8 M hydrochloric acid. Uranium(VI) in the solution was reduced to uranium(IV) with zinc and the solution was transferred to a 25-ml volumetric flask. After addition of 5 ml of 6 M hydrochloric acid, saturated with oxalic acid, and 1 ml of 0.1% (w/v) arsenazo-III solution, the solution was diluted to the mark with 8 M hydrochloric acid. The absorbance was measured at 665 nm in a 5-cm cuvette. The calibration graph was obtained by following the whole procedure.

Results and discussion

A typical voltammogram for uranyl ions, measured after preconcentration, is shown in Fig. 1, curve 1. If the peak current is obtained by correcting for the residual current as shown in the figure, the small blank current which is always observed for solutions free of uranyl ion interferes with the determination of small concentrations of uranyl ions. Therefore, in this work,

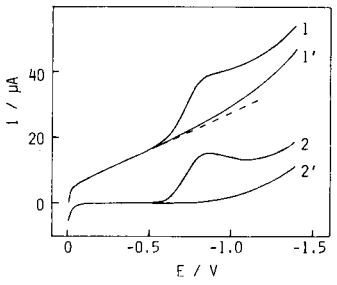

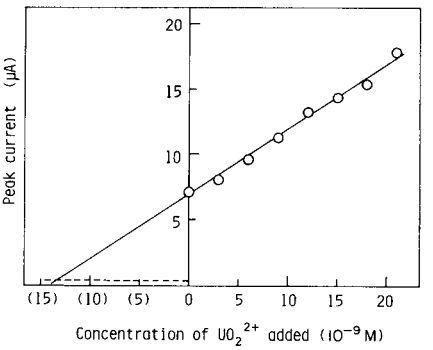

Fig. 1. Voltammograms at the TOPO-coated GC electrode after preconcentration for 20 min at 0 V. Curves: (1 and 2) sea water + 1.5×10^{-8} M UO_2^{2+}; (1', 2') UO_2^{2+}-free artificial sea water. Curves 1 and 1' are without correction; curves 2 and 2' are corrected for the residual current (dashed line).

Fig. 2. Calibration graph obtained by the standard addition of uranyl ions to sea water and the blank current in the artificial sea water (dashed line).

the blank current was kept as small and reproducible as possible in the following ways. First, the dissolved oxygen in the electrolytic solution was removed completely. Secondly, the ratio of the blank current against the peak current was improved by measuring the voltammograms at a high voltage scan rate (10 V s^{-1}). The effect of the scan rate on the ratio was reported previously [2]. Thirdly, the peak current was obtained with the aid of the computer by correcting for the residual current which was obtained from the linear part of the current—potential curve between —0.1 and —0.4 V by the least-squares method. This procedure improved the reproducibility of the results compared with the pen-and-ink recording of the voltammograms.

The blank current was obtained in the artificial sea water of Lyman and Fleming [4] by the same procedures as those applied to the sea water sample. The average value, 0.42 μA, was corrected for in the determination of uranium in the sea water.

An example of the calibration graphs obtained by the standard addition method described in the Experimental part is shown in Fig. 2. The amount of uranium was determined by correcting for the blank current. The average uranium content found was 1.32×10^{-8} M (3.14 μg l^{-1}) with a relative standard deviation of 5.2% (8 measurements).

The uranium content in the sea water sample was also determined spectrophotometrically by the method of Ohnishi et al. [3] as outlined above. The average value found was 1.33×10^{-8} M (3.16 μg l^{-1}) with a relative standard deviation of 2.75% (7 measurements), which is in good agreement with the voltammetric results. Though the voltammetric method is somewhat inferior in precision to the spectrophotometric method, it needs smaller samples and simpler procedures and seems to be an interesting example of practical analytical applications of modified electrodes.

This work was supported by a Grant-in-Aid for Scientific Research from the Ministry of Education of Japan (No. 421707).

REFERENCES

1 K. Izutsu, T. Nakamura and T. Oku, Nippon Kagaku Kaishi, (1980) 1656.
2 K. Izutsu, T. Nakamura, R. Takizawa and H. Hanawa, Anal. Chim. Acta, 149 (1983) 147.
3 K. Ohnishi, Y. Hori and Y. Tomari, Bunseki Kagaku, 26 (1977) 74.
4 J. Lyman and R. H. Fleming, J. Mar. Res., 3 (1940) 134.

Analytica Chimica Acta, 152 (1983) 289—293
Elsevier Science Publishers B.V., Amsterdam — Printed in The Netherlands

Short Communication

BEHAVIOUR OF TRIMETALLIC IRON, RUTHENIUM AND OSMIUM CLUSTERS IN REVERSED-PHASE HIGH-PERFORMANCE LIQUID CHROMATOGRAPHY

A. MANGIA* and G. PREDIERI

Istituto di Chimica Generale ed Inorganica, Università di Parma, Via M. D'Azeglio 85, 43100 Parma (Italy)

E. SAPPA

Istituto di Chimica Generale ed Inorganica, Università di Torino, Corso M. D'Azeglio 48, 10125 Torino (Italy)

(Received 8th March 1983)

Summary. The reversed-phase chromatographic behaviour of some trinuclear carbonyl clusters of iron, ruthenium and osmium, having the same basic triangular ensemble of the parent $M_3(CO)_{12}$, is reported. On a LiChrosorb RP-18 column, compounds having similar structures and different substituents were separated by using acetonitrile or acetonitrile/methanol mixtures as mobile phases. The elution order appears to be related to the nature of the substituents and, in the case of clusters of different metals, to the electronegativity of the metal.

The separation and purification of mixtures of transition organometallic derivatives, after the preparative runs, is frequently accomplished by chromatographic techniques, in particular column chromatography and t.l.c. However, in view of the increasing number of studies on transition organometallic derivatives and on polynuclear clusters, new fast and reliable procedures are needed for separation and identification. High-performance liquid chromatography (h.p.l.c.) has been used to separate organometallic compounds, mostly mononuclear compounds [1, 2] and has also proved of value in following the course of reactions involving polynuclear clusters of iron and ruthenium [3—5].

As part of continued research on the h.p.l.c. of metal complexes [6], investigations on the potential of h.p.l.c. in the separation and determination of polynuclear derivatives were undertaken. The separation of mixtures of bimetallic iron alkyne—carbonyl derivatives proved successful [7]. The separation of complexes containing the same $Fe_2(CO)_6$ basic unit, but with different structures and number of substituents had previously been shown to be possible.

The present communication is concerned with trinuclear iron, ruthenium and osmium clusters which can be obtained easily under different reaction conditions; these complexes contain a triangular arrangement of metal atoms, but have different substituents or structures. The structures of all the

0003-2670/83/$03.00

derivatives are known, in most cases through single-crystal x-ray diffraction analysis.

The following complexes were selected: $M_3(CO)_{12}$, with, as the metal, ruthenium (Ia), osmium (Ib) or iron (Ic) [8]; the hydride $H_2Os_3(CO)_{10}$ (II) [8, 9]; the hydrido-acetylides $HM_3(CO)_9(\mu_3\text{-}\eta^2\text{-}C_2Bu^t)$, with ruthenium (IIIa) or osmium (IIIb) [10—12] and the structurally related non-hydride $Fe_3(CO)_9(\mu_3\text{-}\eta^2\text{-}C_2Et_2)$ (IIIc) [13, 14]; some substituted derivatives of complex IIIa, namely $(PPh_3)AuRu_3(CO)_9(\mu_3\text{-}\eta^2\text{-}C_2Bu^t)$ (IV) [15] and $HRu_3(CO)_8(\mu_3\text{-}\eta^2\text{-}C_2Bu^t)(PPh_3)$ (V) [16, 17] and finally the open cluster $(PPh_2)Ru_3(CO)_9(\mu_3\text{-}\eta^2\text{-}C_2Bu^t)$ (VI) [18]. The structures of these complexes are depicted in Fig. 1.

Experimental

Complexes Ia, b, c and II were obtained by applying well established methods [8]; complexes IIIa, b [10, 12], IIIc [13], IV [15], V [16] were obtained as reported. Complex VI was kindly supplied by A. J. Carty (Dept. of Chemistry, University of Waterloo, Ontario, Canada). The identity and purity of the compounds were checked by i.r. and mass spectrometry (except for V and VI), by using a Perkin-Elmer 580 i.r. spectrophotometer, and a Hitachi-Perkin Elmer RMU 6H mass spectrometer. The u.v. spectra of all compounds were run in acetonitrile solutions, using a Jasco Uvidec 505 spectrophotometer, to assess the conditions for the detection of the column eluates.

A Perkin-Elmer Series 3B liquid chromatograph was used with a Rheodyne 7105 injector and a LC75 variable wavelength u.v.-visible detector. The column was a Lichrosorb RP-18 (Merck) with 10-μm mean particle size. Solvents were h.p.l.c. grade (Carlo Erba, Milano). Isocratic elutions were done at a flow rate of 1 $cm^3\ min^{-1}$. Compounds were injected as acetonitrile solutions, with a metal content of about 100 ng in a 5-μl volume.

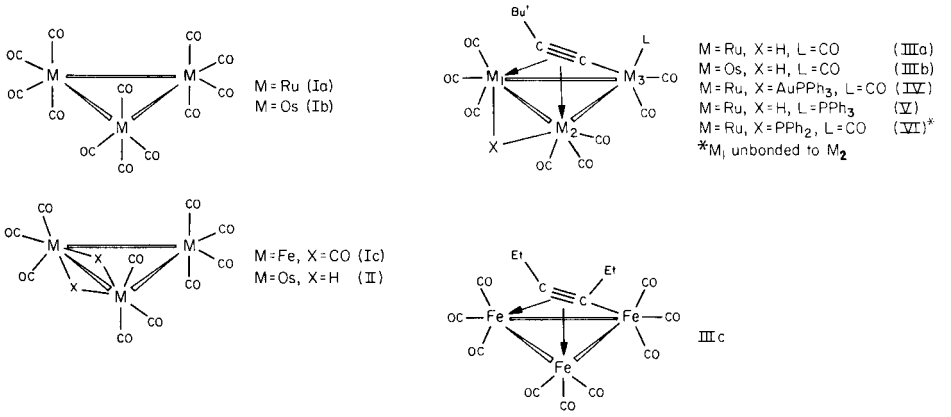

Fig. 1. Schematic representation of the structures.

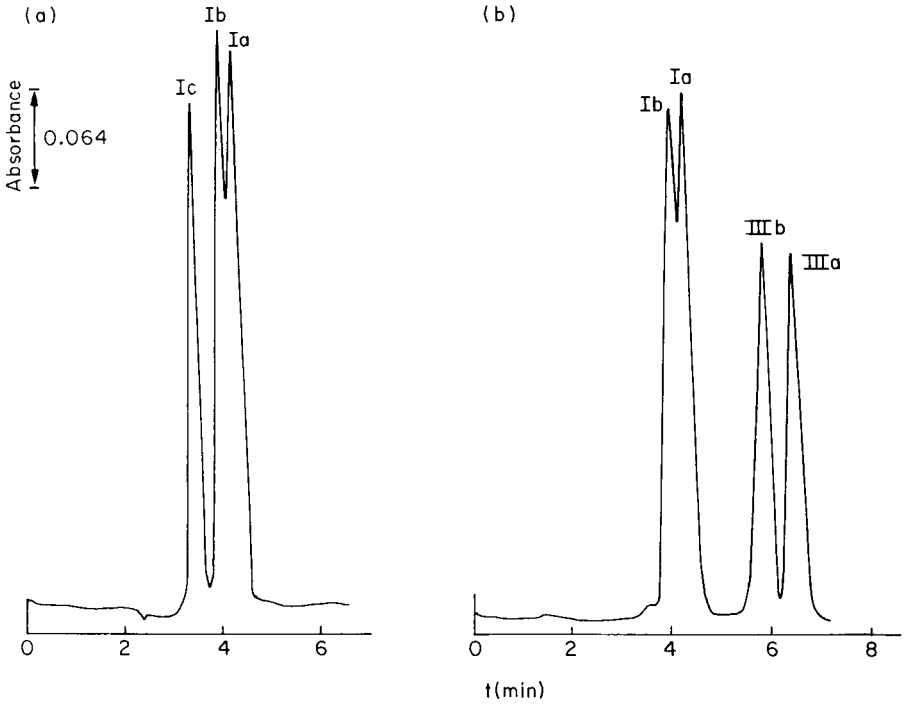

Fig. 2. (a) Separation of $Fe_3(CO)_{12}$ (Ic), $Os_3(CO)_{12}$ (Ib) and $Ru_3(CO)_{12}$ (Ia). LiChrosorb RP-18 column; detection at 265 nm; mobile phase, 1% methanol in acetonitrile; flow rate 1 cm^3 min^{-1}. (b) Separation of $Os_3(CO)_{12}$ (Ib), $Ru_3(CO)_{12}$ (Ia), $HOs_3(CO)_9C_2Bu^t$ (IIIb) and $HRu_3(CO)_9C_2Bu^t$ (IIIa). Mobile phase, acetonitrile; other conditions as in (a).

Results and discussion

For the reversed-phase chromatographic separations, acetonitrile or acetonitrile/methanol mixtures were used as mobile phases. Of interest is the separation, even though not complete, obtained among the trinuclear clusters $Fe_3(CO)_{12}$, $Ru_3(CO)_{12}$ and $Os_3(CO)_{12}$, which have the same basic triangular arrangement of metal atoms (Fig. 2a). The mobile phase used was acetonitrile with 1% of methanol. The elution order (Fe, Os, Ru) does not seem to depend on the bulkiness of the compounds, but is related to the order of decreasing electronegativity of the metals: Fe 1.64, Os 1.52, Ru 1.42 [19]. The value of k' for the iron compound (0.28), significantly different from those of the ruthenium and osmium analogues (0.38 and 0.42), may be due to the slight difference in the structure (Fig. 1), which could enhance the effect of the differing electronegativities.

Figure 2b shows the separation of $Ru_3(CO)_{12}$, $Os_3(CO)_{12}$ and their hydridoacetylide derivatives **IIIa, b**, with acetonitrile as the mobile phase. The retention volumes of these last compounds follow the same trend as those of the corresponding unsubstituted carbonyl compounds. The higher V_R' values for the acetylides could be explained by the presence of alkyne chains with tert-butyl substituents which influence the behaviour of these compounds, although hydrides would be expected to behave like more polar compounds.

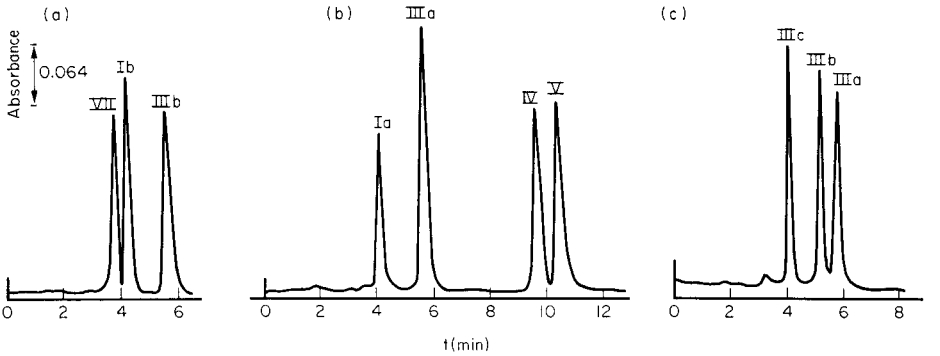

Fig. 3. (a) Separation of $Os_3(CO)_{10}(CH_3CN)_2$(VII), $Os_3(CO)_{12}$ (Ib) and $HOs_3(CO)_9C_2Bu^t$ (IIIb) with acetonitrile as mobile phase. (b) Separation of $Ru_3(CO)_{12}$ (Ia), $HRu_3(CO)_9C_2Bu^t$ (IIIa), $(PPh_3)AuRu_3(CO)_9$ (IV) and $HRu_3(CO)_8C_2Bu^t(PPh_3)$ (V) with acetonitrile/methanol (80/20) as mobile phase. (c) Separation of $Fe_3(CO)_9C_2Et_2$ (IIIc), $HOs_3(CO)_9C_2Bu^t$ (IIIb) and $HRu_3(CO)_9C_2Bu^t$ (IIIa) with acetonitrile/methanol (80/20) as mobile phase. Other conditions as in Fig. 2.

Figure 3a shows the separation of a mixture of the osmium derivatives Ib, II and IIIb in acetonitrile. In effect, peak VII should correspond to the substitution product of $H_2Os_3(CO)_{10}$ (II) with acetonitrile, i.e., $Os_3(CO)_{10}(CH_3CN)_2$ [20], the reaction being confirmed by the fast change of the colour of the acetonitrile solution from bronze to yellow. The shape of the peak suggests high stability of the adduct when acetonitrile is the mobile phase.

The ruthenium derivatives Ia, IIIa, IV, V were separated by using acetonitrile/methanol (80/20) mixture as the mobile phase (Fig. 3b). The presence of bulky substituents causes higher retention volumes for compounds IV and V, and particularly for V, the behaviour of which strongly resembles that of $H_2FeRu_3(CO)_{12}(PPh_3)$ in relation to its parent compound, $H_2FeRu_3(CO)_{13}$ [5]. The separation of the structurally related enneacarbonyl derivatives, III, is shown in Fig. 3c. The elution order is the same as that observed for the other derivatives of these metals. In particular, the retention time of osmium and ruthenium compounds, which are isostructural, seems to be influenced by the nature of the metal.

Complex VI undergoes decomposition under the chromatographic conditions used, during elution, as indicated by broadening of the peak. Nucleophilic attack at the C(σ—π) may occur with consequent modification of this species; the nucleophilic reactivity of this carbon towards isocyanides has been reported [21].

As observed for the binuclear derivatives [7], h.p.l.c. was an effective method of separation for these trimetallic clusters, the only limitation being their inertness towards the solvents used. The separation should prove useful, considering that several of these complexes may be found in the same reaction mixture. Among the factors affecting the separations of the trinuclear

clusters of Fe, Ru and Os, the electronegativity of the metal appears to be important.

Studies are in progress on the chromatographic behaviour of homo- and hetero-tetrametallic clusters, having different cluster shapes.

This work was supported by CNR (Rome), grant no. 81.01664.03. We thank Johnson-Matthey (London) for a gift of ruthenium and osmium salts.

REFERENCES

1 H. Veening and R. B. Willeford, Rev. Inorg. Chem., 1 (1979) 281 and references therein.
2 D. Sellmann, E. Jonk, H. J. Reinecke and T. Würminghausen, Frezenius Z. Anal. Chem., 294 (1979) 372.
3 C. T. Enos, G. L. Geoffroy and T. H. Risby, J. Chromatogr. Sci., 15 (1977) 83.
4 J. R. Fox, W. L. Gladfelter, T. G. Wood, J. A. Smegal, T. K. Foreman, G. L. Geoffroy, I. Tavanaiepour, V. W. Day and C. S. Day, Inorg. Chem., 20 (1981) 3214.
5 H. C. Foley and G. L. Geoffroy, J. Am. Chem. Soc., 103 (1981) 7176.
6 See, e.g., A. Mangia, P. L. Messori, C. Pelizzi and G. Predieri, Inorg. Chim. Acta, 68 (1983) 137 and references therein.
7 A. Mangia, G. Predieri and E. Sappa, Anal. Chim. Acta, 149 (1983) 349.
8 G. Wilkinson (Ed.), Comprehensive Organomet. Chem., 4 (1982), pp. 260, 664, 970—971.
9 M. R. Churchill, F. J. Hollander and J. P. Hutchinson, Inorg. Chem., 16 (1977) 2697.
10 E. Sappa, O. Gambino, L. Milone and G. Cetini, J. Organomet. Chem., 39 (1972) 169.
11 M. Catti, G. Gervasio and S. A. Mason, J. Chem. Soc., Dalton Trans., (1977) 2260.
12 E. Sappa, A. Tiripicchio and A. M. Manotti Lanfredi, J. Organomet. Chem., (1983) in press.
13 E. Sappa, A. Tiripicchio and M. Tiripicchio Camellini, J. Organomet. Chem., 199 (1980) 243 and references therein.
14 J. F. Blount, L. F. Dahl, C. Hoogzand and W. Hubel, J. Am. Chem. Soc., 88 (1966) 292.
15 P. Braunstein, G. Predieri, A. Tiripicchio and E. Sappa, Inorg. Chim. Acta, 63 (1982) 113.
16 C. Jangala, E. Rosenberg, D. Skinner, E. Aime, L. Milone and E. Sappa, Inorg. Chem., 19 (1980) 1571.
17 A. J. Carty, S. A. MacLaughlin, N. J. Taylor and E. Sappa, Inorg. Chem., 20 (1981) 4437.
18 A. J. Carty, S. A. MacLaughlin and N. J. Taylor, J. Organomet. Chem., 204 (1981) C27.
19 A. L. Allred and E. G. Rochow, J. Inorg. Nucl. Chem., 5 (1958) 264.
20 M. Tachikawa and J. R. Shapley, J. Organomet. Chem., 124 (1977) C19.
21 S. A. MacLaughlin, J. P. Johnson, N. J. Taylor, A. J. Carty and E. Sappa, Organometallics, 2 (1983) 352.

Analytica Chimica Acta, 152 (1983) 295—299
Elsevier Science Publishers B.V., Amsterdam — Printed in The Netherlands

Short Communication

AN IMPROVED DISTILLATION APPARATUS FOR A CONTINUOUS FLOW METHOD FOR THE DETERMINATION OF PHENOL IN WASTEWATER

A. E. GOODWIN* and J. L. MARTON
Conoco, Inc., Ponca City, OK (U.S.A.)

(Received 1st April 1983)

Summary. A distillation apparatus for a continuous-flow method for determination of phenol in water is described. The colorimetric measurement step utilizes the familiar 4-aminoantipyrine method. Phenol in water can be measured at a rate of 10 samples per hour, has a sensitivity of 4.0×10^3 $\mu g\ l^{-1}$ per unit absorbance, a limit of detection of 5 $\mu g\ l^{-1}$, and a standard deviation of 1.6 $\mu g\ l^{-1}$ for 20 replicates of a 100-$\mu g\ l^{-1}$ sample.

Attempts to implement a continuous-flow method from the literature to determine phenolic concentrations in water were unsettling, because different heating bath temperatures and different sample-feed rates gave different results [1—3]. No single temperature setting, even as high as 200°C, was considered best and so changes in the design of the distillation assembly were made. This communication describes the new design, the flow manifold, and reagent mixtures which give an improved continuous-flow method.

Experimental

Figure 1 illustrates the flow diagram for this method and lists all the needed components. Figure 2 shows a diagram of the distillation assembly which consists of a distillation coil, a condenser, and a heat exchanger. The distillation coil has an expansion chamber which is partially filled with 1-mm glass beads, a bottoms draw to remove hot acid, and an overhead draw to remove vapors. The cycle time consists of 1 min for sampling and 3 min for washing.

Reagent solutions are prepared from reagent-grade chemicals. The phosphate buffer solution contains 78 g of trisodium phosphate (12-hydrate), 7.4 g of boric acid, and 6.6 g of citric acid per liter of water. The 4-aminoantipyrine (4-AAP) solution contains 0.8 g of 4-AAP per liter of phosphate buffer solution, and the hexacyanoferrate(III) solution contains 5.0 g of potassium hexacyanoferrate(III) per liter of phosphate buffer solution. Both solutions are filtered through glass fiber filter (type A/E, Gelman).

The diluent for standards and samples contains 10 ml of phosphoric acid and 1.0 g of copper(II) sulfate per 4 l of distilled water and stops biodegradation of phenolic standards for at least one week.

0003-2670/83/$03.00

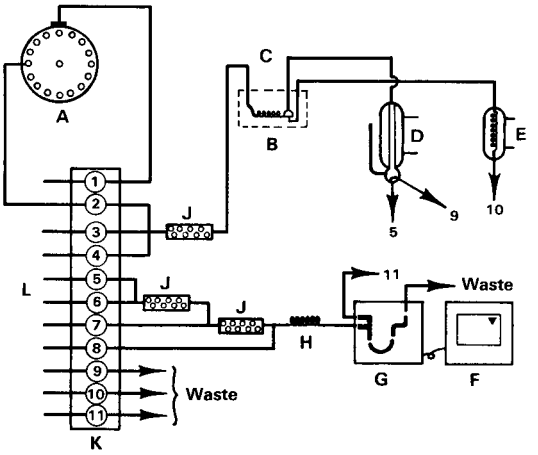

Fig. 1. Manifold for the determination of phenol. A, Sampler (Model IV, Technicon, Tarrytown, NY); B, heating bath with heating rod (Firerod, Model J3A110, Watlow, St. Louis, MO); C, distillation head (see Fig. 2); D, condenser (see Fig. 2); E, heat exchanger (see Fig. 2); F, strip-chart recorder (Omniscribe, Houston Instruments, Austin, TX); G, colorimeter (Model AC-200, Scientific Instruments Corporation, Pleasantville, NY) with a 75-mm flowcell and a 500-nm filter; H, 20-turn mixing coil (Part No. 157-0248-01, Scientific Instruments Corporation); J, single bead-string reactor, 200-mm polyethylene tubing (PE-205, i.d. 1.57 mm, Becton, Dickinson and Company, Parsippany, NJ) filled with glass beads (1 mm solid glass beads, Propper Manufacturing Company, Long Island City, NY); K, peristaltic pump (Model MP13-JG14, Brinkmann Instruments, Westbury, NY); L, peristaltic pump tubing (Technicon). Tube function with flow rate (ml min^{-1}) in parentheses: (1) wash water (3.90); (2) sample (2.00); (3) air (1.00); (4) phosphoric acid (0.60); (5) overhead condensate (1.20); (6) 4-AAP reagent (0.32); (7) Fe(III) reagent (0.32); (8) air (0.60); (9) level control (3.90); (10) bottoms draw (1.00); (11) debubbler draw (1.20).

Results and discussion

An automated method for the determination of phenol was needed, and an attempt was made to implement the EPA procedure. The criterion of acceptability was that the results for phenol by the continuous flow and manual methods should be equivalent. In the general search for operating conditions to meet this criterion, a problem was found with the commercial distillation assembly (Technicon 116-0163-01 and 116-0478-01). Depending on the temperature of the heating bath and the sample flow rate, the apparent phenol content of a real waste sample varied by one order of magnitude (from 0.2 to 2.3 mg l^{-1}). In addition, the concentration of the phosphoric acid used in the distillation affected the results. In one study, results varied from 0.1 to 0.3 mg l^{-1} as acid concentrations varied from 5 to 100%. Because no set of parameters for temperature, sample feed rate, and acid concentration gave results for a sample which were the same as results obtained by the manual method, it became obvious that modifications of the distillation assembly were needed.

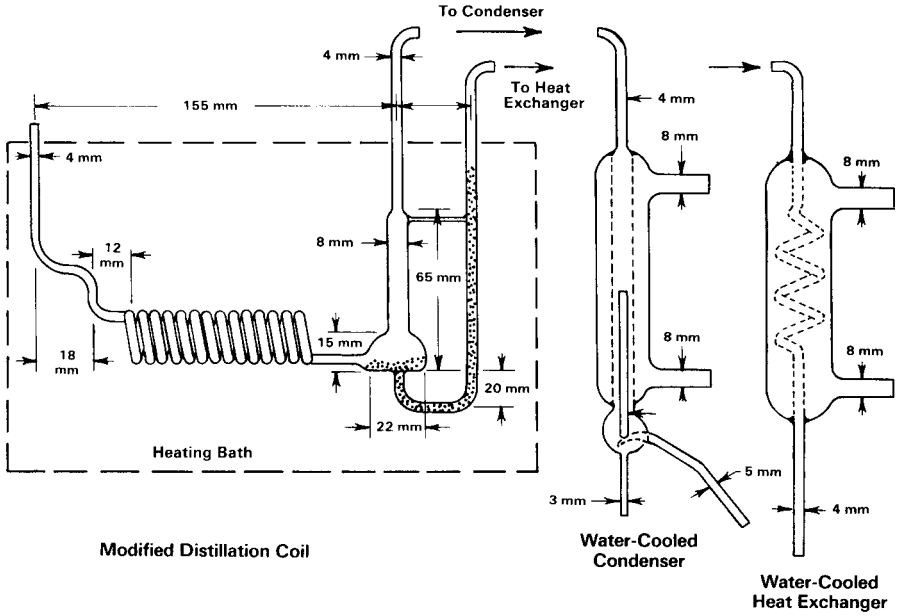

Fig. 2. Modified distillation apparatus for phenol determination.

Figure 2 illustrates the new design. Because an expansion chamber is located in a constant temperature bath, the temperature of the liquid—vapor interface and liquid phase from the bottoms draw is better controlled. The surface area of the expansion chamber is further increased by partially filling it with 1-mm glass beads which reduce bumping at higher temperatures. While 100% recovery for the unsubstituted phenol in samples was achieved at distillation temperatures above 120°C, the percent recovery for other phenols such as resorcinol increased with increasing distillation temperature. This is seen in Fig. 3. Because water is not completely distilled at temperatures less than 120°C, the recovery of phenol appears greater than 100%.

In this study, it was found that chloride ions present in many samples caused interferences with the EPA method. Since the pH in the 4-AAP method requires close control, the chloride ions which distilled as hydro-

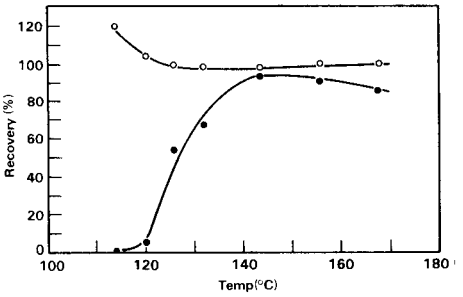

Fig. 3. Recoveries of (○) phenol and (●) resorcinol at various distillation temperatures.

TABLE 1

The dependence of phenol concentration on distillation temperature for waste-water samples

Sample[a]	Phenol found ($\mu g\ l^{-1}$)			
	122°C	144°C	169°C	192°C
Wastewater A	20	49	71	103
Wastewater B	16	49	69	97

[a]Samples taken from two different locations in an oil refinery.

chloric acid overwhelmed the EPA buffer. A phosphate buffer with a higher capacity was formulated into the reagent solutions. It has a pH of 10.2 and a capacity to buffer chloride ion concentrations as high as 1000 mg l^{-1}. It was also discovered that replacement of the 10% phosphoric acid solution with concentrated acid, made it possible to reach a plateau in apparent phenol concentration of real waste samples at distillation temperatures in the range 200—220°C. This is most probably due to the fact that the more complex phenolic compounds that react with 4-AAP require higher distillation temperatures for separation (see Table 1).

The capability to control distillation temperature and the selection of phosphoric acid concentration offer two options in the determination of apparent phenol content in samples. One option is to operate at a tem-

TABLE 2

Comparative data between manual and continuous flow methods for the determination of phenol in waste-water sampled on three different days

Sample[a]	Day	Phenol found (mg l^{-1})	
		Manual	CFA
A	1	16	15
	2	12	11
	3	12	11
B	1	31	29
	2	26	25
	3	35	33
C	1	60	57
	2	52	51
	3	33	32
D	1	0.022	0.021
	2	0.025	0.020
	3	0.028	0.026

[a]Samples taken from four locations in an oil refinery.

perature setting near 124° C and use 10% phosphoric acid to obtain results comparable to the manual method. Table 2 provides comparative data between these methods. The second option is to operate at a temperature setting near 200° C and use concentrated acid to obtain a measure of higher-boiling, substituted phenols.

We thank R. M. Owens, J. W. Wisenhunt, and R. D. Swain, whose ideas led to the design of the distillation assembly, and P. E. Burnett for the drawings. This work was presented at the 183rd National Meeting of the American Chemical Society, March 28, 1982, in Las Vegas, Nevada.

REFERENCES

1 M. A. Franson (Ed.), Standard Methods for the Examination of Water and Wastewater, 14th edn., American Public Health Association, Washington, DC, 1976.
2 Methods for Chemical Analysis of Water and Wastes, STORET Method No. 32730, U.S. Environmental Protection Agency, Cincinnati, OH, 1974.
3 M. E. Gales, Jr. and R. L. Booth, J. Am. Water Works Assoc., 68 (1976) 540.

Analytica Chimica Acta, 152 (1983) 301—306
Elsevier Science Publishers B.V., Amsterdam — Printed in The Netherlands

Short Communication

EXTRACTION OF GOLD, SILVER, MERCURY, PLATINUM(II) AND PALLADIUM WITH *O,O'*-DIISOPROPYL-*S*-BENZYLTHIOPHOSPHATE INTO MOLTEN DIPHENYL

YASUMASA SHIGETOMI* and TAKEHIRO KOJIMA

Department of Chemistry, Okayama College of Science, 1-1 Ridai-chō, Okayama-shi 700 (Japan)

ETSURO IWAMOTO and YUROKU YAMAMOTO

Department of Chemistry, Faculty of Science, Hiroshima University, Hiroshima 730 (Japan)

(Received 18th January 1983)

Summary. Liquid-liquid distribution with *O,O'*-diisopropyl-*S*-benzylthiophosphate (DPBTP), tri-n-octylphosphine oxide, tri-n-butylphosphate, di-n-hexylsulfide (DHS) and *O,O'*-dimethyl-*O*-(3-methyl-4-nitrophenyl)thiophosphate (DMTP) into molten diphenyl was investigated for the extraction of metals from hydrochloric, nitric and sulfuric acid solution. Silver(I), gold(III), mercury(II), platinum(II) and palladium(II) can be selectively extracted with DPBTP, DHS and DMTP.

Liquid—liquid extractions with trialkylphosphates have been widely examined [1]. Less work has been done on extractions with tri-n-butylthiophosphate [2] or dialkylsulfides [3, 4]. Extractions with compounds containing sulfur donors are known to be selective for silver(I) and mercury(II). This communication deals with the extraction behavior of various metals with tri-n-octylphosphine oxide (TOPO), tri-n-butylphosphate (TBP), di-n-hexylsulfide (DHS), *O,O'*-dimethyl-*O*-(3-methyl-4-nitrophenyl)phosphorothioate (DMTP) and *O,O'*-diisopropyl-*S*-benzylthiophosphate (DPBTP). Diphenyl serves as the diluent.

Experimental

Reagents. All reagents were of analytical grade; demineralized water was used throughout. Aqueous standard silver(I) solution (1000 mg l^{-1}) was prepared from silver nitrate. Standard gold(III) solution (1000 mg l^{-1}) was prepared by dissolving the pure metal in aqua regia, evaporating several times with concentrated hydrochloric acid and dissolving the residue in 1 M hydrochloric acid. Stock solutions of other metals (10^{-2} M) were prepared by dissolving suitable salts in appropriate concentrations of nitric acid or hydrochloric acid. The extractants were commercial products, TOPO (Dojindo Co.), TBP (Wako Chemical Co.), DPBTP (Ihara Chemical Co.), DHS (Daihachi Chemical Co.) and DMTP (Sumitomo Chemical Co.), which were used as

0003-2670/83/$03.00

received. The purities of DPBTP, DHS and DMTP were confirmed by CHN determinations.

Procedure. A solution containing 10—1000 μg of the metal under study was transferred to a 100-ml Erlenmeyer flask with a tightly fitting stopper. The acidity was adjusted to 0.1—4 N with nitric acid, hydrochloric acid or sulfuric acid, and the solution was diluted to 20 ml with water. A mixture of 200 mg of the ligand under study and 800 mg of diphenyl were added and the flask was heated on a water-bath at about 70°C until the ligand–diphenyl phase melted completely.

After vigorous shaking for 1 min, the flask was removed from the bath and cooled to room temperature. After the crystalline phase had separated completely, the mixture was filtered through filter paper (No. 5A) and the solid was washed with a little water. The filtrate and washings were transferred to a 50-ml volumetric flask and diluted to the mark with water.

Silver was determined spectrophotometrically in the filtrate with 1,10-phenanthroline and 2,4,5,7-tetrabromofluorescein [5]. Gold(III) was determined spectrophotometrically with 4,4'-bis(dimethylamino)-thiobenzophenone, platinum(II,IV) with tin(II) chloride, palladium(II) with *p*-nitrosodiphenylamine, copper(II) with diethyldithiocarbamate and mercury(II) with dithizone. The other metals were determined by titration with 0.01 M EDTA solution [6]. The distribution ratio was calculated from the concentration of metal ion in the aqueous phase after extraction.

Results and discussion

Effects of extraction parameters. The time required to reach equilibrium at 70°C was examined by measuring the metal concentration in the aqueous phase at different periods. For example, a mixture of 200 mg of DPBTP and 800 mg of diphenyl was shaken with 20 ml of a 10 mg l^{-1} metal solution, acidified with 0.5 M hydrochloric acid. A shaking time of 30 s sufficed for complete extraction of gold, but a period of 1 min was chosen for further experiments. The effect of the amount of DPBTP on the extraction of silver and gold is shown in Fig. 1; the extraction of silver increases regularly as the amount of DPBTP is increased, whereas the extraction of gold is less affected by the excess of DPBTP. Overall, it is advisable to extract with $\geqslant$ 200 mg of DPBTP.

Composition of gold(III) complex. A continuous variations type of experiment with varying amounts of DPBTP and gold(III) indicated that the extracted complex had the composition Au(III): DPBTP = 1:1.9. An examination of the effect of varying the DPBTP concentration on the extraction of hydrochloric acid indicated the formation of a 1:1 complex ($H_3O^+ \cdot$ DPBTP$\cdot$ Cl) when aqueous 0.1 M hydrochloric acid was extracted with DPBTP (0.01—0.5 M) in cyclohexane or diphenyl. When the effect of varying the chloride concentration on the extraction of gold was examined, the logarithmic plot of the distribution ratio against chloride concentration had a slope of approximately −2.5 (Fig. 2). This decrease in the distribution ratio of gold with

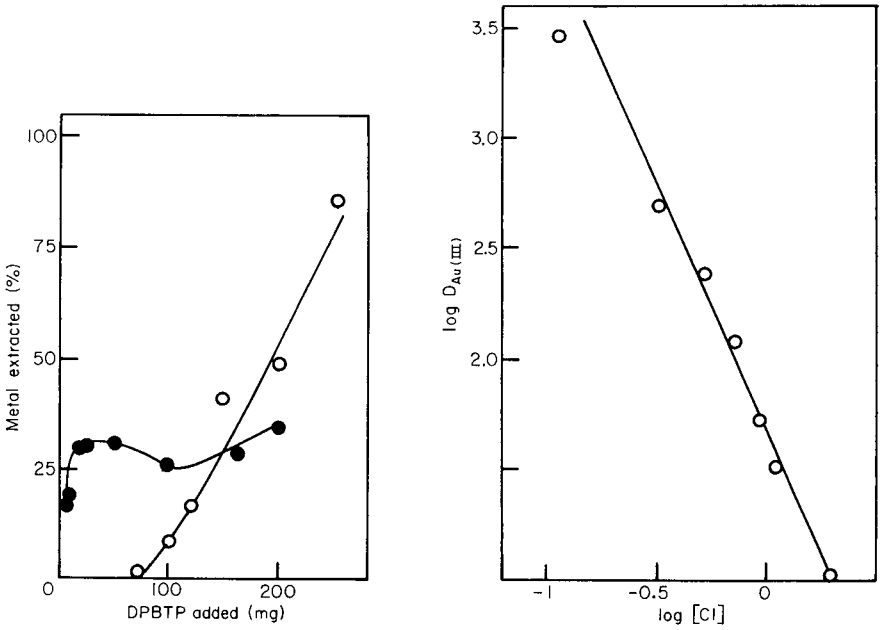

Fig. 1. Effect of amount of DPBTP on the extraction of silver and gold at 70°C. (•) Au(III) 50 mg l^{-1}, 0.5 M HCl; (○) Ag(I) 50 mg l^{-1}, 0.1 M HNO_3. Other conditions as in Procedure.

Fig. 2. Effect of chloride concentration on the extraction of gold(III) with DPBTP in molten diphenyl; 20 ml of 50 mg l^{-1} Au(III) solution extracted with 100 mg of DPBTP in 500 mg of diphenyl.

increasing concentration of chloride can be attributed to the formation of tetrachloroaurate. In the organic phase, the concentration ratio of the chloride to gold extracted was determined with the results given in Table 1. The gold complex formed in the organic phase contains gold:chloride:DPBTP in the molar ratio 1:4:2, indicating the formation of an $HAu \cdot Cl_4 \cdot 2DPBTP$ complex, which is in agreement with the finding of Potts [7].

Extraction of diverse metals from various acid solutions. Extraction of twenty metal ions was examined from 1 N acid solutions with 200 mg of DPBTP and 800 mg of diphenyl. The main results are given in Table 2 along with those for the other extractants studied. Extraction from these acid solutions was negligible for Mg(II), Ca(II), Sr(II), Ba(II), Sc(III), Y(III), La(III), Nd(III), Ce(III), Al(III), Cr(III), Mn(II), Fe(III), Zn(II) and U(VI). From the sulfuric acid solution, silver(I), mercury(II), gold(III) and palladium(II) were selectively extracted with DPBTP in molten diphenyl. Gold(III) was extracted with all the ligands studied. The pattern of distribution ratios for these metals was usually not significantly affected by the mineral acid used, except that silver cannot be extracted from hydrochloric acid. Platinum(IV) was not extracted from any of the acid solutions. The extraction behaviors of silver(I), gold(III), platinum(II) and palladium(II)

TABLE 1

The chloride concentration in the organic phase[a]

Initial $Au(III)_{aq}$ (mmol)	Au(III) extracted (%)	$[Au(III)]_o$ (mmol)	$[Cl]_o$ (mmol)	$[Cl]_o/[Au]_o$
0.025	47.9	0.0122	0.0580	3.5
0.025	49.6	0.0126	0.0621	3.7
0	0	0	0.0153	—

[a]Sample was 25 ml of 200 mg l^{-1} Au(III) solution. The reference was 25 ml of 0.5 M HCl. Chloride in the organic phase was determined by Volhard's method.

TABLE 2

The distribution ratio of various metals from 1 N sulfuric, hydrochloric or nitric acid solution with various extractants in molten diphenyl[a]

Acid	Metal	Distribution ratio				
		TOPO	TBP	DHS	DPBTP	DMTP
H_2SO_4	Cu(II)	N	N	N	N	N
	Ag(I)	N	N	0.6	33.8	N
	Hg(II)	0.6	N	N	95	1.2
	Au(III)	$>10^3$	615	$>10^3$	$>10^3$	$>10^3$
	Pd(II)	N	N	30	30	2.2
					(66.9)	(54.1)
HCl	Cu(II)	N	N	N	2.2	N
	Ag(I)	—	—	—	—	—
	Hg(II)	61.3	N	2.6	4.5	4.5
	Au(III)	$>10^3$	$>10^3$	$>10^3$	$>10^3$	$>10^3$
	Pt(II)	123	$>10^3$	56.8	91.1	26.5
	Pd(II)	126	47.3	209	42.5	25.5
					(46.7)	(113)
HNO_3	Cu(II)	N	N	N	1.4	N
	Ag(I)	N	N	25.9	16.2	5.4
	Hg(II)	0.2	N	22.4	53.9	53.9
	Au(III)	86.4	116	456	64.7	457
	Pt(II)	107	91.7	75.7	66.9	11.7
					(46.7)	(27.6)
	Pd(II)	6.7	0.6	7.8	20	1.9
					(15.8)	(13.8)

[a]N means not extracted. The values in parentheses are the distribution ratios with kerosene as solvent. Conditions: 20 ml of aqueous phase; 20% (w/w) of extractant in organic phase; 50 mg l^{-1} Cu(II), 25 mg l^{-1} Hg(II), 66.5 mg l^{-1} Ag(I), 10 mg l^{-1} Au(III), 2 mg l^{-1} Pt(II) or Pd(II).

are shown in Fig. 3. In hydrochloric acid solutions, the extraction of gold decreases with increasing acidity (cf. Fig. 2). The extractability of silver decreased with increasing nitric acid concentrations. As is clear from Fig. 3, platinum(IV) can be separated from silver, gold and palladium.

Thus, DPBTP can extract selectively metals such as silver, gold, platinum and palladium. It seems that the sulfur atom of the ligand is responsible for these extractions, behaving similarly to the sulfur atom in dioctylsulfide and other sulfides, which has the properties of a soft base [4, 8]. Neutral esters of thiophosphoric acid, thiophosphonic acid, and thiophosphinic acids tend to function through the oxygen atom toward hard metal ions and through the sulfur atom toward soft or borderline metal ions [9]. Although DPBTP exists mainly in the thiol form, its thione form must coordinate easily to these metals, and the selective extraction behavior noted above can be attributed to the thione:

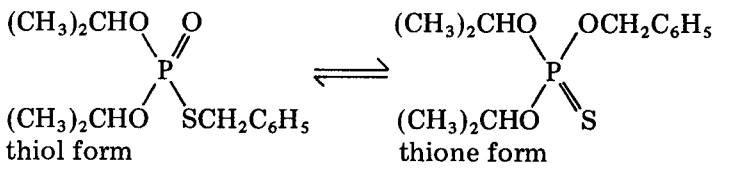

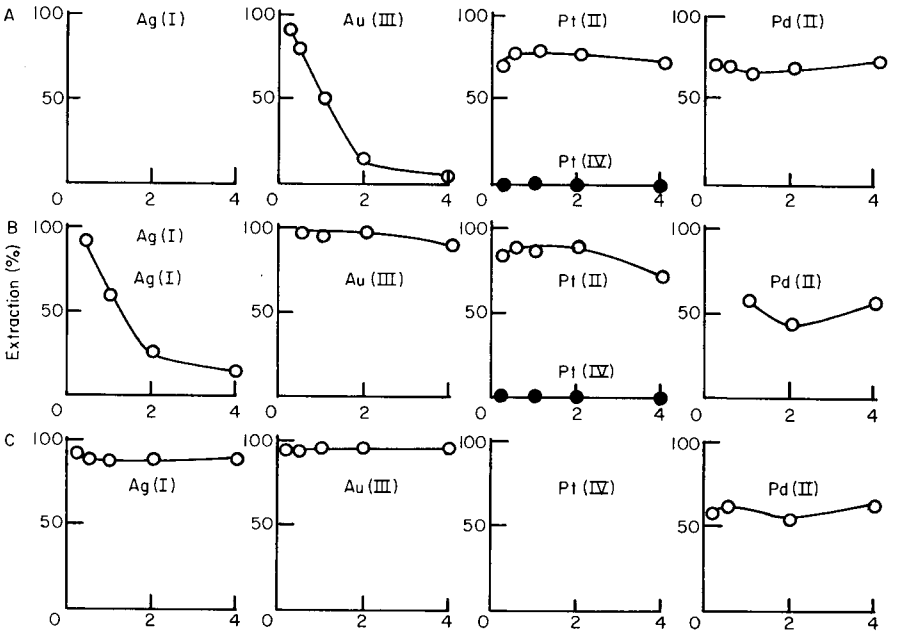

Fig. 3. Effect of the acidity for (A) hydrochloric acid, (B) nitric acid and (C) sulfuric acid on the extraction of Ag(I), Au(III), Pt and Pd(II) into the DPBTP—diphenyl phase at 70°C. Conditions: 200 mg DPBTP, 800 mg diphenyl, 10^{-4}—10^{-5} M metal ion, contact time 1 min.

In conclusion, in nitric acid, DPBTP, DMTP and DHS with sulfur donor atoms selectively extract the soft metals, silver(I) and mercury(II), compared to TOPO and TBP; in sulfuric acid only DPBTP shows selective extraction. Finally, these metals are efficiently concentrated, as the volume of the organic phase is small and separates out easily upon cooling.

REFERENCES

1 See e.g., Y. Marcus and A. S. Kertes, Ion Exchange and Solvent Extraction of Metal Complexes, Wiley, New York, 1969.
2 R. W. Cattrall, A. R. Martin and S. Tribuzio, J. Inorg. Nucl. Chem., 40 (1978) 687.
3 V. A. Mikhailov, N. A. Korol and D. D. Bogdanova, Izv. Sib. Otd. Akad. Nauk SSSR, Ser. Khim. Nauk, 6 (1975) 29; Chem. Abstr., 84 (1976) 80506S.
4 M. Mojski, Talanta, 25 (1978) 163.
5 Mukioyōhishiyoku Bunseki Henshyu Inhen, Mukiouōhishiyoku Bunseki, I (in Japanese), Kyoritsu (1980) p. 234.
6 K. Ueno, Chelate Tekiteihō (in Japanese), Nankodō (1972).
7 R. A. Potts, Inorg. Chem., 9 (1970) 1284.
8 S. Ahrland, J. Chatt and N. R. Davies, Quart. Rev., 12 (1958) 265.
9 C. M. Mikulski, S. Chauhan and R. Rabin, J. Inorg. Nucl. Chem., 43 (1981) 2017.

Analytica Chimica Acta, 152 (1983) 307—314
Elsevier Science Publishers B.V., Amsterdam — Printed in The Netherlands

Book Reviews

E. L. Wehry (Ed.), *Modern Fluorescence Spectroscopy*, Plenum, New York, 1981, *Vol. 3*, xx + 354 pp., price $39.50; *Vol. 4*, xvi + 282 pp., price $35.00.

A few years ago, I had the pleasure of reviewing Vols. 1 and 2 of this series. My comments on the excellence of the contents and the presentation were so glowing that they have been printed on the dust jacket to Vol. 3. It is a pleasure to report, therefore, that Vols. 3 and 4 achieve equally high standards. The intention is to cover new and developing areas of fluorescence as applied in analytical chemistry. A glance at the contents shows how extensive these areas are and how versatile fluorimetry has become. Fluorescence detection in g.c. and h.p.l.c., reaction rate methods involving fluorescence, fluorescence immunoassay, structural interpretation of fluorescence spectra by automated file searching, fluorescence of biologically important molecular complexes, and two chapters on fluorimetry of single cells are in Vol. 3., whereas Vol. 4 deals with laser applications, a theoretical approach to time-resolved fluorimetry, array detectors, synchronous excitation, low temperature studies, luminescence in oil detection, and lanthanide ion emission from solid materials. The articles are comprehensive, and contain a wealth of up-to-date information. Each volume has a subject index. These books deserve to be read by all analytical chemists. They cannot fail to provide inspiration in all sorts of avenues of analytical work, as well as giving an excellent account of progress in modern analytical fluorescence spectroscopy.

A. Townshend

M. Oehme, *Gas-chromatographische Detektoren*, Hüthig, Heidelberg, 1982, S. viii + 104, Preis DM 28.

Das vorliegende Büchlein aus der Reihe ABC der Mess- und Analysen-technik fasst den heutigen technischen Stand auf dem Gebiet der Gaschromatographie-Detektoren zusammen. Die verschiedenen Detektortypen sowie die für das Verständnis wichtigen Grundbegriffe sind in etwa 100 Kurzkapiteln auf etwa 100 Seiten äusserst knapp und doch vorbildlich konzentriert dargestellt. Die alphabetische Ordnung der Stichworte erlaubt die Benutzung als Nachschlagewerk. Die Verwendung als Lehrtext um einen raschen Überblick über das breite Gebiet zu erhalten ist wegen des fehlenden Zusammenhangs eher mühsam. Durch die vielen gut durchdachten Querverweise wird die Frustration aber in erträglichen Grenzen gehalten. Ziel des Buches ist es, durch Beachreibung von Bauform, Funktionsweise, Leistungsfähigkeit und Grenzen der Methoden grundlegende Kenntnisse zu vermitteln, um so dem Praktiker

die Wahl der für seine Probleme best-geeigneten Detektionsart und des passenden Detektors zu erleichtern. Dieses Ziel dürfte nach Meinung des Rezensenten voll erreicht werden.

J. T. Clerc

D. D. Perrin, B. Dempsey, and E. P. Serjeant, *p*K$_a$ *Prediction for Organic Acids and Bases*, Chapman and Hall, London, 1981. 118 pp. + 31 pp. tables, price £10.95.

Chemists who use Albert & Serjeant's excellent book, The Determination of Ionization Constants (1971) will find this volume a worthy companion. For many others it will be an invaluable source of data. The authors' aim is to show how pK_a values can be predicted within a few tenths of a pH unit when direct measurement is unjustified or impractical. They first summarise the definitions and practical importance of pK_a values and their dependence on solvent, temperature, and ionic strength, but particularly on molecular factors such as electronic, steric, and statistical effects, tautomerism, and zwitterion formation. Then many guiding principles of pK_a correlation with molecular structure are introduced, with extensive lists of formulae and numerical parameters in the text and appendix, and references to other compilations. Brief explanations and copious worked examples show how the Taft, Hammett, extended Hammett, and related equations and other empirical rules can be used on a great variety of compounds, from the simple to the very complex. The large amount of information condensed into the book is clearly organised, and the production is pleasing.

A. J. Waring

G. J. Martin, M. L. Martin and J.-P. Gouesnard, *NMR Basic Principles and Progress, Vol. 18, ^{15}N-NMR Spectroscopy*, P. Diehl, E. Fluck and R. Kosfeld (Eds.), Springer-Verlag, Berlin, 1981, vii + 382 pp., price DM 148.

The large amount of tabular data in this volume, amounting to about 5,000 items, testifies to the popularity of nitrogen-15 n.m.r. studies and to the remarkable sensitivity of high-field spectrometers. Indeed, on modern wide-bore instrumentation, ^{15}N spectra can now be obtained routinely at the 0.4% natural abundance level.

The major part of this volume is devoted to tables of ^{15}N chemical shifts, coupling constants and relaxation times for a wide range of synthetic organic and inorganic compounds and natural products. The tables are well organised and the presentation is good within the limitations of the direct reproduction technique employed. However, this volume is not just a data base, as

a significant amount of space is devoted to a discussion of the ^{15}N-n.m.r. parameters. One particularly useful section deals with experimental techniques for obtaining ^{15}N spectra, including modern methods involving polarization transfer. Other sections discuss the problematical area of ^{15}N shift referencing, medium effects, and the application of ^{15}N-n.m.r. to study exchange processes and reaction mechanisms. A useful formula index is provided in addition to the subject index.

This is a comprehensive source of ^{15}N material compiled by authors who have made significant contributions to this field. It is a highly desirable reference book for any laboratory interested in ^{15}N-n.m.r. spectroscopy.

W. B. Jennings

F. L. Boschke (Ed.), *Topics in Current Chemistry, Vol. 100, New Trends in Chemistry*, Springer-Verlag, Berlin, 1982, vii + 213 pp., price DM 98.

This one hundredth volume of Topics in Current Chemistry provides an interesting selection of articles: Trends in Analytical Chemistry (Betteridge and Sly), Topics in Photochemistry (Zimmerman), New Developments in Polymer Synthesis (Saegusa), Biochemical Engineering (Janshekar and Fiechter), Chemistry and Spectroscopy of Rare Earths (Jørgensen and Reisfeld) and Systematization and Structures of the Boron Hydrides (L. Barton). The book concludes with an author index for Vols. 50—100. For the analytical chemist, the first article (42 pp.) is obviously of most interest. It contains brief discussions of the impact of modern electronics, laboratory computers and mathematical methods (including simplex optimization and information gathering) on analytical science, followed by descriptions of some new techniques (flow injection analysis, thin film analysis and acoustic emission) and of "total systems automation". A lot of ground is covered, in conversational style, and should give the non-specialist a readable account of the variety and power of modern analytical developments. The Chapter on rare earth spectra will also be of considerable use to analytical chemists concerned with lanthanide analysis.

A. Townshend

J. Berliner and J. Reuben (Eds.), *Biological Magnetic Resonance, Vol. 4*, Plenum Press, New York, 1982, 340 pp. $42.50.

There is hardly an area of biochemistry or biology to which magnetic resonance techniques have not been applied in recent years. As yet, they do not occupy the central role they enjoy in organic chemistry but they are rapidly establishing themselves as indispensable tools for resolving many of

the dilemmas of molecular biology. The basic physics of the methodology is the same, but the complexity and sophistication of biological systems alter the goals that can be achieved and consequently the general methodology employed differs significantly from that applicable to organic chemistry.

This comprehensive series of volumes covers (or plans to) a diverse range of topics from in vivo metabolism and n.m.r. imaging to studies on protein dynamics and n.m.r. of immobilized/frozen structures (so-called solid-state n.m.r.); each chapter combines the first-hand knowledge and expertise of active workers. The laudable stated aim of the editors is that the coverage of each topic should "approach that found in a textbook and in a reference book .... and not be a mere literature review." In this volume, the individual authors are generally successful in these aims. Each gives a useful, though sometimes brief, introduction to the quirks of their particular methodology and, in general, the examples chosen to illustrate the techniques are well-made and extensive.

This volume contains four chapters. The first, by D. A. Butterfield, is titled "Spin labelling in disease". It largely reviews the use of spin labels as probes of membrane fluidity in the diseased state; surprisingly, no mention was made of the need to omit that constant companion of biochemical buffers, a reducing agent, from solutions of nitroxide spin labels. The potential of ^{113}Cd-n.m.r. as a structural and dynamic probe of various metalloenzymes is discussed by I. M. Armitage and J. D. Otvos. The wide range of the chemical shifts experienced by ^{113}Cd-substituted metalloproteins makes it an extremely sensitive probe for many metal-dependent reactions, particularly those employing Ca^{2+} and Zn^{2+}. Their extensive studies on alkaline phosphate and metallothionein are well featured. Next R. Kaptein eloquently describes his pioneering work on the application of photochemically induced dynamic nuclear polarization to the surface structure of proteins; the greatly increased enhancement of n.m.r. lines caused by free radical reactions has only recently been applied to biochemical problems. Finally, S. J. Perkins relates all the essentials of the application of ring current calculations to protein and *t*-RNA ^{1}H-n.m.r. spectra. This represents the key link between spectroscopy and structure and is elegantly explained.

As with any series of contributed volumes, the whole is inevitably greater than the sum of parts. Some effort has been made to appeal to novices but those with some prior knowledge will benefit most. Nevertheless, I found this volume enjoyable and stimulating to read. This series makes a valuable addition to the magnetic resonance literature and provides extremely useful texts for research workers.

Ian P. Trayer

R. C. Hughes, *Glycoproteins*, Chapman and Hall, London, 1983, 90 pp., price (paperback) £2.95.

No analytical biochemist can underrate the importance of glycoproteins. Sometimes they require analysis, while on other occasions they are important analytical reagents: antibodies and (most) lectins are glycoproteins, for example. Moreover, the study of glycoproteins is developing extraordinarily rapidly, a point acknowledged in this book, as the appendix cites references up to 1982. Dr. Hughes' book makes no attempt to cater specifically for the needs of the analyst; the major methods of analysing for glycoproteins or with glycoproteins are given only passing mention. Nonetheless, it deserves to be widely read, because it provides a stimulating account. The material is inevitably compressed, but it is never dull and the (minute) diagrams are clear and appropriate. The one drawback to the book, always to be especially regretted in a volume intended as a student text, is that the standard of the written English is sometimes rather sloppy. For example "All five classes of human immunoglobulin and probably other species contain carbohydrate"; or "The human red cell membrane consists of relatively few major proteins" (nothing else??). Additionally, more careful proof-reading would have uncovered a number of misprints, including odd cases where two words have apparently been transposed. But the potential reader should not be deterred by these criticisms. Many students and researchers will derive great value and considerable interest from this book.

J. N. Miller

J. W. Bridges and L. F. Chasseaud (Eds.), *Progress in Drug Metabolism, Vol. 6*, Wiley, Chichester, 316 pp., price £24.75.

This excellent review series is intended for all research workers studying the absorption distribution, biotransformation and excretion of drugs or xenobiotics. Volume 6 emphasises the experimental techniques which are so essential to this field, with many useful references. There is a concise account of the factors affecting excretion of compounds in bile, with a comprehensive listing of those xenobiotics known to follow this route. Other chapters discuss the metabolism of the currently-fashionable β-adreno-receptor blocking agents and also more-recently discovered metabolic biotransformation pathways. The comprehensive article on isolation of drug metabolites gives detailed information of methods for identification and determination of many compounds of clinical interest, while the section on whole-body autoradiography provides much-needed advice on the techniques involved in cryosectioning and the use of photographic emulsions to visualise the tissue distribution of radioisotopes. The book is well-produced with clear diagrams of the often complicated structures of the compounds

under discussion, and should prove invaluable as a reference source for all those interested in developments in drug metabolism.

R. H. Waring

Alan Wiseman (Ed.), *Topics in Enzyme and Fermentation Biotechnology, Vol. 6*, Horwood, Chichester, 1982, 232 pp., price £21.50.

This excellent series of widely-varying topics continues with discussion of 4-hydroxycoumarin antibiotics, the discovery of novel secondary metabolites, the yeast mitochondrial system, a test for antimitochondrial drugs and mutagens, and microbial oxygenases. The article by S. A. Barker on new approaches to enzyme stabilization will be of most interest to analytical chemists, in that it discusses means of stabilizing (and destabilizing) enzymes by polysaccharides, polyelectrolytes, colloids and simple ions. Such knowledge is essential if the range of conditions under which enzymes retain their catalytic activity is to be expanded. Finally, the description of developments in beer fermentation will provide useful reading for all interested in the production of their favourite beverage! As a bonus, the introduction contains a useful compilation of patents covering immobilization of enzymes and of cells, and there is a cumulative index for volumes 1—5 (why not 1—6?) as well as a separate index to volume 6.

A. Townshend

J. D. Lee and T. D. Lee, *Statistics and Computer Methods in BASIC*, Van Nostrand Reinhold, Wokingham, 1982, 206 pp., price £11.50 (hardback), £5.50 (paperback).

This book introduces the main statistical techniques which are useful for scientists, and provides computer programs to be used with them. It would be suitable for undergraduates or those whose statistics have become rusty. Clear explanations are given of types of errors, the properties of populations and of common distributions. Tests of significance, correlation and ranking are described, and methods are given for fitting straight lines or polynomials to data and for solving equations by analytical and simple iterative procedures. Numerical integration and a chapter on sorting of numerical data complete the text. The mathematics is kept simple, but the scope of validity of each statistical technique is stressed. An unusual feature is the complete listing, with typical output and explanation, of computer programs to perform most of the calculations and report the significance of the results. The programs, in a simple subset of BASIC, should be easily modified for one's own microcomputer, have extensive error-trapping procedures and are designed to be

robust for use by the inexpert. Some statistical tables are provided, but the programs do not call upon them. The book has many clearly worked examples, often based on chemical experiments, and questions (with answers) to test one's progress.

A. J. Waring

D. J. Fabian, H. Kleinpoppen and L. M. Watson (Eds.), *Inner-shell and X-ray Physics of Atoms and Solids*, Plenum Press, New York, 1981, xxv + 950 pp., price £66.50.

These proceedings of an international conference held in 1980 at Stirling, Scotland provide abundant confirmation, if any is needed, that atomic physics, understood so well in principle, is still capable of yielding abundant riches. The work under review consists of over 150 articles on inner-shell processes, and provides an account, which is comprehensive in depth as well as extent, of the present state of this important field. The book contains substantial sections in inner-shell ionisation by light and heavy ions, and by electron impact. There are also several articles on the theory of these processes. Much attention is devoted to the emission of photo- and Auger electrons, and the book includes detailed studies of chemical bonding effects in x-ray spectra. There are naturally many papers on experimental techniques, covering all branches of x-ray physics. All research groups whose work lies in any of these fields will require a copy of this well-produced book. It can also be strongly recommended for purchase by all libraries seeking to provide academic support for such groups. It is a work of considerable significance which deserves to become widely known.

N. A. Dyson

P. L. Chambers and C. M. Chambers (Eds.), *New Toxicology for Old. A Critique of Accepted Requirements and Methodology*, Springer-Verlag, Berlin, 1982, 394 pp., price DM 94.

This fifth supplement to the Archives of Toxicology is the proceedings of the meeting of the European Society of Toxicology held in Dublin in August 1981. It contains 66 papers and 6 abstracts of papers, arranged under the following headings: critical evaluation of protocols used in routine toxicity studies; neurotoxicity; non-invasive and invasive techniques, drugs in obstetrics and gynaecology, statistics in toxicology, histopathology of toxic agents, and a miscellaneous section. Also included are the Young Scientists Award lecture, and author and subject indexes.

Douglas A. Skoog and Donald M. West, *Principles of Instrumental Analysis*, 2nd edn., Saunders College, Philadelphia, 1980, xi + 769 pp., price U.S. $25.

The first edition of this book was one of the most popular student texts on instrumental analysis during the past decade. This second edition, which has been considerably modified and updated, should ensure that this popularity will continue well into the 1980's. Among the major innovations are two chapters on electrical circuitry and elementary electronics, the latter including operational amplifiers, noise and computer interfacing. Microprocessors receive a brief mention. The treatment of instrumentation for optical spectroscopy has been re-organized, and there is a new chapter on thermal methods. Chromatography has been considerably revamped and appears as three chapters: a general treatment, liquid chromatography (and electrophoresis) and gas chromatography, reflecting the current importance of chromatography in general, and high performance liquid chromatography in particular, in modern analytical chemistry. The remainder of the book, which contains accounts of all the major aspects of current instrumental analysis, has received much careful detailed modification. The outcome is a comprehensive, up-to-date, and easily read account, suitable for undergraduate students, and which could provide a basis for more detailed study by more advanced students.

A. Townshend

ANALYTICA CHIMICA ACTA, VOL. 152 (1983)

AUTHOR INDEX

ACA announcements

ANNOUNCEMENTS OF MEETINGS

ANALYTICAL METHODS AND PROBLEMS IN BIOTECHNOLOGY – AN INTERNATIONAL SYMPOSIUM, NOORDWIJKERHOUT, THE NETHERLANDS, APRIL 17–19, 1984

The development of analytical methods for biotechnological applications is an area of growing importance. Analytical methods currently available are now being adapted for practical use in biotechnological research, development and industrial production. But a large gap remains to be bridged between experts in analytical methodology and experts in biotechnology. It is the purpose of this Symposium to outline the problems in this field and to describe the rapid developments taking place. The Symposium is aimed at an interdisciplinary audience of those involved in industrial and academic biotechnology, as well as analytical chemists.

The Scientific Committee expects the Symposium to cover a wide and representative range of current research activity on all aspects of analytical chemistry related to biotechnology. The Scientific Programme will consist of invited plenary lectures, invited and submitted research papers (both oral and poster presentations) and discussion sessions. The following topics will be covered: on-line *vs.* discontinuous analysis; (on-line) sampling (incl. asepsis); on-line process analysis; gas-phase analysis (sensors, optical techniques, mass spectrometry, gas chromatography); liquid-phase analysis (sensors, immunoassay, h.p.l.c., optical techniques, etc.); biomass (cell counts, population density, cell constituents, enzyme activities, nuclear magnetic resonance spectroscopy, immobilized systems, etc.); data evaluation and process control; biochips; and process control planning.

The Symposium will be held at the Leeuwenhorst Congress Center in Noordwijkerhout (The Netherlands), under the auspices of the Royal Netherlands Chemical Society (KNCV), Analytical Division, and The Netherlands Biotechnological Society (NBV). The conference language will be English.

Papers presented at the conference will be published (subject to normal refereeing processes) in a special issue of *Analytica Chimica Acta*. A selection of review papers will be considered for publication in *TrAC – Trends in Analytical Chemistry*.

Further information may be obtained from: W.A. Scheffers, Symposium Analytical Methods and Problems in Biotechnology, Delft University of Technology, Laboratory of Microbiology, Julianalaan 67A, NL-2628 BC Delft, The Netherlands. Tel.: (015)-782411.

INTERNATIONAL SYMPOSIUM ON LIQUID CHROMATOGRAPHY IN THE BIOMEDICAL SCIENCES, RONNEBY, SWEDEN, JUNE 18–21, 1984

The above-mentioned symposium will cover the following main areas: theory; ion-pair chromatography; microcolumns; separation of optical isomers; separation of peptides and proteins; new trends; detectors; and determination of bioactive compounds in biological material.

For further information contact: Swedish Academy of Pharmaceutical Sciences, P.O. Box 1136, S-111 81 Stockholm, Sweden.

CALENDAR OF FORTHCOMING MEETINGS

Oct. 5–7, 1983 Ulm-Donau, F.R.G.	**Ulmer Symposium Analtyical Chemistry 1983** Contact: Dr. U. Reuter, Department of Analytical Chemistry, University of Ulm, P.O. Box 4066, D-7900 Ulm-Donau, F.R.G. Tel.: (0731) 176-2181.
Oct. 10–12, 1983 Tarrytown, NY, U.S.A.	**Capillary Chromatography – 2nd International Symposium** Contact: Professor A. Zlatkis, Department of Chemistry, University of Houston, Houston, TX 77004, U.S.A. (Further details published in Vol. 148.)

Oct. 12–14, 1983 London, Great Britain	**Analyticon 83** Contact: Mr. G.C. Young, SIMA, Leicester House, 8 Leicester Street, London WC2H 7BN, Great Britain.
Oct. 17–21, 1983 Neubrandenburg, G.D.R.	**Analytiktreffen 1983: Fortschritte in der Gas- und Flüssigkeits-Chromatographie** Contact: Dr. sc. W. Engewald, Karl-Marx-Universität Leipzig, Sektion Chemie, Leibigstrasse 18, DDR-7010 Leipzig, G.D.R.
Oct. 18–19, 1983 Saarbrücken, G.F.R.	**"Dünnschichtchromatographie – Säulenflüssigkeitschromatographie: Partner oder Konkurrenten?"** Contact: Gesellschaft Deutscher Chemiker, Abteilung Fachgruppen, Postfach 90 04 40, D-6000 Frankfurt am Main 90, G.F.R. Tel.: (0611) 7917-366.
Nov. 10–16, 1983 Düsseldorf, G.F.R.	**9th International Congress and Exhibition for Instrumentation and Automation (INTERKAMA 83)** Contact: INTERKAMA 83, Düsseldorfer Messegesellschaft mbH, NOWEA, Postfach 32 02 03, D-4000 Düsseldorf 30, G.F.R.
Nov. 14–16, 1983 Monte Carlo, Monaco	**3rd International Symposium on HPLC of Proteins, Peptides and Polynucleotides** Contact: Shirley E. Schlessinger, 400 East Randolph, Chicago, IL 60601, U.S.A. Tel.: (312) 527-2011.
Nov. 16–18, 1983 New York, NY, U.S.A.	**22nd Eastern Analytical Symposium** Contact: Norman Gardner, 73 Ethel Street, Metuchen, NJ 08840, U.S.A. Tel.: (201) 548-7377.
Nov. 24–25, 1983 Lausanne, Switzerland	**Workshop on Handling of Environmental and Biological Samples in Chromatography** Contact: Prof. R.W. Frei, The Free University of Amsterdam, Department of Analytical Chemistry, De Boelelaan 1083, 1081 HV Amsterdam, The Netherlands. (Further details published in Vol. 148.)
Dec. 7–10, 1983 Singapore, Singapore	**Chem Asia '83 Conference** Contact: Singapore Exhibition Services, Ltd., 601 Cathay Building, Singapore 0922, Singapore.
Jan. 2–6, 1984 San Diego, CA, U.S.A.	**1984 Winter Conference on Plasma Spectroscopy** Contact: Dr. Ramon M. Barnes, Conference Chairman, Department of Chemistry, GRC Towers, University of Massachusetts, Amherst, MA 01003-0035, U.S.A. Tel.: (413) 545-2294.
Jan. 19–20, 1984 Amsterdam, The Netherlands	**Workshop on Low Dispersion Liquid Chromatography** Contact: LDLC Workshop Office, Department of Analytical Chemistry, Free University, De Boelelaan 1083, 1081 HV Amsterdam, The Netherlands. (Further details published in Vol. 151, No. 1.)
March 5–9, 1984 Atlantic City, NJ, U.S.A.	**35th Pittsburgh Conference and Exposition on Analytical Chemistry and Applied Spectroscopy** Contact: Linda Briggs, Pittsburgh Conference, 437 Donald Road, Dept. J-005, Pittsburgh, PA 15235, U.S.A.
March 26–30, 1984 London, Great Britain	**APCOM '84 – 18th International Symposium on the Application of Computers and Mathematics in the Mineral Industries** Contact: The Conference Office, The Institute of Mining and Metallurgy, 44 Portland Place, London W1N 4BR, Great Britain.

April 8–13, 1984 St. Louis, MO, U.S.A.	**187th National Meeting of the American Chemical Society** Contact: Meetings Department, American Chemical Society, 1155 Sixteenth Street, NW, Washington, DC 20036, U.S.A.
April 10–13, 1984 Munich, G.F.R.	**9th Conference on Biochemical Analysis (BIOCHEMISCHE ANALYTIK 84) & ANALYTICA 84 Exhibition** Contact: Secretary General, Dr. Rosmarie Vogel, Abteilung für Klinische Chemie und Klinische Biochemie in der Chirurgischen Klinik Innenstadt der Universität München, Nussbaumstrasse 20, D-8000 München 2, G.F.R. Tel.: (089) 15 30 32; Telex: 5 216 018 bird d. (Further details published in Vol. 151, No. 1.)
April 16–19, 1984 New York, NY, U.S.A.	**20th International Symposium on Advances in Chromatography** Contact: Professor A. Zlatkis, Chemistry Department, University of Houston, Houston, TX 77004, U.S.A.
April 17–19, 1984 Noordwijkerhout, The Netherlands	**Analytical Methods and Problems in Biotechnology – An International Symposium** Contact: W.A. Scheffers, Symposium Analytical Methods and Problems in Biotechnology, Delft University of Technology, Laboratory of Microbiology, Julianalaan 67A, NL-2628 BC Delft, The Netherlands. Tel.: (015)-782411.
April 29–May 4, 1984 Rio de Janeiro, Brazil	**12th International Congress of Clinical Chemistry, 7th Latin American Congress of Clinical Biochemistry, & 12th Brazilian Congress of Clinical Analysis** Contact: 12th International Congress of Clinical Chemistry, Rua Vicente Licinio 95, Tijuca, 20270 Rio de Janeiro, RJ, Brazil.
May 9–11, 1984 Dourdan, France	**4th Weurman Flavour Research Symposium** Contact: J. Adda, Laboratoire de Recherches sur les Arômes, 17 rue Sully, 21034 Dijon Cedex, France.
May 15–18, 1984 Ghent, Belgium	**5th International Symposium on Mass Spectrometry in Life Sciences** Contact: Prof. Dr. A. De Leenheer, Symposium Chairman, Laboratoria voor Medische Biochemie en voor Klinische Analyse, Harelbekestraat 72, B-9000 Ghent, Belgium. Tel.: (091) 21.89.51.
May 20–25, 1984 New York, NY, U.S.A.	**8th International Symposium on Column Liquid Chromatography** Contact: Professor Cs. Horváth, Mason Laboratory, Yale University, P.O. Box 2159, Yale Station, New Haven, CT 06520, U.S.A. (Further details published in Vol. 146.)
June 12–14, 1984 Szeged, Hungary	**2nd Symposium on the Analysis of Steroids** Contact: Professor S. Görög, Chairman of the Organizing Committee of the 2nd Symposium on the Analysis of Steroids, c/o Hungarian Chemical Society, H-1061 Budapest, Anker köz 1, Hungary.
June 18–21, 1984 Ronneby, Sweden	**International Symposium on Liquid Chromatography in the Biomedical Sciences** Contact: Swedish Academy of Pharmaceutical Sciences, P.O. Box 1136, S-111 81 Stockholm, Sweden.
Aug. 21–24, 1984 Colombo, Sri Lanka	**Analytical Chemistry in Development** Contact: Centre for Analytical Research and Development, Department of Chemistry, University of Colombo, Colombo, Sri Lanka; or, Trace Analysis Research Centre, Chemistry Department, Dalhousie University, Halifax, N.S. B3H 4J1, Canada. (Further details published in Vol. 151, No 1.)

Aug. 26–31, 1984 Philadelphia, PA, U.S.A.	**188th National Meeting of the American Chemical Society** Contact: A.T. Winstead, American Chemical Society, 1155 16th Street, NW, Washington, DC 20036, U.S.A.
Aug. 26–Sept. 1, 1984 Cracow, Poland	**EUROANALYSIS V – 5th European Conference on Analytical Chemistry** Contact: Professor Zygmunt Kowalski, Secretary-General, Euroanalysis V, Academy of Mining and Metallurgy, Mickiewicza 30, 30-059 Kraków, Poland. (Further details published in Vol. 148.)
Sept. 2–6, 1984 Hradec Králové, Czechoslovakia	**4th International Symposium on Isotachophoresis – ITP 84** Contact: ITP 84, Dr. Z. Prusik, C.Sc., Institute of Organic Chemistry and Biochemistry, Czechoslovak Academy of Sciences, Flemingovo nám. 2, CS-166 10 Praha 6, Czechoslovakia. (Further details published in Vol. 146.)
Sept. 23–28, 1984 Philadelphia, PA, U.S.A.	**11th Annual Meeting of the Federation of Analytical Chemistry and Spectroscopy Societies** Contact: R.F. Hirsch, Division of Analytical Chemistry, American Chemical Society, 304 Beach Wood, Orange, NJ 07050, U.S.A.
Oct. 1–5, 1984 Nürnberg, G.F.R.	**15th International Symposium on Chromatography** Contact: Gesellschaft Deutscher Chemiker, Abteilung Fachgruppen, Postfach 90 04 40, Varrentrappstrasse 40–42, D-6000 Frankfurt (Main) 90, G.F.R.
Oct. 8–10, 1984 Tarrytown, NY, U.S.A.	**3rd International Symposium on Capillary Chromatography** Contact: Dr. A. Zlatkis, Chemistry Department, University of Houston, Houston, TX 77004, U.S.A.
Oct. 24–26, 1984 Montreux, Switzerland	**Third Workshop on LC–MS and MS–MS** Contact: Professor Dr. R.W. Frei, Department of Analytical Chemistry, Free University, De Boelelaan 1083, 1081 HV Amsterdam, The Netherlands. (Further details published in Vol. 151, No. 1.)
Nov. 19–24, 1984 Barcelona, Spain	**EXPOQUIMIA 84 – Salón Internacional de la Quimica** Contact: EXPOQUIMIA, Feria de Barcelona, Barcelona 4, Spain.
Nov. 22–24, 1984 Barcelona, Spain	**14th Annual Symposium on Analytical Chemistry of Pollutants** Contact: 3rd International Congress on Analytical Techniques in Environmental Chemistry/EXPOQUIMIA, Av. Reina Ma. Christina, Palacio No. 1, Barcelona 4, Spain. Tel.: 223.31.01; telex: 50458 FOIMB-E.
Nov. 22–24, 1984 Barcelona, Spain	**3rd International Congress on Analytical Techniques in Environmental Chemistry** Contact: 3rd International Congress on Analytical Techniques in Environmental Chemistry/EXPOQUIMIA, Av. Reina Ma. Christina, Palacio No. 1, Barcelona 4, Spain. Tel.: 223.31.01; telex: 50458 FOIMB-E.
Feb. 25–March 1, 1985 New Orleans, LA, U.S.A.	**36th Pittsburgh Conference and Exposition on Analytical Chemistry and Applied Spectroscopy** Contact: Linda Biggs, Pittsburgh Conference, 437 Donald Road, Dept. J-005, Pittsburgh, PA 15235, U.S.A.
April 28–May 3, 1985 Miami Beach, FL, U.S.A.	**189th National Meeting of the American Chemical Society** Contact: Meetings Department, American Chemical Society, 1155 Sixteenth Street, NW, Washington, DC 20036, U.S.A.

July 1–5, 1985 Edinburgh, Scotland, Great Britain	**9th International Symposium on Column Liquid Chromatography** Contact: J.H. Knox, Department of Chemistry, University of Edinburgh, Edinburgh EH9 3JJ, Scotland, Great Britain.
Sept. 8–13, 1985 Chicago, IL, U.S.A.	**190th National Meeting of the American Chemical Society** Contact: Meetings Department, American Chemical Society, 1155 Sixteenth Street, NW, Washington, DC 20036, U.S.A.
Sept. 9–13, 1985 Manchester, Great Britain	**30th International Congress of Pure and Applied Chemistry** Contact: The Royal Society of Chemistry, Burlington House, London W1V 0BN, Great Britain.

(continued from outside back cover)

CONTENTS

(Abstracted, Indexed in: Anal. Abstr.; Biol. Abstr.; Chem. Abstr.; Curr. Contents Phys. Chem. Earth Sci.; Life Sci.; Index Med.; Mass Spectrom. Bull.; Sci Citation Index; Excerpta Med.)

(continued on inside back cover)